The University Of Sheffield.

Analysis of *cd9b* in CXCR4b signalling

By:

Sarah Greaves

A thesis submitted for the degree of
Doctor of Philosophy

The University of Sheffield
Faculty of Science
Department of Biomedical Science

May 2016

Abstract

CXCR4b, CXCR7b and their ligand, CXCL12a, are essential for the migration of the posterior lateral line primordium (pLLP) and primordial germ cells (PGCs) in zebrafish (Dambly-Chaudière et al. 2007, Boldajipour et al. 2008). A number of tetraspanins have been shown to affect CXCR4-mediated processes through regulating CXCR4 trafficking or downstream signalling (Yoshida et al. 2008, Li et al. 2011, Leung et al. 2011). Based upon these results we set out to identify candidate tetraspanins that may play a similar role in CXCR4b signalling during pLLP and PGC migration. CD9b, one of the zebrafish homologs of human CD9, was identified as a good candidate gene. Morpholino knock down of *cd9b,* using either a translation-blocking or splice-site blocking morpholino, resulted in reduced neuromast deposition and abnormal structure of the posterior lateral line. However, morpholinos often have nonspecific effects and so two CD9b knockout lines were created using TALENs. Surprisingly CD9b homozygous mutants showed normal lateral line structure. Preliminary results suggest that the phenotype differences between CD9b morphants and mutants may be due to residual functionality in the wildtype N-terminal of CD9b, upstream of the mutation site, in CD9b mutants.

As well as assessment of PGC and pLLP migration, CD9b mutants were also assessed for fertility defects. Significantly reduced numbers of pups are born to CD9 knockout mice. This is due to a requirement of CD9 on the egg membrane for efficient sperm-egg fusion in the CD9-/- female mice (Kaji et al. 2000, Le Naour et al. 2000, Miyado et al. 2000). CD9b -/- zebrafish also appear to have fertility defects. Fewer eggs were laid by CD9b -/- zebrafish pairs and of the eggs laid, a lower percentage were fertilised.

Contents

List of Abbreviations

ACKR3	Atypical chemokine receptor 3
aLL	Anterior lateral line
ApE	A plasmid editor
BSA	Bovine serum albumin
CXCL12	Chemokine CXC motif ligand 12
CXCR4	Chemokine CXC motif receptor 4
DIG	Digoxigenin
dpf	Days post fertilisation
DSBs	Double strand breaks
E	Embryonic day
Env	HIV-1 Envelope glycoprotein
ERK1/2	Extracellular-signal-related kinases 1/2
GPCR	G-protein coupled receptor
HB-EGF	Heparin-binding epidermal growth factor-like
HIV-1	Human immunodeficiency virus-type 1
hpf	Hours post fertilisation
HSCs	Hematopoietic stem cells
ID	Identify
IDT	Integrated DNA Technologies
IL-8	Interleukin-8
indels	Insertion and/or deletions
JAK	Janus kinases
LESTRE	Leukocyte derived seven transmembrane domain receptor
mAb	Monoclonal antibody
MAPK	Mitogen-activated protein kinases
MIF	Migration inhibitory factor
MMP-9	Matrix metalloproteinase
MO	Morpholino oligonucleotides
NEB	New England Biolabs Inc.
NHEJ	Non-homologous end joining
NMD	Nonsense-mediated decay
PCR	Polymerase chain reaction
PBS	Phosphate buffered saline
PFA	Paraformaldehyde
PGC	Primordial germ cells
PI3K	Phosphatidylinositol-3-kinase
PLC-β	Phospholipase C-beta
pLL	Posterior lateral line
pLLP/Prim I	Primary posterior lateral line primordium
Pro-K	Proteinase-K
PSG17	Pregnancy-specific-glycoprotein 17
qRT-PCR	Quantitative reverse transcription PCR
Rgs14a	Regulator of G-protein signalling 14a protein
SAP	Shrimp alkaline phosphatase

SDF-1	Stromal cell derived factor-1
SDS	Sodium dodecyl sulphate
SLS	Scientific Laboratory Supplies
SSCs	Spermatogonial stem cells
STAT	Signal transducer and activator of transcription protein
TALEN	Transcription activator-like effector nuclease
TBE	Tris-borate-EDTA
TEM	Tetraspanin enriched microdomain
TIMP-1	Tissue inhibitor of metalloproteinases
TPAR-1	TPA repressed gene 1
VCAM-1	Vascular cell adhesion molecule-1
WHIM	Warts, hypogammaglobulinemia, infection and myelokathexis
wt	Wildtype

Chapter 1: Introduction

1.1 CXCR4

CXCR4 (chemokine CXC motif receptor 4) was originally cloned from human monocytes and named LESTR (leukocyte derived seven transmembrane domain receptor) by Loetscher et al. in 1994. The 352 amino acid protein was found to have considerable sequence identity with the bovine neuropeptide Y receptor boLCR1 (96%) and interleukin-8 (IL-8) receptors (34%) which were known G-protein coupled receptors and chemokine receptors at the time (Rimland et al. 1991, Loetscher et al. 1994). It was noted by Loetscher et al., that the predicted structure had many typical G-protein coupled receptor (GPCR) domains, including seven transmembrane domains, a binding site for the G_i-subtype of G-proteins, potential N-glycosylation sites in the N-terminus and putative intracellular substrate motifs for protein kinase C. The high abundance of CXCR4 mRNA in human leukocytes led Loetscher et al., to speculate that CXCR4 functions in the activation of leukocytes, though the relevant ligand could not be identified.

A function for CXCR4 was soon found by Yu et al. 1996, as a co-receptor for T-cell-tropic, but not macrophage-tropic, HIV-1 (human immunodeficiency virus-type 1) in CD4+ cells. Expression of CXCR4 in CD4+, human or non-human cells allowed HIV-1 envelope glycoprotein (Env) mediated fusion, syncitium formation and HIV-1 infection in normally non-permissive cells. CD4- cells were also rendered susceptible to T-cell-tropic Env mediated cell fusion by co-expression of human CD4 and CXCR4, even in non-human cell lines. Sole expression of either CD4 or CXCR4 did not permit Env-mediated fusion in normally non-permissive cells (Yu et al. 1996, Berson et al. 1996).

Soon after the discovery of CXCR4's function in HIV-1 infection its ligand, CXCL12 (chemokine CXC motif ligand 12), was found. Previously known as SDF-1 (stromal cell derived factor 1), CXCL12, was shown to inhibit T-cell tropic HIV-1 infection in CXCR4+ and CD4+ cells. CXCL12 was also shown to act as a highly efficient chemoattractant, inducing Ca^{2+} release from and internal actin polymerization in CXCR4-transfected cells and leukocytes, supporting the hypothesis made by Loetscher et al., in 1994 (Bleul et al. 1996a, 1996b, Oberlin et al. 1996).

Cloning of the murine CXCR4 homolog revealed high amino acid identity with human CXCR4 (91%) and identical responses of CXCR4+ cells to murine CXCL12. It was also noted that CXCR4 was expressed in embryos at embryonic day 7.5-17.5 (E7.5-E17.5) as well as in a number of adult tissues such as the spleen, thymus, brain and kidney (Nagasawa et al. 1996b, Heesen et al. 1996). To investigate the potential role of CXCR4 in these tissues and others, CXCR4 homozygous knockout mice were made by a number of groups. CXCR4-/- embryos were viable until E15.5 after which the majority of the embryos died. Only 50% of the expected number of pups were seen at E17.5 and the few pups that survived to full term died within a few hours of being born. The viable CXCR4-/- embryos were observed to have a number of defects including reduced body size, defective B-cell lymphopoiesis and bone-marrow myelopoiesis as well as a cardiac ventricular septal defect, all of which mirrored the defects seen in CXCL12-/- mice previously (Nagasawa et al. 1996a, Tachibana et al. 1998, Zou et al. 1998, Ma et al. 1998).

Lack of CXCR4 also affected the migration or positioning of many neuronal cells and neural progenitors. CXCR4 deficient embryos showed an ectopic granule cell layer in the cerebellum, an underdeveloped hippocamal dentate gyrus due to defective progenitor cell migration and premature differentiation as well as ectopic migration of interneurons in the neocortex (Zou et al. 1998, Ma et al. 1998, Lu et al. 2002, Stumm et al. 2003). Migratory defects were not only seen in neuronal cells, but also in progenitor muscle cells and germ cells where CXCR4 appears to also regulate survival of these cell types (Molyneaux et al. 2003, Vasyutina et al. 2005). It was also noted by Tachibana et al. 1998 that CXCR4-/- embryos often displayed multiple haemorrhages or vascular congestions in the small intestines. It was found that CXCR4 was required for correct vascularization of the small intestines after E11.5, with CXCR4 mutants showing decreased vascular branching and re-modelling after this time point. While a reduced number of large vessels were seen in the small intestine, they were completely absent in the stomach of CXCR4-/- embryos, a phenotype which was also attributed to defective branching and re-modelling (Tachibana et al. 1998).

Since the creation of CXCR4-/- mice, CXCR4 and CXCL12 signaling has been found to guide or regulate the migration of numerous cell types, with similar functions found in multiple other models including human cell culture and zebrafish.

1.1.1 CXCR4 and WHIM

With the embryonic lethality of CXCR4-/- it is unsurprising that no human homozygous CXCR4 mutations have been reported, however, heterozygous C-terminal CXCR4 mutations have been reported to cause the disorder WHIM (warts, hypogammaglobulinemia, infection, and myelokathexis) (Hernandez et al. 2003). WHIM syndrome was first described in 1990, and is caused by a gain of function mutation in CXCR4 which results in neutrophil retention and apoptosis in the bone marrow and consequently increased infection rates (Wetzler et al. 1990, Hernandez et al. 2003, Busillo and Benovic 2007, Pawig et al. 2015).

This syndrome appears to result from the dysregulation of CXCR4 signaling upon CXCL12 stimulation. In WHIM syndrome patients, the C-terminal truncated CXCR4 displays heightened and prolonged G-protein activation due to the inability to uncouple from its G-protein and internalize upon CXCL12 binding (Balabanian et al. 2005b, Busillo and Benovic 2007). This lack of internalization has been suggested to be due to the loss of phosphorylation sites in the C-terminus of CXCR4, which then results in the impaired ability of GRK3 (GPCR kinase-3) to bind and induce the internalization of CXCR4 (Balabanian et al. 2008). As well as increased G-protein signaling, enhanced β-arrestin2 signaling via ERK1/2 has been suggested to contribute to the augmented chemotactic response to CXCL12 by WHIM leukocytes (Lagane et al. 2008).

1.1.2 CXCR4 and cancer

Many cell types have been reported to require CXCR4 for correct migration and so it is also unsurprising that CXCR4 has become associated with metastasis for many different cancers including breast, prostate, ovarian, pancreatic, colon cancers, T-cell hybridoma, and melanoma (Zeelenberg et al. 2001, 2003, Murakami et al. 2002, Singh et al. 2004, Saur et al. 2005, Gladson and Welch 2008, Barbolina et al. 2010, Chatterjee et al. 2014). Originally it was found that breast cancer cells require CXCR4/CXCL12 signalling for metastasis (Müller et al. 2001). Breast cancer cells exhibit significantly up regulated CXCR4 expression compared to healthy mammary gland tissue and commonly metastasise to organs which express high levels of CXCL12, such as lymph nodes, lungs, liver and bone marrow. Neutralisation of CXCR4 signalling using an anti-CXCR4 antibody resulted in a significant reduction of metastasis *in vivo* (Müller et al. 2001). CXCR4 overexpression has been reported in >23 human cancers, with

implications not only in metastasis and invasion but also in tumour survival through growth, angiogenesis and treatment resistance (Chatterjee et al. 2014). The effects mediated by CXCR4 on cancer cell behaviours are diverse, often depending on the cancer type and the partner proteins or downstream signalling activated. For example, CXCR4 mediates migration and invasion of many different cancer cell types. In breast cancer, CXCR4 interaction with CXCL12 leads to the transactivation of the receptor HER-2/neu (human epidermal growth factor receptor 2/ receptor tyrosine-protein kinase erbB-2), which is essential for HER-2-mediated metastasis (Balkwill 2004, Cabioglu et al. 2005). In multiple myeloma CXCR4 mediates migration and homing through G-protein signalling to activate the PI3K and ERK/MAPK pathways (Alsayed et al. 2007). While ovarian cancers also use MAPK and PI3K to promote invasion, these pathways are activated via αvβ6 integrin expression, which is upregulated by CXCR4 (Xue et al. 2013).

As well as promoting migration, CXCR4 is often important for tumour cell survival (Chatterjee et al. 2014). In leukaemia CXCR4 and CXCL12 interaction helps to protect cancerous cells from chemotherapy-induced apoptosis through the phosphorylation of PI3K/AKT, MAPK and ERK. Similarly, MEK/ERK signalling is activated by CXCR4 in prostate cancer cell, however, this then leads to the activation of NF-κB which was suggested to be important for tumour cell survival (Chatterjee et al. 2014). The activation of MAPK is also used by small cell lung cancer to inhibit chemotherapy-induced cell death. However, the mechanism is slightly different. CXCR4 activates actin polymerisation and MAPK signalling which leads to adhesion of small cell lung cancer cells to the surrounding extracellular matrix (Sethi et al. 1999, Burger et al. 2003). This adhesion results in increased β1, α3, α6 and αv integrin expression and increased tyrosine-kinase activity therefore preventing caspase activation and inhibiting chemotherapy-induced cell death (Sethi et al. 1999, Chatterjee et al. 2014).

1.1.3 CXCR4 and alternative ligands

Although CXCL12 was originally thought to be the sole ligand for CXCR4, a number of other ligands have since been identified. Migration inhibitory factor (MIF), Ubiquitin and gp120 have all been shown to bind and activate CXCR4. MIF was shown to stimulate T-cell chemotaxis through CXCR4 as well as activating G-protein signaling and adhesion of partner proteins such as VCAM-1 (vascular cell adhesion molecule-1)

(Bernhagen et al. 2007, Pawig et al. 2015). Extracellular ubiquitin has also been shown to activate G-protein signaling upon binding to CXCR4 in monocyte and macrophage cell lines, resulting in a Ca^{2+} release as seen with CXCL12 binding (Saini et al. 2010). Lastly the HIV-1 envelope glycoprotein gp120 has been shown to induce rapid CXCR4 internalization upon binding, in both CD4+ and CD4- cells (Tarasova et al. 1998).

1.2 CXCL12

Originally cloned in 1993 murine CXCL12, formerly named SDF-1 or TPAR1 (TPA repressed gene 1), was found to produce two different isoforms as a result of alternative splicing. The 89 and 93 amino acid sequence forms (where the first 89 amino acids are identical), CXCL12-α and CXCL12-β respectively, were found to be part of the CXC subfamily of the cytokine family, having high similarity with the cytokine IL-8 and the characteristic CXC motif (Tashiro et al. 1993, Jiang et al. 1994, Shirozu et al. 1995). The human homologs of CXCL12-α and CXCL12-β were cloned in 1995 and were found to have >92% identity with their murine counterparts.

Additional isoforms, CXCL12-γ, CXCL12-δ, CXCL12-ε and CXCL12-φ, resulting from alternative splicing events were found in 2006. All six isoforms appear to produce functional proteins, which are expressed in different tissues and appear to have different functions. For example CXCL12-α appears most widely expressed, however, it is broken down rapidly in the bloodstream unlike CXCL12- β which is consequently more highly expressed in highly vascularised organs and functions in angiogenesis (Yu et al. 2006, Janowski 2009). CXCL12- α has been the most widely studied and is the isoform of interest for this work, so any reference to CXCL12 in mammals refers to CXCL12-α unless otherwise stated.

While mammals have a single *cxcl12* gene zebrafish have two, *cxcl12a* and *cxcl12b* (David et al. 2002). Unlike the mammalian homolog, multiple isoforms of these genes have yet to be identified.

1.2.1 CXCL12 and CXCR4 signalling

Upon ligand binding, freely diffusing CXCR4 is immobilised in the plasma membrane. Immobilisation is dependent on and correlates with G-protein dependent signalling and occurs prior to subsequent receptor trafficking. Immobilisation of the receptor is suggested to be due to the formation of a supramolecular scaffold or signalosome

comprising of the G-protein dependent signalling pathways activated upon ligand binding (Beletkaia et al. 2016).

The G-protein complex associated with CXCR4 comprises of three subunits, Gα, Gβ, and Gγ. Receptor activation leads to dissociation of GβGγ from Gα, allowing Gα to activate extracellular-signal-related-kinases (ERK1/2), the phosphatidylinositol-3-kinase pathway (PI3K) and Rho leading to downstream effects such as chemotaxis, promotion of cell survival and transcription. The GβGγ subunit also activates PI3K, along with phospholipase C-β (PLC-β) and Rac leading to Ca^{2+} release and chemotaxis (Figure 1.1) (Ganju et al. 1998, Tan et al. 2006, Busillo and Benovic 2007, Teicher and Fricker 2010, Pawig et al. 2015).

G-protein independent signalling has also been reported, with β-arrestin shown to promote ERK1/2 activation as well as p38 mitogen-activated protein kinase (p38MAPK) activation (Busillo and Benovic 2007, Pawig et al. 2015). The Janus kinase/Signal Transducer and Activator of Transcription protein (JAK/STAT) pathway has also been implicated in CXCR4 signalling. Vila-Coro et al. 1999 reported the association of activated JAK2 and JAK3 with CXCR4 after ligand binding and receptor dimerization, leading to the recruitment of several STAT proteins (Figure 1.1).

Ligand binding not only induces downstream signalling but also ligand trafficking, with the endocytosis of up to 60% of surface CXCR4 (Tarasova et al. 1998, Förster et al. 1998). The receptor is endocytosed by clathrin-coated pits, with β-arrestin acting as a mediator between CXCR4 and clathrin (Tarasova et al. 1998, Förster et al. 1998, Busillo and Benovic 2007, Pawig et al. 2015). The receptor is then targeted to the lysosomes for degradation following the ubiquitination of lysine residues in the C-terminal degradation motif SSLKILSKGK by the E3 ubiquitin ligase AIP4 (Marchese and Benovic 2001, Marchese et al. 2003). Recycling of internalised CXCR4 after ligand binding was reported to occur, albeit inefficiently (Tarasova et al. 1998). Interestingly, CXCR4 crosslinking using an anti-CXCR4 antibody did result in rapid and efficient receptor internalisation and recycling (Förster et al. 1998).

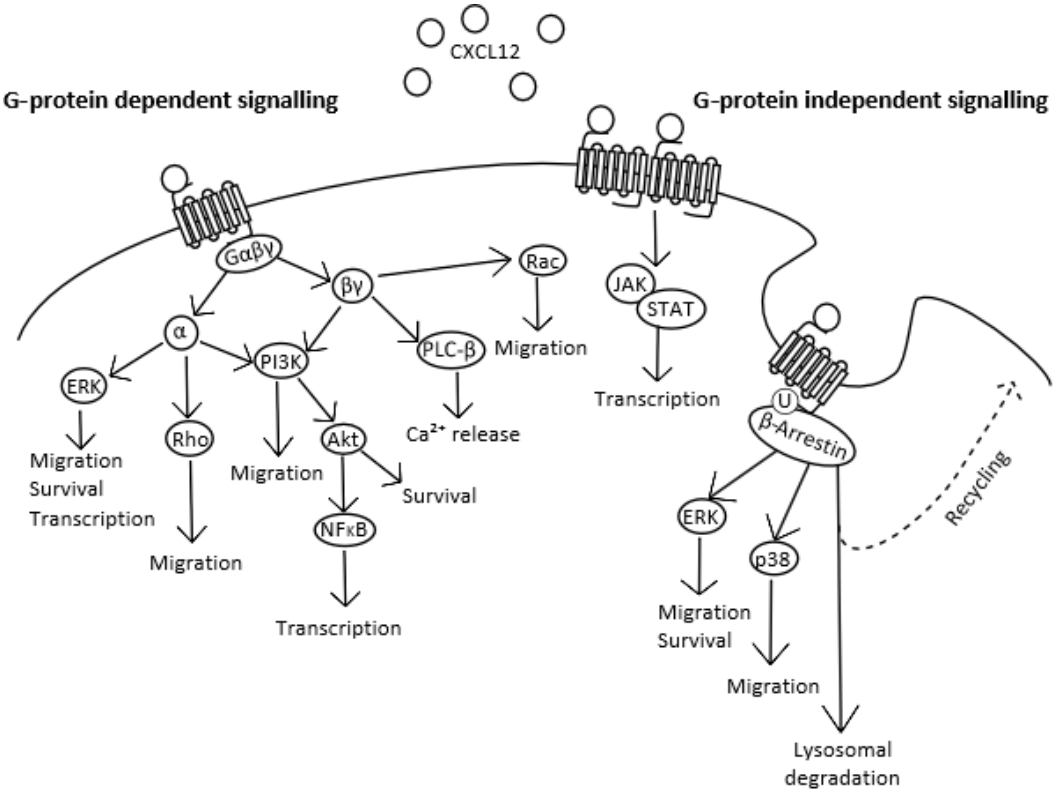

Figure 1.1 Diagram showing the signalling pathways of CXCR4.
ERK (Extracellular signal-regulated kinases), Gαβγ (G-protein), JAK (Janus kinase), PI3K (phosphoinositide 3-kinase), PLC-β (Phospholipase C-β), STAT (signal transducer and activator of transcription), U (Ubiquitination)

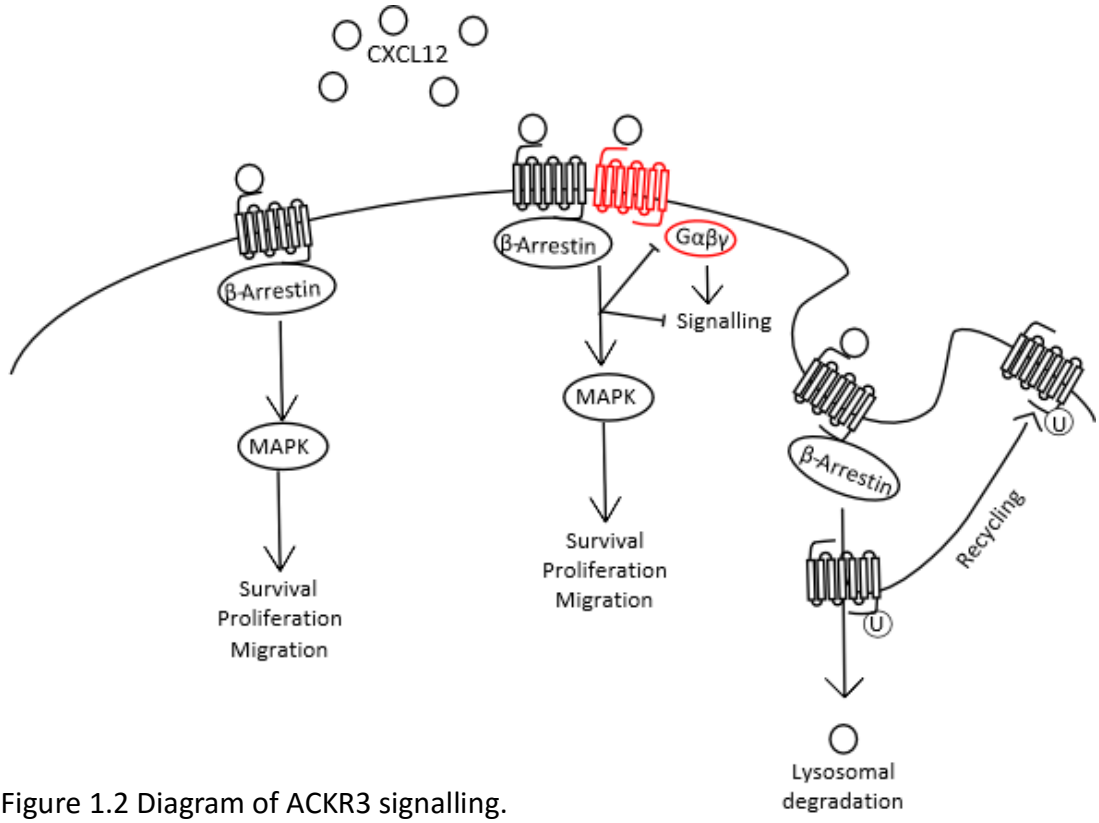

Figure 1.2 Diagram of ACKR3 signalling.
ACKR3 (black) and CXCR4 (red) can heterodimerise to regulate G-protein and β-Arrestin signalling. U (Ubiquitination), MAPK (Mitogen-activated protein kinases)

1.3 ACKR3 (Atypical chemokine receptor 3)

A second CXCL12 receptor, ACKR3, was originally known as the orphan receptor RDC1 or CXCR7. ACKR3 was initially grouped with GPCRs due to the presence of typical GPCR features such as 7 transmembrane domains, an extracellular N-terminus and intracellular C-terminus as well as characteristic conserved cysteines (Libert et al. 1989, Heesen et al. 1998).

Adopted by CXCL12 in 2005 and CXCL11 in 2006, ACKR3 was shown to be expressed on T lymphocytes and tumour cell lines with the ability to bind CXCL12 with higher affinity than CXCR4 (Balabanian et al. 2005a, Burns et al. 2006). Despite the similarities in protein domains, ACKR3 has been reported to be unable to elicit G-protein signalling or bind to G-proteins on multiple occasions (Burns et al. 2006, Sierro et al. 2007, Rajagopal et al. 2010, Canals et al. 2012, Kumar et al. 2012, Hoffmann et al. 2012), although this has been challenged by Odemis et al. 2012 who demonstrated ACKR3 signalling via G-proteins in rodent astrocytes and human glioma cells. This predominant lack of G-protein association is thought to be due to differences in the C-terminal domain and second intracellular loop between CXCR4 and ACKR3. CXCR4 contains a DRYLAIV motif in the second intracellular loop that is considered critical for G-protein association. In ACKR3 this motif is altered to DRYLSIT and substitution of the CXCR4 C-terminal with ACKR3 C-terminal renders CXCR4 unable to bind G-proteins (Sierro et al. 2007, Naumann et al. 2010, Hoffmann et al. 2012). However, replacement of either or both of these domains with the equivalent CXCR4 domain is not sufficient to render ACKR3 the ability to bind G-proteins (Naumann et al. 2010, Hoffmann et al. 2012).

Despite this apparent lack of signalling via G-proteins, ACKR3 has been shown to have a wide variety of functions and is highly conserved between species with 92% similarity between humans and mice (Heesen et al. 1998, Sierro et al. 2007). ACKR3-/- mice died at birth, displaying ventricular septal defects and decreased expression of factors important in endothelial cell growth and survival, angiogenesis and vessel protection; however, haematopoiesis appeared unaffected unlike CXCR4-/- and CXCL12-/- embryos (Sierro et al. 2007). Roles for ACKR3 in cell chemotaxis, growth, survival, positioning and adhesion have been reported in multiple cell types including T lymphocytes, breast cancer cells, lung cancer cells, renal progenitor cells, interneurons,

marginal zone B-cells and melanoma cells (Balabanian et al. 2005a, Burns et al. 2006, Miao et al. 2007, Mazzinghi et al. 2008, Wang et al. 2011b, 2012, Kumar et al. 2012, Liedtke et al. 2014).

The functionality of ACKR3 has been shown to use multiple different pathways including acting as a ligand sink for CXCL12, signalling through β-arrestin upon CXCL12 binding or forming heterodimers with CXCR4 to down regulate G-protein signalling and up regulate β-arrestin signalling pathways (Figure 1.2). The rapid recycling of ACKR3 and high affinity for CXCL12 renders the receptor well suited as a ligand scavenger, efficiently binding, internalising and degrading CXCL12 before recycling back to the cell membrane (Naumann et al. 2010, Canals et al. 2012, Hoffmann et al. 2012). This allows ACKR3 to regulate chemotaxis by moderating chemokine gradients, as well as regulating CXCR4 function and cell reactivity to CXCL12 (Boldajipour et al. 2008, Naumann et al. 2010, Sánchez-Alcañiz et al. 2011, Canals et al. 2012, Hoffmann et al. 2012).

Whilst scavenging roles for ACKR3 do not report any subsequent signalling after ligand binding, many cell types have shown ligand induced ACKR3 signalling via β-arrestin to activate MAP kinases resulting in enhanced cell survival, proliferation, chemotaxis or trans-endothelial migration (Figure 1.2) (Zabel et al. 2009, Rajagopal et al. 2010, Odemis et al. 2010, Wang et al. 2011b, Kumar et al. 2012).

Although monomeric signalling has been shown by ACKR3, it has also been shown to hetero-dimerise with CXCR4 upon CXCL12 binding which causes conformational changes in the pre-formed CXCR4-G-protein complex. These changes lead to the inhibition of G-protein and CXCR4 coupling, subsequently downregulating G-protein signalling pathways and upregulating β-arrestin signalling pathways via MAP kinases (Levoye et al. 2009, Décaillot et al. 2011). This switch in cell signalling allows ACKR3 to regulate and enhance cell survival, proliferation or migration (Décaillot et al. 2011).

1.4 CXCR4 in zebrafish

Due to a fish specific genome duplication, many mammalian genes have two homologous genes in teleost fish (Meyer and Van de Peer 2005, Brunet et al. 2006). This is true for *cxcr4, cxcl12* and *ackr3* in zebrafish, with homologous genes labelled *a* or *b* (Chong et al. 2001, David et al. 2002, Miyasaka et al. 2007) (Table 1.1).

Human gene	**Mouse gene**	**% Identity to human**	**Zebrafish gene**	**% Identity to human**
CXCR4	Cxcr4	88	cxcr4a	66
			cxcr4b	62
ACKR3	Ackr3	93	ackr3a	47
			ackr3b	54
CXCL12	Cxcl12	71	cxcl12a	42
			cxcl12b	42

Table 1.1 Percentage identity of the mouse and zebrafish homologs to human *CXCR4, ACKR3* and *CXCL12*. Data from ensembl.org (Herrero et al. 2016).

The expression of *cxcr4a* and *cxcr4b* are predominantly mutually exclusive in the developing zebrafish embryo, with the genes only being co-expressed in the lateral mesoderm and posterior midbrain (Chong et al. 2001). Together *cxcr4a* and *cxcr4b* are expressed in the majority of cell types that have been reported to express *cxcr4* in mammals, leading to Chong et al. 2001 hypothesising that the functions of mammalian CXCR4 may be split between CXCR4a and CXCR4b in zebrafish.

This appears to be true, with CXCR4a and CXCR4b regulating different biological processes during development reminiscent of those controlled by CXCR4 in mammals, for example CXCR4a is required for vasculogenesis and angiogenesis whereas CXCR4b controls neutrophil chemotaxis and germ cell migration (Table 1.2) (Doitsidou et al. 2002, Siekmann et al. 2009, Walters et al. 2010, Harrison et al. 2015). These functions require the activation of CXCR4a and CXCR4b through the specific binding of either CXCL12a or CXCL12b. Whilst some functions have been shown to use CXCR4a and CXCL12a, predominantly it has been shown that CXCR4a and CXCL12b or CXCR4b and CXCL12a interact to elicit specific functions (Dufourcq and Vriz 2006, Boldajipour et al.

2011). This preference has been shown to be due to a single amino acid in the CXCL12 ligands which confers higher affinity with one of the CXCR4 receptors (Boldajipour et al. 2011). However, due to the high identity between CXCL12a and CXCL12b at the amino acid level (82%), these ligands have been shown to be partially functionally redundant for posterior lateral line primordium migration (Li et al. 2004).

CXCR4a function	**Reference**	**CXCR4b function**	**Reference**
Angiogenesis	Harrison et al. 2015	Cardiomyocyte migration	Itou et al. 2012
Endodermal cell migration	Mizoguchi et al. 2008	Germ cell migration	Doitsidou et al. 2002
Epidermal cell proliferation	Dufourcq & Vriz 2006	GnRH3 (Hypothalamic gonadotropin-releasing hormone) neuron migration	Palevitch et al. 2010
Neural crest cell migration	Boer et al. 2015	Neutrophil chemotaxis/ WHIM-syndrome	Walters et al. 2010
Fast muscle formation	Chong et al. 2007	Olfactory neuron precursor migration	Miyasaka et al. 2007
Slow muscle migration	Chong et al. 2007	Posterior lateral line primordium migration	David et al. 2002
Vasculogenesis	Siekmann et al. 2009	Retinal ganglion cell axon migration	Li et al. 2005
		Trigeminal sensory neuron migration	Lewellis et al. 2013

Table 1.2 Reported functions of CXCR4a and CXCR4b in zebrafish.

1.4.1 Primordial germ cell migration

One of the most well characterised functions of CXCR4 in zebrafish is the regulation of primordial germ cell (PGC) migration by CXCR4b and CXCL12a. PGCs are specified early on during embryogenesis, at 3-4hpf, by the segregation of germ plasm RNAs into future PGCs (Yoon et al. 1997, Weidinger et al. 1999, 2003). PGCs cluster at four locations, which are dependent on the orientation of the earlier cleavage planes, although these planes are random in respect to the future dorsoventral body axis (Yoon et al. 1997, Weidinger et al. 1999). Immediately after specification PGCs are indistinguishable from their somatic neighbours as both cell types present a round non-motile morphology (Blaser et al. 2005). Following this, PGCs start to extend multiple protrusions in multiple directions, although remain immotile and appear unable to respond to CXCL12a (Blaser et al. 2005, Raz and Reichman-Fried 2006). Transition to motile cell behaviour is acquired in co-ordination with the expression of CXCL12a, a process which is regulated by Rgs14a (regulator of G-protein signalling 14a protein), E-cadherin levels and function of the RNA-binding protein Dead end (Weidinger et al. 2003, Blaser et al. 2005, Goudarzi et al. 2012, Hartwig et al. 2014, Paksa and Raz 2015).

Directed cell migration is mediated by CXCR4b-expressing PGCs actively and individually migrating towards CXCL12a expressing tissues (Doitsidou et al. 2002, Knaut et al. 2003). The expression pattern of CXCL12a is dynamic and changes throughout development, leading the PGCs to initially cluster bilaterally at somites 1-3 before migrating posteriorly to the region where the gonads will later develop (Figure 1.3) (Weidinger et al. 1999, 2002, Doitsidou et al. 2002, Knaut et al. 2003). This dynamic chemoattractant pattern is fine tuned into an effective chemotactic gradient at the protein level by ACKR3 and at the mRNA level by miR-430 (Boldajipour et al. 2008, Staton et al. 2011). ACKR3 is expressed by somatic cells and acts as a ligand sink, binding, internalising and degrading CXCL12a before recycling back to the cell surface. The degradation of CXCL12a generates sharp gradients of diffusible chemokine, allowing PGCs to follow the dynamic pattern of *cxcl12a* transcription and migrate to the new source of transcription (Mahabaleshwar et al. 2008, 2012, Boldajipour et al. 2008) (Figure 1.3). miR-430 aids this fine-tuning of gradients by removing *cxcl12a* transcripts from previous expression domains and regulating the levels of *ackr3*

(Staton et al. 2011, 2013). This function for miR-430 in PGC migration has been debated by Goudarzi et al. 2013 as they found the results reported by Staton et al., could not be reproduced. However, this mechanism of ligand clearance has been reported in a second CXCR4b-mediated process, the migration of trigeminal sensory neurons (Lewellis et al. 2013).

When following the chemotactic gradient of CXCL12a PGCs perform a 'run and tumble' behaviour. During run phases polarised cells actively migrate in a single direction, whilst direction can be changed by entering a tumbling phase in which cells lose their polarity, extend filopodia around the cell surface, before re-polarising to correct the migration path and entering a new run phase (Reichman-Fried et al. 2004). Correct polarisation of cells, and therefore correct migration, relies on CXCR4b-CXCL12a signalling. PGC filopodia allow the cells to detect the chemokine gradient and polarise towards the source of the gradient (Meyen et al. 2015). CXCL12a binds to CXCR4b on the filopodia, activating the scaffold protein Irsp53 which promotes the formation of more actin-rich filopodia at the cell front, increasing CXCL12a binding potential and the resulting signal (Meyen et al. 2015). CXCL12a binding CXCR4b induces G-protein signalling, specifically signalling by the Gβγ subunits. This results in an elevated pH at the cell front, mediated by Carbonic Anhydrase 15b, that promotes polarised Rac1 activity and actin polymerisation (Dumstrei et al. 2004, Kardash et al. 2010, Xu et al. 2012, Meyen et al. 2015, Tarbashevich et al. 2015).

Although actin polymerisation is upregulated at the cell front in response to the CXCL12a gradient, it does not power cell migration as it does cell polarisation (Blaser et al. 2005, Meyen et al. 2015). Migration of PGCs occurs by blebbing. At sites of high levels of free calcium, myosin contraction is activated. This contraction causes local separation of the acto-myosin cortex from the plasma membrane, allowing an influx of cytoplasm which creates a bleb (Blaser et al. 2006, Goudarzi et al. 2012). The local increase in free calcium which initiates bleb formation has been hypothesised to be due to activation of CXCR4b on CXCL12a binding (Blaser et al. 2006).

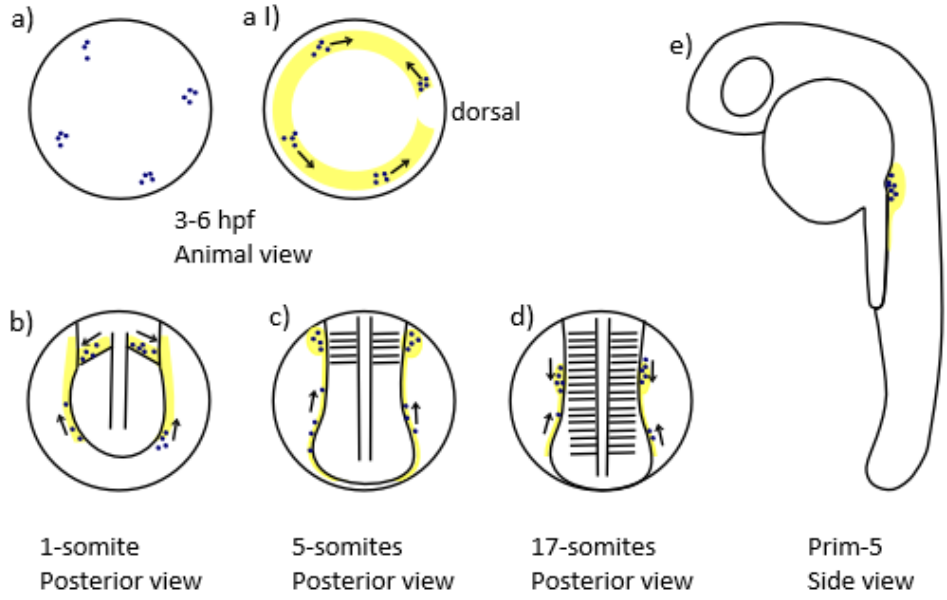

Figure 1.3 Illustration of PGC migration and *cxcl12a* expression.
Four clusters of non-motile PGCs (a) become motile upon *cxcl12a* expression (yellow) (a I). The motile PGCs move dorsally but are repelled from the dorsal midline (a I). At the 1-somite stage, PGCs move laterally and anteriorly to position adjacent to developing somites (b). PGCs continue to migrate towards and cluster at somites 1-3 (c) before migrating posteriorly to cluster adjacent to somites 8-10 (d). This final cluster position is just above the anterior yolk extension, where the gonads will later develop (e). Based on Weidinger et al. 1999; Weidinger et al. 2002; Doitsidou et al. 2002; Blaser et al. 2005.

1.4.2 Posterior lateral line migration

The lateral line is a mechanosensory organ which allows fish to detect water movements, facilitating behaviours such as prey detection, predator avoidance and schooling (Dambly-Chaudière et al. 2003, Ghysen and Dambly-Chaudiere 2004, Suli et al. 2012). Water flow is detected by individual sense organs called neuromasts, which are comprised of central hair cells surrounded by support cells. Neuromasts on the head and neuromasts on the trunk make up the two different lateral line systems, the anterior lateral line (aLL) and the posterior lateral line (pLL) (Gompel et al. 2001).

The adult zebrafish posterior lateral line consists of more than 1000 neuromasts, which are loosely arranged in dorso-ventral rows called stitches (Ledent 2002, Sapede et al. 2002). The embryonic posterior lateral line structure is much simpler, comprising of 7-8 neuromasts on both sides of the embryo along the horizontal myoseptum (Metcalfe et al. 1985, Metcalfe 1985, Gompel et al. 2001). The development of the posterior lateral line from the simple embryonic to the complex adult organ requires the migration of multiple primordia, the formation of intercalary neuromasts from interneuromast cells deposited by these primordia and budding of new neuromasts from primary neuromasts (Ledent 2002, Sapede et al. 2002, Grant et al. 2005, López-Schier and Hudspeth 2005, Nuñez et al. 2009, Sarrazin et al. 2010).

The development of the embryonic posterior lateral line has been extensively studied and become a popular model for collective cell migration and tissue morphogenesis, with implications for cancer metastasis (Ma and Raible 2009, Friedl and Gilmour 2009, Sarrazin et al. 2010, Aman et al. 2011). The 7-8 embryonic neuromasts are deposited by a single primordium of ~100 cells, the primary posterior lateral line primordium (Prim I/ pLLP), which migrates along the horizontal myoseptum between ~20-42hpf, depositing clusters of cells which later develop into neuromasts (Metcalfe 1985, Kimmel et al. 1995, Gompel et al. 2001). As in PGC migration, CXCL12a acts as a chemoattractant for the pLLP cells expressing CXCR4b (Gompel et al. 2001, David et al. 2002, Haas and Gilmour 2006). Just prior to pLLP migration, at ~20hpf, CXCL12a starts to be expressed by cells in the horizontal myoseptum (David et al. 2002, Li et al. 2004). The expression of CXCL12a provides the pathway for the pLLP to migrate along; however it does not provide the directionality as the pathway contains no chemokine gradient (Haas and Gilmour 2006). Directionality is imparted by the CXCL12a receptors,

ACKR3a and ACKR3b, which are expressed in the anterior-most third of the primordium, complimentary to CXCR4b (David et al. 2002, Dambly-Chaudière et al. 2007, Valentin et al. 2007, Venkiteswaran et al. 2013, Donà et al. 2013). Unlike CXCR4b which induces Gβ1 signalling and actin polymerisation, ACKR3 does not induce downstream signalling and cell migration upon ligand binding (Venkiteswaran et al. 2013, Donà et al. 2013). ACKR3 functions as a ligand sink, allowing the formation of a local CXCL12a gradient around the primordium and preventing the more anteriorly expressed CXCR4b from binding CXCL12a. This results in directed migration of the primordium down the CXCL12a pathway towards the caudal fin (Dambly-Chaudière et al. 2007, Valentin et al. 2007, Venkiteswaran et al. 2013, Donà et al. 2013) (Figure 1.4).

The expression pattern of the CXCL12a receptors is highly regulated and remains the same throughout the entire primordium cycle of pre-neuromast rosette formation, deposition, leading to cell proliferation and new rosette formation. Antagonistic interactions between the receptors have been reported. Dambly-Chaudière et al. 2007 and Gamba, Cubedo, Ghysen, et al. 2010 have shown that knockdown of *cxcr4b* expression or activation results in an expansion of the *ackr3* expression domain in the primordium. However, this antagonistic interaction has been disputed by Valentin et al. 2007, who found no expansion of the *ackr3* expression domain in CXCR4b mutants.

ackr3 expression has also been shown to be regulated by Wnt signalling through Hoxb8a, with this signalling also playing a role in maintaining *cxcr4b* expression at the leading edge (Aman and Piotrowski 2008, Matsuda and Chitnis 2010, Breau et al. 2013). *cxcr4b* appears to be excluded from the anterior-most third of the primordium by the presence of oestrogen receptor ESR1, which acts independently of Wnt signalling (Gamba et al. 2010a) (Figure 1.4).

Wnt signalling in the leading cells is important in a number of primordium functions other than regulating receptor expression, including leading cell proliferation, Fgf ligand production and regulating Fgf signalling in the trailing cells (Figure 1.4) (Nechiporuk and Raible 2008, Aman and Piotrowski 2008, 2011, Matsuda and Chitnis 2010, Gamba et al. 2010b, Aman et al. 2011, McGraw et al. 2011, Valdivia et al. 2011, Matsuda et al. 2013). Fgf signalling in turn regulates Wnt signalling in the leading cells, as well as being essential for the formation of rosettes and correct neuromast

deposition (Nechiporuk and Raible 2008, Aman and Piotrowski 2008, Matsuda and Chitnis 2010, Harding and Nechiporuk 2012, Durdu et al. 2014) (Figure 1.4).

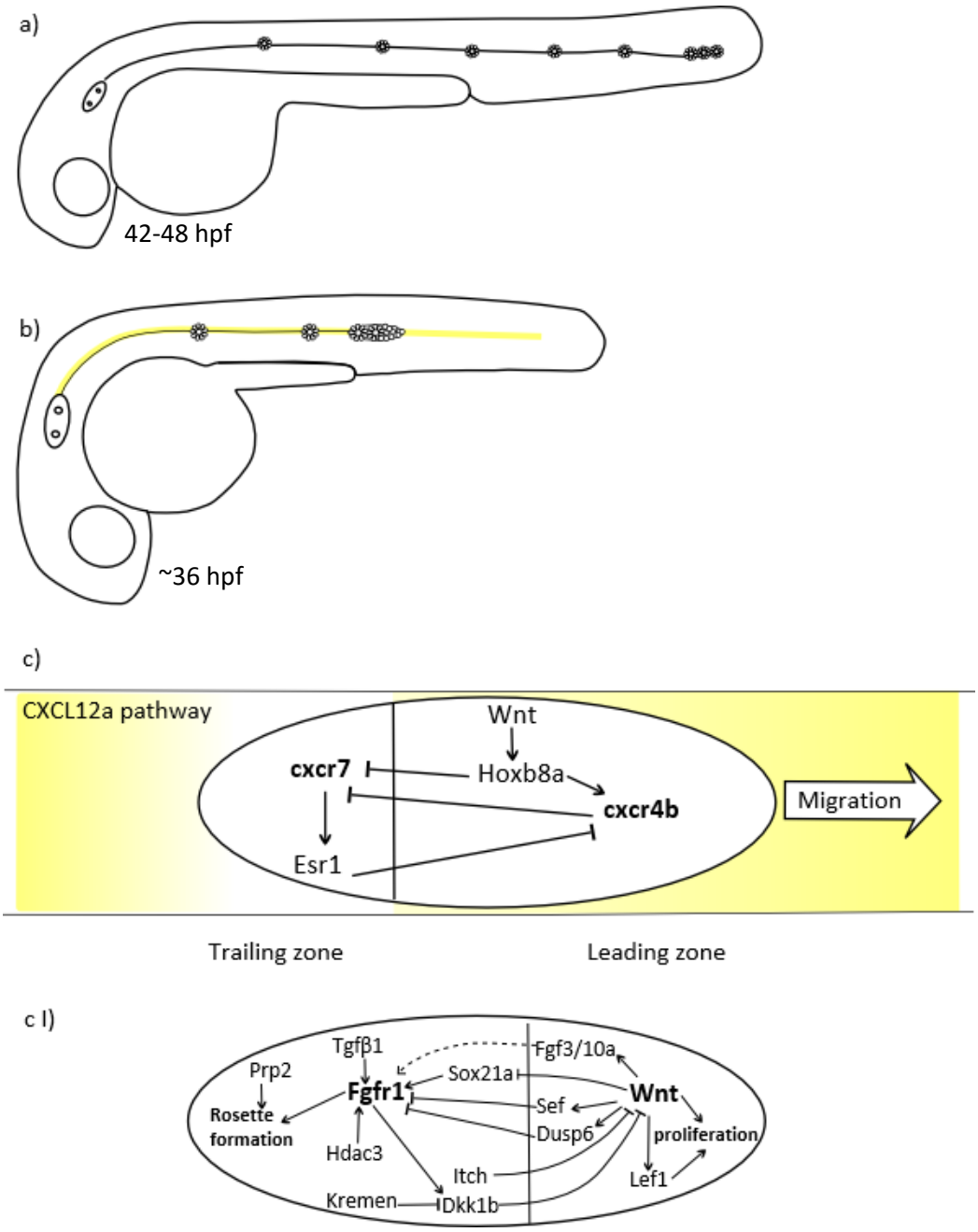

Figure 1.4 Illustration of the embryonic pLLP migration and signalling.
The completed embryonic pLLP consists of 7-8 neuromasts by 42-48hpf (a). Prim 1 migrates from the ear to the tail, along a pathway of *cxcl12a* (yellow), depositing neuromasts along the way (b). Directed migration is a result of the internal signalling within the primordium (c). CXCR4b and ACKR3 are restricted to the leading and trailing edge respectively. With ACKR3 acting as a ligand sink, this creates a CXCL12a gradient along the primordium (c). Proliferation, rosette formation and neuromast deposition are controlled by Wnt and Fgf signalling respectively (c I). Wnt and Fgf signalling inhibit the expression of the other to maintain distinct domains, although the Wnt domain produces Fgf ligands which diffuse (dashed line) to the Fgf domain to active Fgfr1 (c I). Based on Dambly-Chaudière et al. 2007; Donà et al. 2013; Angers & Drapeau 2014; Huc-Brandt et al. 2014; McGraw et al. 2014; Ariza-Cosano et al. 2015; He et al. 2015; Xing et al. 2015.

1.5 Tetraspanins

Tetraspanins are large family of small membrane proteins, which have been shown to be involved in a wide variety of cellular functions. Discovered in 1990, tetraspanins have since been found in a range of diverse organisms from the amoeba *Entamoeba histolytica*, fungus *Coprinopsis cinerea* and ascidian *C.intestinalis* to mice, zebrafish and humans (Oren et al. 1990, Szala et al. 1990, Boucheix et al. 1991, Huang et al. 2005, 2010, Garcia-España et al. 2008). In mice, humans and zebrafish there are currently 34, 33 and 50 known members of the tetraspanin family, respectively (Garcia-España et al. 2008, Huang et al. 2010).

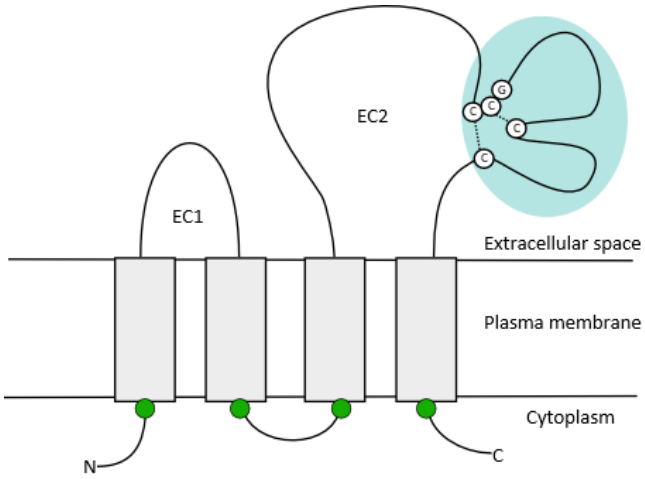

Figure 1.5 Diagram of Tetraspanin structure.
Tetraspanins have a consistent structure of four transmembrane domains (grey), intracellular N- and C- termini, a small intracellular loop and two extracellular loops (EC1, EC2). The large extracellular loop (EC2) can be split into constant and variable (blue) domains. Within the variable domain are conserved cysteine residues and CCG motif which form structural di-sulphide bonds. Most tetraspanins also contain palmitoylated juxta-membrane cysteines (green).

Tetraspanins are characterised by four transmembrane domains (TM1-4), a short intracellular loop and two extracellular domains, flanked by short intracellular N- and C-termini domains (Figure 1.5) (Oren et al. 1990, Szala et al. 1990, Boucheix et al. 1991, Wright and Tomlinson 1994). The larger of the two extracellular domains, EC2, contains a highly conserved CCG motif with an additional 2-6 cysteine residues, which form disulphide bonds to stabilise the correct folding of the domain (Wright and Tomlinson 1994, Kitadokoro et al. 2001, Seigneuret et al. 2001). This structural model

of the tetraspanin EC2 is based on the crystal structure of the EC2 of tetraspanin CD81 reported by Kitadokoro et al. in 2001. The structure and sub-domains of other tetraspanin EC2 domains have been inferred from the CD81 EC2 crystal structure using homology modelling (Seigneuret et al. 2001).

The EC2 also contains two sub-domains: a conserved region and a variable region (Seigneuret et al. 2001). The variable region has been shown to contain critical protein-protein interaction sites, which allows tetraspanins to interact with their respective direct partner proteins (Higginbottom et al. 2000, Berditchevski et al. 2001, Zhu et al. 2002, Stipp et al. 2003, Shoham et al. 2006). The conserved region, in contrast has been suggested to allow homo-dimerization and hetero-dimerization of tetraspanins, a function which has been shown to be conducted by the transmembrane domains through chemical cross-linking and FRET (Förster resonance energy transfer) experiments (Kitadokoro et al. 2001, Stipp et al. 2003, Kovalenko et al. 2004, Barreiro et al. 2008). The four transmembrane domains have been shown to not only be sites of inter- molecular interactions but also intra-molecular interactions, with interactions between TM1 and TM2 required for the tetraspanins correct folding and transport (Cannon and Cresswell 2001, Stipp et al. 2003, Kovalenko et al. 2005, Shoham et al. 2006). The intracellular N- and C-termini can also contribute to tetraspanin functions in numerous ways. Some tetraspanins, such as CD63 contain tyrosine-based internalisation motifs in their C-termini which allow them to mediate the endocytosis and trafficking of their partner proteins to late endosomes via interactions with adaptor protein complexes (Berditchevski and Odintsova 2007, Pols and Klumperman 2009). CD63 also contains a PDZ-binding motif in its C-terminus which allows binding of the protein syntenin, which has been suggested to negatively regulate CD63 endocytosis (Latysheva et al. 2006). Other tetraspanins also display PDZ-domains, suggesting the ability to bind syntenin or other PDZ-domain containing proteins intracellularly (Berditchevski and Odintsova 2007, Charrin et al. 2014). The N- and C-termini have also been shown to be directly involved in signal transduction. For example, upon ligation CD37 becomes tyrosine phosphorylated at both termini, leading to the recruitment and activation of other enzymes and signalling molecules such as SHP1 or PI3K. This directly triggers the activation of two cell survival signalling pathways (Lapalombella et al. 2012). A link between tetraspanins and the cytoskeleton

has also been suggested to occur via the C-terminus as the tetraspanins CD81 and CD9 have been shown to interact with proteins such as RAC1 and ezrin (Sala-Valdes et al. 2006, Tejera et al. 2013, Arnaud et al. 2015).

The tetraspanin structure allows them to interact with a variety of membrane and intracellular proteins, including immunoglobulin superfamily members, integrins, GPCRs, growth factors, growth factor receptors, Rac1 and phosphatidylinositol 3-kinase (Boucheix and Rubinstein 2001, Yáñez-Mó et al. 2009, Lapalombella et al. 2012, Arnaud et al. 2015).

Interactions with partner proteins and other tetraspanins allow the formation of multi-molecular complexes named TEMs (tetraspanin enriched microdomains). TEMs are constructed from by individual tetraspanins recruiting one or more of their partner proteins and then forming larger complexes via tetraspanin-tetraspanin interactions. Formation of these complexes is supported by the palmitoylation of juxtamembrane cysteines in tetraspanins (Yang et al. 2002, Stipp et al. 2003, Delandre et al. 2009). Within TEMs there are three different types of protein interactions: direct, indirect and tetraspanin-tetraspanin interactions. Direct interactions between tetraspanins and partner protein were originally found by co-immunoprecipitation following the use of harsh detergents such as 1% NP-40. Similarly indirect tetraspanin-protein interactions were discovered using co-immunoprecipitation following cell lysis, however, these interactions were only seen when mild detergents, that preserve tetraspanin-tetraspanin interactions, were used (Charrin et al. 2014). These interactions suggested that tetraspanins were able to form larger membrane complexes and may play a role in membrane compartmentalization, a hypothesis which was supported by the discovery that tetraspanins act in a similar manner to components of lipid raft micro-domains in sucrose gradients after cell lysis, signifying that tetraspanins are associated with detergent-resistant membranes (Claas et al. 2001, Berditchevski et al. 2002, Charrin et al. 2014).

Originally it was thought that TEMs were highly diverse, containing a variety of partner proteins and tetraspanins depending on the cell type and tetraspanins included (Rubinstein et al. 1996a, Boucheix and Rubinstein 2001, Yáñez-Mó et al. 2009). However, recent work has suggested that tetraspanins form individual adjacent

tetraspanin clusters, with little overlap between different tetraspanin clusters which challenges the prior view of diverse tetraspanin-containing regions (Zuidscherwoude et al. 2015).

The ability to form TEMs, whether composed of individual tetraspanins or several, is hypothesised to facilitate the spatial organisation of membrane proteins by tetraspanins. In addition to this, tetraspanins have been shown to regulate their partner proteins through multiple other mechanisms (Charrin et al. 2014). This includes the ability to regulate the degradation, secretion, expression, multimerization and intracellular signalling of many different membrane proteins (Berditchevski and Odintsova 2007, Charrin et al. 2009, 2014, Yáñez-Mó et al. 2009).

Trafficking of membrane proteins by tetraspanins has been demonstrated for both endocytic and secretory pathways. Many proteins, including CXCR4, synaptotagmin 7 and H^+/K^+ ATPases, have been shown to be internalised and/or trafficked to the lysosomes by CD63 (Pols and Klumperman 2009, Flannery et al. 2010). For some tetraspanins, such as CD63, internalisation and trafficking of partner proteins appears to be their primary function. Other tetraspanins, like CD81, are required for the secretion of their partner proteins. A mutation in CD81 results in an impaired humoral immune response due to a lack of surface CD19, which is an important B-cell receptor co-stimulatory molecule (Charrin et al. 2014). CD81 associates with CD19 early in biosynthesis at the endoplasmic reticulum and supports the entire process from exiting the endoplasmic reticulum to functioning on the plasma membrane (Shoham et al. 2006).

Another method used by tetraspanins to affect partner function is to regulate their multimerization but not the trafficking of the partner protein (Charrin et al. 2014). The elevation of Norrin/β-Catenin signalling by TSPAN12 is one example of this. TSPAN12 is a component of the Norrin receptor complex, which also contains Frizzled-4 and lipoprotein-related protein 5, and promotes the oligomerization of the receptor complex to enhance the signalling response to Norrin binding (Junge et al. 2009).

Lastly, several tetraspanins have displayed the ability to modulate the downstream signalling of their partner proteins. Both indirect and direct partner proteins have been shown to be affected in this way. The signalling of tyrosine kinase receptors, such

as epithelial growth factor receptor and vascular endothelial growth factor receptor-3, has been shown to be modulated by the expression or deletion of CD9 or CD82, although no direct interactions have been found between the tetraspanins and the receptors so far (Odintsova et al. 2000, Murayama et al. 2008, Iwasaki et al. 2012, Charrin et al. 2014). In contrast, CD151 has been shown to directly interact with several laminin-binding integrins and appears to moderate the activation of several of their downstream signalling molecules, including Akt, Src and focal adhesion kinase (Yauch et al. 1998, Serru et al. 1999, Takeda et al. 2007, Yang et al. 2008, Yamada et al. 2008, Charrin et al. 2014).

This diverse range of functions, partner proteins and their expression in all cell types means that the tetraspanin family have been found to be involved in a variety of processes including proliferation, cell motility, angiogenesis, host-pathogen interactions, antigen presentation, tumour development and metastasis (Miyazaki et al. 1997; Boucheix & Rubinstein 2001; Zhang et al. 2009; Monk & Partridge 2012; Detchokul et al. 2014; Jiang et al. 2015; Rocha-Perugini et al. 2015; Y.-G. Yang et al. 2016).

1.6 Tetraspanins in zebrafish

Not only are tetraspanins found in evolutionarily diverse organisms but they are also fairly highly conserved between organisms. Zebrafish tetraspanin genes show between ~45- 80% identity with their human orthologs (Table 1.3). However, protein identity between zebrafish and human orthologs differs dramatically within the tetraspanin structure (Stipp et al. 2003). Stipp et al analysed the identity of different domains of four tetraspanins, CD9, CD81, CD151 and Tspan7 in human and zebrafish. They found the transmembrane domains and intracellular structures to be the most highly conserved between orthologs, with 83% and 72-78% identity. Polar residues within the transmembrane domains and membrane-proximal cysteines were 100% conserved between humans and zebrafish. These high identities are consistent with these regions or residues having important conserved functions. This is in contrast to the EC1 and EC2 which displayed 43-58% identity, suggesting some potential diversification in function or protein partners (Stipp et al. 2003).

Though tetraspanins are fairly highly conserved between humans and zebrafish there is not much known about the function or expression pattern of tetraspanins in zebrafish. As shown in Table 1.4, only 18 of the 50 zebrafish tetraspanins have had their expression patterns described in any detail.

Tetraspanins have been reported in a number of gene expression screens, suggesting roles in various systems including the immune response, posterior lateral line development, hair cell regeneration, photoreceptor function and hypertrophic muscle growth (Pujic et al. 2006, Johnston et al. 2009, Gallardo et al. 2010, Yang et al. 2012, Steiner et al. 2014). However, few studies have focused on tetraspanin functions in zebrafish.

Research looking at the functions of tetraspanins in zebrafish has so far only described functions for Tspan 18, Tspan 36, CD63 and Upk3a-l. Tspan 18 was described in a PhD thesis by Li in 2011, to play a role in angiogenesis through the regulation of Vegfr2 and notch pathways (Li 2011). A Tspan 36 mutant, *deli,* displayed abnormal skin pigment pattern formation which was shown to be due to defective melanophore migration and irregular interactions between melanophores and xanthophores (Inoue et al. 2014). Knock-down of CD63 using morpholinos rendered zebrafish embryos unable to

hatch from their chorion, a phenotype which appeared to result from an absence of secreted proteolytic enzymes which are required for chorion softening (Trikić et al. 2011). Lastly, knockdown of Upk3a-l caused reduced pronephros function due to defective epithelial cell polarisation and morphogenesis (Mitra et al. 2012).

Human gene	**Mouse gene**	**% Identity to human**	**Zebrafish gene**	**% Identity to human**
Tspan 7	Tspan 7	98	tspan 7b	84
CD9	Cd9	90	cd9a	60
			cd9b	59
CD63	Cd63	79	cd63	45
CD81	Cd81	92	cd81a	65
			cd81b	60
CD151	Cd151	94	cd151	65
			cd151-L	71

Table 1.3. Percentage identity of the mouse and zebrafish homologs to a number of human tetraspanins. Data from ensemble.org (Herrero et al. 2016)

Tetraspanin	hpf	Expression	Reference
Tspan 1	96	Anterior neuromast mantle cells	Steiner et al. 2014
Tspan 2a	19-60	Olfactory placode, brain, retina	Thisse et al. 2001
Tspan 3a	Adult	Brain, eye, heart, skin, melanocyte, ovary, testis, xanthophore	Inoue et al. 2014
Tspan 3b	Adult	Brain, eye, ovary, testis	Inoue et al. 2014
Tspan 5a	10-60	CNS, olfactory placode	Thisse & Thisse 2004
Tspan 7b	16-60	Notochord, brain, spinal cord, pancreatic bud	Thisse & Thisse 2004
Tspan 18	24-60	Yolk vessel, intersegmental vessels, post cardinal vein, caudal vein, heart	Li 2011
Tspan 35	16-60	Pronephric duct, olfactory organ	Thisse & Thisse 2004
Tspan 36	16-Adult	Retina, neural crest, melanocyte, xanthophore, ovary, testis, skin, heart, brain	Thisse et al. 2001; Pujic et al. 2006; Inoue et al. 2014
CD9a	19-60	Heart, liver, retina, telencephalon	Thisse & Thisse 2004
CD9b	16-60	Otic placode, pronephric duct, skin, olfactory organ, lateral line primordium, neuromasts, pharynx	Thisse & Thisse 2004; Gallardo et al. 2010
CD63	19-120	Hatching gland, pronephric duct, dorsal fin, notochord, pharynx	Rauch et al. 2003; Thisse & Thisse 2004; Trikić et al. 2011
CD81b	19-60	Cephlic floor plate, cerebellum, hindbrain, cleithrum	Thisse & Thisse 2004
CD82a	19-60	CNS, brain, pectoral fin, otic vesicles	Kudoh et al. 2001; Thisse & Thisse 2004
CD151	10-60	Skin, slow muscle, heart, pectoral fin, swim bladder bud,	Thisse & Thisse 2004
CD151-L	10-60	Notochord, pronephric ducts, skin, pharynx, forebrain	Thisse & Thisse 2004
Upk3a-L	48	Retina, ganglia, pronephric tubules	Mitra et al. 2012

Table 1.4 Known expression patterns of zebrafish tetraspanins. Data from zfin.org (D. Howe et al. 2013)

1.7 Tetraspanins and CXCR4

A link between CXCR4 and tetraspanins was initially found in CD4+ human cell lines when a CD63 mutant prevented infection by CXCR4-using T-cell Tropic Human Immunodeficiency Virus Type 1 (HIV-1). Both mutant and wildtype CD63 was shown to inhibit CXCR4 surface expression, although the N-terminal deletion mutant was dramatically more efficient (Yoshida et al. 2008). CD63 binds CXCR4 at the Golgi apparatus via N-linked glycans in its EC2, allowing CD63 to regulate CXCR4 trafficking. It was found that the CD63 N-terminal deletion mutant exclusively trafficked CXCR4 to the late endosomes/lysosomes, whereas wildtype CD63 could also be found at the plasma membrane bound to CXCR4 (Yoshida et al. 2008, 2009). This role for CD63 in CXCR4 trafficking has also been replicated in activated B-cells, where CXCR4 cell surface expression was shown to be downregulated by CD63(Yoshida et al. 2011).

Since CD63, three other tetraspanins, Tspan3, CD82 and CD9, have been functionally linked with CXCR4 (Li et al. 2011, Leung et al. 2011, Yang et al. 2016). Most recently, loss of Tspan3 in leukemic cells was shown to reduce CXCR4 phosphorylation and impair the response to CXCL12 which resulted in the ectopic localisation of the leukemic cells (Yang et al. 2016).

CD82 functions with CXCR4 in early human pregnancy to prevent the over invasion of embryonic trophoblasts into the maternal tissue. To prevent over-invasion CXCL12-CXCR4 signalling on embryonic trophoblasts acts in both a paracrine and an autocrine manner. When acting in an autocrine manner, CXCL12 promotes invasion of the maternal tissue by the trophoblasts. However, when acting in a paracrine manner CXCL12 produced by the trophoblasts binds CXCR4 on the maternal decidual stromal cells which results in the upregulation of CD82 expression. CD82 upregulation promotes TIMP1 (tissue inhibitor of metalloproteinases) expression which in turn inhibits trophoblast invasion (Li et al. 2011, Meng et al. 2012).

Lastly, Leung et al. 2011 found that CD9 was upregulated by CXCL12-CXCR4 signalling in hematopoietic stem cells (HSCs). A functional role for CD9 in CXCL12-mediated migration and *in vivo* homing of HSCs was suggested due to the inhibition of these functions in HSCs treated with an anti-CD9 antibody.

To investigate whether tetraspanins could play a role in CXCR4b signalling in the pLLP or PGC migration, the expression patterns of CD63, CD82 and CD9 zebrafish orthologues were assessed. As shown in Table 1 4, CD63 and CD82a are not expressed in the pLLP or the PGCs. With a lack of CD82b expression data, this left the CD9 orthologues, CD9a and CD9b. Of the two orthologues, CD9b has been shown to be expressed in the pLLP and in the region to which PGCs migrate, making it a good candidate for playing a role in CXCR4b signalling (Figure 1.7) (Thisse and Thisse 2004, Gallardo et al. 2010).

1.8 CD9

First described in 1981 to be expressed on acute lymphoblastic leukaemia cells, CD9 has since been found to have an almost ubiquitous expression pattern in normal human tissues (Kersey et al. 1981, Maecker et al. 1997, Sincock et al. 1997). Along with normal tissues, CD9 has been associated with multiple cancers including myeloma, breast cancer and small-cell lung cancer (reviewed in Xuan et al. 2014).

CD9 has been reported to modulate many different cellular functions in cancer pathogenesis, including adhesion, proliferation, apoptosis and stem cell properties (Ovalle et al. 2007, Yamazaki et al. 2011, He et al. 2013, Xuan et al. 2014). Most predominantly CD9 has been reported to affect the migration and metastasis of multiple cancer cell types. Initially it appeared that CD9 acted as a metastasis suppressor, with inverse correlations found between metastasis and CD9 expression in melanoma, breast, colon and ovarian cancers (Si and Hersey 1993, Miyake et al. 1995, Mori et al. 1998, Houle et al. 2002). Experimental data appears to support these findings for a number of cancer types including: melanoma, fibrosarcoma, renal cell carcinoma, lung and prostate cancer (Ikeyama et al. 1993, Huang et al. 2004, Copeland et al. 2013, Garner et al. 2016). By contrast, lymphoblastic leukaemia, fibrosarcoma and esophageal squamous cell carcinoma displayed positive correlations between CD9 expression and cancer cell migration or metastasis (Herr et al. 2013, Jian et al. 2015, Arnaud et al. 2015). Interestingly, conflicting reports have been described for breast cancer. Patient samples displayed an inverse correlation between CD9 and breast cancer metastasis, data supported by experimental evidence showing an increase in integrin α5β1-mediated migration of CD9-deficient breast cancer cells (Miyake et al. 1995, Powner et al. 2011). However, more recent data has shown significant CD9

overexpression in breast cancer bone metastases from patients, as well as decreased migration of breast cancer cells *in vivo* upon CD9 knockdown (Kischel et al. 2012, Rappa et al. 2015).

In non-cancerous cells, CD9 shows similar functions with roles in cell proliferation, adhesion and migration (Takemura et al. 1999, Shi et al. 2000, Cook et al. 2002, Leung et al. 2011, Yang et al. 2012, Jiang et al. 2013). CD9 has been shown to promote migration in a number of different cell types, including human cord blood cells, satellite cell-derived myoblasts, embryonic stem cells, megakaryocytes and endothelial cells (Deissler et al. 2007, Leung et al. 2011, Kamisasanuki et al. 2011, Iwasaki et al. 2012, Brzoska et al. 2015, Desterke et al. 2015). A study by Iwasaki et al. in 2012 showed that knockdown of CD9 resulted in a decrease in the migration of lymphatic endothelial cells. The authors also found that loss of CD9 reduced the creation of complexes between vascular endothelial growth factor receptor-3 and integrins α5 and α9, which resulted in the inhibition of downstream ERK and p38 MAPK signalling upon vascular endothelial growth factor-C binding. Similar results were seen by Kamisasanuki et al. 2011, who also found that knockdown of CD9 reduced the vascular endothelial growth factor or hepatocyte growth factor stimulated endothelial cell migration during angiogenesis. Whilst they did not observe any difference in growth factor signalling, they did report the abnormal localisation of integrins and membrane type-1 matrix metalloproteinase upon CD9 knockdown (Kamisasanuki et al. 2011). CD9 deficiency has been reported to cause altered signalling and reduced migration in megakaryocytes and re-epithelialization during wound healing, with the focal adhesion kinase and c-Jun NH2-terminal kinase/ matrix metalloproteinase-9 pathways affected respectively (Zhang et al. 2012, Desterke et al. 2015).

CD9 has also been reported to function in cell proliferation and apoptosis (Shi et al. 2000, Murayama et al. 2004, Iwasaki et al. 2012). By directly interacting with transforming growth factor-β (TGF-β), CD9 expression augments the activation of EGFR by TGF-β and increases proliferation in a juxtacrine manner. However, this co-expression also resulted in decreased the autocrine proliferative activity (Shi et al. 2000). Anti-CD9 antibodies have also been shown to give anti-proliferative effects, which Murayama et al. 2004 suggested was due to the inhibition of ERK1/2 activity. Interestingly, the same CD9 antibody was shown to induce apoptosis via the activation

of c-Jun NH2-terminal kinase/stress-activated protein kinase, p38 MAPK and caspase-3 (Murayama et al. 2004).

Lastly, cell adhesion to fibronectin has been shown to be repressed by CD9 in a number of studies (Cook et al. 2002, Leung et al. 2011, Wang et al. 2011a). This function was not observed in a C-terminal deletion mutant by Wang et al. 2011a, which would suggest involvement of the C-terminal. However, Cook et al. 2002 had previously shown that the EC2 of CD9 was important in the regulation of cell adhesion. Cook et al. also reported that CD9 co-localised with F-actin and integrin α5β1 at cell margins and affected the localisation of focal adhesion kinase and α-actinin. They suggested that CD9 could affect adhesion by regulating the formation of adhesion complexes.

The co-ordination of these functions allows CD9 to mediate processes such as wound repair, lymphangiogenesis and angiogenesis (Deissler et al. 2007, Kamisasanuki et al. 2011, Zhang et al. 2012, Iwasaki et al. 2012, Jiang et al. 2013). CD9 is also known to be important inhibitor of muscle cell, macrophage and HIV-1-induced cell fusion (Takeda et al. 2003, Gordón-Alonso et al. 2006, Charrin et al. 2013). Although a recent paper by Brzoska et al. 2015 did report a positive impact of CD9 expression on myoblast fusion, which could suggest contradictory functions for CD9 in cell fusion.

With the variety of cell functions regulated by CD9, it is surprising that cell fusion appeared to be the only CD9 function affected in CD9 knockout mice. Female homozygous CD9-/- mice were showed severely impaired fertility which resulted from defective gamete fusion (Le Naour et al. 2000, Miyado et al. 2000, Kaji et al. 2002). The apparent lack of widespread phenotypes in CD9-/- mice is most likely due to redundancy between tetraspanins. For example, the fertility phenotype can be rescued by injection of CD81 and lymphangiogenesis defects can only be seen in CD9/CD81-double knock-out mice but not in single knock-out mice (Kaji et al. 2002, Iwasaki et al. 2012).

1.9 CD9a and CD9b

The zebrafish homologs of human CD9, CD9a and CD9b, show high amino acid identity to each other (63%) and to their human counterpart (60%, 59% respectively) (Table 1.3 and Figure 1.6a). The highly similar hydrophobicity plots of the three homologs suggest many structural similarities although the second hydrophilic domain, the predicted EC2, appears the most diverse (Figure 1.6b). This correlates with a previous report which showed the EC2 is the least conserved domain between zebrafish and humans (Stipp et al. 2003). These differences may suggest divergent functions, even between the two zebrafish paralogs. This would not be unexpected as other zebrafish paralogs, such as CXCR4a and CXCR4b, show complimentary expression patterns and functions (Chong et al. 2001). As shown in Table 1.4 and Figure 1.7, CD9a and CD9b also appear to have distinct expression patterns.

Neither CD9a nor CD9b have been studied extensively and so the functions of these proteins are not yet clear. CD9a may play a role in the immune response as two reports have shown CD9a to be differentially regulated upon viral infection or vaccine immunisation (Encinas et al. 2010, Yang et al. 2012). While CD9b was not reported in either of those studies, it was shown to be upregulated in muscle fibres in the hypertrophic phenotype in comparison to muscle fibres in the hyperplastic phenotype, suggesting a role in muscle growth (Johnston et al. 2009). A role in the lateral line has also been suggested for CD9b. It is highly expressed in the lateral line primordium cells in comparison to surrounding cells and a brief proof-of-principle experiment by Gallardo et al. 2010 showed that knockdown of CD9b using a morpholino resulted in abnormal lateral line primordia structure in 50% of the injected embryos at 36hpf and reduced neuromast number at 48hpf.

a)

```
CD9   MPVKGGTKCIKYLLFGFNFIFWLAGIAVLAIGLWLRFDSQTKSIFEQETNNNNSSFYTGV
CD9a  MGVEGCPKCIKYSMFLLNSVFWIAGTAVLAVGLWLRFDPKTKSLFEGE--NSPYVFYTGV
CD9b  MAAGGGLQCIKYLLFIFNFIFWLAGTGVLAVGLWLRFDAKTKEFFTAE--NGQTVFLTGV
      * . *  :**** :* :* :**:** .***:*******.:**.:*  *  *.   * ***

CD9   YILIGAGALMMLVGFLGCCGAVQESQCMLGLFFGFLLVIFAIEIAAAIWGYSHKDEVIKE
CD9a  YILIAAGALMMVVGFFGCCGAIQESPCMLGLFFFFLLVIFAVEVAAGIWGFSNQTKVTED
CD9b  YILIVAGAVMMVVGFLGCCGAIKESACMLGLFFMFLLVIFAAEVAAGIWGLSNKDKIVSD
      **** ***:**:***:*****::** ******* ******* *:**.*** *:: :: .:

CD9   VQEFYKDTYNKLK-TKDEPQRETLKAIHYALNCCGLAGGVEQFISDICPKKDVLETFTVK
CD9a  ITTFYRQTYDTYQQSKQEALKKTLRLFQHGLNCCGPSGNMQESLDETCPKKEGLDNLIIK
CD9b  IQQFYTQTVKNYKESPDGPLKETLTAIHFSLQCCGPTGLVTDGVSVTCPKQEGLANVITT
      :  ** :* .. : : : . .:**  ::..*:*** :* : : :.  ***:: * ..  .

CD9   SCPDAIKEVFDNKFHIIGAVGIGIAVVMIFGMIFSMILCCAIRRNREMV
CD9a  SCPDAIDEVFNSKLHIIGGVGIATGVIMIFGMIFSMMLCCAIRKTREIV
CD9b  GCSSVIQDMFNSRLHVIGGVGIGIGVIMVFGMIFSMLLCCAIRRTRDIV
      .*...*.::*:..:*:**.***. .*:*:*******:******..*::*
```

b)

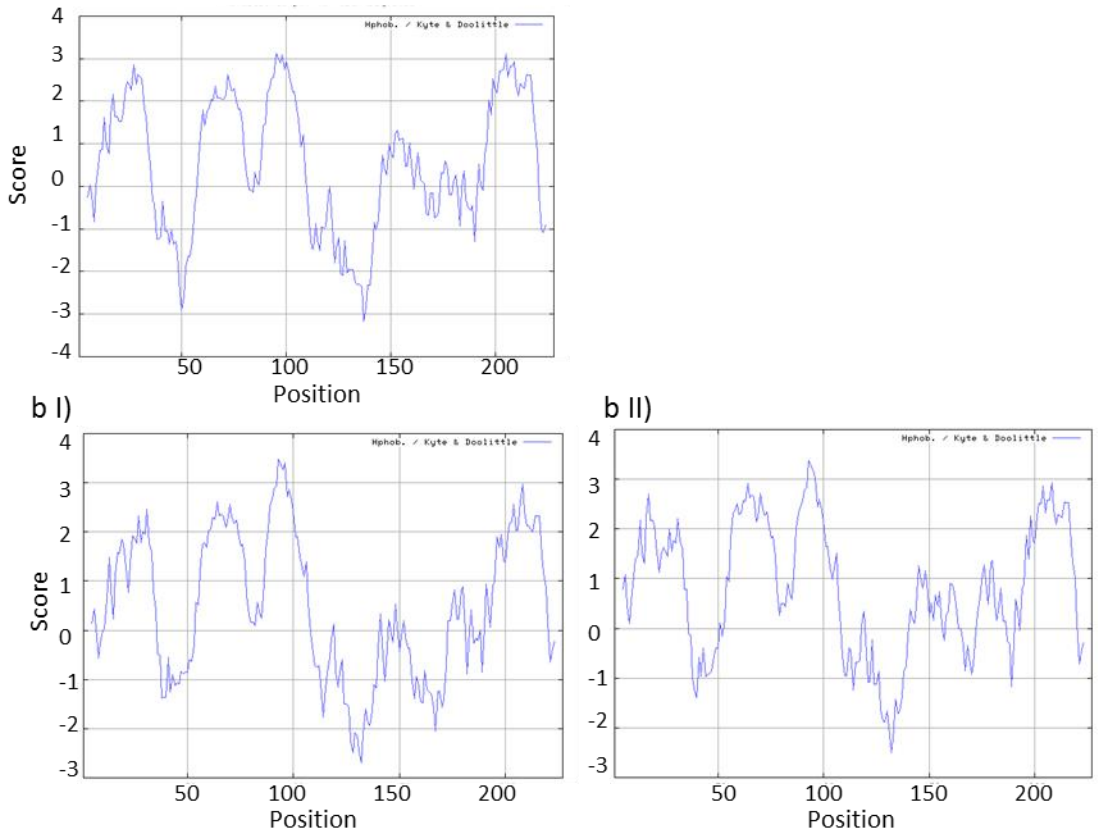

Figure 1.6 Sequence alignment (a) and hydrophobicity plots (b) of human CD9 (a, b) and zebrafish CD9a (a, b I) and CD9b (a, b II).
Sequences aligned using MUSCLE (Edgar 2004). *,:, ., indicate fully conserved residues, strongly similar and weakly similar residues respectively. Kyte and Doolittle hydrophobicity plots where scores of >0 indicate hydrophobic regions (Gasteiger et al. 2005).

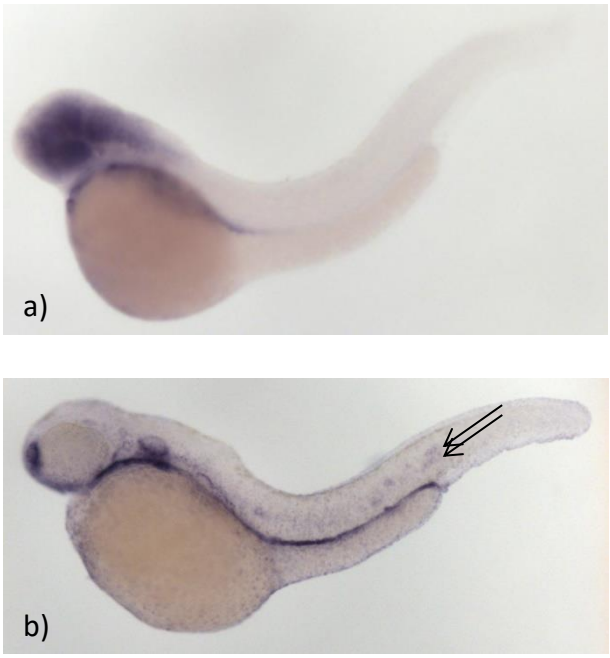

Figure 1.7 *cd9a* (a) and *cd9b* (b) *in situ* hybridisation at stage Prim-15 to Prim-25 by Thisse, B. and Thisse, C. 2004. Reproduced with the authors' permission. Black arrows indicate the two pLLP from either side of the embryo.

1.10 Aims and objectives

This project aimed to investigate whether CD9b played a role in CXCR4b-mediated PGC and pLLP migration. To accomplish this, a reverse genetics approach was taken.

Aims:

1) To investigate whether CD9b knockdown causes abnormal PGC or pLLP migration.
2) To investigate whether any of the PGC or pLL phenotypes seen in the CD9b morphants are replicated in CD9b homozygous mutants.
3) To assess any novel PGC or pLL phenotypes seen in the CD9b mutants.
4) To elucidate the mechanism in which the lack of CD9b is causing the phenotypes seen.
5) To analyse and assess any other phenotypes observed in the CD9b mutants.

Objectives:

1) Use morpholinos to knockdown *cd9b* and visualise the completed migration of PGCs or the pLLP using *in situ* hybridisation.
- Develop assays to accurately quantify differences observed in PGC migration and clustering in CD9b morphants.
- Develop assays to accurately quantify differences observed in pLLP migration and pLL structure in CD9b morphants.
2) Create homozygous CD9b mutants using TALENs.
- Use same assays to analyse PGC and pLLP migration in CD9b mutants.
3) Develop assays to accurately quantify novel PGC and pLL phenotypes in CD9b mutants.
4) Analyse CXCR4b trafficking and internalisation in CD9b mutants using CXCR4b-EGFP and CXCL12a-Venus.
- Analyse whether CD9b is upregulated upon CXCR4b signalling.
- Assess CXCR4b and CXCL12a expression in CD9b mutants.
5) Develop assays to quantify any observed morphological differences in the CD9b mutants.
- Develop assays to evaluate the fertility of CD9b mutants.

Whilst the majority of these aims and objectives were met, the fourth aim was not fully investigated due to the CD9b mutants not replicating the pLL phenotypes seen in the CD9b morphants. In light of this a new aim was developed 'To investigate why CD9b morphants and CD9b mutants show different pLL phenotypes'. To explore this aim, redundancy, morpholino off-target effects and residual CD9b function in the CD9b mutants were assessed.

Chapter 2: Materials and Methods

2.1 Materials

2.1.1 General laboratory reagents

Water

All unspecified water used was ultrapure (Type 1) water, often labelled MQH_2O, which had been purified using Synergy Water Purification System from Merck Millipore. During RNA and DNA sensitive experiments, nuclease-free water from Ambion was used.

Chemicals

All chemicals used were analytical grade or equivalent and purchased from Sigma, Aldrich, VWR International or Fluka, unless stated otherwise.

2.1.2 General laboratory equipment

Equipment	Supplier
Agarose gel documentation	Alrad Camera, UVP 2UV transilluminator
Agarose gel electrophoresis	Biorad gel box, Biorad PowerPac 300
Balances	Scientific Laboratory Supplies (SLS) Explorer Pro and Adventurer Pro
Centrifuges	Hettich Mikro 22, Sigma 1-14, Hermle Z 306
Flaming/Brown Micropipette Puller	Sutter Instrument Company
Forceps	Dumont
Graticule	Pyser-SGI Ltd.
Incubators (fish)	Sanyo, SLS LMS cooled incubator
Incubator (microbiology)	Neuberger
Orbital Shaker	Stuart
Pasteur pipettes (glass)	Volac
Pasteur pipettes (plastic)	SLS
pH meter	Mettler Toledo
Pipettes (manual)	Gilson
PV800 Pneumatic PicoPump	World Precision Instruments
Spectrophotometers	Eppendorf BioPhotometer, Nanodrop ND-1000
Thermal Cyclers	Biorad S1000, Techne TC-412
Water baths	Grant- JB Nova

Table 2.1 General Laboratory equipment

Microscopy related equipment	Manufacturer
AxioCam ERc 5s Camera	Zeiss
AxioCam MRm Camera	Zeiss
Axioskop 2 mot plus microscope	Zeiss
Axioskop microscope	Zeiss
AxioVision Software	Zeiss
Fluoview software	Olympus
FV1000 Confocal	Olympus
MS5 Dissecting microscope	Leica
Prog Res C14 camera	Jenoptik
Prog Res Capture Pro Software	Jenoptik
Zoom.V16 microscope	Zeiss

Table 2.2 Microscopy equipment

2.1.3 General laboratory consumables

Equipment	Supplier
1.5mL pestle, disposable	Sigma
1.5mL RNAse –free tubes	TreffLab
1.5mL tubes	Eppendorf, TreffLab
100mm petri dishes	Thermo Scientific
12-well plates	Costar, Corning Inc.
96 well PCR plates	StarLab
Borosilicate glass capillaries	Harvard Apparatus
Cover slips No.0	SLS
Falcon tubes	Becton Dickinson and Co.
Glass slides	VWR International or Fisherbrand
Gloves	Microflex
PCR tubes	StarLabs
Pipette tips	StarLabs

Table 2.3 General Laboratory Consumables

2.1.4 General laboratory buffers

Buffer	Preparation
Phosphate Buffered Saline (PBS) 0.01M, pH7.4	One tablet (Sigma) per 200 mL of deionized water
PBS / 0.05% Tween 20 (PBST)	50mL 1x PBS, 25µL Tween 20
Tris-Borate-EDTA (TBE) (5X)	54g Tris base, 27.5g Boric Acid, 20mL 0.5M EDTA in 1L water, pH to 8
Tris-HCl (1M)	121 g Tris base in 1 L water. pH to 8.2 or 9.5 depending on requirements
20% Tween-20	10mL Tween-20 with 40mL MQH_2O, kept in dark

Table 2.4 General Laboratory Buffers

2.1.5 Solutions for microbiology

Buffer/Solution	Preparation
LB	Re-suspend 25g LB broth powder (Sigma) in 1L water, then autoclave to sterilize
SOC Outgrowth Medium	Provided by New England Biolabs Inc. (NEB) with NEB 10- beta competent E.Coli. Contains 2% Vegetable Peptone, 0.5% Yeast Extract, 10 mM NaCl, 2.5 mM KCl, 10 mM MgCl2, 10 mM MgSO4, 20 mM Glucose

Table 2.4 Solutions for microbiology

2.1.6 Solutions and reagents for zebrafish work

Solution/Reagent	**Preparation**
E3 Methyl-Cellulose	3% Methyl cellulose dissolved in 1X E3
1X E3	5 mM NaCl, 0.17 mM KCl, 0.33 mM $CaCl_2$, 0.33 mM $MgSO_4$, 10^{-5}% Methylene Blue
4% Paraformaldehyde (PFA)	4% PFA dissolved in PBS containing 1 mM NaOH
20X Ringer's buffer	2.3M NaCl, 58 mM KCl, 36 mM $CaCl_2$, 100 mM HEPES in water, pH 7.2.
Tricaine (Ethyl 3-aminobenzoate methanesulfonate)	400 mg Tricaine, 2.1 mL 1M Tris pH9 in 97.9mL water to pH 7. Used at 4.2%

Table 2.5 Solutions for zebrafish work

2.1.6.1 Solutions and reagents for *in situ* hybridisation

Solution	Preparation
20X SSC	In 800mL H_2O, 140.2g 3M NaCl, 65.8g 0.3M NaCitrate dihydrate to pH 7.0. Or taken from readymade 20X SSC(Sigma)
BCIP	50mg 5-Bromo 4-Chloro3Indolyl Phosphate in 1mL anhydrous Dimethyl-formamide
Bleaching solution	0.5X SSC containing 10% H_2O_2 and 5% Formamide
Blocking buffer	50mL PBST containing 1mL Sheep serum and 100mg BSA
Hyb-	25mL Formamide, 12.5mL 20X SSC, 250µ 20% Tween-20, 460µL 1M Citric Acid and H_2O to 50mL
Hyb+	25mL Formamide, 25mg tRNA, 12.5mL 20X SSC, 250µ 20% Tween-20, 50µL Heparin (50mg/mL), 460µL 1M Citric Acid and H_2O to 50mL
NBT	50mg Nitro Blue Tetrazolium and 0.7mL anhydrous Dimethyl-formamide added to 0.3mL H_2O
PTU	0.089g PTU (N-Phenylthiourea) + 25ml MQH_2O
Staining buffer	5mL 1M Tris pH9.5, 2.5mL 1M $MgCl_2$,1.66mL 4M NaCl, 250µL 20% Tween-20 to 50mL with H_2O
Staining solution	25mL Staining buffer with 112.5µL NBT and 87.5µL BCIP
0.2 X SSCT or 2X SSCT	Dilute 20X SSC by 1:10 or 1:100. To 50mL 0.2 X or 2X SSC add 250µL 20% Tween-20

Table 2.6 Solutions for ISH

2.1.7 Oligonucleotides for zebrafish work

Primers

All primers were purchased from IDT (Integrated DNA Technologies). Primers were re-suspended in MQH_2O to give 100µM primer concentration and stored at -20°C.

Morpholinos

Morpholinos (MOs) were purchased from Gene Tools LLC and re-suspended in MQH_2O to give a stock concentration of 1mM. CD9b MOs were stored at room temperature in parafilm wrapped Eppendorf tubes as recommended by Gene Tools LLC. The mismatch MO was stored at -20°C and was incubated at 65°C for 20 minutes before use to ensure the MO was completely soluble. The mismatch MO is the same mismatch MO used by Trikić et al. 2011, which had been stored at -20°C since purchase.

MO name	Activity	Sequence 5'-3'
CD9b MO1	Translation blocker	tttatgaggagaaacccaagactga
CD9b i2e3	Splice-site blocker	aacccctgaacacagagaaacaaca
Mismatch MO	None	tttccctgctgcttatacagcgatg

Table 2.7 Morpholino activity and sequence

2.1.8 Analysis software

Software	Reference/Origin
ApE v2.0.47	M. Wayne Davis http://biologylabs.utah.edu/jorgensen/wayned/ape/
Excel	version 14.0.7166.5000, Microsoft
GraphPad Prism version 6	GraphPad Software, La Jolla California USA, www.graphpad.com
Image J/Fiji	Schindelin et al. 2012; Schneider et al. 2012

Table 2.8 Software used for data analysis

2.2 Methods

2.2.1 Molecular techniques

2.2.1.1 PCR

PCR reactions were assembled on ice in PCR tubes or 96 well plates, depending on the number of reactions to be run. The reactions were set up as displayed below in Table 2.9 and run in a PCR machine using the thermal cycle seen in Table 2.10. The annealing temperature shown in Table 2.10 is an example but would have depended on the primers used, with the annealing temperature generally being 5°C below the Tm of the primers.

Upon completion of the reaction, 1-5µL of the PCR product was run on a 1-1.5% agarose (VWR) TBE gel containing 0.5 µg/mL ethidium bromide (VWR), at 80V for 15-40 minutes depending on the length of the product and the band separation needed. A 1kb or 100bp ladder (NEB) was run alongside the PCR products.

Component	**Volume (µL)**	**Concentration**
10x PCR Buffer	2.5	1x
2.5mM NTPs	1	100 µM
Taq polymerase	0.5	5 units
10µM Forward Primer	1	0.4 µM
10µM Reverse Primer	1	0.4 µM
DNA	1	Variable
MQH_2O	18	-

Table 2.9 PCR reaction

Thermal Cycle	**Temperature (°C)**	**Time**
Initial Denaturation	96	45 seconds
35 Cycles	94	30 seconds
	55 (variable)	30 seconds
	72	1 minute per kb
Final Extension	72	5 minutes

Table 2.10 PCR thermal cycle

2.2.1.2 Genotyping

2.2.1.2.1 Using gDNA sequencing for genotyping

Genotyping was carried out either on fin clips from live adult fish or on the heads of fixed embryos. gDNA was extracted from the tissue sample using the method described by Meeker et al. 2007, which firstly used heated sodium hydroxide to lyse cells and denature the gDNA. The solution was then neutralised and centrifuged to pellet cell debris. The supernatant, which contains the gDNA, can then be used in PCR to amplify the relevant section of gDNA using the primers in Table 2.12. The PCR products were checked on a gel before being cleaned using either ExoSAP or Sodium acetate/Ethanol (see below for method). Once cleaned, the PCR products were sent for sequencing with a sequencing primer (Table 2.13). Sequencing results were analysed using ApE v2.0.47 (a plasmid editor).

Cleaning PCR products for sequencing

Sodium Acetate/Ethanol

To 18µL PCR product, 2µL 3M sodium acetate (Sigma) and 50µL 100% ethanol (Fisher scientific) were added before mixing then cooling at -20°C for 30 minutes. The products were then centrifuged for 30 minutes at maximum speed at 4°C. The pellet was washed once with 500µL PE buffer (QIAGEN) then re-suspended in 50µL EB buffer (QIAGEN). 1-4µL was then used for sequencing.

ExoSAP

ExoSAP clean-up of PCR products used SAP (Shrimp-Alkaline Phosphatase) (NEB) and Exonuclease 1 (Exo1) (NEB) to remove unused primers and NTPs from the finished reaction. SAP and Exo 1 were added to the PCR products, on ice, before immediately incubating the mix at 37°C for 45 minutes (Table 2.11). After 45 minutes, the enzymes were de-activated by incubating at 80°C for 15 minutes. 10µL of PCR product was then sent for sequencing with a relevant sequencing primer (IDT) (Table 2.13).

Component	Volume (µL)
PCR	16
SAP (1000units/mL)	4
Exonuclease 1	0.5

Table 2.11 ExoSAP reaction

Genotyping and sequencing PCR primers

Target	Primer	Sequence (5'-3)
CD9b TALEN 1 cut site	CD9b T1 F1	ggaaaggtacatttctcaggtgctcag
CD9b TALEN 1 cut site	CD9b T1 R1	atcctcacaacaacacaatcaagcct
CD9b TALEN 2 cut site	CD9b T2 F1	tgattgggatgtgcagttcagtttctg
CD9b TALEN 2 cut site	CD9b T2 R1	atttacaccgttcaaaacaaacagaa
CD9b TALEN 1 cut site	CD9b T1 F1 1.4.15	gcttgactaatccgcatttagactc
CD9b TALEN 1 cut site	CD9b T1 R1 1.4.15	ccagcctagatacaatcacacaaac

Table 2.12 Genotyping PCR primers

Sequencing Primer	Sequence (5'-3')
CD9b T1 F2	cgagtcaaaacccaaagagg
CD9b T1 R2	acacacttatttcaccatct
CD9b T2 F2	aaactaaacattttcttagt
CD9b T2 R2	aattgaataataaaaggtga
CD9b T1 F2 1.4.15	tatctatgctctttcccatgggacc
CD9b T1 R2 1.4.15	ctcacaacaacacatcaagcctta

Table 2.13 Sequencing primers

2.2.1.2.2 Using restriction digest for genotyping

Restriction digest using the enzyme Mbo II (NEB), was used on gDNA extracted from offspring from potential founder fish (F0s). The gDNA was extracted as described by Meeker et al. 2007 and the TALEN cut site amplified using the PCR primers CD9b T1 F1 and CD9b T1 R1 or CD9b T2 F1 and CD9b T2 R1 (Table 2.12). The PCR reaction and thermal cycle are described below (Tables 2.14, 2.15). 3µL of the PCR reaction was checked for a single amplicon on a 1% agarose gel alongside a 100bp ladder. Once a single amplicon was obtained, 1µL Mbo II was added to the remaining 17µL PCR reaction and incubated at 37°C for 3 hours. 15µL of the reaction was then checked for digestion on a 3% agarose gel containing 2% high resolution agarose (Sigma) and 1% normal agarose, alongside a 100bp ladder.

Component	**Volume (µL)**
ReddyMix (Sigma)	10
100µM Forward Primer	0.1
100µM Reverse Primer	0.1
gDNA	1.5
MQH_2O	8.3

Table 2.14
PCR reaction for restriction digest

Thermal Cycle	**Temperature (°C)**	**Time**
Initial Denaturation	94	2 minutes
34 Cycles	94	20 seconds
	55 (variable)	20 seconds
	72	45 seconds
Final Extension	72	3 minutes

Table 2.15 Restriction digest PCR reaction thermal cycle

2.2.1.3 Making injectable mRNA

Transforming competent bacteria

After defrosting NEB 10-beta competent E.Coli on ice, 2.5µL plasmid DNA was added to the cells and left for 30 minutes at room temperature. The cells were subsequently heat shocked at 40°C for 30 seconds then placed on ice for 5 minutes. 400µL SOC medium was added and the cells incubated with agitation for 1 hour at 37°C. The bacteria were then plated onto agar plates containing the relevant antibiotic and incubated overnight at 37°C.

Plasmid	Obtained	Vector	Resistance conferred	Restriction enzyme (NEB)	Mini or Midi Prep
CXCR4b-EGFP-globin	E.Raz (Minina et al. 2007)	pSP64T	Ampicillin (Sigma)	Xba1	Mini
CXCL12a-Venus-globin	E.Raz (Minina et al. 2007)	pSP64T	Ampicillin	Xba1	Mini
CD9b-T1-L	ZGENEBIO Biotech INC.	pZGB4L	Kanamycin (Sigma)	Not1	Midi
CD9b-T1-R	ZGENEBIO Biotech INC.	pZGB4L	Kanamycin	Not1	Midi
CD9b-T2-L	ZGENEBIO Biotech INC.	pZGB4L	Kanamycin	Not1	Midi
CD9b-T2-R	ZGENEBIO Biotech INC.	pZGB4L	Kanamycin	Not1	Midi

Table 2.15 Plasmids used to make injectable mRNA

Amplification of plasmid DNA

QIAGEN Plasmid Mini- or Midi- Kits were used to amplify and purify the plasmid DNA, with the resulting DNA stored in TE buffer at -20°C before linearization. The protocol followed was per the manufacturer's instructions. Briefly, plasmid DNA was amplified by creating starter cultures of transformed bacteria in 14mL falcon tubes containing 2mL LB and the relevant antibiotic (1µL/mL), which were then incubated for 8 hours at 37°C (Table 2.15). Midi-prep kits then used a secondary culture step in which starter

cultures were diluted in LB and incubated overnight at 37°C. Bacterial cells were harvested by centrifugation, re-suspended and lysed using the kit buffers P1 and P2. DNA was precipitated using the buffer P3 and incubating on ice before separation from proteins and cell debris by centrifugation. DNA was cleaned further using a QIAGEN-tip, which binds DNA and allowed residual contaminants to be washed away using the supplied buffer QC. DNA was eluted from the tips using the kit buffer QF before precipitating the DNA using isopropanol and centrifugation. Pellets were washed with 70% ethanol and re-suspended in TE buffer.

Linearization of plasmid DNA

The plasmids were then linearized using a relevant restriction digest as shown in Tables 2.15, 2.16, incubated at 37°C for 2 hours. Bovine Serum Albumin (BSA) was added to the reaction to help prevent loss of the restriction enzyme through adhesion to reaction tubes and pipette tips. 10µL of each digest and 1µL of each uncut plasmid was run on a 0.8% agarose gel for 45 minutes at 65V to check for complete digestion.

Reaction component	**Volume (µL)**
7µg Plasmid	variable
Relevant buffer (NEB)	10
Restriction enzyme (NEB)	3
BSA (Sigma)	1
MQH_2O	to 100

Table 2.16 Restriction digest reaction for plasmid linearization

Purification and extraction of DNA

The linearized DNA template was cleaned by adding 200µg/mL Proteinase K (Pro-K) (Sigma) and 0.5% SDS (sodium dodecyl sulfate) (Fluka) and incubating for 50 minutes at 50°C to remove any remaining proteins. A further 10 minute incubation at 95°C was used to de-activate the Pro K. The DNA template was then extracted and precipitated using phenol:chloroform:isoamyl alcohol (25:24:1) (phenol/chloroform) (Sigma) and ethanol using the following protocol.

The DNA templates were transferred to 1.5mL Eppendorf tubes and equal volume of phenol/chloroform was added before centrifuging for 5-10 minutes at maximum speed. To fresh RNAse free tubes, an equal volume of chloroform (Sigma) was added. The aqueous phase from the centrifuged tubes was immediately transferred to the fresh chloroform containing tubes and centrifuged at max speed for 3 minutes. After centrifugation, the aqueous phase was transferred to new RNase free tubes. 1 in 10 volume of sodium acetate and 110µL Isopropanol (Sigma) was added, before cooling for 30 minutes at -20°C to precipitate the DNA. After centrifugation at 10,000-20,000g at 4°C for 30 minutes, the pellets were washed with 70% EtOH and then air dried. The pellets were then re-suspended in nuclease free water and stored at -20°C.

Transcribing mRNA for microinjection

The DNA templates were transcribed into injectable mRNA using the mMESSAGE mMACHINE SP6 Transcription Kit (Ambion) and 1µg DNA per template. Residual nucleotides and proteins were removed and mRNA was precipitated by adding 30µL nuclease-free water and 30µL lithium chloride and cooling at -20°C for 30 minutes before centrifuging for 15 minutes at 20,000g at 4°C. The RNA pellets were then washed with 70% EtOH, air dried and re-suspended in 20µL nuclease-free water before storing at -80°C.

2.2.1.4 Making cDNA

To extract RNA, 1-10 embryos were placed in Eppendorf tubes containing 0.3mL TRI Reagent (Sigma) and homogenized. An additional 0.6mL TRI Reagent was added and the tubes agitated for 5 minutes on an orbital shaker. If low numbers of embryos were used per tube (1-4 embryos), 5µL glycogen (20mg/ml Roche) was added as an inert co-precipitant. 0.2mL chloroform was added, the tubes inverted to mix, then left at room temperature for 3 minutes before centrifuging at 12,000g, 4°C for 15 minutes to partition the RNA into the aqueous phase. 500µL Isopropanol was then added to 500µL supernatant, the tubes inverted then left at room temperature for 10 minutes before centrifugation for 10 minutes at 12,000g at 4°C to precipitate the RNA. The RNA pellet was then washed once with 70% EtOH, and then re-suspended in nuclease-free water.

The RNA was then reverse transcribed to cDNA using the Applied Biosystems High Capacity RNA-to-cDNA kit and stored at -20°C.

2.2.1.5 qRT-PCR

qRT-PCR (quantitative reverse transcription-PCR) was conducted on single embryo cDNA using the Sigma S5193 kit and run on a Stratagene qPCR machine using MXPro software. Each reaction was set up as shown in Table 2.17 and followed the thermal cycle shown in Table 2.18. A reaction master-mix was created using the components shown in Table 2.17 and 15µL of the master-mix was aliquoted per well. To each well, 5µL of 1:20 diluted cDNA was also added. When trialling the primers, to test for a single PCR product, a mix of diluted cDNAs was used but cDNA from individual embryos was used to look at the relevant expression of β-actin2, CD9b C-terminal RNA and CD9b N-terminal RNA in AB, CD9b -1/-1 and CD9b -8/-8 embryos . Four primer sets were trialled but only β-actin-2, CD9b C-term and CD9b N-term 1 primer pairs were used subsequently (Table 2.19).

The fold expression of CD9b C-terminal RNA and CD9b N-terminal RNA in CD9b mutants was calculated by initially normalising the expression of CD9b C-terminal RNA and CD9b N-terminal RNA to the control gene, β-actin-2. Differences in fold expression between mutants and wildtype AB embryos were then calculated by normalising the mutant expression of the RNAs to the wildtype AB.

The standard curves for the primer pairs were conducted on a mix of diluted AB cDNA. A serial dilution of the cDNA was carried out with 1, 1/4, 1/16, 1/64, 1/256 and 1/1024 dilutions used. The last two dilutions didn't appear to yield reliable results and so only the first four dilutions were analysed.

Component	**Volume (µL)**
each 7.5µM Primer	1
25mM $MgCl_2$	2.8
ROX Reference Dye	0.2
SYBR Green Ready Mix (Jumpstart)	10
1:20 cDNA	5

Table 2.17 qPCR reaction

Thermal Cycle	Temperature (°C)	Time
Initial Denaturation	95	3 minutes
40 Cycles	95	15 seconds
	57	15 seconds
	72	20 seconds
Dissociation	95	1 minute
	55	30 seconds
	95	30 seconds

Table 2.18 qPCR thermal cycle

qPCR Primers	Sequence (5'-3')
β-actin2 Forward	ggacctgtatgccaacactg
β-actin2 Reverse	tgatctccttctgcatcctg
CD9b C-term Forward	gaacccgtgacatcgtgtaa
CD9b C-term Reverse	tacaacaggacaaccactcg
CD9b N-term1 Forward	aattctcaggtgctcagtctt
CD9b N-term1 Reverse	ttgatacactgaagtccacc
CD9b N-term2 Forward	aaggtcaattctcaggtgct
CD9b N-term2 Reverse	gcggccatggcttaaaaag

Table 2.19 qPCR primers

2.2.2 Zebrafish work and related methods

2.2.2.1 Home Office regulation

All experiments were carried out following the Home Office requirements for the use of animals in scientific research. The majority of experiments were classed as unregulated procedures and carried out under the UK Home Office project license 40/3459. Regulated procedures were conducted by colleagues under their UK Home Office personal project licenses.

2.2.2.2 Maintenance of adult zebrafish

Adult zebrafish were housed and bred in the UK Home Office approved Bateson centre aquaria at the University of Sheffield, which follow a regulated 14:10 hour light: dark cycle.

2.2.2.3 Zebrafish strains

Wildtype AB zebrafish were used as controls for all experiments, unless otherwise stated, and are maintained as breeding stocks in the aquaria. Heterozygous and Homozygous CD9b mutants (46delA or 42_49delCTTTATCT) were created from AB embryos and maintained on an AB background. Breeding stocks of CD9b mutants were maintained in the aquaria.

Claudinb:GFP+/-;CD9b +/-8 adult females were produced from a Claudinb:GFP X CD9b -8/-8 cross to produce embryos for the migration speed assay. This strain was not maintained after the migration speed assay experiments.

2.2.2.4 Pair mating

Adult pairs were placed in clear, plastic breeding tanks containing aquarium water in the late afternoon, the day before embryos were required. The breeding tanks consist of two parts, a breeding chamber and a larger water holding tank. The breeding chamber sits inside the water holding tank and has a perforated base that allows eggs to fall into through the larger tank, preventing the eggs from being eaten by the adult fish. Overnight the two adults are separated by a clear plastic divider. This divider is removed the next morning after the lights have been switched on. Zebrafish are photoperiod breeders and so spawn after the lights are switched on (Legault 1958). Embryos were collected by transferring the breeding tank containing the adult fish to a new water holding tank, then the embryos are sifted out of the water of the original water holding tank. Embryos were collected every 20 minutes after divider removal when embryos of the same developmental stage were required or after 2.5 hours if embryos of the same stage were not required.

2.2.2.5 IVF

Fish were paired as described in the Pair Mate protocol, four days before the IVF procedure and then transferred back to their normal tanks. The fish were paired again, the afternoon before the IVF, but the dividers are not removed. The next morning fish of the same genotype are placed together in larger tanks, as zebrafish will not normally lay when grouped. Individual males and females were then anaesthetised in tricaine and patted dry before extraction of the gametes. Sperm was extracted from male fish using 10 µl capillaries (Hirschmann) and suction, whereas females were gently squeezed on the abdomen to release eggs. The sperm and eggs were mixed together and incubated for 30 seconds before adding 750 µl aquarium water to the eggs and incubating for a further 2 minutes. 9 ml of aquarium water was then added and the gametes incubated for 4 hours at 28°C. The numbers of fertilised and unfertilised eggs was then assessed. Dead eggs were immediately discarded after extraction from the females and so were not included in the analysis.

2.2.2.6 General embryo preparation

Embryos were raised at 28°C in petri dishes containing E3 solution. E3 was changed daily and dead embryos removed. At the required time point, embryos were anaesthetised using tricaine, then fixed using 4 % PFA (Aldrich) in PBS. If the embryos remained in their chorions, the embryos were dechorionated using forceps before fixation. The fixed embryos were left in 4% PFA overnight at 4°C before being washed twice with PBST the following morning. Embryos were then put through a MeOH/PBS series using 30%, 60% and 100% MeOH before being stored in 100% MeOH (Sigma-Aldrich) at -20°C.

2.2.2.7 Survival curves and general phenotype assessment

Embryos were left uninjected or injected with a morpholino or TALEN at various volumes during the 1- or 2- cell stage. Embryos were then placed in petri dishes containing E3 and transferred to a 28°C or 22°C incubator. No more than 60 embryos were placed in a single dish and embryos were evenly distributed between dishes. At the designated time points, up to five days post fertilisation (dpf), the number of surviving embryos was assessed and any dead embryos were removed. Survival of embryos was calculated as a percentage of the original number of embryos at 0dpf. To assess toxicity of MOs or TALENs, general embryo morphology was analysed and categorised by eye at the same designated time points using a dissecting microscope.

2.2.2.8 Microinjection

A Flaming/Brown micropipette puller was used to create micro-injection needles from borosilicate glass capillary tubes. Needles were filled with 3-4µL of injection material using 20µL microloader tips (Eppendorf) and the needle tip seal broken using forceps. The PV800 Pneumatic PicoPump, as part of the micro-injection jig, was set up to release the required amount of injection material by adjusting the air pressure and air expulsion time. To determine the amount (nL) of injection material ejected, injections were first carried out into mineral oil (Sigma) over a graticule (Pyser-SGI) to allow the bolus size to be measured. Bolus size correlates to the volume (nL) of injection material, allowing final concentration within the embryo to be calculated. For example,

injection of 0.5nL of 1mM injection material into a 1µL embryo will give a 0.5µM final concentration in the embryo (Table 2.20).

Diameter (0.1mm)	Volume (nL)
1	0.5
1.25	1.0
1.5	1.76
1.70	2.57
1.75	2.80
1.80	3.05
2.0	4.18
2.20	5.58
2.25	5.96

Table 2.20 Bolus size to volume conversion table

Embryos were injected individually at the 1- or 2- cell stage with a stock concentration of injection material. When multiple concentrations were needed, a single stock solution was used at multiple volumes to create different final concentrations within the embryos, with the smallest volume injected first. To increase the final concentration, the bolus size was increased and re-measured before injecting the next group of embryos.

2.2.2.9 Internalisation assay

240pg CXCR4b-EGFP-globin and 384pg CXCL12a-Venus-globin mRNA was injected into individual blastocysts in 8-cell stage AB embryos, with either a single fluorescent construct per embryo or both constructs in separate blastocysts. The embryos were then incubated at 28°C before imaging at 6hpf. Embryos were imaged live using the Olympus Confocal microscope using 20X and 60X objectives, with the embryos held in 3% methyl-cellulose between a glass slide and coverslip. CXCR4b-EGFP-globin was captured using excitation and emission wavelengths of 484/507 nanometers, whereas CXCL12a-Venus-globin used 515/528 nanometers.

2.2.2.10 *In situ* hybridisation

In situ hybridisation was carried out as described by Thisse & Thisse in 2008, with a few minor changes which are outlined subsequently. The protocol was carried out with embryos being treated in Eppendorf tubes for the entirety of the first two days, after which they were held in 12-well plates for staining before transferring back to Eppendorf tubes for storage.

Day 1

Embryos were taken through a reverse MeOH series, from 100% to 30%, before washing with PBST. Embryos were digested with Pro-K (10µg/mL) using the timings described in Table 2.21, which are slightly different to those reported by Thisse & Thisse, although digestion time also depended on the freshness of the Pro-K aliquot. A water bath at 20°C was used during the digestion step to remove the effect of a variable room temperature on Pro-K digestion times. After re-fixing embryos in 4% PFA and washing with PBST, embryos were incubated with Hyb+ for 2 hours at 70°C. The Hyb+ then was replaced with 200µL Hyb+ containing 1-4µL RNA probe and left to hybridise overnight at 70°C.

Day 2

Salt washes were carried out initially at 70°C and then at room temperature to remove excess probe and non-specific hybridisation. After blocking for 3-4 hours with blocking buffer, embryos are incubated with anti-DIG-AP-Fab fragments (1:10000) (Roche) overnight at 4°C with agitation.

Day 3

Embryos were washed multiple times for 15-20 minutes in PBST to remove any unbound antibody before washing in staining buffer and incubating in staining solution containing NBT/BCIP (Sigma). Staining was monitored periodically using a dissecting microscope. After stopping the staining reaction with PBST 1mM EDTA, embryos were fixed with 4% PFA for 30 minutes at room temperature before conducting a MeOH series. Embryos were washed with 30% then 60% MeOH/PBS for 10 minutes before maintaining in 100% MeOH for up to 2 hours to remove excess non-specific staining. The MeOH series was then reversed and embryos washed twice with PBST for 5

minutes before washing with 50% glycerol. The embryos were then stored in 80% glycerol at room temperature in the dark.

Stage	Time (minutes)
1-cell to 1 somite	0.5
1-8 somites	1
9-18 somites	3
18-24 somites	10
24 hours	15
30 hours	22
36-48 hours	30
60 hours	40
72 hours	50

Table 2.21 Digestion times using 10mg/mL Pro-K

ISH probe synthesis

Digoxigenin (DIG)-11-UTP (Roche) was used to create DIG-labelled antisense RNA probes for *in situ* hybridisation. The DNA templates for RNA ISH probes were produced predominantly using nested PCR; however the *vasa* probe was produced using a modified mini prep on transformed bacteria. Both protocols are described in further detail below.

DNA template synthesis using a modified Mini Prep

Vasa cDNA was provided by H.Knaut (NYU Medical Center and School of Medicine), as part of pBS+ cloning vector which conferred ampicillin resistance and contained surrounding M13 primer binding sites. The plasmid was transformed into NEB 10-beta competent E.Coli and left overnight.

The next morning, bacterial cultures were transferred to 1.5mL Eppendorf tubes and centrifuged for 30 seconds at 14,000g. The resulting pellet was then treated with buffers from the Qiagen QIAprep Spin Miniprep Kit, using the following modified mini

prep protocol. 200µl P1 buffer was added, to re-suspend the pellet, on ice. 200 µl P2 buffer was then added and the Eppendorf inverted multiple times then left at room temperature for 5 minutes to lyse the cells. 200µl neutralising P3 buffer was then added, the tube inverted to mix, then centrifuged for 3 minutes at 14,000g. 600µl Isopropanol was placed in a fresh Eppendorf tube, to which the supernatant from the centrifuged tube was added and then placed at -20°C for 30 minutes. The tube was removed from the freezer and centrifuged for 30 minutes at 16,000g at 4°C to pellet the DNA. The supernatant was removed and the pellet washed gently with 700µl PE buffer. 50µl TE buffer was added to the dry pellet, mixed, and then left at room temperature for 5 minutes.

After adding PB buffer to the mini prep at 5x the volume of DNA, the DNA was transferred to a QIAprep spin column (QIAGEN) and centrifuged for 15 seconds at 14,000g. The pellet was washed twice using 500µl PE buffer and centrifuged for 15 seconds at 14,000g. A further centrifugation of the column, without buffer, was carried out for 3 minutes at 14,000g before allowing the column to dry for 5 minutes. DNA was then eluted by adding 50µl EB, incubating for 3 minutes at room temperature, and centrifuging the DNA into a fresh Eppendorf for 2 minutes at 14,000g.

The amount of cleaned DNA was determined using a spectrophotometer, 20ng of which was then used in a PCR reaction to create the DNA template. The PCR reaction is shown in Table 2.22 and the thermal cycle used was the same as shown in Table 2.10. The primers used are displayed in Table 2.24.

Component	**Volume (µL)**	**Concentration**
10x PCR Buffer	10	1x
10mM NTPs	1	100 µM
Taq polymerase	2	5 units
25µM Forward Primer	1	0.25 µM
25µM Reverse Primer	1	0.25 µM
20 ng DNA	variable	-
MQH_2O	to 85	-

Table 2.22 PCR reaction for making a DNA template from plasmid DNA

DNA template synthesis using Nested PCR

Nested PCR uses two PCR reactions to create a DNA template containing a T3/T7 binding site from whole transcriptome cDNA. The first reaction amplifies the relevant section of cDNA and the second adds a T3/T7 binding site and further amplifies the cDNA. The first PCR reaction used the protocol in Table 2.9 and thermal cycle in Table 2.10 with one difference, the denaturation step during the 35x cycles, was 45 seconds instead of 30 seconds. 1µL of the PCR product was then run on a 1% agarose gel to ensure amplification. The second PCR reaction used the same forward primer but a different reverse primer which targets upstream of the initial reverse primer and contains a T3 or T7 binding site (Table 2.24). The second PCR reaction used the same thermal cycle as the first but a slightly different PCR mix (Table 2.23). The PCR product, the DNA template, was then cleaned and transcribed as described below.

Component	**Volume (µL)**	**Concentration**
10x PCR Buffer	10	1x
10mM NTPs	1	100 µM
Taq polymerase	2	5 units
25µM Forward Primer	1	0.25 µM
25µM Reverse Primer	1	0.25 µM
1st PCR product	1	Variable
MQH_2O	84	-

Table 2.23 Second nested PCR reaction

Probe	Primer name	Sequence (5'-3')
Claudin b	Claudinb Forward	tttgctttttcgtaccgtag
Claudin b	Claudinb Reverse	gaggctgtttcaaacgtggt
Claudin b	Claudinb Rev T3	ggatccattaaccctcactaaagggaatgagcctcaatgtccaacaa
CD9a	CD9a Forward	ctgaagcatctttcgctcaca
CD9a	CD9a Reverse	gttggcttttatttgagccatgt
CD9a	CD9a Rev T3	ggatccattaaccctcactaaagggaatgagccatgtgcaccaatgt
CD9b	CD9b Forward	cttcgccacaagtgcctgat
CD9b	CD9b Reverse	acatgttactttctctccaaactcc
CD9b	CD9b Rev T3	ggatccattaaccctcactaaagggaagttactttctctccaaactcccat
Vasa	pBS forward M13	gtaaaacgcggccagt
Vasa	pBS reverse M13	ggaaacagctatgaccatg

Table 2.24 Primers for making ISH probes

Cleaning the DNA template

400µL nuclease-free water was added to an Amicon 50K centrifugal filter unit along with the DNA template. The filter unit was then centrifuged at 14000g for 5 minutes. This wash was repeated twice more, adding 500µL nuclease-free water each time. The filter unit was then inverted in a new nuclease-free Eppendorf and spun at 1000g for 2 minutes. 1µL of the product was then run on a 1% agarose gel to check for a single product of the anticipated size.

DIG-NTP-RNA transcription of the DNA template to create an ISH probe

The transcription reaction was set up on ice to the specifications shown in Table 2.25 and then incubated for 2 hours at 37°C. 18µL nuclease-free water and 2µL RNAse-free DNAse (Roche) was added to the transcription mix before a further incubation for 30 minutes at 37°C. Aldrich-Sigma spin filters were centrifuged empty for 2 minutes at 750g, after which they were transferred to new nuclease-free Eppendorfs that contain 14µL RNA-later (Sigma). The transcription mix was then added to the filters and centrifuged for 4 minutes at 750g. The resulting RNA was stored at -20°C, after

checking for successful transcription by running 1µL of the RNA and complimentary DNA template on an agarose gel.

Component	Volume (µL)	Supplier
DNA to 1 µg	variable	-
Nuclease-free water	to 30	-
Transcription buffer	3	NEB
NTP-DIG-RNA	3	Roche
RNAsin	1.5	Promega
T3/T7 RNA polymerase	1.5	NEB

Table 2.25 Transcription reaction

2.2.2.11 Imaging embryos

Embryos in 80% glycerol were transferred to glass slides using a glass pipette. Cover slips, with a drop of 80% glycerol, were placed over the embryo and maneuvered to position the embryo in the desired orientation. Plasticine between the coverslip and glass slide was used to hold the coverslip in the appropriate position. Embryos were then imaged at various magnifications using a microscope mounted camera and imaging software (Table 2.2). The lateral views of the whole embryo or embryo tail were imaged using 5X and 10X objectives. Images of single neuromasts or primordia were imaged using 20X or 63X objectives.

2.2.2.12 Using To-Pro-1 Iodine to stain neuromasts

Dechorionated 51 hpf embryos were placed, 10 embryos per well, in a 12-well plate containing E3 with 1µM To-Pro-1 (Invitrogen) and tricaine. The embryos were incubated in the dark for 15 minutes at 28°C and fluorescent staining of neuromasts was visualised using the YFP settings (515/531) on a Zeiss Zoom microscope. The embryos were then washed twice with E3 before imaging the embryos, using the Zeiss Zoom microscope, at 52hpf. The embryos were then fixed in 4% PFA at 52hpf for a subsequent ISH experiment.

2.2.2.13 Developmental assays

Staging and developmental assays were carried out as described by Kimmel et al. 1995, on live embryos. Three assays were used, embryo length, head-tail angle and otic vesicle length, which describes the number of otic vesicles which could be fitted between the otic vesicle and the eye.

2.2.2.14 Migration speed assay

The offspring from the cross between claudinb:GFP+/-;CD9b +/-8 adult females and CD9b -8/-8 adult males were initially sorted for claudinb:GFP. These embryos were then incubated at 28° until reaching 26 or 59 hpf. At these timepoints, the embryos were imaged using the Zeiss Zoom microscope before being returned to the incubator until 31 or 59hpf. At the later time points, the same embryos were imaged again and the primordium migration speed calculated using the distance travelled by the primordium during the incubation time.

2.2.3 Analysis

2.2.3.1 PGC assays

PGCs were firstly stained using a *vasa in situ* hybridisation and then PGC migration was analysed using two assays. Firstly, the distance between the most anterior and posterior PGCs was measured following the body axis. Secondly, the number of ectopic PGCs was also assessed. Ectopic PGCs were defined as being outside of the mean measurement between the most anterior and posterior PGCs in control embryos (Figure 2.1). Measurements were taken using Image J software and statistically analysed using Excel and GraphPad Prism.

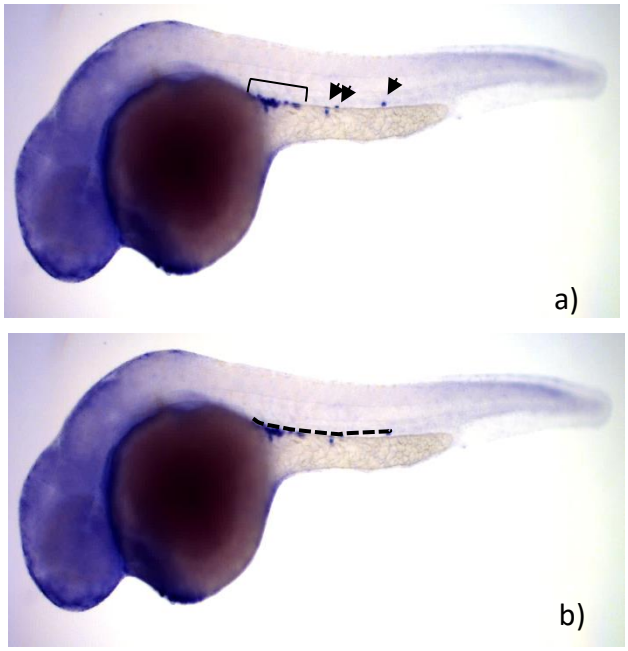

Figure 2.1 Assessment of ectopic PGCs (a) and the distance between the most anterior and posterior PGCs (b).

(a) PGCs outside the mean control group cluster measurement (bracket) were considered ectopic (arrowheads). The mean control group cluster measurement bracket was placed over the main cluster for each embryo.

(b) the distance between the most anterior and posterior PGCs was measured following the body axis (dashed line).

2.2.3.2 pLLP assays

Neuromasts and the pLLP were stained prior to analysis using a *claudin b in situ* hybridisation. Five different assays were then used to analyse lateral line structure and primordium migration as shown in Figure 2.2. The measurement of trunk length was taken from the posterior side of the otic placode to the tail tip, following the body axis. Similarly, the total body length was measured following the body axis and ends at the tail tip but starts at the tip of the nose. The distance between the 1st and last neuromasts and between the 1st and 2nd neuromasts was measured then reported as a percentage of the total body or trunk length. Migration of the primordium was

measured from the posterior side of the otic placode to the posterior side of the primordium and reported as a percentage of trunk length. A percentage of trunk or total body length was used to eliminate the variability of embryo size and remove the possibility that a difference seen was solely due to embryo size. The same software was used to analyse the pLLP as was used for PGC migration.

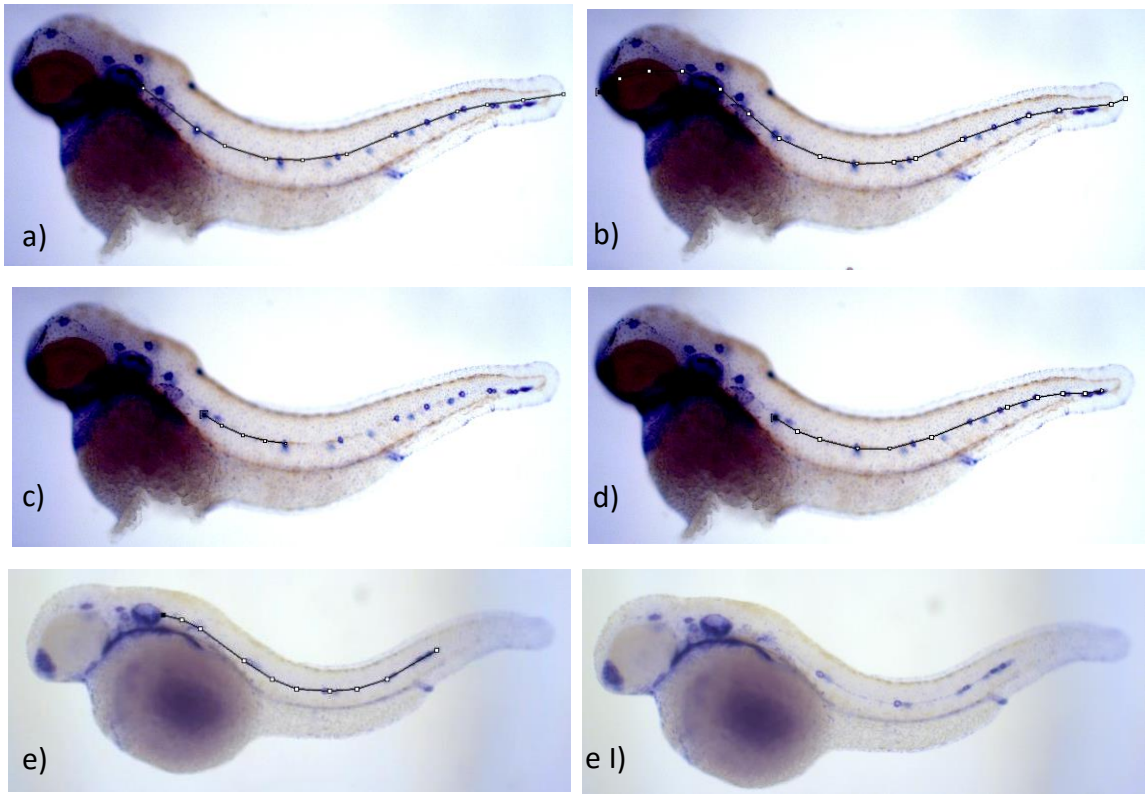

Figure 2.2 pLLP Assay measurements

Representative images showing the measuring process for the pLLP assays.

The trunk length (a) and total body length (b) were measured to the tail tip, starting from either the ear (a) or the nose (b). The distance between the 1st and 2nd neuromasts (c) or 1st and last neuromasts (d) was measured from the centre of the 1st neuromast to the centre of the 2nd or last neuromast. Primordium migration (e) was measured from the otic placode to posterior primordium edge. e I) shows the unmeasured image for comparison.

2.2.3.3 Statistics

All statistical analyses were carried out using GraphPad Prism version 6 and Microsoft Excel, on data obtained using Image J/Fiji.

Normality of data distribution was assessed by conducting a D'Agostino-Pearson omnibus K2 normality test on the experimental residuals and creating a histogram of residuals. Looking at the residuals allows normality to be assessed over the whole experiment and not just individual conditions as residuals report the difference between individual measurements and the condition group mean.

Normality tests are very sensitive to outlier results which can lead to an inaccurate normality result and so the histogram was created and used to check this result. The histogram allows the shape and distribution of the data to be assessed by eye and compared to Gaussian distribution. The D'Agostino-Pearson omnibus K2 normality test was chosen over the Shapiro-Wilke normality test as the Shapiro-Wilke test works best when every value in a data set is unique but is less efficient when multiple values are the same, whereas the D'Agostino-Pearson omnibus K2 normality test is more versatile.

For normally distributed data, parametric tests such as an Un-paired T-test or ANOVA with Dunnet's multiple comparisons test were used. The ANOVA post-hoc tests, Sidak and Holms-Sidak multiple comparisons tests were used when more power was required. For non-normally distributed data non-parametric tests were used, most often Mann-Whitney U test or Kruskal-Wallis with Dunn's multiple comparisons test.

Percentages

Percentages were first assessed for normal distribution and if found to be normally distributed were treated the same as all other parametric data. Percentage data that was found to be not normally distributed was transformed using the $\log_{10}$ transformation for continuous data and the arcsine transformation for non-continuous count data.

Pooling data

Before pooling data from experimental repeats, data of the same condition, e.g. control data, were compared for significant differences. If no significant differences were found, the data was pooled but if significant differences were found the experiments were not pooled and trends between experiments were studied.

n numbers

n numbers for all experiments, except pLL assays where n= number of lateral lines analysed, refer to individual embryos unless otherwise stated.

2.2.3.4 Graphs

Graphs are presented showing the mean ±SEM unless otherwise stated. Significance was calculated using GraphPad Prism with $p<0.05$ and indicated graphically using the notations described in Table 2.26.

Symbol	**P value**
NS (non-significant)	≥0.05
*	0.01 to 0.05
**	0.001 to 0.01
***	0.0001 to 0.01
****	<0.0001

Table 2.26 Statistical significance symbols

Chapter 3: CD9b Morpholinos

3.1 Introduction

Morpholino oligonucleotides (MOs) were used to investigate the effect of *cd9b* knockdown on PGC and pLLP migration. Morpholinos are synthetic nucleic acid analogs that can bind to specific complementary RNA sequences using Watson-Crick base pairing (Summerton and Weller 1997, Nasevicius and Ekker 2000) (Figure 3.1). Although MOs can bind to complementary nucleic acids, the MO structure is different to that of RNA. The differences are advantageous as MOs gain resistance to nuclease digestion and inhibition of non-specific protein interactions (Figure 3.1) (Summerton and Weller 1997, Ekker 2000, Corey and Abrams 2001). Injection of morpholinos into the yolk of 1-4 cell stage embryos can cause efficient and specific gene knockdown through embryonic development up to 50hpf (Nasevicius and Ekker 2000, Ekker 2000, Corey and Abrams 2001, Draper et al. 2001).

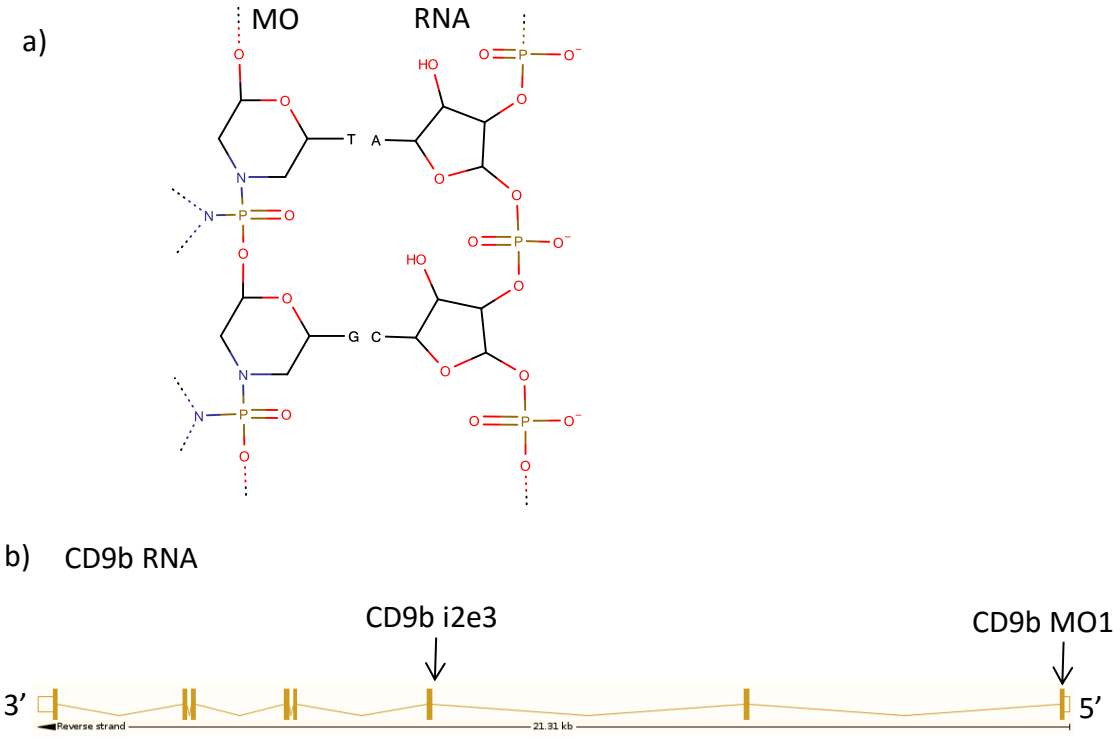

Figure 3.1 Diagram of the structure and binding of CD9b morpholinos
Representative morpholino structure and its interaction with RNA (a). Two MOs were designed to bind *cd9b* RNA (b) (*cd9b* RNA diagram from ensemble.org). CD9b MO1 was designed to bind to the 5' UTR of *cd9b* RNA, causing a *cd9b* knockdown by inhibiting the progression of the ribosomal initiation complex and therefore preventing translation. CD9b i2e3 is a splice-site morpholino which binds to pre-mRNA and prevents splicing, causing aberrant protein production.

MOs have been used to successfully phenocopy a number of previously studied mutants, for example no-tail (*T,brachyury homolog a*), nacre (*microphthalmia-associated transcription factor a*) and ace (*fgf8a*). However, it has been noted that many morphants showed unexpected additional phenotypes such as gnarled tails, elevated neural cell death or overall degeneration, which are often caused by off-target activation of p53 (Nasevicius and Ekker 2000, Ekker 2000, Araki and Brand 2001, Draper et al. 2001, Ekker and Larson 2001, Sumanas and Larson 2002, Robu et al. 2007, Bedell et al. 2011). Off-target effects are a relatively common occurrence with morpholinos, so a number of controls were used to help verify that any phenotypes seen were CD9b-knockdown specific. Firstly, uninjected embryos were raised and stained under the same conditions as injected embryos to ensure that phenotypes were not due to abnormal embryo batches. Secondly, a 5bp mismatch control which has previously been used by Trikic et al., was injected at the highest CD9b MO concentration to confirm that the morpholino structure was not causing any toxicity at the concentrations used (Trikić et al. 2011). Thirdly, two different MOs were designed to target *cd9b,* one as a translation-site blocker (CD9b MO1) and the other as a splice-site inhibitor (CD9b i2e3). These MOs were injected independently to ensure that they produce the same phenotype (Figure 3.1b). Lastly, embryos were injected with a range of CD9b MO concentrations to verify that the phenotypes were not only present in embryos showing general morphological defects. (Sumanas and Larson 2002, Eisen and Smith 2008, Bedell et al. 2011)

3.2 Results

3.2.1 MO toxicity

Injection of morpholinos at high concentrations can have a toxic effect on embryonic development and is often fatal. To ensure that the concentrations of the translation blocking CD9b morpholino, CD9b MO1, would not be completely lethal, 1-cell stage embryos were injected with different volumes of CD9b MO1 at a single concentration. This produced a range of final concentrations within the batch of embryos. The survival of the embryos with different final concentrations of CD9b MO1 was then recorded over 96hpf (Figure 3.2). Uninjected, pierced and ringer's buffer injected embryos showed high viability with ~80-90% of the embryos surviving over four days. Pierced embryos, where the needle was inserted into the yolk but no liquid injected, were used to check whether the micro-injection technique was causing decreased survival. Ringer's buffer was injected at the largest drop size used for the CD9b MO1 injections to control for any effects caused by the amount of liquid injected. Embryos injected with CD9b MO1, to give a final concentration of 0.5-2.0µM inside the embryo, showed a dramatic decrease in survival with only ~30-50% of the embryos surviving over 96hpf (Figure 3.2d). Injection of lower concentrations of CD9b MO1 resulted in a higher percentage of morphants surviving, ~50-80%, with one concentration even showing the same level of viability as the controls (Figure 3.2a-c). Similar results were seen in multiple experimental repeats and surprisingly the ringer's buffer injected embryos always showed similar survival rates to CD9b MO1 0.2µM injected embryos (Figure 3.2b-c).

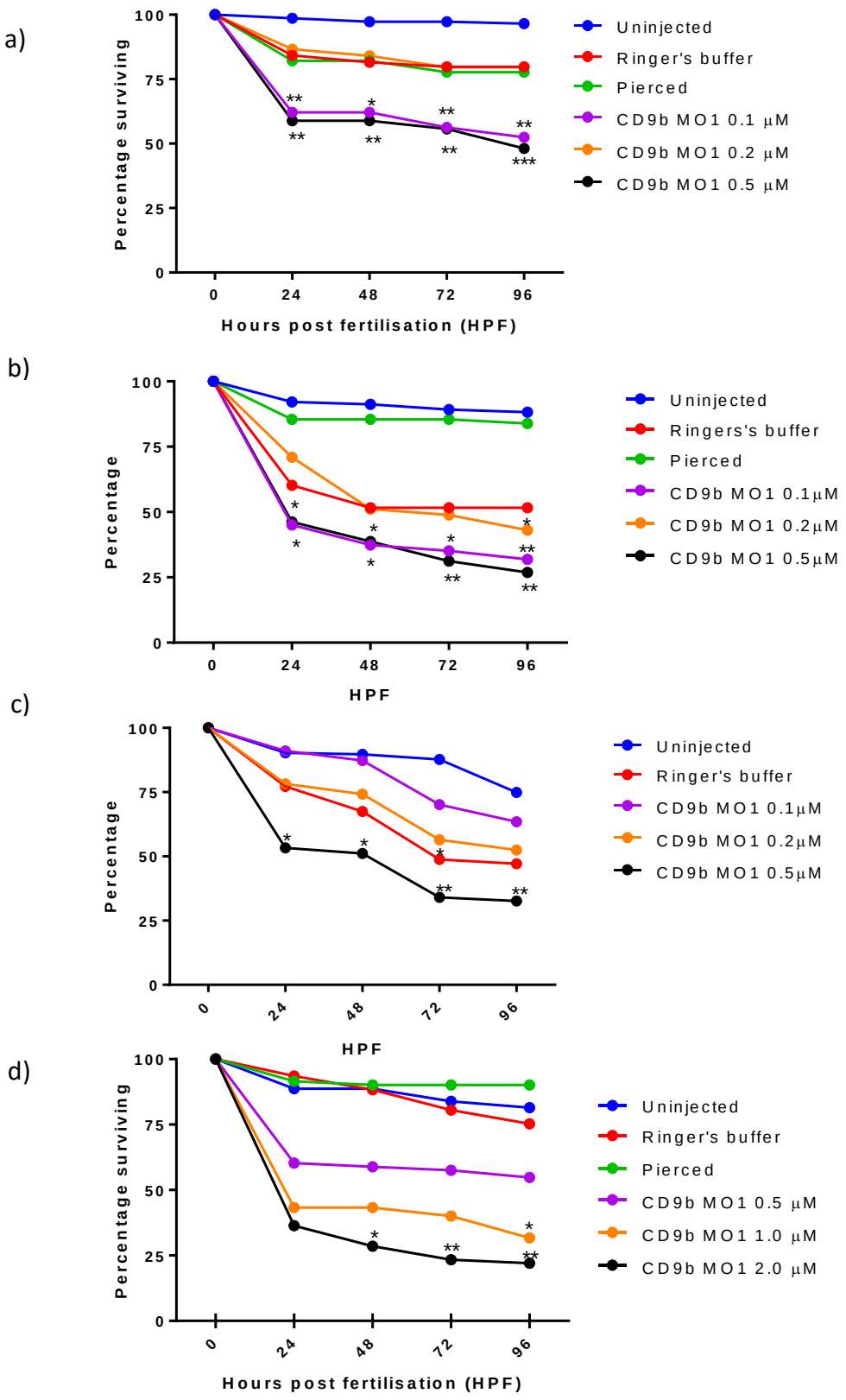

Figure 3.2 Embryos injected with the translation blocker CD9b MO1 show decreased viability compared to the uninjected controls.
Viability curve showing the survival of embryos, injected with CD9b MO1 0.1- 0.5µM (a-c) or 0.5-2.0µM (d) over 96 hpf. n= minimum 100 (a,c), and 60 (b,d) embryos for each condition. Two-Way ANOVA with Dunnett's multiple comparisons test on untransformed (a-c) or $\log_{10}$ transformed data (d). p = <0.05. All graphs show data from individual experiments.

Amongst the surviving embryos, it was noted that a proportion of the CD9b MO1 injected embryos showed abnormal developmental phenotypes (Figure 3.3a). The extent to which abnormal development affects CD9b MO1 injected embryos was assessed by evaluating embryos daily, over four days, for general phenotypes ranging from wildtype to mild, moderate and severe abnormal phenotypes (Figure 3.3-3.5). Phenotypes seen included pericardial or yolk oedema, a kinked, curly or shorter tail, wrinkled or decreased fin fold area, and decreased overall development (Figure 3.3a). Embryos were categorised as mild, moderate or severe depending on the number and severity of any abnormal phenotypes they had developed. While the majority of uninjected, pierced and ringer's buffer injected embryos displayed wildtype phenotypes, a considerable percentage of CD9b MO1 injected embryos displayed abnormal phenotypes (Figures 3.3b-e, 3.4a-d, 3.5a-d). In embryos with lower final concentrations of CD9b MO1 (0.1-0.5µM), approximately 20% of the embryos showed abnormal phenotypes at 24hpf rising to 30-50% of embryos by 96hpf. The majority of the abnormal embryos only showed mild phenotypes, although the severity appears to increase with morpholino concentration and time (Figure 3.3b-e). Similar results were seen in the experimental repeat, although the range of phenotypes was more evenly distributed than seen in Figures 3.3b-e (Figure 3.4).

Injecting higher concentrations of CD9b MO1, to give final concentrations of 0.5-2.0µM, appears to recapitulate this result with a similar percentage of embryos showing abnormal phenotypes over the 96 hours; however the phenotypes seen were more severe (Figure 3.5). Higher concentrations of CD9b MO1 induced noticeably more moderate and severe phenotypes than lower concentrations, as well as a decrease in embryos showing wildtype phenotypes (Figures 3.3 – 3.5).

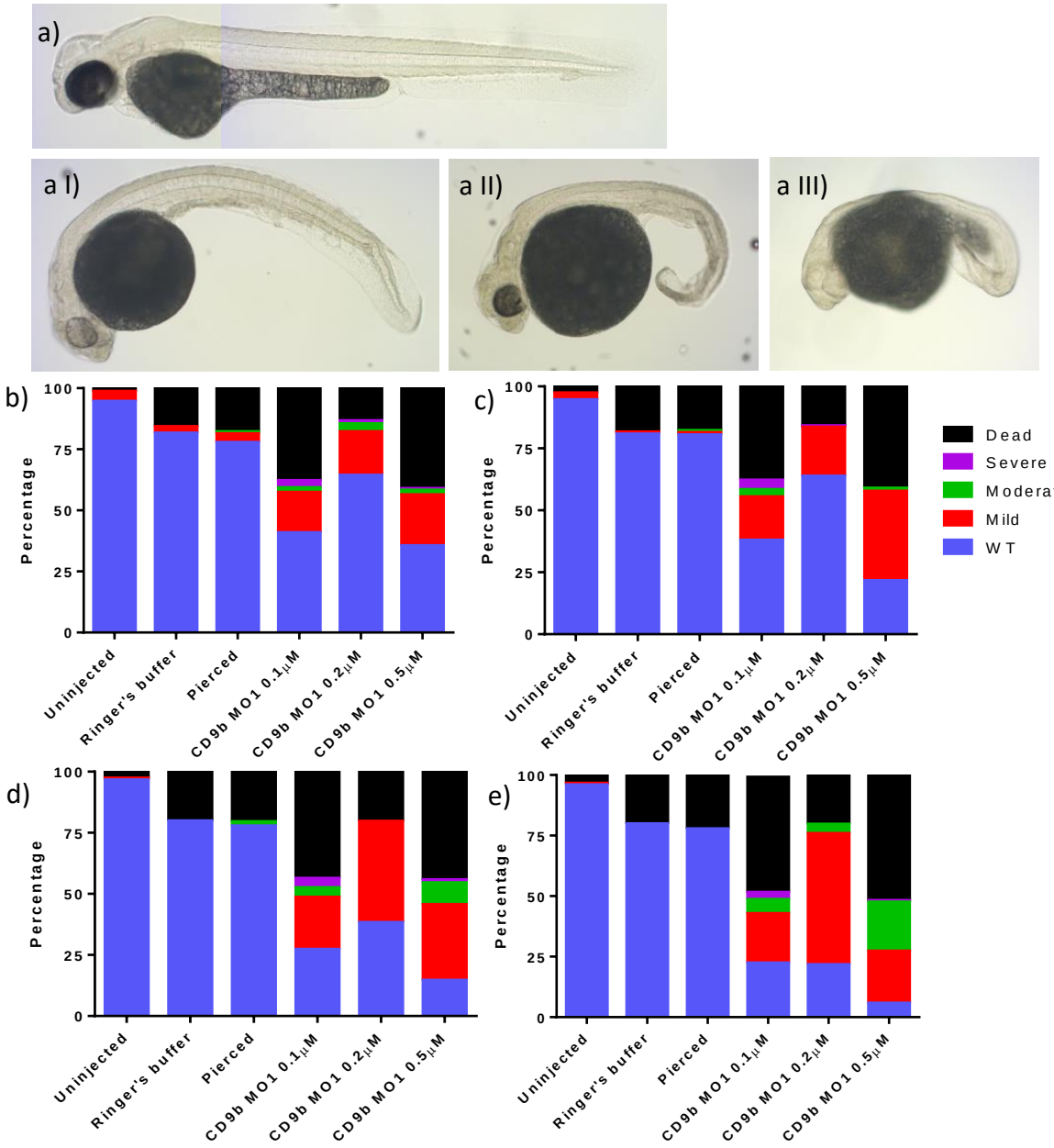

Figure 3.3 Embryos injected with 0.1-0.5µM CD9b MO1 show abnormal phenotypes more often than control embryos.

Representative images of the fixed embryos showing wildtype (a), mild (a I), moderate (a II) and severe (a III) phenotypes observed in 48hpf CD9b MO1 injected embryos. Abnormal phenotypes seen include pericardial oedema, kinked or curly tail, shorter tail, wrinkled or decreased fin fold, large yolk and decreased overall development. The lack of pigmentation is due to bleaching of the embryos post-fixation.

Representative graphs of gross phenotypes shown by CD9b MO1 injected embryos at 24 (b), 48(c), 72 (d) and 96 (e) hpf, where mild embryos showed one or two minor defects, moderate showed multiple abnormalities, often including delayed overall development and severe displayed the most extreme phenotypes. n= minimum 100 embryos for each condition. This figure shows data from a single experiment, see Figure 3.4 for experimental repeat.

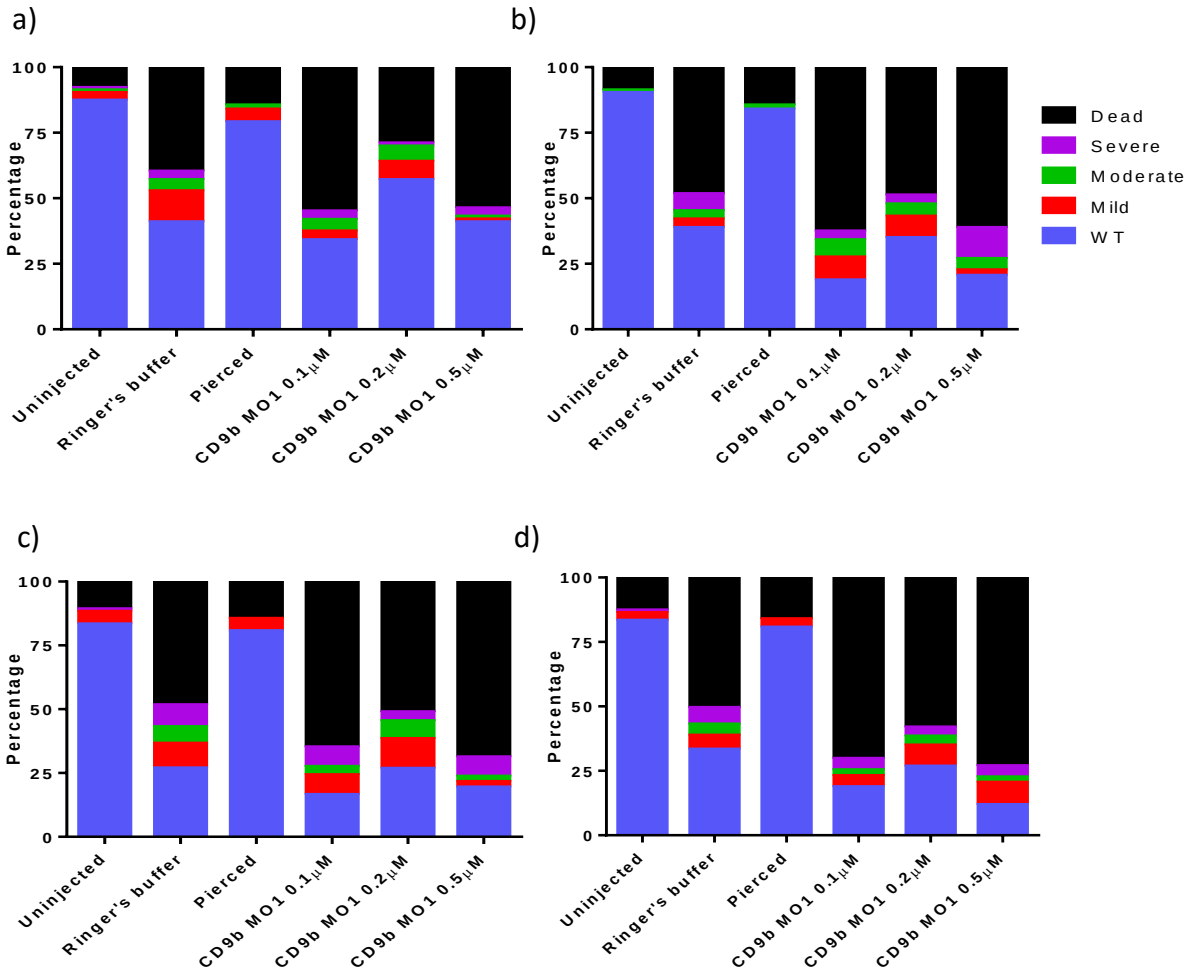

Figure 3.4. Ringer's buffer and CD9b MO1 injected embryos show increased frequencies of abnormal phenotypes at 24 (a), 48(b), 72 (c) and 96 (d) hpf. The ringer's buffer injected control embryos do show a decreased percentage of wildtype phenotypes compared with the other controls, however this may be due to micro-injection inexperience during this experiment as the experimental repeat (Figure 3.3) displays no such decrease. Phenotypes were categorised as described in Figure 3.3. n=minimum 60 embryos per condition

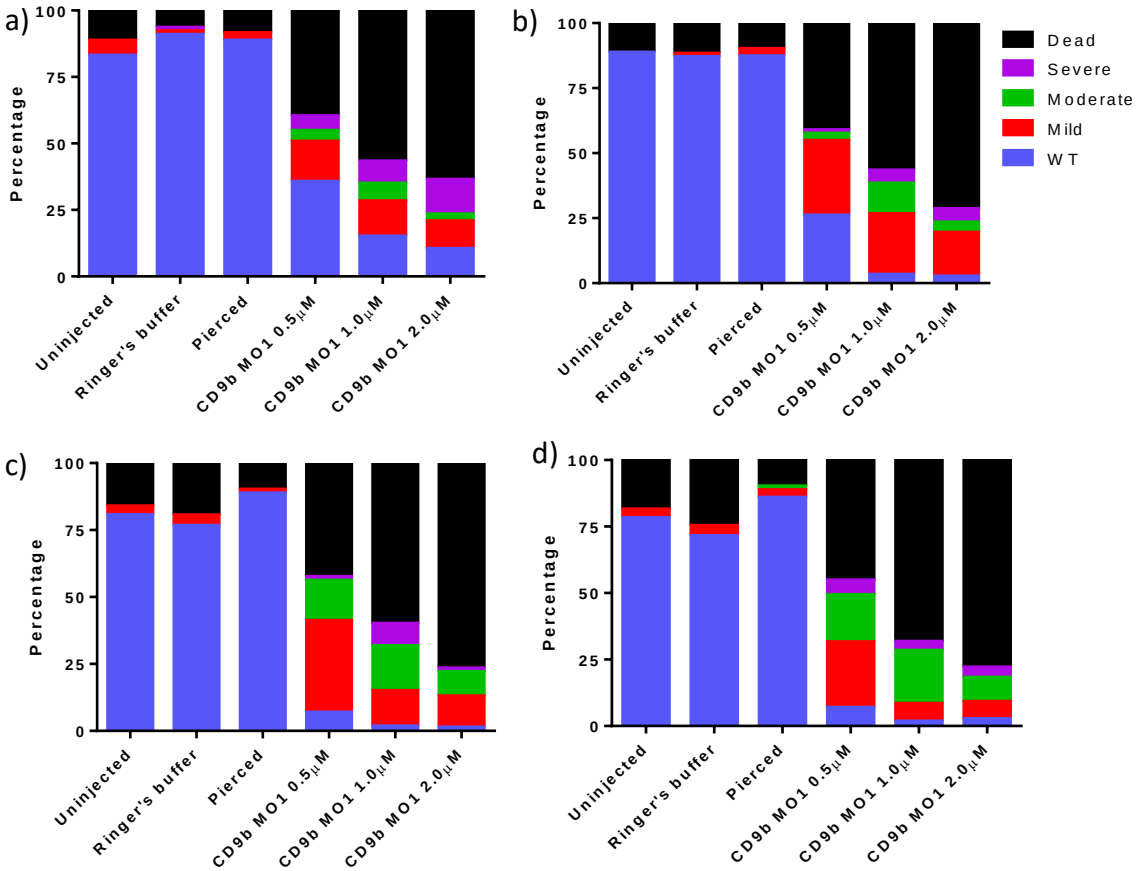

Figure 3.5 Embryos injected with 0.5-2.0µM CD9b MO1 show abnormal phenotypes more often than control embryos.
Graphs of general phenotypes shown by CD9b MO1 injected embryos at 24 (a), 48(b), 72 (c) and 96 (d) hpf. n=minimum 60 per condition. Phenotypes were categorised as described in Figure 3.3. Data from a single experiment.

While the higher concentrations of CD9b MO1 do cause increased lethality and abnormal phenotypes, a percentage of the injected embryos were viable and showed wildtype phenotypes, especially at 24 and 48hpf (Figure 3.5). It was decided that concentrations of 0.5, 1.0 and 2.0µM CD9b MO1 would be used initially to investigate the effect of CD9b knockdown on PGC and pLLP migration (Figures 3.6 and 3.9). This decision was made based on the fact that morpholinos act in a knockdown capacity and if no phenotypes were seen using the lower concentrations it could be due to incomplete knockdown of CD9b.

3.2.2 PGC migration in CD9b morphants

The effect of CD9b knockdown on PGC migration was investigated by injecting embryos to give final concentrations of 0.5, 1.0 or 2.0µM CD9b MO1 at the 1-cell stage, raising these to 30hpf before fixing and staining for the PGCs (Figure 3.6a). An antisense DIG-labelled RNA *in situ* hybridisation probe against *vasa* RNA was produced and used to stain the PGCs as *vasa* RNA is sequestered by PGCs (Braat et al. 1999).

As well as uninjected controls, ringer's buffer was injected to show any effects caused by the injection technique and a mismatch MO, which should not bind specifically to RNA, was injected to negate any effects the morpholino structure may have. Though PGC migration finishes at ~24hpf, embryos were fixed at 30hpf to ensure that any PGC phenotypes seen were not just due to general developmental delay in the CD9b morphants (Doitsidou et al. 2002). Whilst staining with the *vasa* probe was poor, PGCs could still be distinguished in the trunk although often not in the head. With this in mind, PGCs were cautiously identified and the distance between the most anterior and posterior PGC was measured following the body axis (Figure 3.6b). This measurement was taken to quantify the observed phenotype of more widely spaced PGCs in CD9b morphants when compared to uninjected or mismatch MO embryos. Interestingly, a mutant with a CXCR4b-internalisation defect has been previously shown to have abnormal PGC migration, with PGCs overshooting their target region, causing a spread out phenotype (Minina et al. 2007). In CD9b morphants a small but significant increase in the mean distance between the most anterior and posterior PGC was seen compared to the uninjected (Figure 3.6b).

To determine whether this significance was due to single PGCs migrating incorrectly or a mass disruption of PGC migration, the number of ectopic PGCs was also analysed. Germ cells were defined as ectopic if they were outside the mean uninjected PGC cluster size. The mean cluster size was taken as the mean distance between the most anterior and posterior PGC in the uninjected embryos for that experimental repeat. There was no significant difference in the number of ectopic PGCs in CD9b morphants and though there is a clear trend of embryos with increased numbers of ectopic PGCs in the CD9b morphants, the majority of embryos still had 0 or 1 ectopic PGCs. Wildtype embryos and injected embryos showing non-specific or off-target effects often have single ectopic PGCs (Weidinger et al. 1999, Goudarzi et al. 2013) (Figure 3.6c). This lack

of ectopic PGCs in CD9b morphants suggests the increase in spread of PGCs seen in Figure 3.6b may be due to a few individual PGCs migrating incorrectly and not due to a general spreading out of the germ cells.

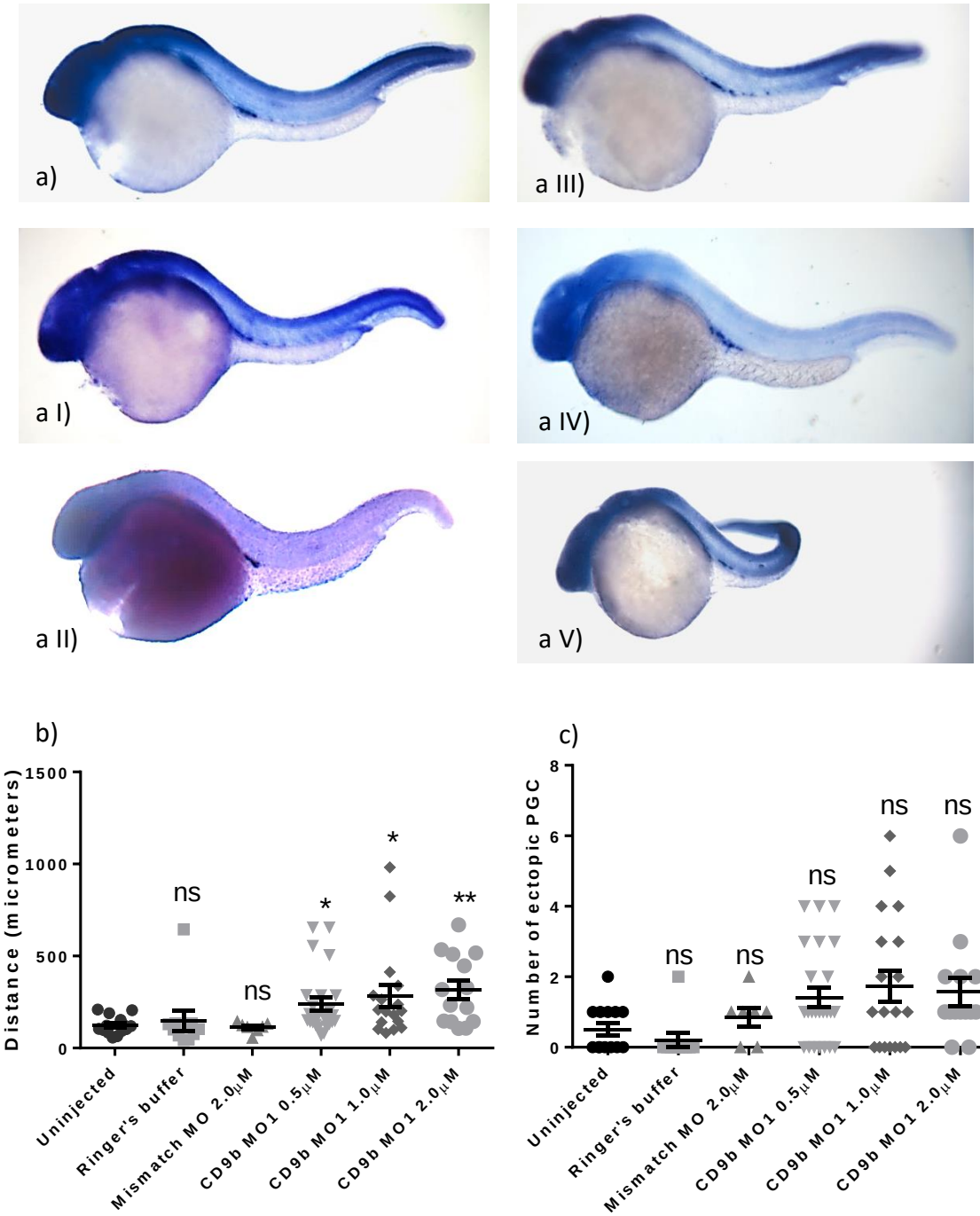

Figure 3.6 30hpf embryos injected with 0.5-2.0μM CD9b MO1 show increased distance between the most anterior and posterior PGCs.
Representative images of uninjected (a), Mismatch MO 2.0μM (a I), Ringer's buffer 2.0μM (a II), CD9b MO1 0.5μM (a III), CD9b MO1 1.0μM (a IV) and CD9b MO1 2.0μM (a V). A significant increase in the mean distance between the most anterior and posterior PGC (b) but no significant increase in the number of ectopic PGC in CD9b MO1 injected embryos (c) was seen using a Kruskal-Wallis ANOVA with Dunn's multiple comparisons test. n= minimum 7. P= <0.05. Pooled data of two experiments.

Thus, in CD9b morphants a small number of PGCs were failing to migrate correctly more frequently than in control embryos. However, it has been observed that PGCs can be easily perturbed in embryos that are developmentally abnormal (private communication, D. Gilmour, Heidelberg University, EMBL). While the more phenotypically normal embryos were fixed for the *in situ* hybridisation, between the decreased survival rate and low percentage of embryos showing wildtype phenotypes, embryos with mild or occasionally moderate abnormal phenotypes had to be used (Figure 3.2d and 3.5a). To evaluate whether CD9b knock down or abnormal embryo development was causing the significant increase in distance between the most anterior and posterior PGC in CD9b morphants, the experiment was repeated using lower concentrations of CD9b MO1 (0.1-0.5µM) (Figure 3.7). While the CD9b morphants appeared to show a slight spreading out of the germ cells, it appeared that the uninjected and mismatch MO injected embryos also showed this phenotype (Figure 3.7a). There was no significant difference in the distance between the most anterior and posterior PGCs or in the number of ectopic PGCs, although a small increase trend can be seen in both (Figures 3.7b-c). It was surprising that no significant difference was found for embryos with 0.5µM CD9b MO1 as this morpholino concentration had previously produced a significant phenotype, however, this may be due to differences in the uninjected control between the experiments (Figures 3.6b and 3.7b).

To be certain that CD9b knockdown was not causing a significant effect on PGC migration a splice-blocking morpholino, CD9b i2e3, was injected into 1-cell stage embryos and the PGC positions analysed at 30hpf (Figure 3.8). Initially it appeared that a concentration of 0.5µM CD9b i2e3 caused a PGC spreading out phenotype in 30hpf embryos (Figure 3.8b I, Figure 3.8a IV), however this significance was not seen in two further experiments (Figure 3.8b, b II). Whilst the distance between the most anterior and posterior PGC could not be pooled due to differences in the uninjected populations, the number of ectopic PGCs from each experiment could be. Consistent with previous results, no significant difference was found in the number of ectopic PGCs (Figure 3.8c).

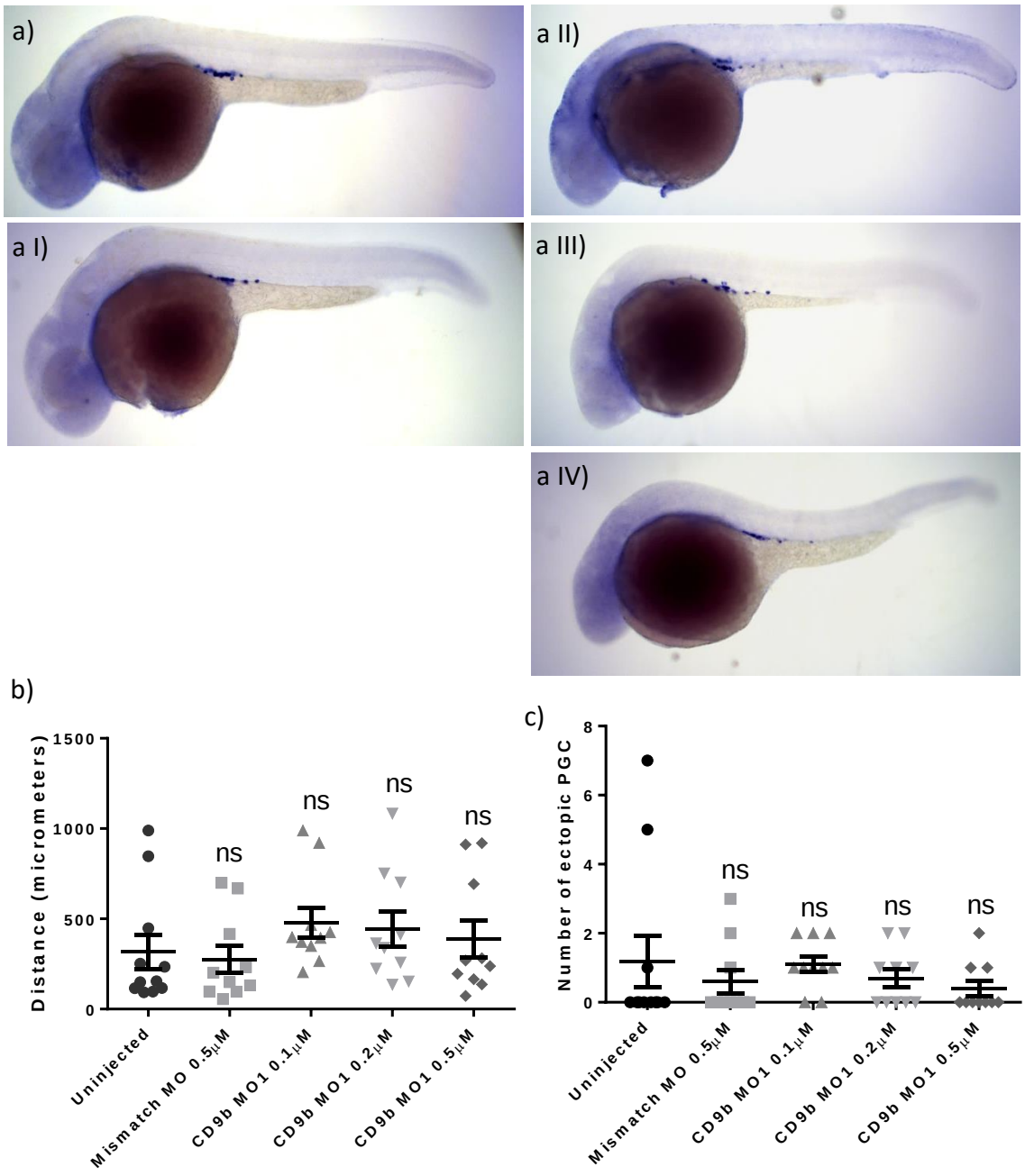

Figure 3.7 No significant difference in PGC migration was observed in embryos injected with 0.1-0.5µM CD9b MO1 compared to uninjected controls. Representative images of 30hpf uninjected (a), Mismatch MO 2.0µM (a I), CD9b MO1 0.1µM (a II), CD9b MO1 0.2µM (a III) and CD9b MO1 0.5µM (a IV). No significant increase in the mean distance between the most anterior and posterior PGC (b) or in the number of ectopic PGC in CD9b MO1 injected embryos (c) was seen. Kruskal-Wallis ANOVA with Dunn's multiple comparisons test. n= minimum 10. P= <0.05. Data from a single experiment.

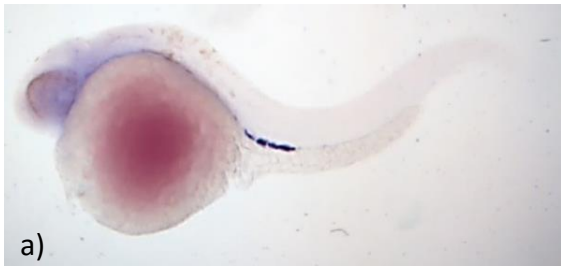
a)

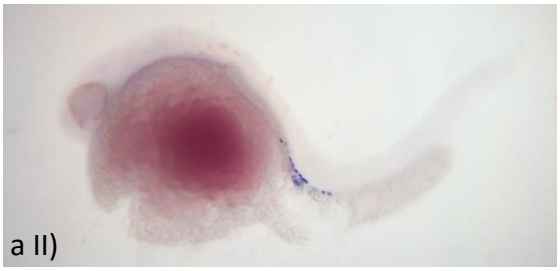
a II)

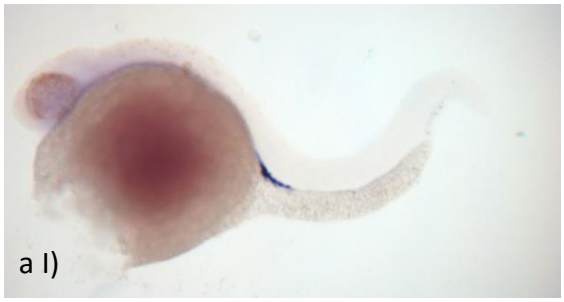
a I)

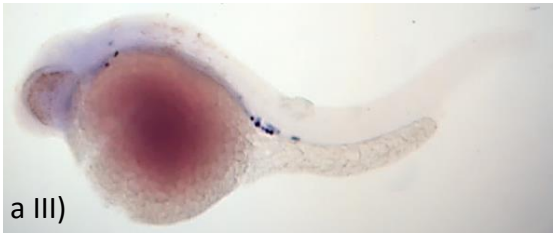
a III)

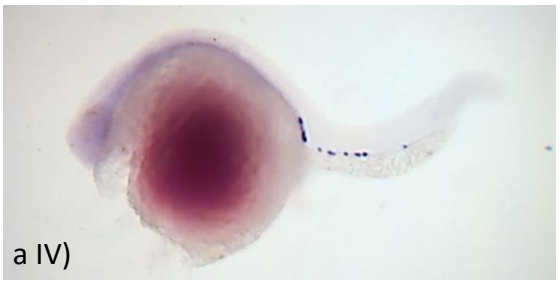
a IV)

b)

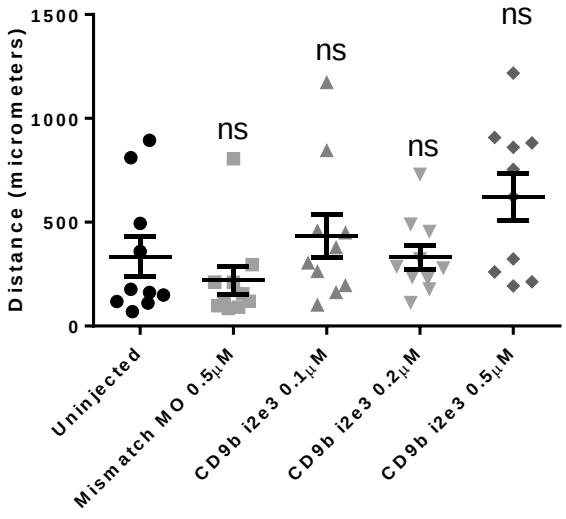
Distance (micrometers)
1500
1000
500
0
ns
ns
ns
ns
Uninjected
Mismatch MO 0.5μM
CD9b i2e3 0.1μM
CD9b i2e3 0.2μM
CD9b i2e3 0.5μM

c)

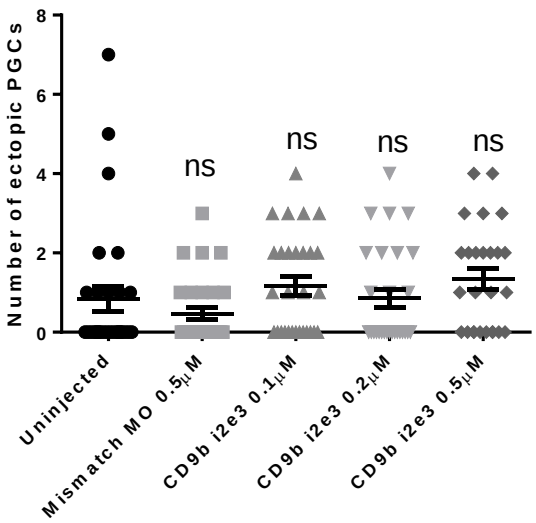
Number of ectopic PGCs
8
6
4
2
0
ns
ns
ns
ns
Uninjected
Mismatch MO 0.5μM
CD9b i2e3 0.1μM
CD9b i2e3 0.2μM
CD9b i2e3 0.5μM

b I)

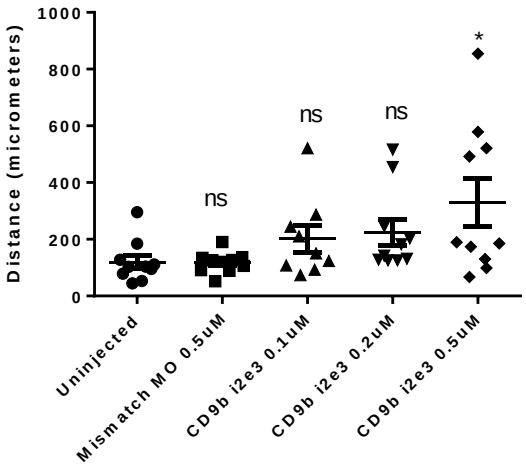
Distance (micrometers)
1000
800
600
400
200
0
ns
ns
ns
*
Uninjected
Mismatch MO 0.5uM
CD9b i2e3 0.1uM
CD9b i2e3 0.2uM
CD9b i2e3 0.5uM

b II)

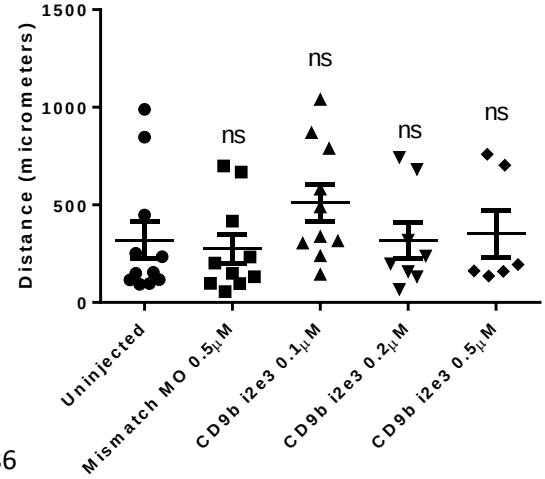
Distance (micrometers)
1500
1000
500
0
ns
ns
ns
ns
Uninjected
Mismatch MO 0.5μM
CD9b i2e3 0.1μM
CD9b i2e3 0.2μM
CD9b i2e3 0.5μM

Figure 3.8 No significant difference in PGC migration was observed in CD9b i2e3 injected and uninjected control embryos .
Representative images of v*asa* RNA *in situ* hybridisation on 30hpf AB embryos which are (a) Uninjected or injected with (a I) Mismatch control morpholino 0.5µM, (a II) CD9b i2e3 0.1µM, (a III) CD9b i2e3 0.2µM or (a IV) CD9b i2e3 0.5µM. No significant difference in the distance between the most anterior and posterior PGC (b) or in the number of ectopic PGC (c). Kruskal-Wallis test with Dunn's multiple comparison test. n= minimum 6 (b II), 10 (b, bI) or 26 (c) per condition. b)- b II) are graphs of individual experimental repeat whereas (c) shows the pooled data of three experiments. p=<0.05

3.2.3 pLLP migration in CD9b morphants

As well as looking at PGC migration, the posterior lateral line was assessed in CD9b morphants. The protocol used was similar to the method used to investigate PGC migration except embryos were allowed to develop to 52hpf, though the pLLP should finish migration by ~42hpf, and the *in situ* hybridisation used a *claudin b* RNA probe as *claudin b* is expressed in the neuromasts and posterior lateral line primordium (Kimmel et al. 1995, Gompel et al. 2001, Haas and Gilmour 2006). Upon injection of CD9b MO1 to give final concentrations of 0.5-2.0µM, it was immediately clear that CD9b morphants had significantly fewer neuromasts deposited and that spacing between the neuromasts was irregular (Figure 3.9a -b). After analysing the lateral line, a significant decrease in the percentage of total body length between the 1st and last deposited neuromasts was also found (Figure 3.9c). This suggested two hypotheses: i) the pLLP is migrating normally and the embryos are just developmentally delayed or ii) the pLLP is migrating abnormally and depositing less neuromasts. If hypothesis i) were correct, it would be expected that the spacing between the 1st and 2nd neuromasts would remain the same as in uninjected embryos. While there is no significant difference in the mean spacing between the 1st and 2nd neuromasts, there is an obvious increase in the variability of spacing between these neuromasts in CD9b morphants (Figure 3.9d). This is also clear in the representative images in Figure 3.9a, in particular 3.9a II, where the second neuromast is almost at the end of the tail. This variability suggests that hypothesis ii) may be correct.

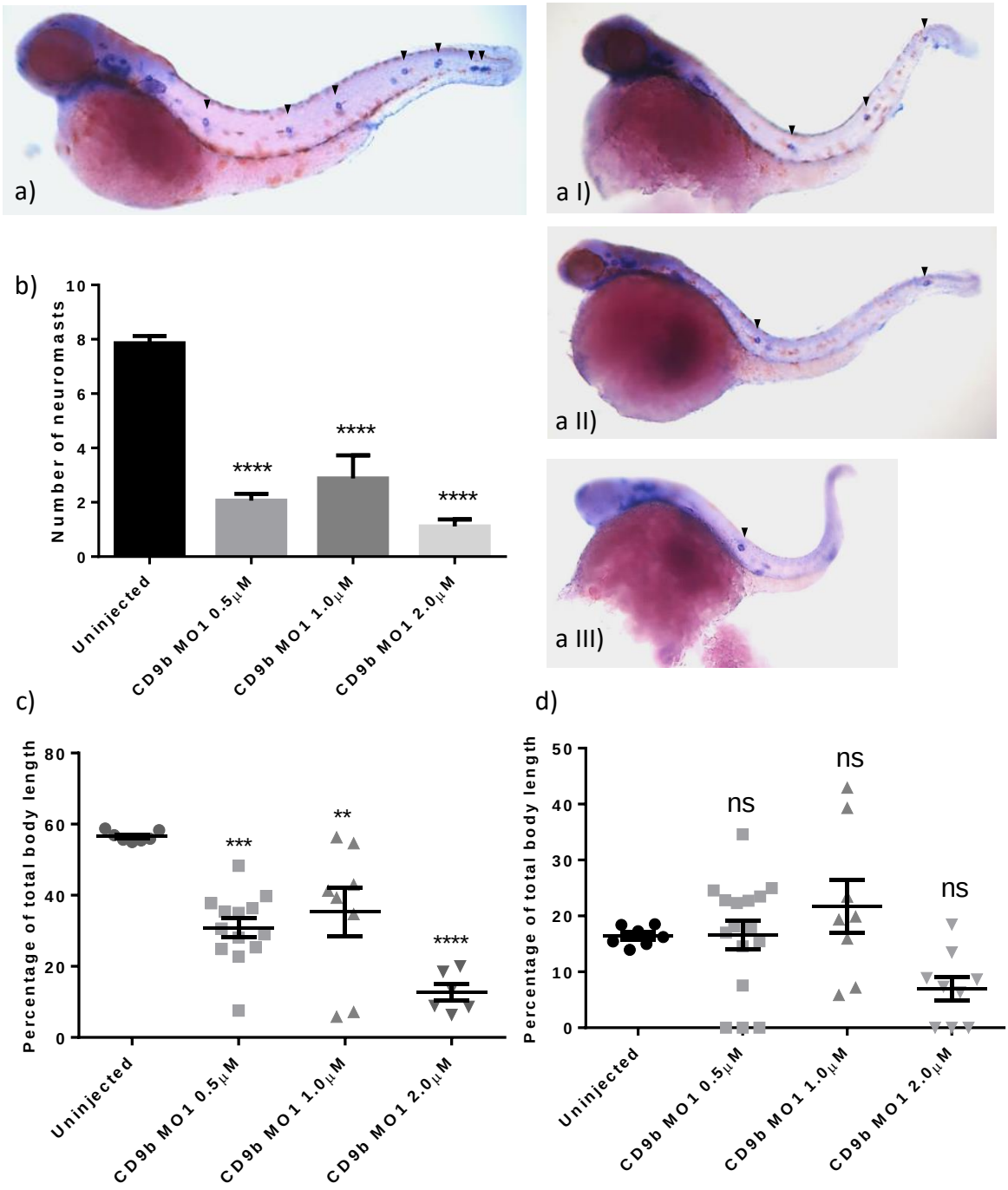

Figure 3.9 Injection of 0.5-2.0µM CD9b MO1 significantly decreases the number of neuromasts deposited by the pLLP and affects their spacing.
Representative images of ISH using a probe for *claudin b* RNA on 52hpf AB embryos that are uninjected (a) or injected with 0.5µM CD9b MO1 (a I), 1.0µM CD9b MO1 (a II) or 2.0 µM CD9b MO1 (a III). Neuromasts indicated by black arrowheads.
There is a significant decrease in the number of neuromasts deposited (b) and the percentage of total body length between the 1st and last neuromast (c) but no change in the mean percentage of total body length between the 1st and 2nd neuromasts (d). ANOVA with Dunnet's multiple comparisons test. n= minimum 6. p=<0.05. Data from a single experiment.

Whilst the lateral line phenotype appears to be strong and specific, the experiments were repeated using lower final concentrations of CD9b MO1 (0.1-0.5µM) to see if the phenotype was still present in embryos that showed fewer developmental abnormalities. CD9b morphants showed the same significant phenotype at the lower final concentrations as seen in embryos with the higher final concentrations of CD9b MO1 (Figure 3.9, 3.10). This was observed in two individual experimental repeats which have been pooled for Figure 3.10. Lower MO1 concentrations caused decreased neuromasts deposition, irregular spacing between neuromasts and less spacing between the first and last neuromasts (Figure 3.10). Although the CD9b morphants in Figures 3.9 and 3.10 appear slim in comparison to their uninjected counterparts, it does not seem likely that the lateral line phenotype is a consequence of the embryos general morphology. A further repeat of this experiment was carried out and the same lateral line phenotype was seen, even though the embryos appeared to have noticeably more wildtype morphology than the CD9b morphants in Figures 3.9 and 3.10 (Figure 3.12a). This repeat was not pooled with the rest of the lateral line data as the experiment was carried out later on in the project and the CD9b MOs had to be re-optimised as the concentrations of the MOs had increased during storage.

A second MO, CD9b i2e3, was used to confirm that the lateral line phenotypes seen were not off target effects of CD9b MO1. The same lower concentrations (0.1-0.5µM) were used and embryos were raised and stained using the same protocol. CD9b i2e3 morphants appeared to develop less general abnormalities (Figure 3.11a) and yet still showed a significant decrease in the number of neuromasts deposited in both experimental repeats (Figure 3.11b - b I). Only embryos with 0.5µM CD9b i2e3 showed a slight decrease in the percentage of body length between the first and last neuromast, indicating that the lack of neuromasts was not due to delayed primordium migration (Figure 3.11b - c). There was also irregular spacing seen between the 1st and 2nd neuromast in CD9b i2e3 morphants and embryos with 0.2µM CD9b i2e3 showed a significant increase in the mean spacing between these neuromasts, a phenotype which was replicated for multiple concentrations of CD9b MO1 and CD9b i2e3 in Figure 3.12e.

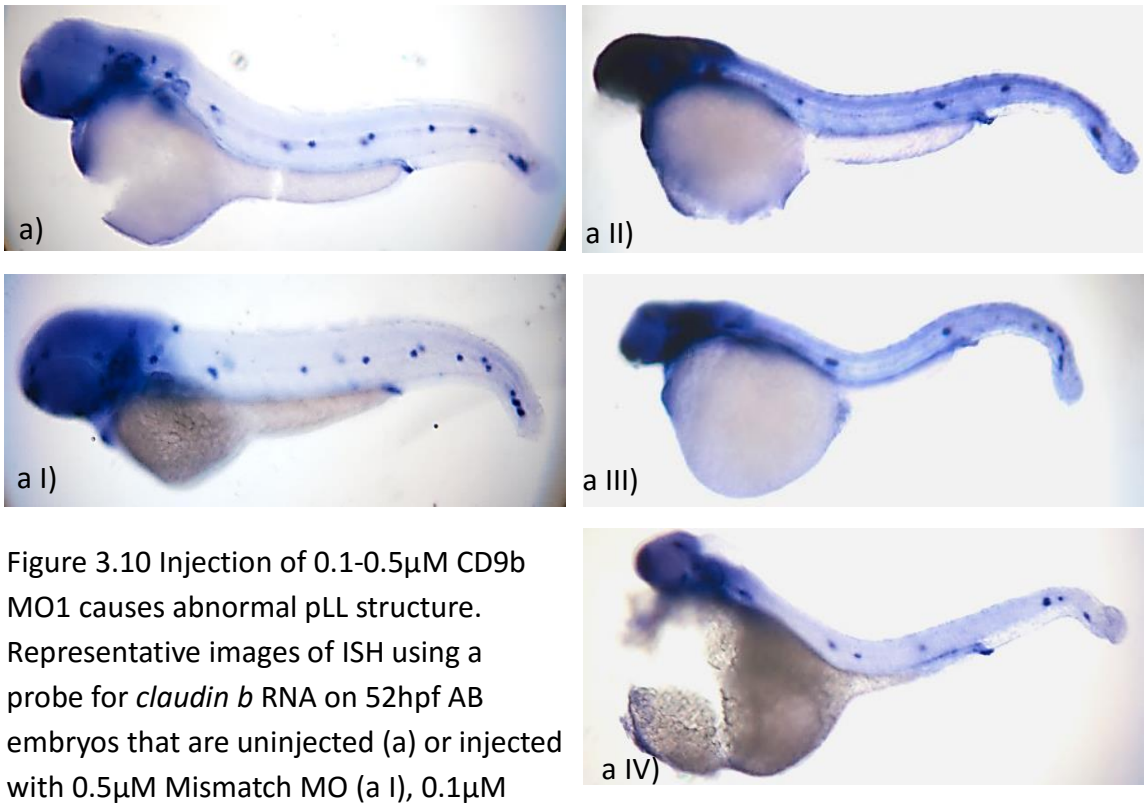

Figure 3.10 Injection of 0.1-0.5µM CD9b MO1 causes abnormal pLL structure. Representative images of ISH using a probe for *claudin b* RNA on 52hpf AB embryos that are uninjected (a) or injected with 0.5µM Mismatch MO (a I), 0.1µM CD9b MO1 (a II), 0.2µM CD9b MO1 (a III) or 0.5 µM CD9b MO1 (a IV). There is a significant decrease in the number of neuromasts deposited (b) and the percentage of total body length between the 1st and last neuromast (c) but no change in the mean percentage of total body length between the 1st and 2nd neuromasts (d). ANOVA with Dunnett's multiple comparisons test. n= minimum 9 (c,d) and minimum 12 (b). p=<0.05. Pooled data from two experiments.

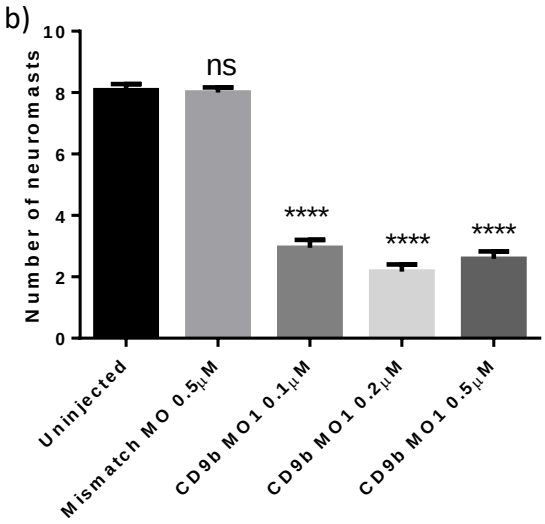

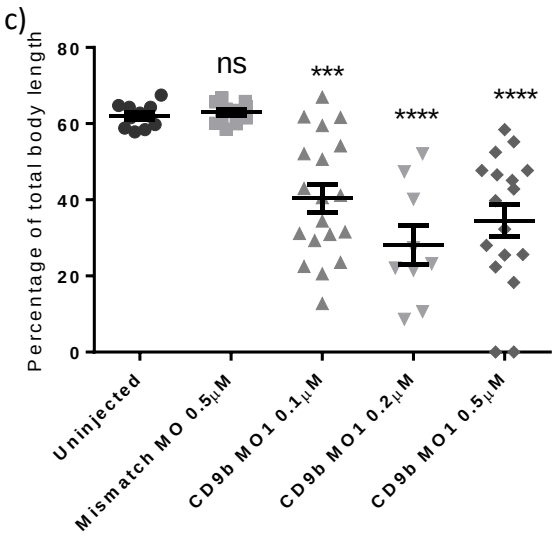

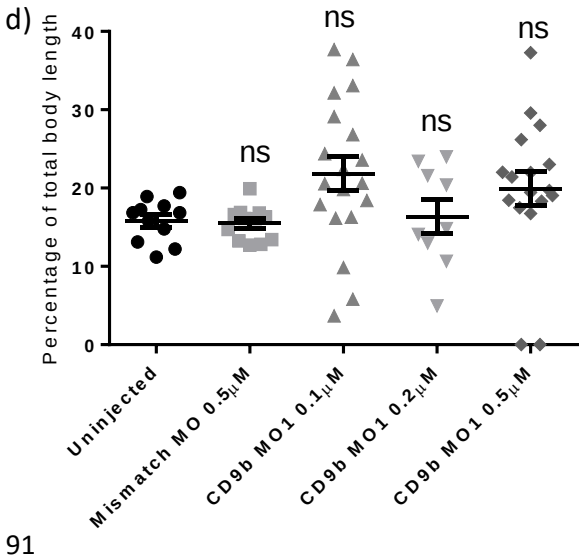

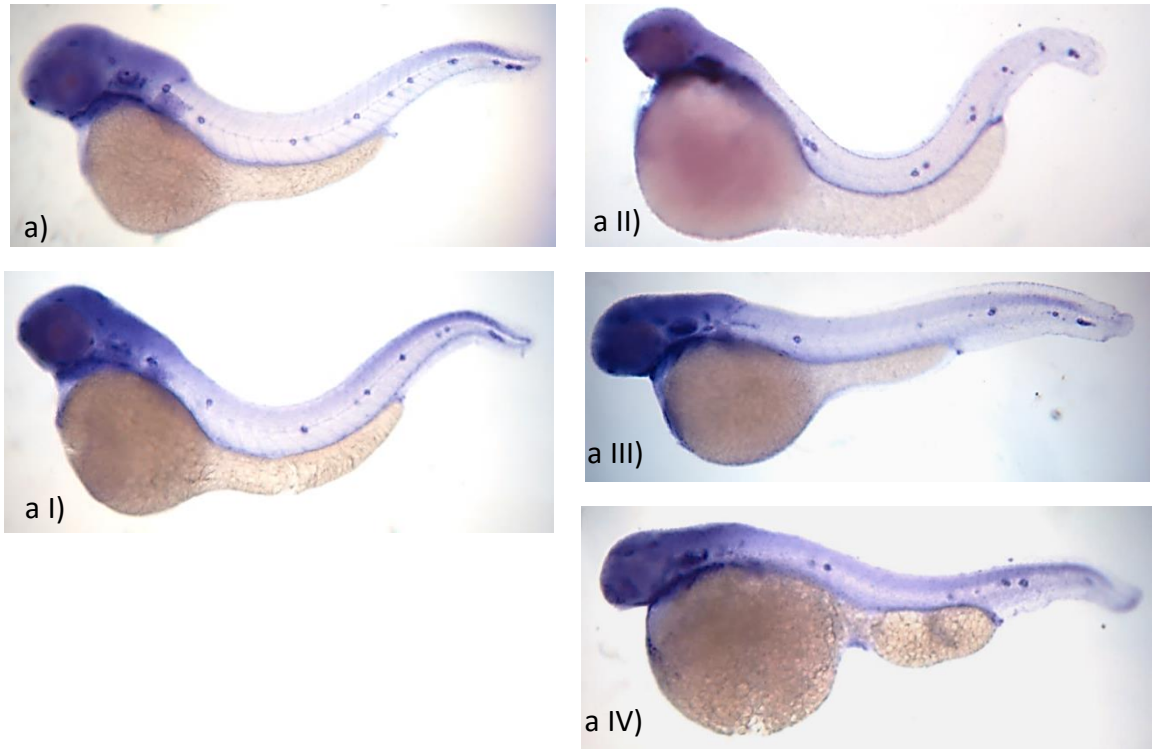

Figure 3.11 Injection of 0.1-0.5µM CD9b i2e3 causes abnormal pLL structure. Representative images of *claudin b in situ* hybridisation on 52hpf AB embryos that are (a) Uninjected or injected with (a I) 0.5µM Mismatch MO, (a II) 0.1µM CD9b i2e3, (a III) 0.2µM CD9b i2e3 or (a IV) 0.5µM CD9b i2e3.

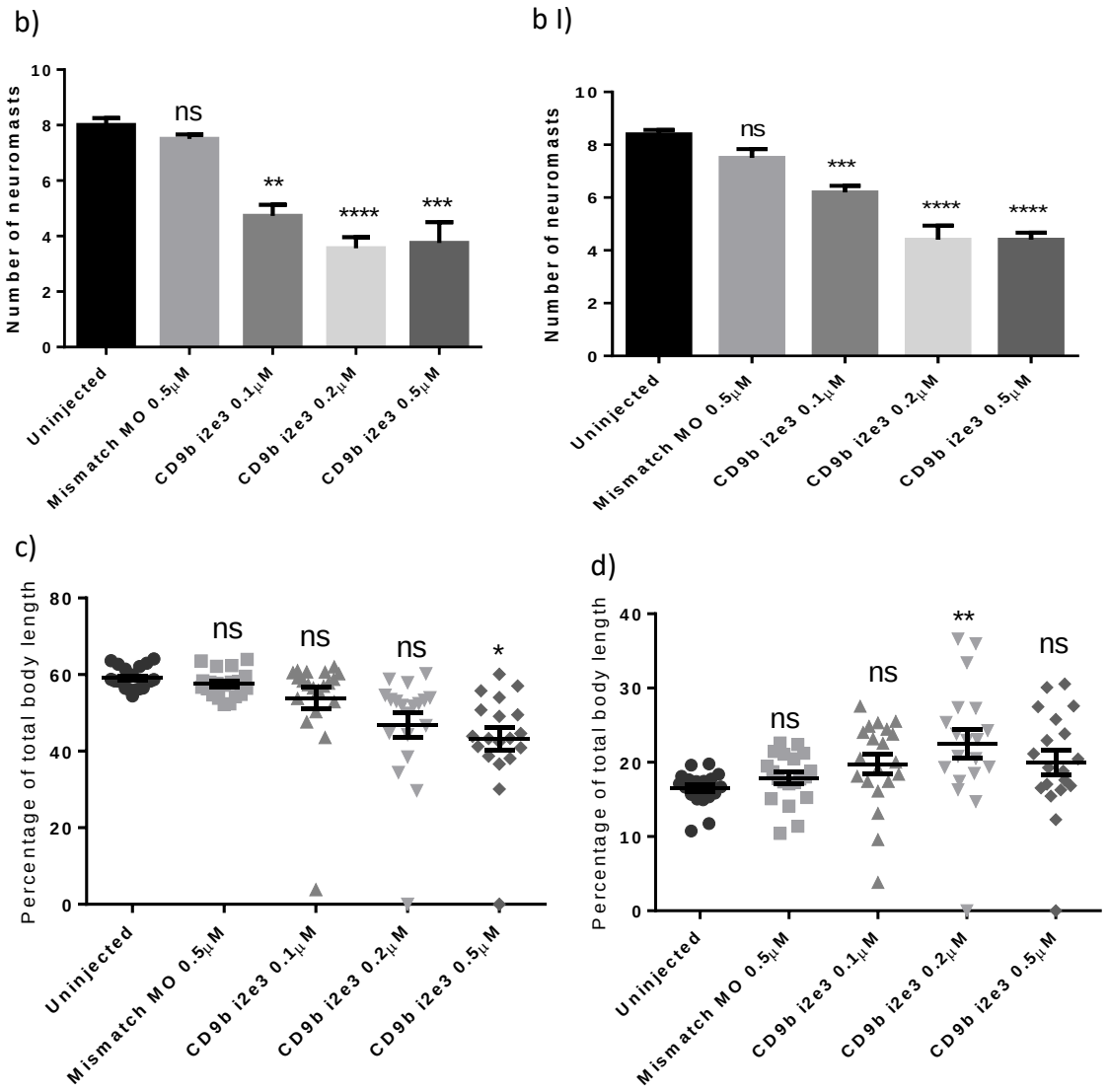

Figure 3.11 Injection of 0.1-0.5µM CD9b i2e3 causes abnormal pLL structure continued.

A Kruskal-wallis test with Dunn's multiple comparisons test shows a significant decrease in the number of neuromasts deposited (b- b I). After $\log_{10}$ transforming the data, an ANOVA with Dunnett's multiple comparisons test found no difference in the percentage of total body length between the 1st and last neuromasts (c) and limited significance in the percentage of total body length between the 1st and 2nd neuromasts (d). n= minimum 10 (b, b I), minimum 19 (c,d). b and b I show data from individual experiments, c-d show pooled data of two experiments. p=<0.05

The data shown in Figure 3.12 is from experiments conducted further on in the project during the re-optimisation of the CD9b MO concentrations for an alternative experiment, to make sure these concentrations produced the same phenotypes as seen previously. Embryos born to the same set of adult fish were injected with either CD9b MO1 or CD9b i2e3 during a single experiment and so any differences seen between the morpholinos will not be due to environmental or genetic background differences. Embryos injected with either CD9b MO1 or CD9b i2e3, but not the mismatch or uninjected embryos, showed a significant decrease in neuromasts deposited (Figure 3.12a, c). In embryos injected with CD9b i2e3, there was no difference in the percentage of trunk length between the 1st and last neuromast or in the percentage of trunk length between the ear and the last neuromast/primordium (Figure 3.12b, d). This suggests that primordium migration was not stalled and the deposition of the 1st and last neuromasts were in the expected positions, however, there are fewer neuromasts deposited within this space (Figure 3.12b-d).

For embryos injected with CD9b MO1, there is a decrease in the percentage of trunk length between the 1st and last neuromasts. This could either be due to the primordium not migrating as far in the CD9b MO1 morphants or the 1st neuromast being deposited in a more posterior position (Figure 3.12d). The additional assay, displaying the percentage of trunk length between the ear and the last neuromast/primordium, shows that the primordium has migrated as far in embryos with 0.1µM CD9b MO1 as in uninjected embryos, suggesting the latter may be the case for these embryos. Embryos with 0.2 or 0.4 µM CD9b MO1 show a decrease in the percentage of trunk length between the ear and primordium as well as a decrease in the percentage of trunk length between the 1st and last neuromasts. However, there is a larger decrease in the percentage of trunk length between the 1st and last neuromasts. This suggests that the 1st neuromast may have been deposited in a more posterior position and the primordium is stalling prematurely or migrating more slowly (Figure 3.12b, d). Irregular spacing was seen in all of the CD9b morphants with an obvious variation or increase in the percentage of trunk between the 1st and 2nd neuromasts (Figure 3.12e).

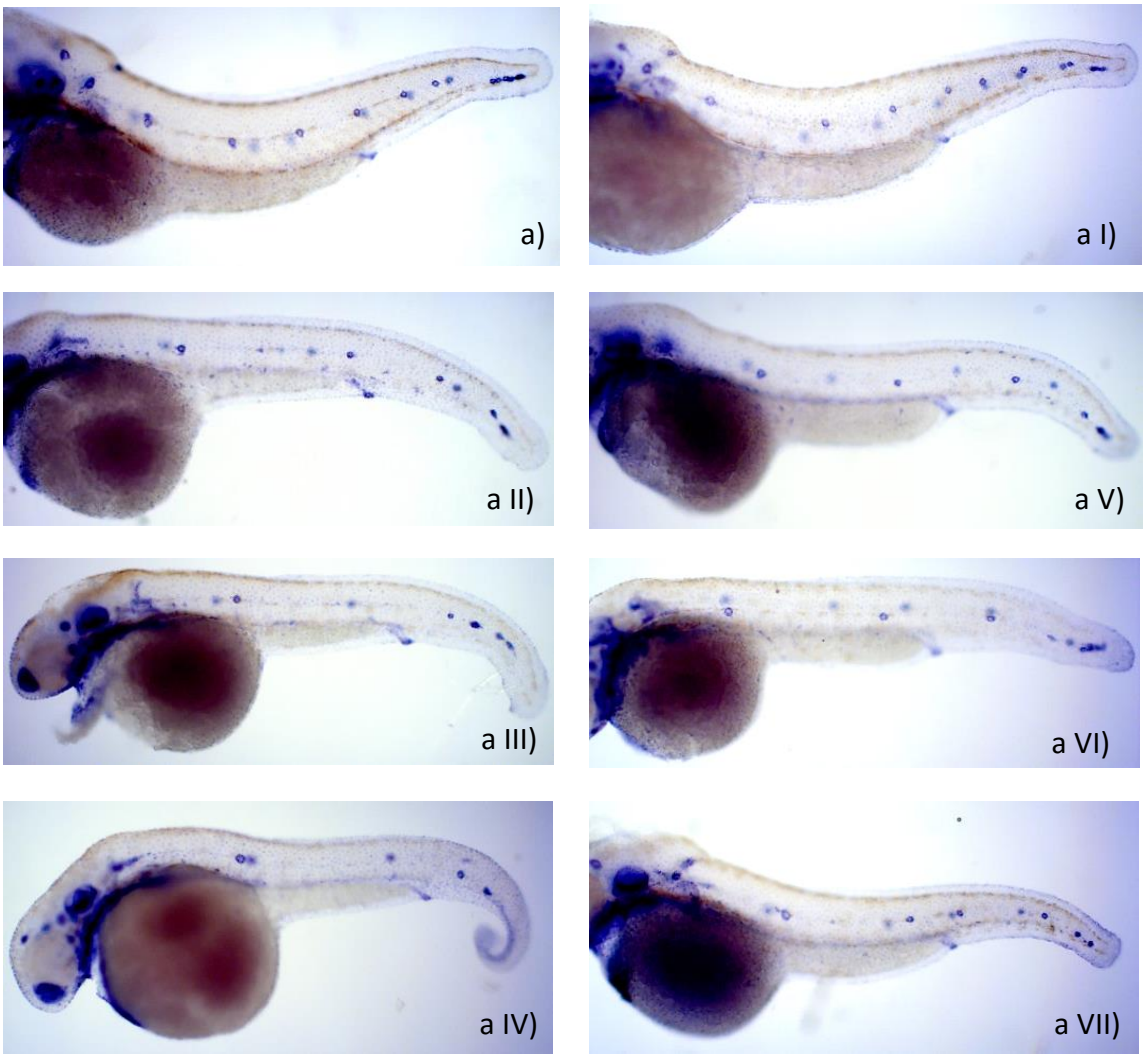

Figure 3.12 Injection of either CD9b MO1 or CD9b i2e3 causes abnormal pLL structure.

Representative images of uninjected (a) embryos and embryos injected with 0.5µM Mismatch MO (a I), 0.1µM CD9b MO1 (a II), 0.2µM CD9b MO1 (a III), 0.4µM CD9b MO1 (a IV), 0.1µM CD9b i2e3 (a V), 0.2µM CD9b i2e3 (a VI) or 0.4µM CD9b i2e3 (a VII), stained for *claudin b*.

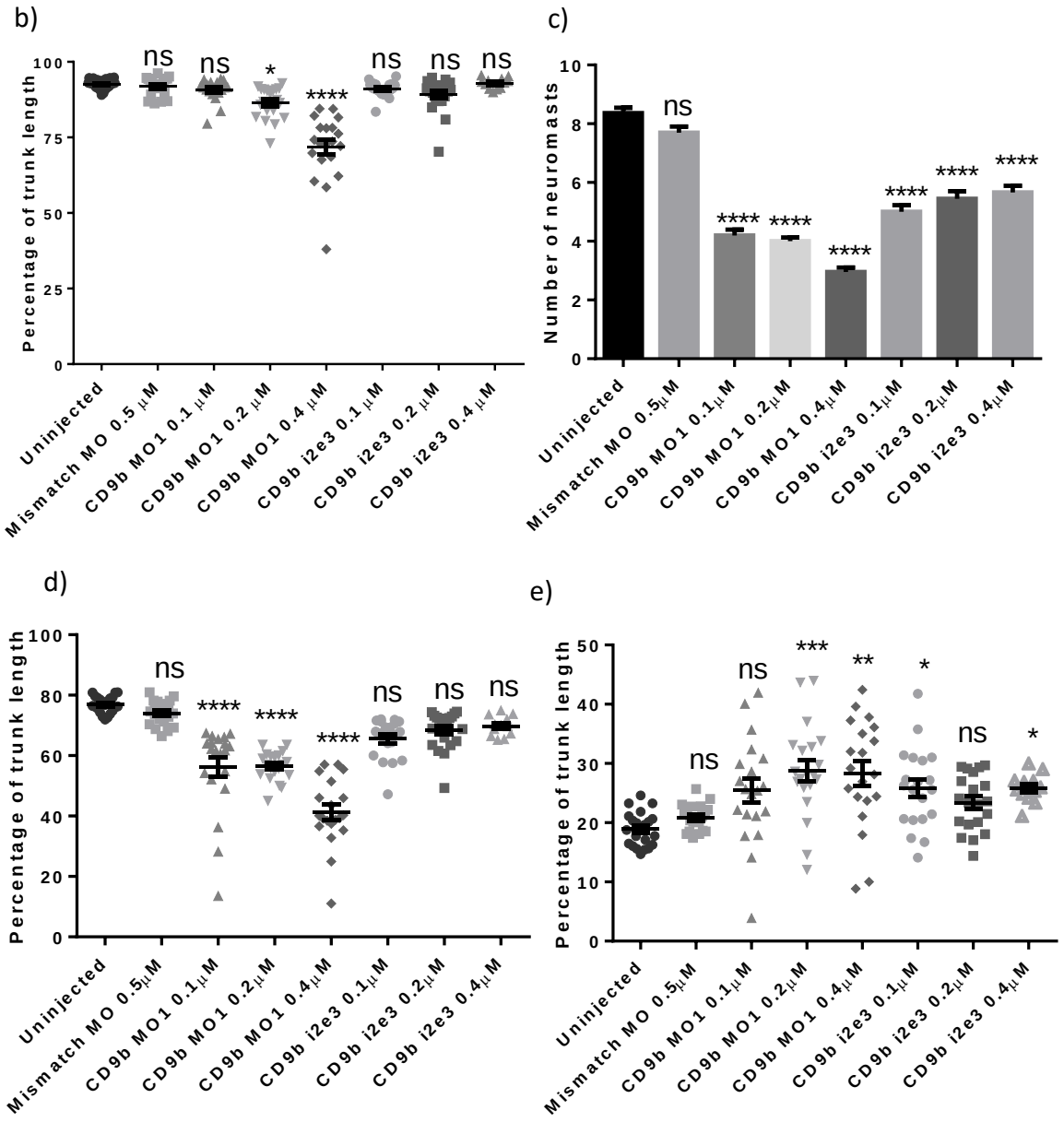

Figure 3.12 continued. Injection of either CD9b MO1 or CD9b i2e3 causes abnormal pLL structure.

The percentage of trunk length between the ear and last neuromast/primordium remains the same in most of the CD9b morphants (b), however the number of neuromasts deposited in this space is significantly decreased (c). The percentage of trunk length between the 1st and last deposited neuromast is decreased in CD9b MO1 morphants but not CD9b i2e3 morphants (d) and the percentage of trunk length between the 1st and 2nd neuromasts is highly variable in CD9b morphants but the mean is often significantly larger (e).

The percentage of trunk length, defined as between the ear and tail tip, was used as the experiment was carried out after TALEN work where this measurement had been preferable. ANOVA with Dunnett's multiple comparisons test was used for all data sets, although b,d and e were $\log_{10}$ transformed beforehand. n= minimum 12 lateral lines analysed per condition. p=<0.05. Data from a single experiment.

3.3 Discussion

In this chapter morpholinos against *cd9b* were used to assess whether *cd9b* knockdown affected the CXCR4b-mediated processes of PGC and pLLP migration. While initial results suggested that CD9b may play a role in PGC migration, this significance was only seen with one morpholino, CD9b MO1, when injected at higher volumes and was seen in the only experiments where the controls showed no abnormally migrated PGCs (Figures 3.6-3.8). The lack of change in the number of ectopic PGCs seen in CD9b morphants supports the hypothesis that the significance seen in Figure 3.6b is due to single PGCs migrating abnormally and not due to a mass disruption of PGC migration. Together these results suggest that CD9b does not play a significant role in PGC migration.

It appears more likely that CD9b plays a significant role in correct neuromast deposition by the pLLP. In CD9b morphants the pLL, while able to complete migration, always displayed decreased numbers of neuromasts in CD9b morphants. The neuromasts were consistently deposited in an irregular fashion, as displayed by the wide range of percentages of total body/trunk length between the 1^{st} and 2^{nd} neuromasts, often with an average overall increase in the spacing between these neuromasts. Many CD9b MO1 injected embryos also showed a decrease in the percentage of trunk between the first and last neuromasts, as well as a decrease in the percentage of trunk migrated by the primordium, suggesting that the pLLP has delayed or slower migration. This phenotype is only observed once in 0.5 µM CD9b i2e3 injected embryos (Figure 3.11) which are also the only CD9b i2e3 morphants to show general morphological abnormalities. This decrease in the percentage of trunk between the first and last neuromasts is not repeated in 0.5 µM CD9b i2e3 injected embryos in Figure 3.12 that do not show general abnormalities. One potential explanation for this difference could be that the delayed migration is an off-target effect of the general abnormalities seen in CD9b MO1 morphants and the morphants with 0.5µM CD9b i2e3 in Figure 3.11. The difference in the mechanisms of CD9b MO1 and CD9b i2e3 action could be a second explanation for this phenotype difference. As a translation-blocker, CD9b MO1 prevents translation of both maternal and zygotic transcripts (Nasevicius and Ekker 2000). In contrast, CD9b i2e3 blocks a splice acceptor site which would be expected to cause a loss of function through exon deletion

(Draper et al. 2001, Morcos 2007). As maternal transcripts are already spliced, CD9b i2e3 only causes knockdown of zygotic transcripts. This could suggest that the decrease in the percentage of trunk between the first and last neuromasts and the decrease in the percentage of trunk migrated by the primordium seen in CD9b MO1 could be due to loss of maternal *cd9b* RNA. However, the significant decrease in the percentage of trunk between the first and last neuromasts seen in CD9b i2e3 injected embryos in Figure 3.11 does not support this hypothesis. Lastly, the efficiency of CD9b i2e3 knockdown of *cd9b* could also explain the different phenotypes. It would be expected that CD9b i2e3 would result in the deletion of exon 3, causing a loss of protein function. However, it is possible that either a partially or differentially functional protein was produced or a cryptic splice site was activated (Draper et al. 2001, Morcos 2007). Either of these results would decrease the efficiency of CD9b knockdown and could explain the decreased severity in phenotypes seen with CD9b i2e3 compared to CD9b MO1. It appears unlikely; however, that a cryptic splice site would be activated as CD9b i2e3 is a splice acceptor site blocker not a splice donor site blocker. Splice acceptor sites are more complicated than splice donor sites and must be adjacent to a polypyrimidine tract therefore CD9b i2e3 is less likely to have revealed a cryptic splice acceptor site (Morcos 2007). This hypothesis could be investigated further by conducting RT-PCR on CD9b i2e3 injected embryos to characterise the outcomes of blocking the intron 2 – exon 3 splice site. Not only would this show whether exon 3 was deleted or whether a cryptic splice site was activated but it would also show the efficiency of the splice blocking due to the ratios of the different PCR products that the alternative splicing events would create.

The decreased numbers of neuromasts and irregular spacing between them do appear to be specific to *cd9b* deficiency. These neuromast phenotypes were consistently seen in CD9b morphants, in embryos with and without general morphological abnormalities. They were reproduced in multiple experimental repeats and seen using both CD9b MO1 and CD9b i2e3 morpholinos which bind to different sequences in *cd9b.* The lack of disrupted neuromast deposition in the uninjected, ringer's buffer injected or mismatch MO injected embryos indicate that the phenotype is not due to the embryos used, injection technique or morpholino structure toxicity and so supports the hypothesis that these phenotypes are specific.

This recapitulates and expands on the work by Gallardo et al., 2010 which suggested a role for CD9b in the lateral line development.

The specificity of the MO phenotypes could be investigated further using a number of different experiments, such as mRNA rescue or co-injection with a p53 MO. RT-PCR could also be used to assess the specificity of the phenotypes seen. The efficiency of CD9b i2e3 splice-blocking activity at a range of concentrations could be analysed by looking at the ratio of the normal to abnormally spliced PCR products. These efficiencies could then be compared to the general abnormalities and the pLL phenotypes seen in CD9b i2e3 morphants. If concentrations are found where the splice-blocking efficiency is high and the pLL phenotypes are observed but the general abnormalities are not, this would support the hypothesis that the pLL phenotypes are specific to *cd9b* knockdown. However, recapitulation of a MO phenotype in a mutant line is currently the gold standard. Therefore, I decided to create CD9b knock-out mutant lines to see if the phenotypes could be reproduced.

Chapter 4: CD9b deletion mutants

4.1 Introduction

TALENs (transcription activator like effector nucleases) are comprised of two different domains, a customisable DNA binding domain and a nuclease domain (Figure 4.1) (Miller et al. 2011, Zhang et al. 2011). The DNA binding domain is made from a modified TALE, Transcription Activator Like Effector protein, from the plant pathogen *Xanthomonas* (Boch et al. 2009, Miller et al. 2011, Zhang et al. 2011). The DNA binding ability of TALE proteins comes from a central repeat domain where every repeat contains the same 34 amino acids, except for two hypervariable amino acids at positions 12/13. Each repeat corresponds to a single base in the target DNA and amino acids at positions 12/13 dictate which base the repeat binds to, for example a repeat with the amino acids N I at positions 12/13 will bind an adenine base (Figure 4.1) (Boch et al. 2009). Different combinations of these repeats allow sequence specific DNA binding domains to be created.

After the discovery of the TALE repeat- DNA base code, Miller et al., 2011 created TALENs. They found that modified TALEs could be coupled to the catalytic domain of the endonuclease FokI, which activates to create double strand DNA breaks (DSBs) upon dimerization. Two sequence specific TALE binding domains, each coupled to a FokI nuclease domain allowed Miller et al., 2011 to specifically target and induce mutations in two human genes, *NTF3* and *CCR5* (Figure 4.1). Mutations were induced through the error-prone endogenous repair of the TALEN-induced DSBs by non-homologous end joining (NHEJ).

TALENs have since been used successfully in zebrafish embryos to produce mutations in many target genes (Huang et al. 2011, Sander et al. 2011, Dahlem et al. 2012, Moore et al. 2012, Cade et al. 2012). Embryos injected with varying amounts of TALENs, from 4-600pg, showed higher mutation frequencies, lower toxicity rates and higher specificity than Zinc Finger Nucleases, which had been used previously to induce targeted mutations. The mutations induced were commonly small insertions and/or deletions (indels) of approximately 10bps, although mutations of a few hundred base pairs were also reported. These

indels often caused frameshifts and nonsense stop codons. (Huang et al. 2011, Sander et al. 2011, Dahlem et al. 2012, Moore et al. 2012, Cade et al. 2012)

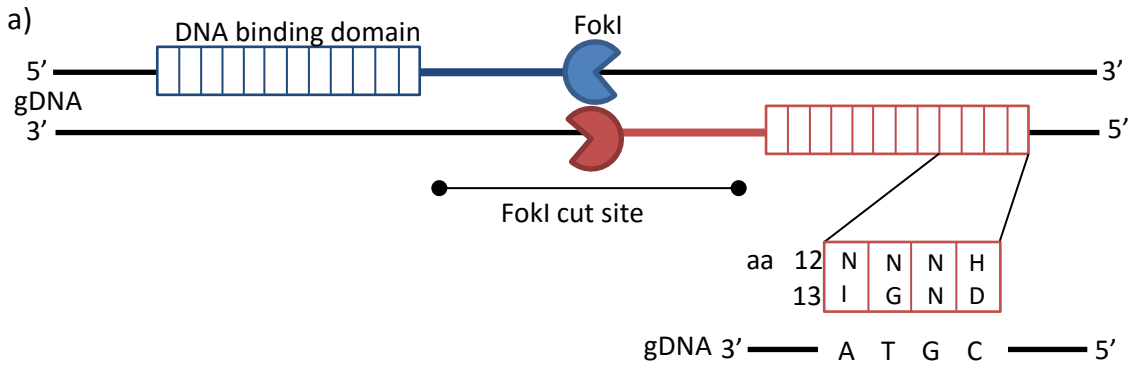

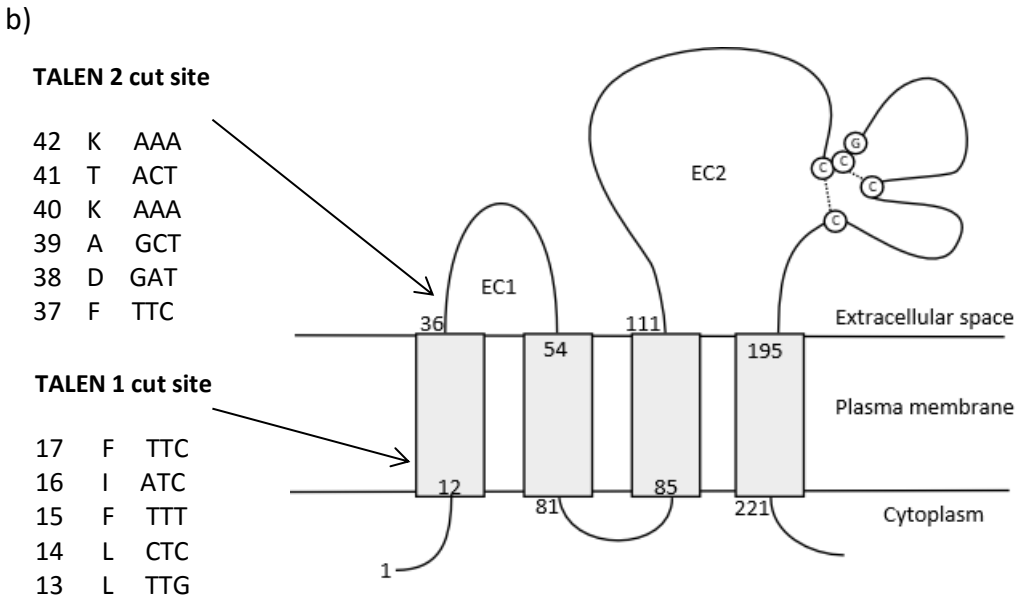

Figure 4.1 Diagram of *cd9b* TALEN structure (a) and their predicted cut sites in CD9b (b).
The cut sites in (b) are represented by amino acid number, their one letter code and nucleic acid sequence, from left to right respectively. The numbers on the diagram of CD9b in (b) show the amino acid number at that part of the structure. The di-sulphide bonds between the conserved CCG motif and conserved cysteines are indicated by the dashed lines. EC1/2= Extracellular domain 1/2, aa= amino acid

Two CD9b TALENs were designed by ZgeneBio using the program 'TEL Effector Nucleotide Targeter 2.0'. The TALENs were designed to target Exon 1, with TALEN 1 predicted to cut in the 1st transmembrane domain and TALEN 2 in the EC1 (Figure 4.1b). With these TALENs, pLLP and PGC migration was analysed in CD9b mosaic embryos as well as in CD9b homozygous mutants, which were created as described by Figure 4.2.

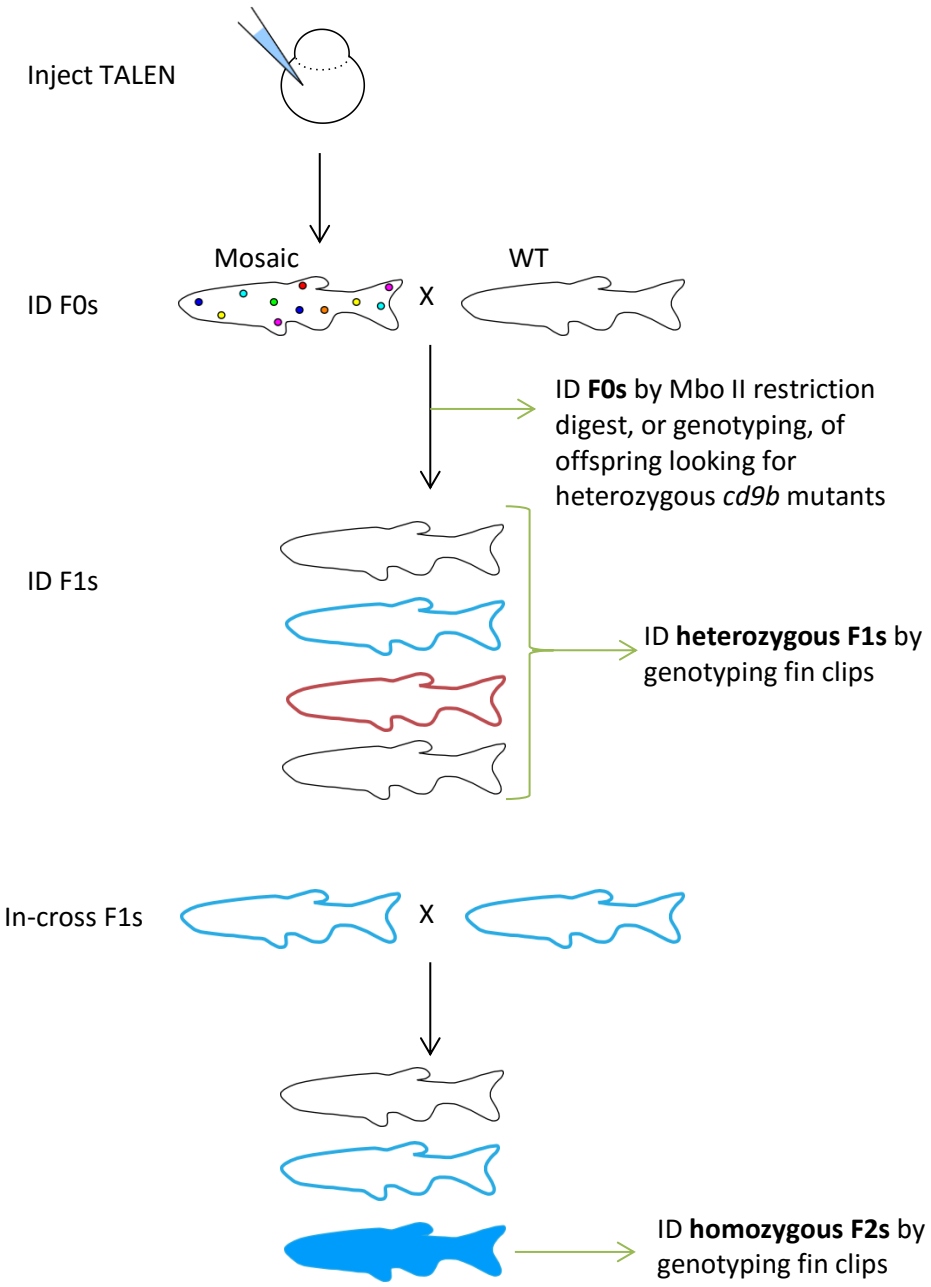

Figure 4.2 Diagram showing the production of homozygous mutants from TALEN injected embryos.
Wildtype fish are shown as a black outline, heterozygous mutants display a coloured outline, different colours indicate different mutant alleles, and homozygous mutants are colour filled. Fish were raised for roughly 3 months before fin clips were taken or the fish were first crossed. ID = identify
F0s are mosaic fish that have mutations in their germ cells and so have offspring that carry a mutation.

4.2 Results

4.2.1 Assessment of TALEN toxicity

Viability curves looking at the survival of embryos injected with a range of TALEN amounts, were initially created to find out how much TALEN mRNA to inject to create mosaic adults (Figures 4.3a,4.4a). Embryos injected with 400pg TALEN 1 showed decreased embryo survival over the first 24hpf. However, injection of 50 or 200pg of TALEN 1 did not induce decreased embryo survival compared to uninjected embryos (Figure 4.3a).

The general morphology of the injected embryos was also assessed over the same time period as the viability curves. Again it appeared that only the embryos injected with 400pg TALEN 1 showed any difference to the uninjected embryos, with an increased percentage of embryos displaying severe phenotypes at 24hpf (Figure 4.3b). Phenotypes seen in TALEN injected embryos included delayed development, smaller heads and kinked tails. Any phenotypes seen in TALEN 1 injected embryos appeared to be rescued over the next 48 hours, with the majority of embryos showing wildtype phenotype by 48 and 72hpf (Figures 4.3c,d). It was decided that using 400pg TALEN 1 would be investigated further as the decrease in survival suggests that the TALEN is active but there is still a ~25% survival rate and the embryos appear to recover from any initial developmental delay (Figure 4.3).

Survival and general phenotypes were also assessed in TALEN 2 injected embryos (Figure 4.4). Interestingly, TALEN 2 appeared more toxic than TALEN 1 with both 200 and 400pg TALEN 2 inducing decreased survival (Figure 4.4a). This was also reflected in the general phenotypes seen, as both 200 and 400pg TALEN 2 caused an increase in the percentage of embryos with mild, moderate and severe phenotypes in comparison to uninjected embryos. Unlike TALEN 1 injected embryos, TALEN 2 injected embryos did not appear to recover as efficiently from the abnormal phenotypes seen at 24hpf with a percentage of TALEN 2 injected embryos still showing moderate and severe phenotypes at 72hpf (Figure 4.4b-d).

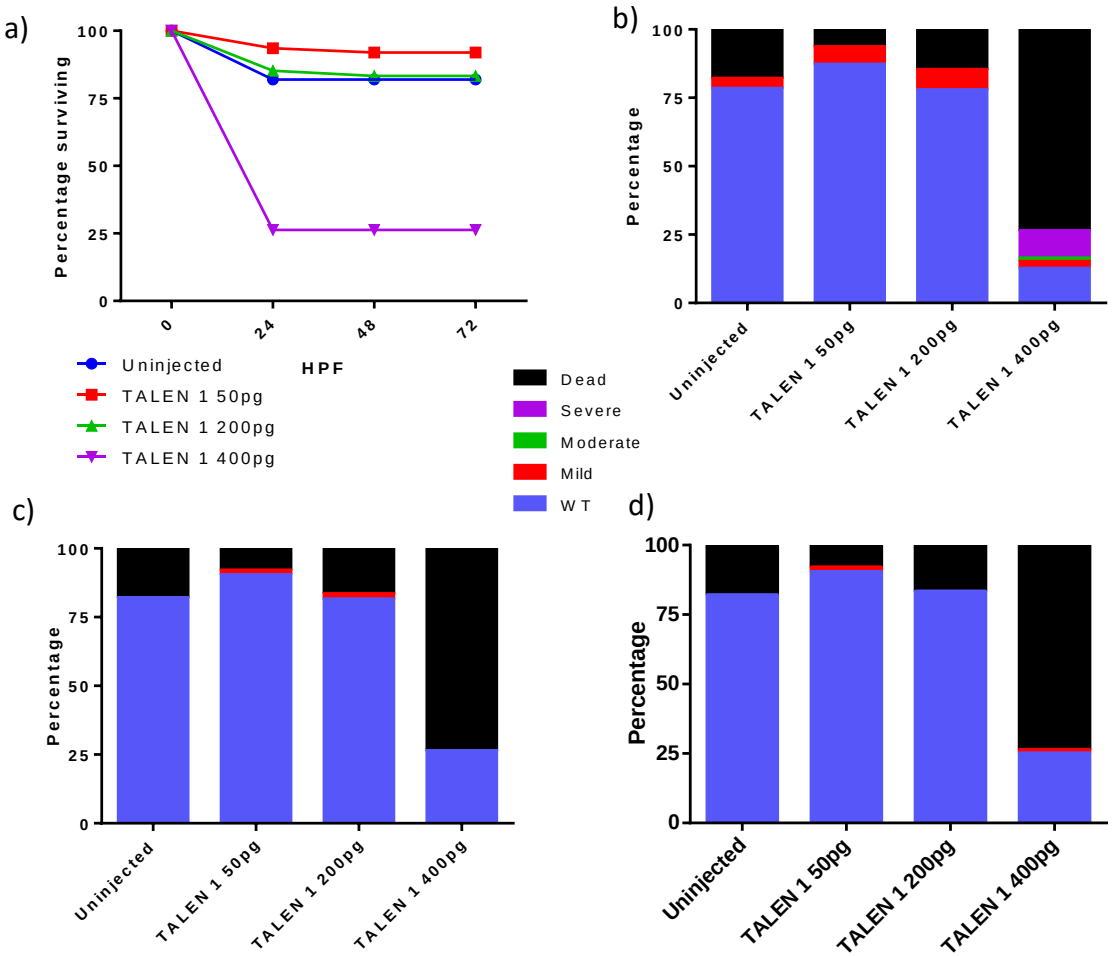

Figure 4.3 Embryos injected with 400pg TALEN 1 show decreased viability and an increase in abnormal phenotypes at 24hpf.

Viability curve showing survival of TALEN 1 injected embryos over 72hpf (a). General abnormal phenotypes seen in TALEN 1 injected embryos at 24 (a), 48 (b) and 72 (c) hpf. Phenotypes defined as described in Chapter 3, Figure 3.3. n= minimum 50 per condition. Data from single experiment.

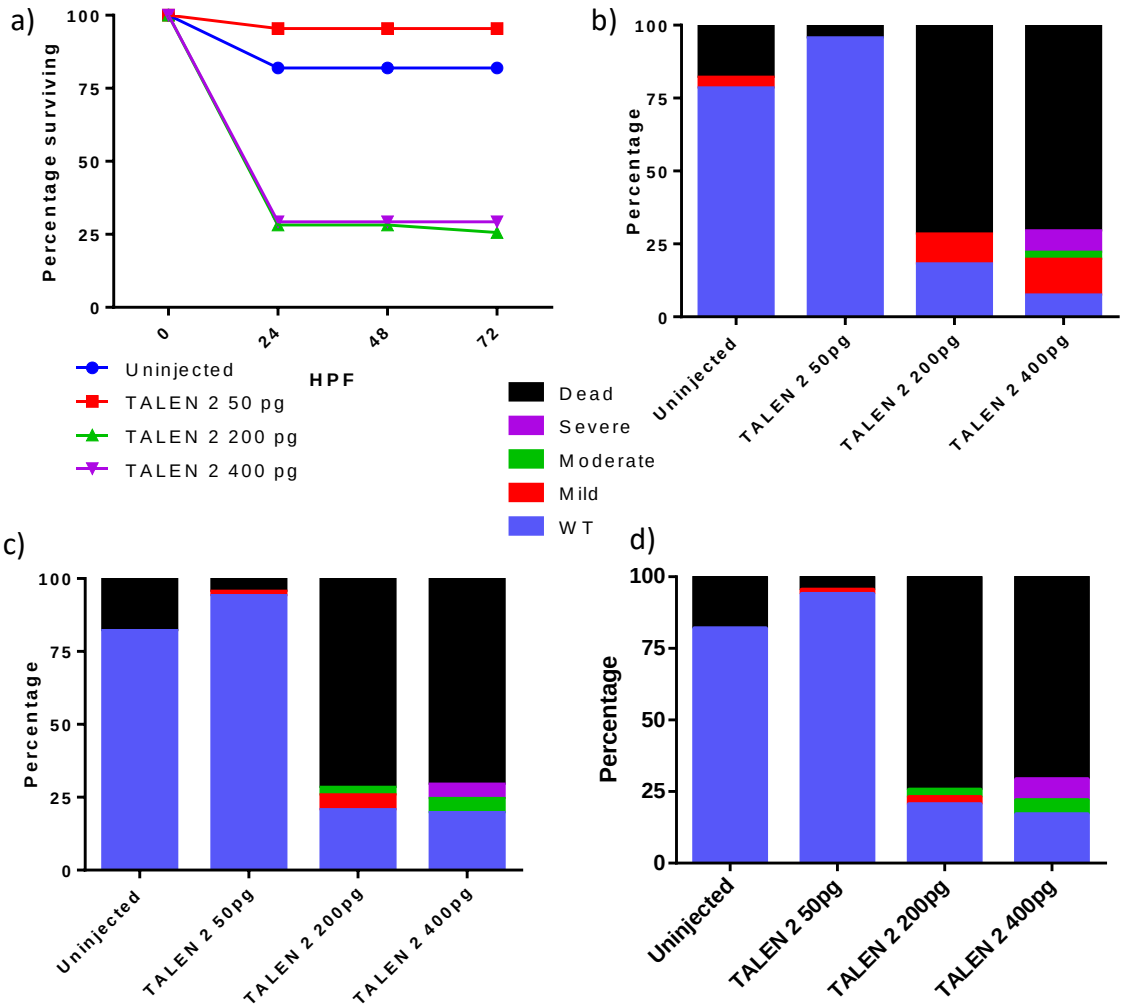

Figure 4.4 Embryos injected with 200pg or 400pg of TALEN 2 show decreased viability and an increase in abnormal phenotypes oer 72hpf.

Viability curve showing survival of TALEN 2 injected embryos over 72hpf (a). General abnormal phenotypes seen in TALEN 2 injected embryos at 24 (a), 48 (b) and 72 (c) hpf. Phenotypes defined as described in Chapter 3, Figure 3.3. n= minimum 39 per condition. Data from single experiment.

4.2.2 Creating *cd9b* mosaic zebrafish

As 400pg of TALEN 1 and TALEN 2 had a ~25% survival rate and showed predominantly wildtype embryos by 72hpf, embryos injected with TALEN 1 or TALEN 2 were genotyped at 72hpf to assess whether the TALENs were inducing mosaicism. Whilst the uninjected embryos showed homozygous wildtype sequence around the TALEN 1 cut site, embryos injected with 400pg TALEN 1 showed clear mosaicism around the TALEN cut site (Figure 4.5).

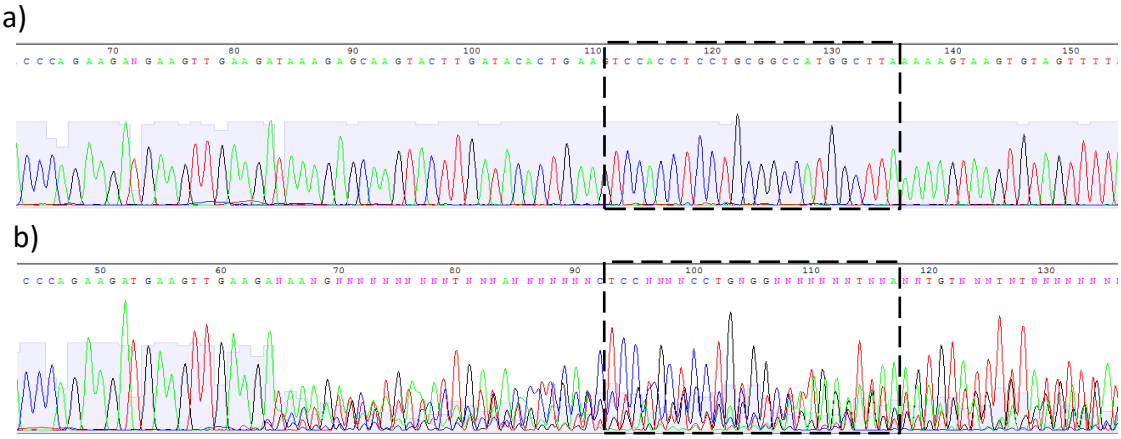

Figure 4.5 Injection of 400pg *cd9b* TALEN 1 at the 1-cell stage causes mosaicism in the genomic sequence of *cd9b* in 72hpf embryos.
Uninjected (a) embryos show the wild-type *cd9b* sequence whereas TALEN 1 (b) injected embryos show large amounts of mosaicism around the cut site (dashed box). n= 4 per genotype. Data from a single experiment.

TALEN 2 injected embryos did not show any mosaicism around the TALEN cut site and appeared no different to the uninjected embryos (Figure 4.6). None of the 14 TALEN 2 injected embryos assessed showed mosaicism, suggesting that the lack of mosaicism is not due to selecting an unaffected embryo by chance.

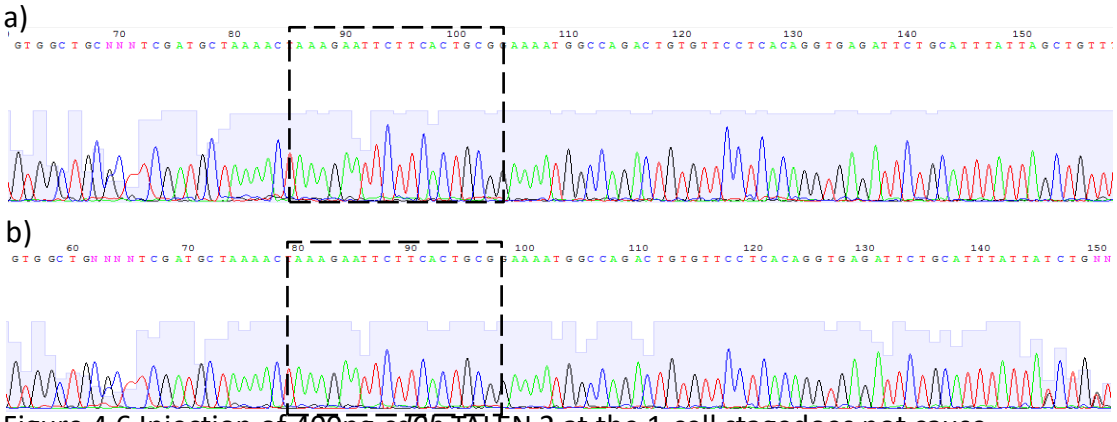

Figure 4.6 Injection of 400pg *cd9b* TALEN 2 at the 1-cell stagedoes not cause mosaicism in the genomic sequence of *cd9b* in 72hpf embryos.
Uninjected (a) and TALEN 2 injected (b) embryos show the wild-type *cd9b* sequence around the cut site (dashed box), suggesting that TALEN 2 is not inducing double-strand breaks in *cd9b*. n= 8 (a), 14 (b). Data from two experiments.

As TALEN 2 does not appear to causing mosaicism in the predicted site, 400pg TALEN 1 was injected into 1-cell stage AB embryos to create mosaic adult F0s. While the embryos were being raised to adulthood, which takes roughly 3 months, mosaic TALEN injected embryos were examined for PGC and pLLP phenotypes. Though a PGC phenotype was not expected, due to the absence of a phenotype in CD9b morphants, PGC migration was assessed in TALEN 1 injected embryos. As expected, TALEN 1 injected embryos did not show any PGC phenotypes, neither the distance between the most anterior and posterior PGCs or the number of ectopic PGCs were significantly different (Figure 4.7).

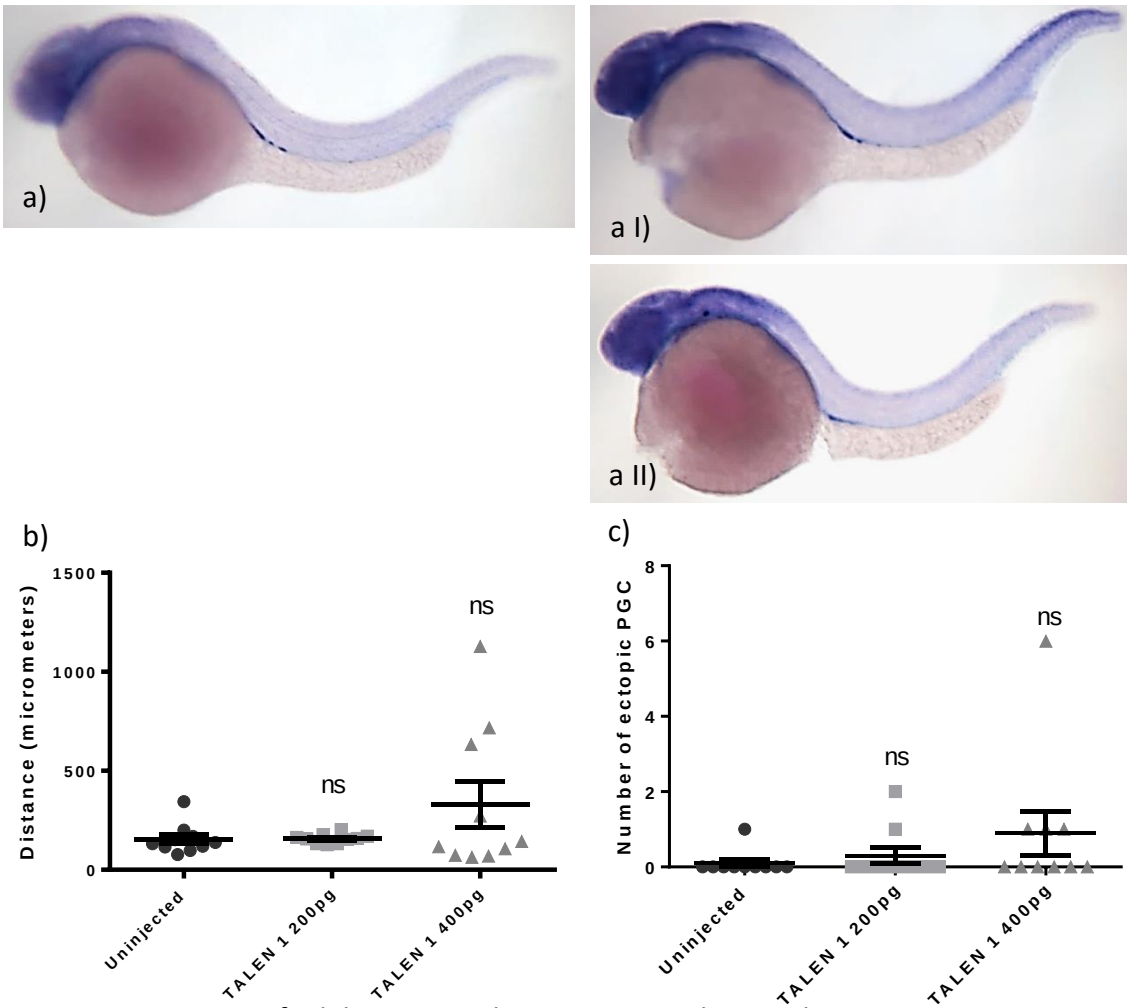

Figure 4.7 Injection of *cd9b* TALEN 1 does not cause abnormal PGC migration.

Vasa in situ hybridisation on 30 hpf AB embryos (a) uninjected or injected with (a I) 200pg *cd9b* TALEN 1, (a II) 400pg *cd9b* TALEN 1. No significant difference in the distance between most anterior and posterior PGC in *cd9b* TALEN 1 injected embryos (b) or in the number of ectopic PGC (c), was seen using a Kruskal-Wallis with Dunn's multiple comparisons test. n=10 per condition. p=<0.05. Data from a single experiment.

PGC migration was also assessed in TALEN 2 injected embryos. As TALEN 2 does not appear to cause mosaicism at its cut site, it was thought that TALEN 2 injection could be used as a control for the TALEN construct. Surprisingly, TALEN 2 injected embryos show a small but significant increase in both the distance between the most anterior and posterior PGCs and the number of ectopic PGCs (Figure 4.8). While it could be that TALEN 2 is cutting elsewhere in *cd9b* or a different gene, it should be noted that TALEN 2 injection caused a large percentage of the embryos to show general abnormal phenotypes and a PGC phenotype was only seen in CD9b morphants which also showed abnormal morphologies (Figure 4.4 and Chapter 3, Figures 3.4-3.5). This could support the hypothesis that the significance seen here is not caused by CD9b knockdown but is rather a consequence of the general abnormal phenotypes induced by TALEN 2 toxicity.

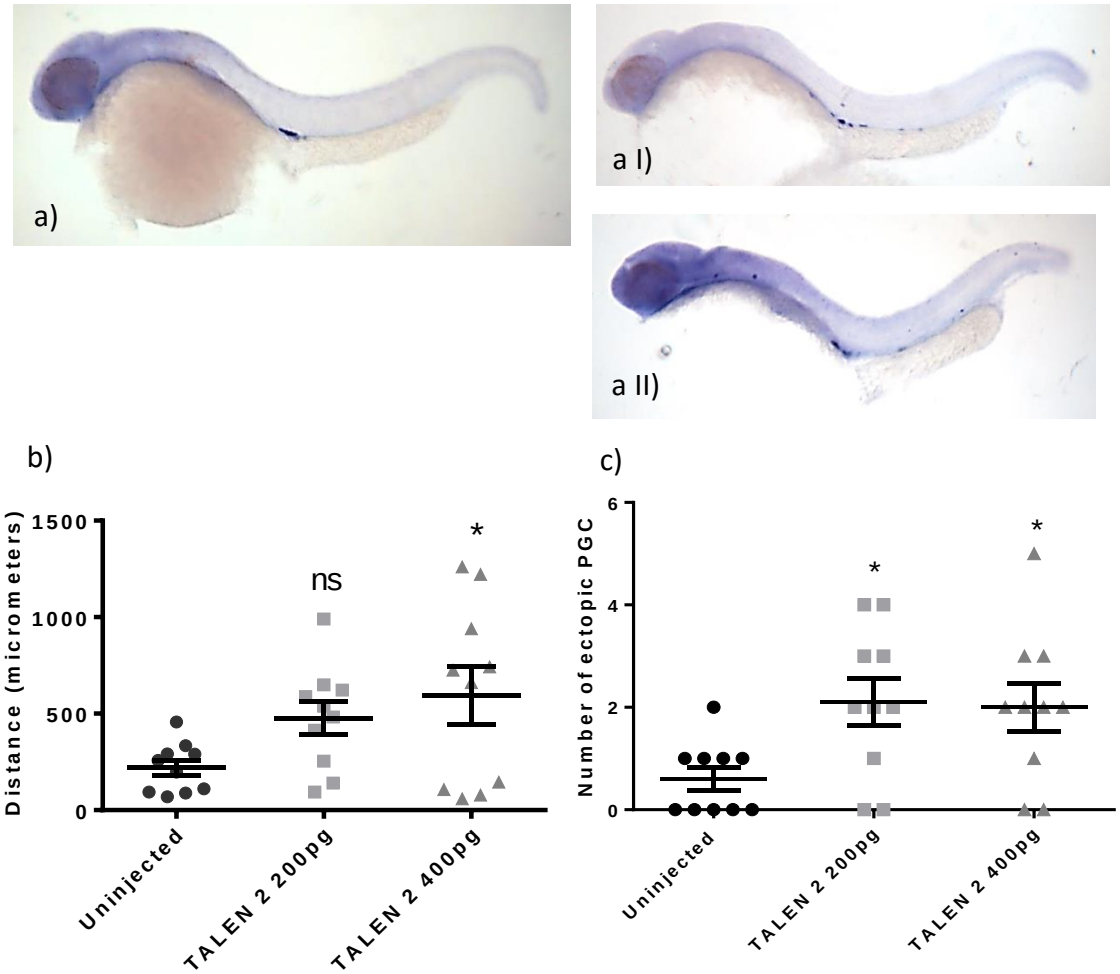

Figure 4.8 Injection of *cd9b* TALEN 2 does cause abnormal PGC migration. *Vasa in situ* hybridisation on 30 hpf embryos (a) uninjected or injected with (a I) 200pg *cd9b* TALEN 2, (a II) 400pg *cd9b* TALEN 2. A small significant difference can be seen in the distance between the most anterior and posterior PGCs (b) and the number of ectopic PGCs (c) using ANOVA with Dunnett's multiple comparisons test. n= minimum 10 per condition. p=<0.05. Data from a single experiment.

The effect of TALEN 1 injection on lateral line migration was also analysed (Figure 4.9). A decrease in the number of neuromasts and irregular spacing was expected as this would replicate the phenotypes seen in CD9b morphants. A significant decrease in the number of neuromasts was seen in embryos injected with 400pg TALEN 1, however, the mean number of neuromasts in these embryos is still within the normal range of 7-8 neuromasts deposited in wildtype embryos (Gompel et al. 2001) (Figure 4.9b). A decrease in the percentage of total body length between the 1st and last neuromasts was also seen with 400pg TALEN 1, which could suggest that the primordium had not completed migration or that the 1st neuromast was deposited in a slightly more posterior position to normal (Figure 4.9c). The increase in variation in the percentage of total body length between the 1st and 2nd neuromasts may support the latter hypothesis, as it suggests irregular neuromast spacing in TALEN 1 injected embryos (Figure 4.9d). The observations that TALEN 1 injected embryos do not show any obvious developmental delay and their recovery from any general abnormal phenotypes by 48hpf also supports this hypothesis (Figures 4.3c, 4.9a).

Embryos injected with TALEN 2 were also assessed for lateral line phenotypes (Figure 4. 10). No significant difference in the number of deposited neuromasts or in the percentage of total body length between the 1st and 2nd neuromasts was seen but there was a significant decrease in the percentage of total body length between the 1st and last neuromasts in embryos injected with 400pg TALEN 2 (Figure 4.10b-d). Embryos injected with 400pg TALEN 2 had primordia that were noticeably delayed and showed general morphological defects, which could explain the decrease in the percentage of total body length between the 1st and last neuromasts.

Figure 4.9 Injection of 400pg *cd9b* TALEN 1 causes a small but significant effect on thepLL structure. *claudin b in situ* hybridisation on 52hpf AB embryos uninjected (a) or injected with 200pg *cd9b* TALEN 1 (a I), 400pg *cd9b* TALEN 1 (a II).

A small but significant decrease in the number of neuromasts deposited (b) and the percentage of total body length between the 1st and last neuromast (c) in embryos injected with 400pg TALEN 1. While there is no significant difference in the mean spacing between the 1st and 2nd neuromast (d), there is a significant difference in the standard deviation between the groups, indicating irregular spacing as seen with CD9b MOs (Bartlett's test, p = 0.0050). n= 10 per column, ANOVA with Dunnett's multiple comparisons test. p=<0.05. Data from single experiment.

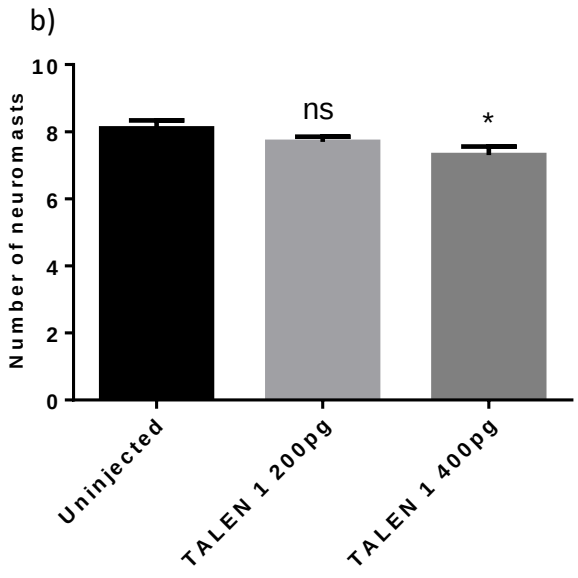

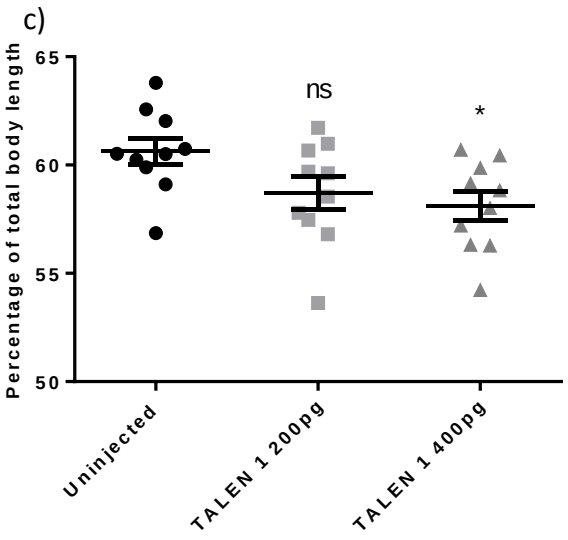

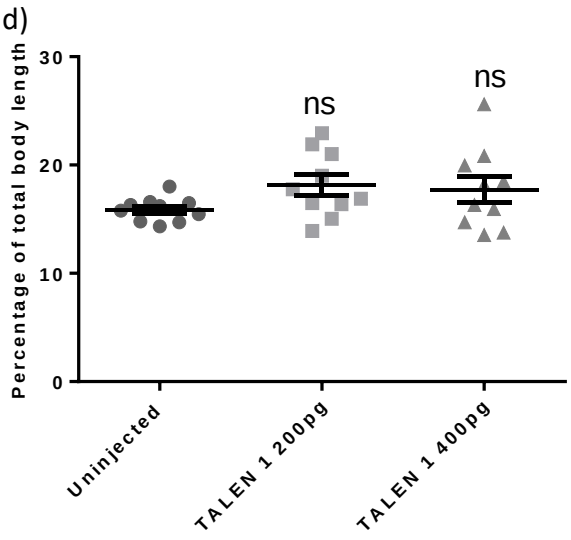

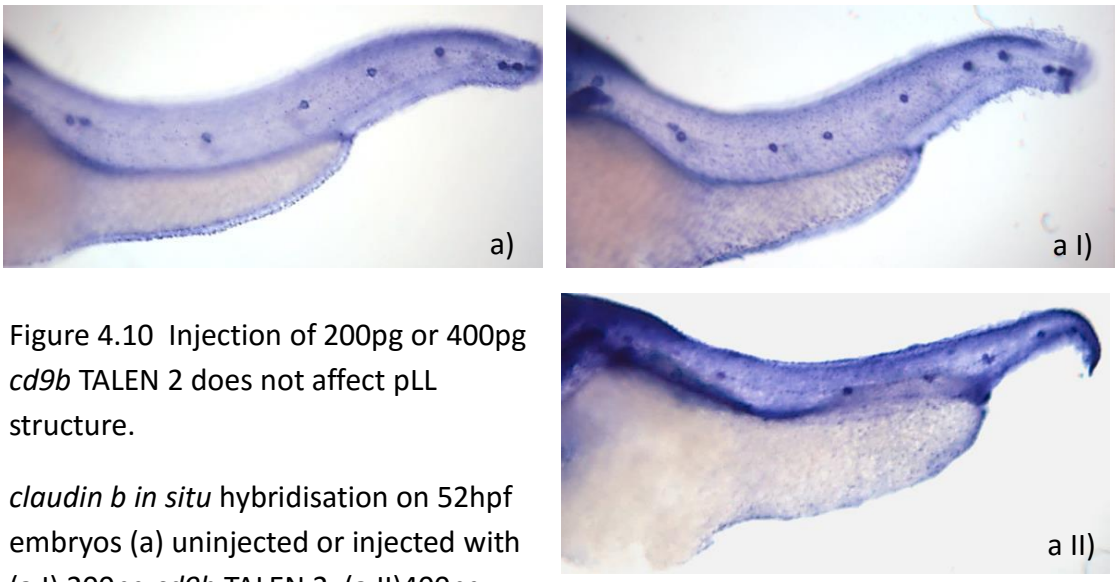

Figure 4.10 Injection of 200pg or 400pg *cd9b* TALEN 2 does not affect pLL structure.

claudin b in situ hybridisation on 52hpf embryos (a) uninjected or injected with (a I) 200pg *cd9b* TALEN 2, (a II)400pg *cd9b* TALEN 2. A significant difference can be seen in the percentage of total body length between the 1st and last neuromast (c) but not in the percentage of total body length between the 1st and 2nd neuromasts (d) or the number of neuromasts (b). ANOVA with Dunnett's multiple comparisons test. n= minimum 6 per column. p=<0.05. Data from a single experiment.

4.2.3 Creating CD9b homozygous mutants

After raising the TALEN 1 injected embryos to maturity, F0s that successfully transmitted CD9b mutations through the germ line were identified (Figure 4.2). These F0s were out-crossed with AB fish and the resulting F1 offspring were raised. The offspring contained a mixture of wildtype and CD9b heterozygous mutants, depending on whether the germ cell had originally been mutated in the mosaic parent. Heterozygous F1s were identified by genotyping fin clips and five mutant alleles were identified (Figure 4.11). Four of these alleles induce nonsense stop codons and result in a frameshift. Initially, F1s were randomly in-crossed to create compound heterozygotes. These embryos showed no PGC phenotype and only a slight pLLP phenotype where there was a small but significant increase in the percentage of trunk length between the 1st and 2nd neuromasts (Figures 4.12, 4.13). The percentage of trunk length was used instead of the percentage body as the embryonic heads were removed prior to ISH for genotyping.

Figure 4.11 Most *cd9b* deletion alleles identified were predicted to cause frameshifts and nonsense stop codons. Predicted open reading frames (red), potential start sites (blue) and stop codons (bold) for the 5 alleles found in *cd9b* heterozygous mutants (F1s) are shown. Nucleotide mutations are given after their assigned name. Predictions made using ExPASy (Artimo et al. 2012).

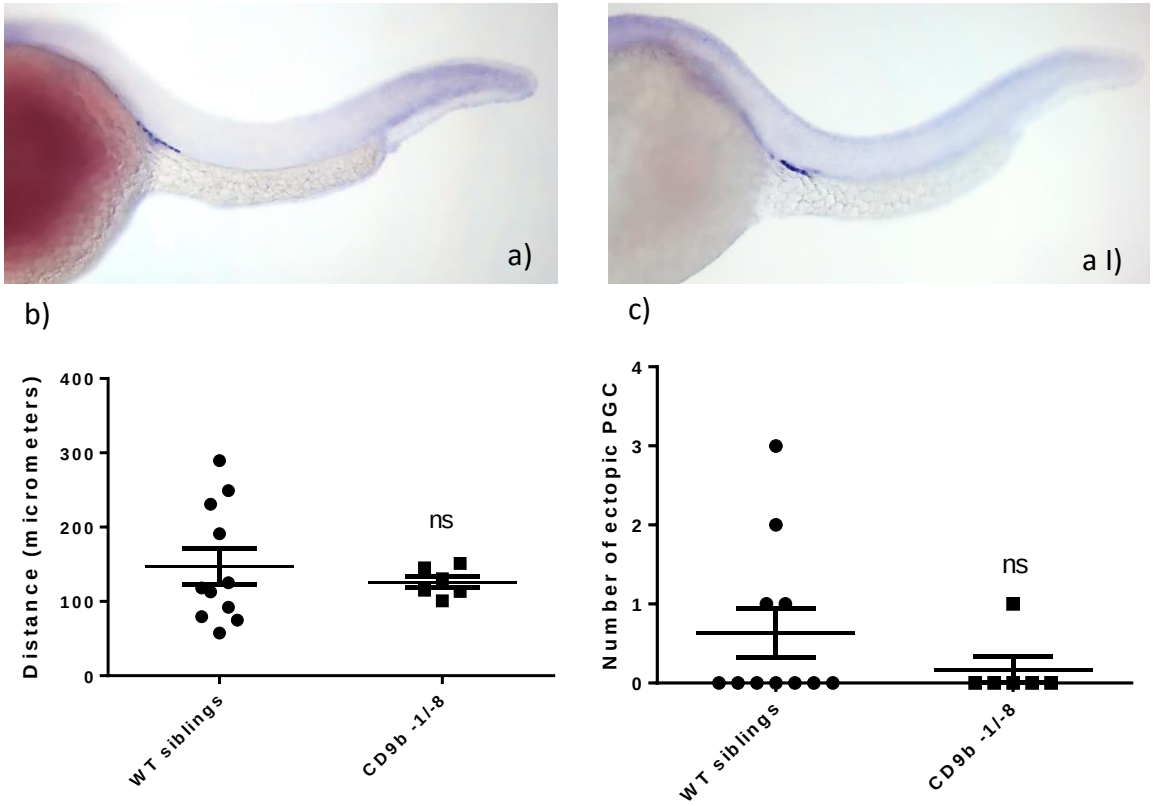

Figure 4.12. CD9b compound heterozygotes (-1 T/-8) appear to have no PGC migration defects.
vasa in situ hybridisation on 30hpf CD9b -1/-8 (a I) or wt sibling (a) embryos. No significant difference in the distance between the most anterior and posterior PGCs (b) or in the number of ectopic PGCs (c) is seen in CD9b compound heterozygotes. n= minimum 6 per condition. Unpaired T test (a) and Mann-Whitney U test (b). p=<0.05

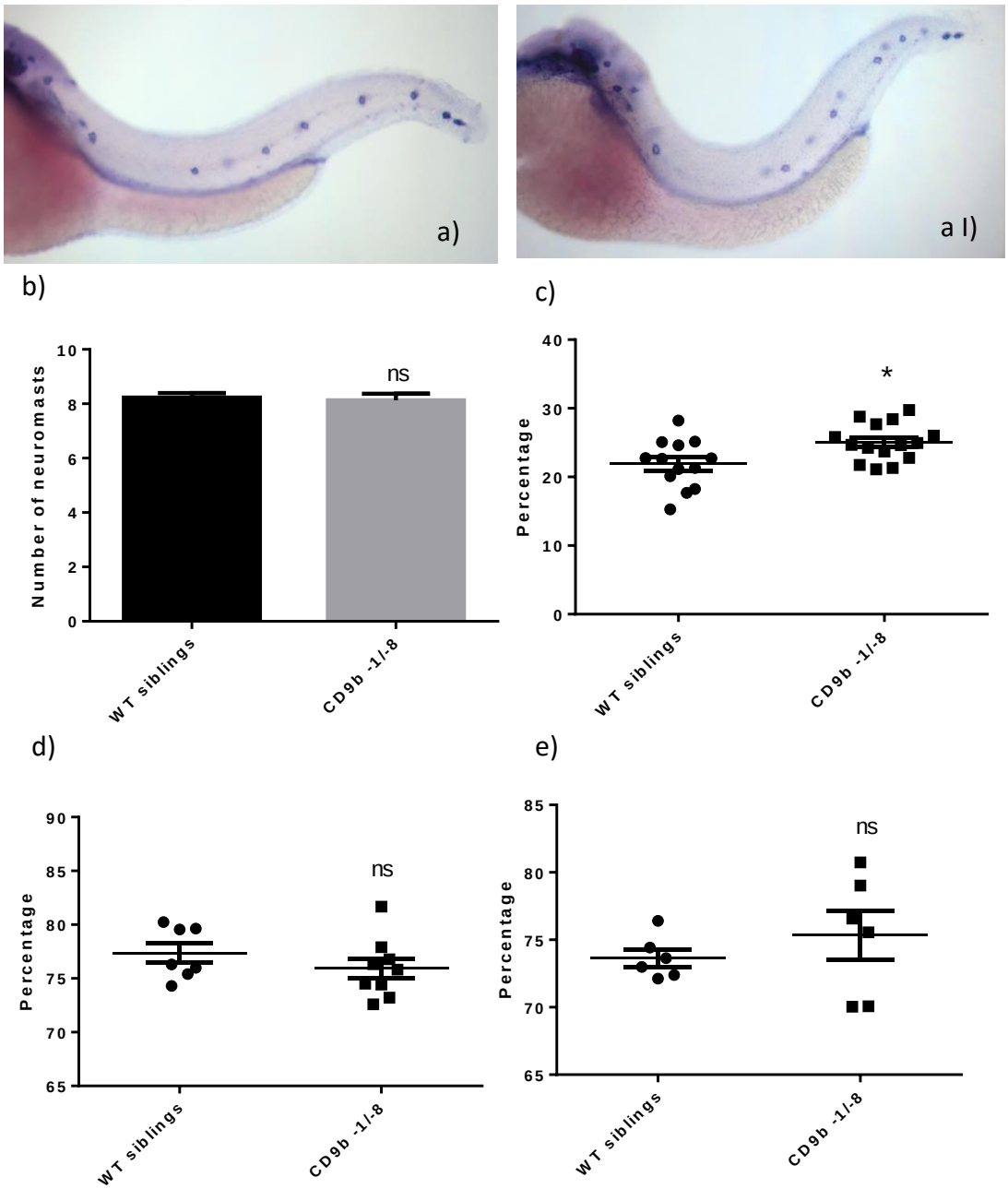

Figure 4.13.The pLL in CD9b compound heterozygotes shows slight neuromast spacing differences.
claudin b in situ hybridisation on 52hpf CD9b -1T/-8 (a l) or wt siblings (a). No significant difference was found in the number of neuromasts deposited (b) or the percentage of trunk length between 1st and last neuromast (d and e). However, a small significant increase in the percentage of trunk length between the 1st and 2nd neuromasts (c) was seen. Unpaired T test, p=<0.05. n = minimum 6 per genotype. (d) and (e) are two experiments that could not be pooled due to significantly different controls. (b) and (c) show the pooled data of two experiments.

To create a CD9b homozygous mutant line with a single mutant allele, F1s with the 42_49delCTTTATCT mutation, hereafter called CD9b -8, were in-crossed and the resulting offspring were raised to adulthood (Figure 4.2). This allele was used as it had the largest deletion and caused the earliest nonsense stop codon (Figure 4.11). Homozygous CD9b -8/-8 adults were identified by genotyping fin clips taken from the adult offspring from the F1 in-cross. CD9b knockout was then confirmed in the homozygous mutant line using a *cd9b* ISH on 36hpf AB and CD9b -8/-8 embryos (Figure 4.14).

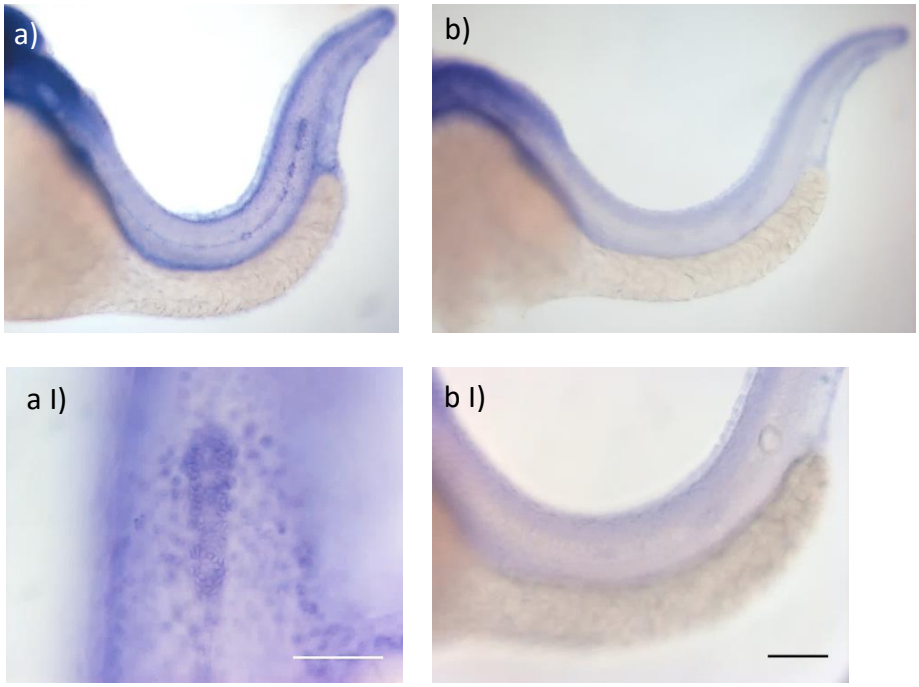

Figure 4.14 CD9b -8/-8 embryos show dramatically reduced *cd9b* RNA compared to AB embryos.
Representative images of a *cd9b in situ* hybridisation on 36hpf AB (a) and CD9b -8/-8 homozygous embryos (b). a I) and b I) show the staining in the posterior lateral line primordium. Scale bar 50µM (a I) and 100µM (b I). n= minimum 3 imaged but 10 observed per genotype. Images and observations from a single experiment.

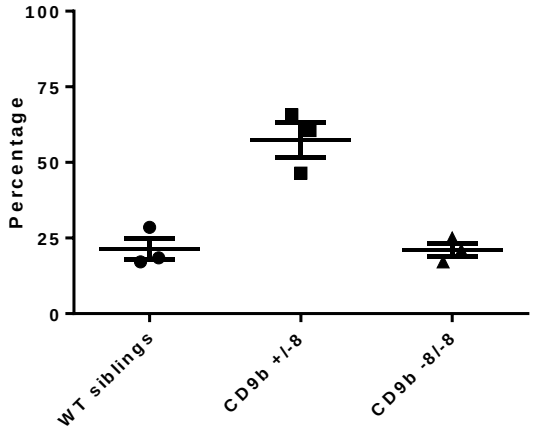

Figure 4.15 The expected percentages of wt siblings, heterozygous and homozygous mutant embryos were observed in three heterozygous F1 in-crosses. Embryos were fixed at 30 or 52hpf before genotyping for use in further experiments. Mean genotype ratios from three experimental repeats. n= minimum 28 embryos per experiment

4.2.4 CD9b homozygous mutants

While the CD9b -8/-8 homozygous mutant line was being raised, CD9b +/-8 adults were in-crossed to generate CD9b -8/-8 progeny. Embryos from these in-crosses were fixed at either 30 or 52hpf, then genotyped. The genotype ratios were assessed to investigate the early viability of CD9b homozygous mutants and to find homozygous mutants for later experiments. The expected ratio of wt, heterozygous and homozygous mutants was seen each time, showing that the CD9b homozygous mutants are viable during the first 50 hours of embryonic development (Figure 4.15).

4.2.4.1 PGC migration in CD9b homozygous mutants

While no PGC phenotype is expected in CD9b mutants, due to the majority of CD9b morphants not showing a significant phenotype, PGC migration was analysed to ensure that CD9b deficiency does not cause a PGC phenotype. As expected, no significant difference in the distance between the most anterior and posterior PGC, was found (Figure 4.16).

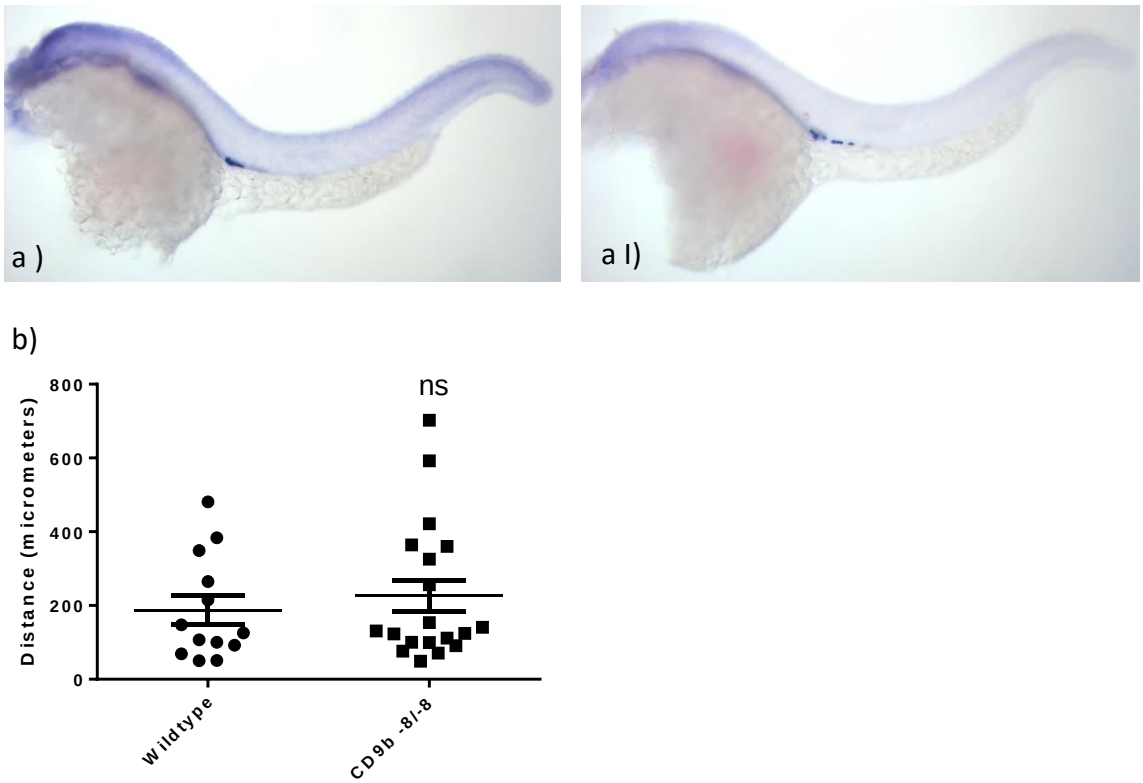

Figure 4.16 PGC migration is not affected in CD9b homozygous mutants.
vasa ISH on 30hpf WT (a) and CD9b -8/-8 (a I) embryos. There is no significant difference in the distance between the most anterior and posterior PGC (b) as shown by a Mann-Whitney U test. n= minimum 13. p=<0.05. Pooled data from two experiments.

4.2.4.2 pLL phenotypes in CD9b homozygous mutants

Due to the phenotypes seen in CD9b morphants, it was expected that a lateral line phenotype would be seen in CD9b mutants with a decreased number of neuromasts deposited and irregular spacing between them. Initially, it appeared that the opposite phenotype might be occurring, with an additional neuromast being deposited (Figure 4.17b). A closer inspection of the additional structure seen in CD9b -8/-8 embryos suggested that the structure may actually be a secondary primordium and not an additional neuromast (Figure 4.17 b I-II).

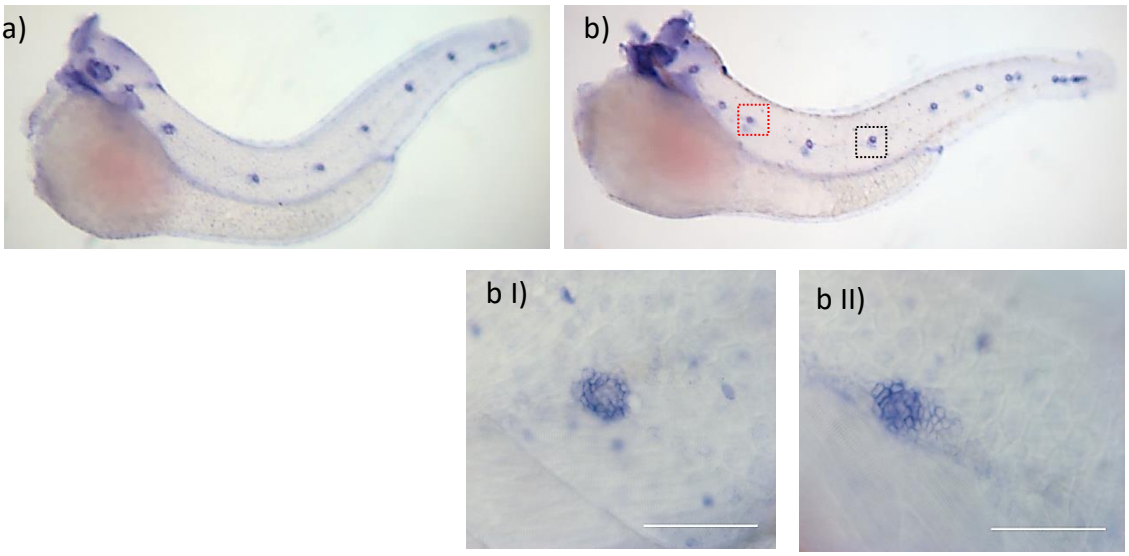

Figure 4.17 CD9b -8/-8 embryos may show an additional neuromast.
claudin b ISH on 52hpf WT siblings (a) and CD9b -8/-8 (b) embryos. An additional neuromast-like structure was seen in CD9b -8/-8 embryos (b, redbox/ b II). However, b II shows a more elongated structure than the circular neuromast shown in b I)/black box. Scale bar 50µM. n= minimum 8 per genotype. Images from a single experiment.

To confirm whether the structure was a neuromast or not, embryos were first incubated with To-Pro-1 and imaged (Figure 4.18 a I, III, b I, III). To-Pro-1 is a cell impermeable fluorescent nucleic acid stain that is able to enter neuromast cells but not primordium cells. The same embryos were then put through a *claudin b in situ* hybridisation to highlight both neuromast and primordia structures. If the structure was an additional neuromast, it would be seen with both To-Pro-1 and *claudin b in situ*, however if the structure was the secondary primordium it would only be seen after the ISH. Figure 4.18 shows that the additional structure is only visible in the *claudin b in situ* and therefore was actually Prim II, a secondary posterior lateral line primordium that migrates along the horizontal myoseptum depositing additional

neuromasts after the primary posterior lateral line primordium (Prim I) has completed migration (Ledent 2002, Sapede et al. 2002, Nuñez et al. 2009).

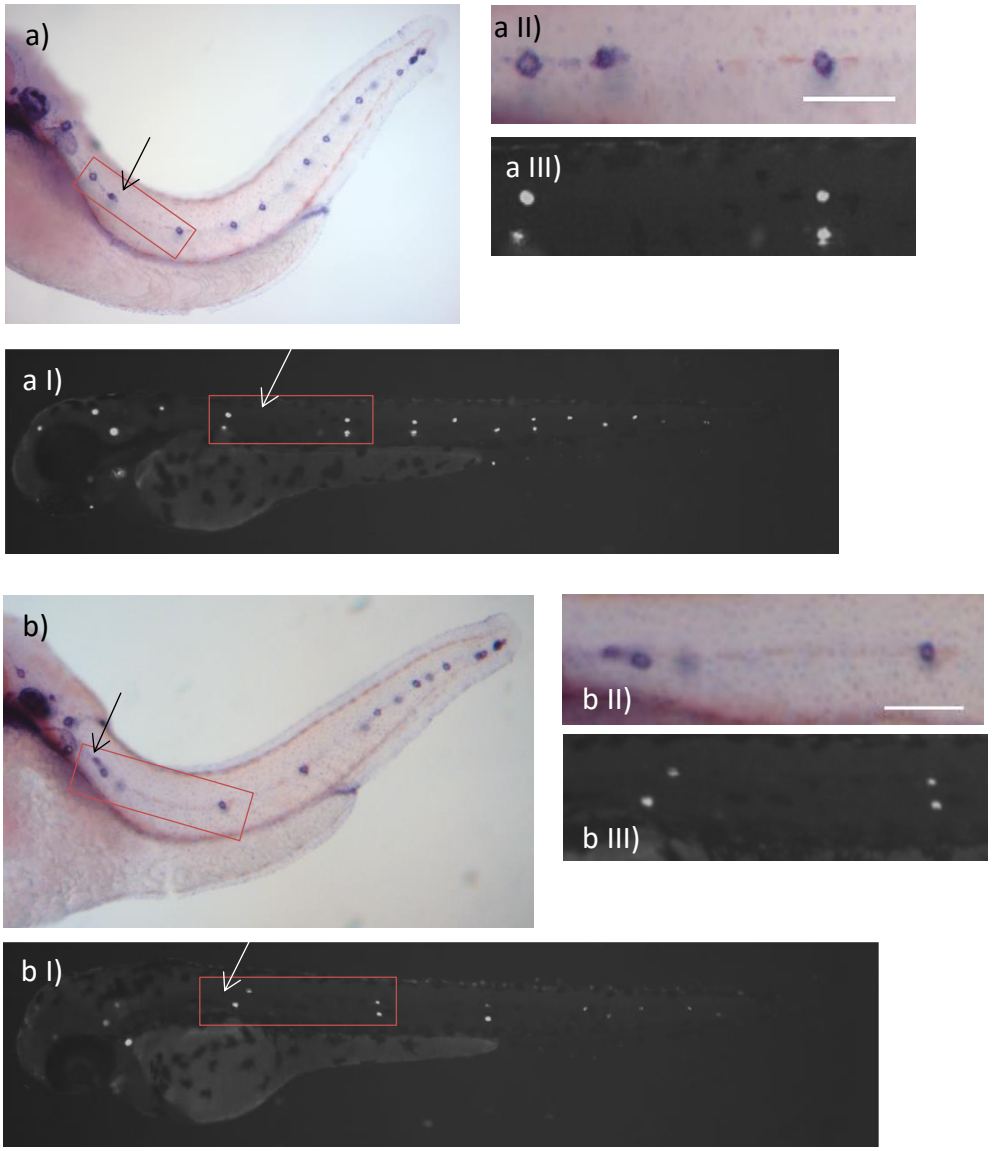

Figure 4.18 The ‘ additional neuromast’ is Prim II.

Neuromasts in AB (a) and CD9b -8/-8 (b) 52hpf embryos were stained with To-Pro-1 (a I,b I) before using a *claudin b in situ* hybridisation (a,b) to highlight both Prim II and the neuromasts. a II), b II) and a III), bIII) show relevant close ups of the red boxes in a), aI), b) and b I). Comparison of a II) to a III) and b II) to b III) clearly show that the ‘extra neuromast’ seen in a) and b) is absent in a I) and b I) (red boxes), suggesting the structure is Prim II. Scale bars are 100µM (a II, b II). n= 8 per genotype. Images from a single experiment.

Having shown that the 'additional neuromast' was actually Prim II, the CD9b -8/-8 embryos were re-assessed for lateral line phenotypes. As the heads of the embryos had been removed for genotyping prior to the ISH, distances were calculated as a percentage of trunk length. Trunk length was measured from the otic vesicle to the tail tip.

No significant difference was found in the number of neuromasts, the percentage of trunk length between the 1st and last neuromasts or the percentage of trunk length between the 1st and 2nd neuromasts (Figure 4.19a-c). This is summarised by the mean neuromast positions as shown in Figure 4.19d.

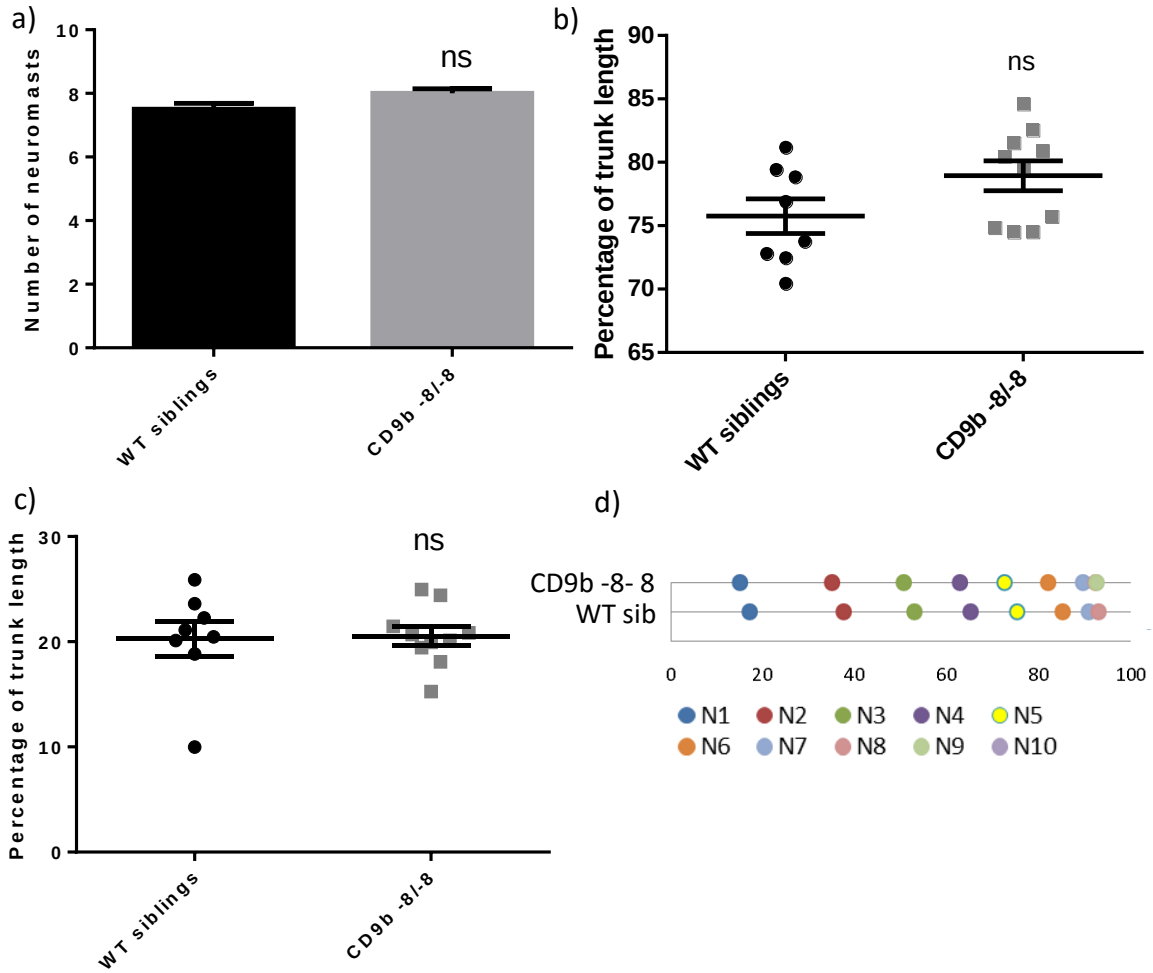

Figure 4.19 CD9b mutants show normal primary posterior lateral line structure. There is no significant difference in the number of neuromasts at 52hpf (a), the percentage of trunk length between the 1st and last neuromasts (b) or in the percentage of trunk length between the 1st and 2nd neuromasts (c). No difference in the mean position of each neuromast, between the ear (0) and tail tip (100), is seen between CD9b mutants and WT siblings using an ANOVA with Sidak's multiple comparisons test (d). The percentage of trunk length was used as the heads were removed prior to the ISH for genotyping. Significance was determined using an unpaired T-test, on $\log_{10}$ transformed data for (c) and untransformed data for (a) and (b) . n= minimum 8, p=<0.05. Data from a single experiment.

4.2.4.3 Prim II migration in CD9b homozygous mutants

With the position of Prim II initially causing confusion in the CD9b -8/-8 mutants, I decided to look at the position of Prim II in both the mutants and WT siblings. To do this, the distance migrated by Prim II was measured from the otic vesicle as a percentage of trunk length. Initially it appeared that Prim II had migrated further in mutant embryos than the wt siblings by 52hpf (Figure 4.20a). However, when the position of Prim II was assessed in the embryos from Figure 4.18, it appeared that the position of Prim II was significantly more posterior than in the AB embryos (Figure 4.20b). One of the differences between the two experiments was the genealogy of the embryos; the embryos in Figure 4.20a are from CD9b +/-8 parents whereas the mutant embryos from Figure 4.20b are from CD9b -8/-8 parents with AB WT controls.

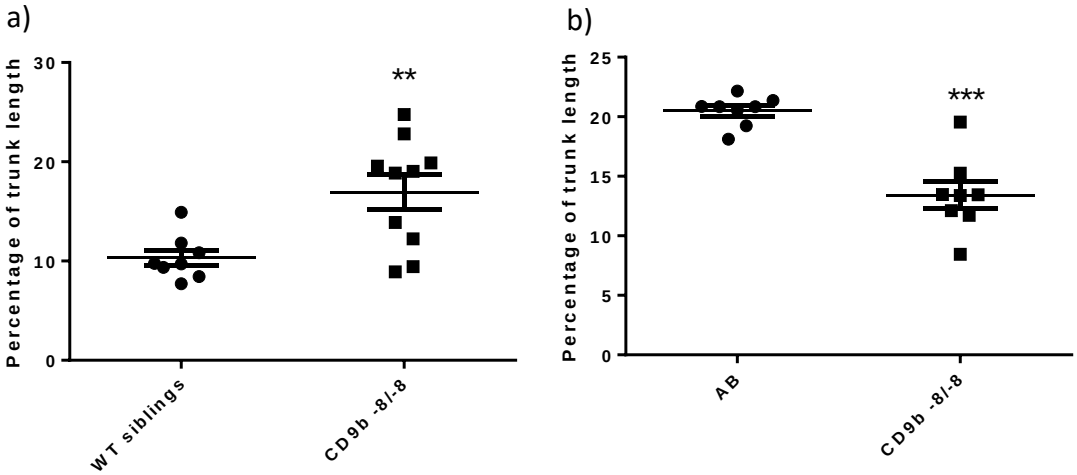

Figure 4.20 CD9b homozygous mutant embryos show an increase in trunk migrated by Prim II when compared to WT siblings (a), but a decrease in migration when compared to AB embryos (b) at 52hpf. Unpaired T test (a, b), on untransformed (a) or $\log_{10}$ transformed data for (b). n= minimum 8 per genotype. p=<0.05. Data from two experiments.

4.2.4.4 Prim I migration and early pLL phenotypes in CD9b homozygous mutants

Due to the similarities between the primary (Prim I) and secondary (Prim II) posterior lateral line primordiums, the observed changes in Prim II migration may also suggest a role for CD9b in Prim I migration (Ledent 2002, Sapede et al. 2002, Nuñez et al. 2009, Sarrazin et al. 2010). Migration of Prim I as well as lateral line structure was assessed at 36hpf. Structure was analysed because although the primary posterior lateral line shows no structural abnormalities in CD9b mutants at 52hpf, it is possible that CD9b

mutants show a lateral line phenotype earlier in development and have recovered by 52hpf (Figure 4.19).

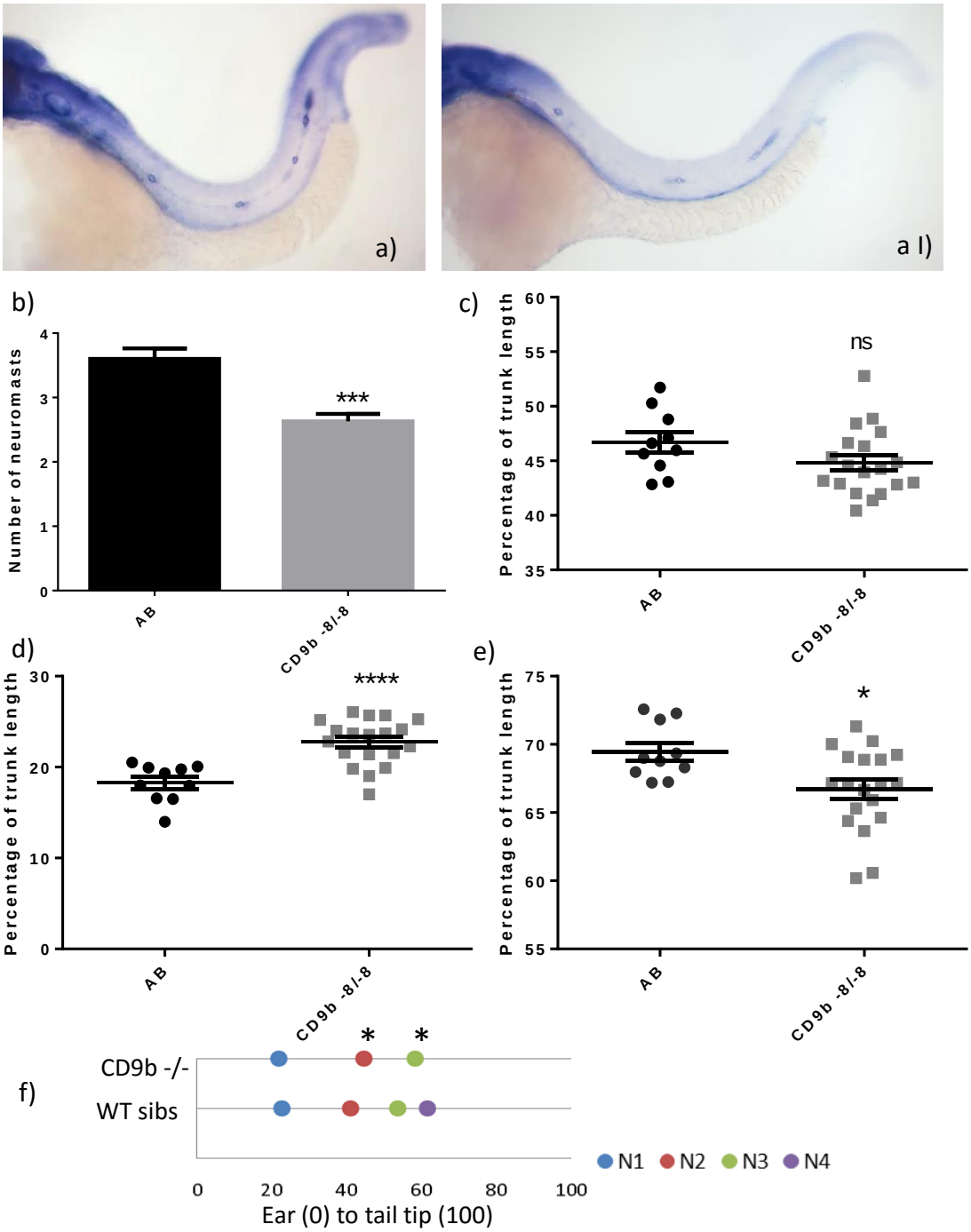

Figure 4.21 CD9b mutants show delayed Prim I migration and increased spacing between deposited neuromasts at 36hpf.
claudin b ISH on AB (a) and CD9b -8/-8 (a I) embryos showed a decrease in the number of neuromasts deposited by 36hpf (b), and an increase in the percentage of trunk length between the 1st and 2nd neuromasts (d). While there was no difference in the percentage of trunk length between the 1st and last neuromasts (c), there was a decrease in the percentage of trunk length migrated by Prim I from the otic vesicle (e). The mean neuromast positions can be seen in (f). Mann-Whitney U test (b) and Unpaired T tests (c-f), with Holm-Sidak correction for multiple comparisons in (f). n= minimum 10 per genotype. p=<0.05. Data from a single experiment.

By 36hpf, CD9b -8/-8 mutants have deposited significantly fewer neuromasts and show a significant increase in the percentage of trunk between the 1st and 2nd neuromasts but no difference in the percentage of trunk between the 1st and last neuromast. This shows that within the same neuromast deposition space less neuromasts have been deposited in CD9b mutants (Figure 4.21 a-c,f). This phenotype is summarised in Figure 4.21f where the mean positions of deposited neuromasts are shown. The 2nd and 3rd neuromasts have been deposited in significantly more posterior positions in the CD9b mutants. Delayed Prim I migration is also seen in Figure 4.21e, where the percentage of trunk length between the otic vesicle and primordium tip is measured. Interestingly, the CD9b-8/-8 embryos used were the offspring of CD9b homozygous mutants and so the delayed Prim I migration mirrors the delayed Prim II migration seen in CD9b -8/-8 embryos from homozygous mutant parents (Figures 4.20b, 4.21e).

4.2.4.5 Does genealogy affect primordium migration in CD9b homozygous mutants?

To see whether the pattern of delay or increase in migration of Prim I and Prim II could be seen at both 36 and 52hpf, CD9b +/-8 adults were in-crossed and the resulting wt siblings and homozygous mutant embryos analysed at 36hpf. Unfortunately, the otic vesicles were cut off during the genotyping of the embryos and so only the number of neuromasts deposited by Prim I at 36hpf could be analysed, whereas migration was assessed for Prim II. As is evident in Figure 4.22, it appears that there is a pattern to the data when experiments are separated according to the parents' genotypes. It appears that CD9b -8/-8 embryos from homozygous parents show delayed migration of Prim I and Prim II whereas CD9b -8/-8 embryos from heterozygous parents show an increase in Prim I and Prim II migration (Figure 4.22). The delay seen in embryos from homozygous parents is also apparent at later stages of development, with embryos at 72 and 96hpf also showing delayed Prim II migration (Figure 4.23).

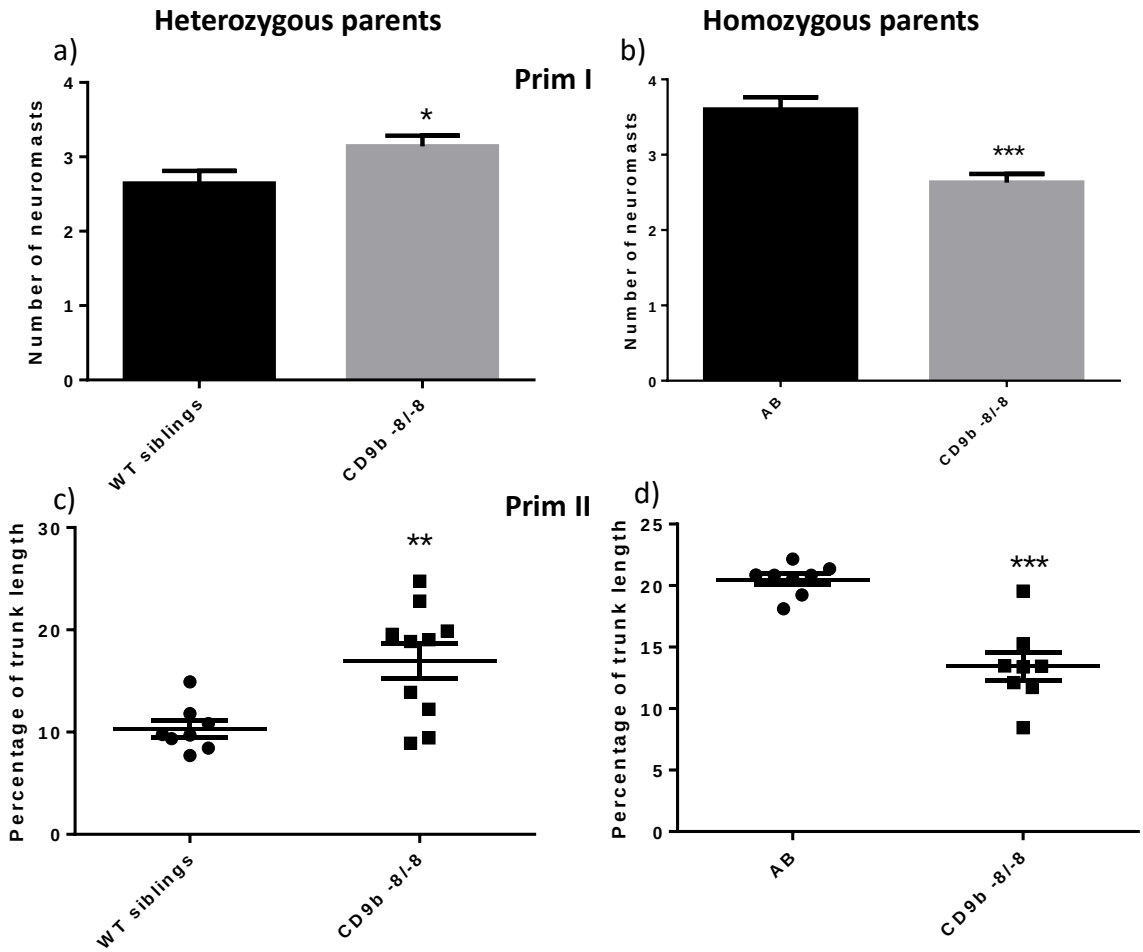

Figure 4.22 The migration of Prim I and Prim II appear to be affected differently in CD9b mutant embryos depending on their parents.
The number of neuromasts deposited by Prim I by 36 hpf seems to be increased in CD9b -8/-8 embryos from heterozygous parents (a) but decreased in embryos from homozygous parents (b). This difference is replicated at 52hpf, looking at the percentage of trunk length migrated by Prim II in 52hpf embryos from heterozygous parents (c) or homozygous parents (d). Mann-Whitney U test (b), unpaired T test (a,c) and unpaired T test on $\log_{10}$ transformed data (d). n= minimum 14 (a), 10 (b), 8 (c,d) p=<0.05. Data from four individual experiments.

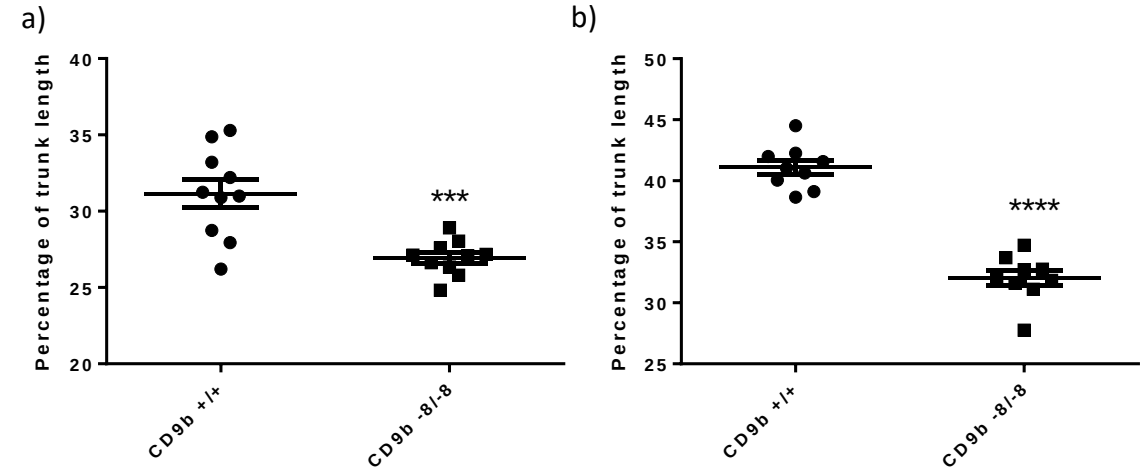

Figure 4.23 The delay in Prim II migration is also seen at 72 (a) and 96 (b) hpf in embryos from CD9b homozygous mutant parents. Unpaired T test on n= minimum 10 (a) and 9 (b) p=<0.05. Data from a single experiment.

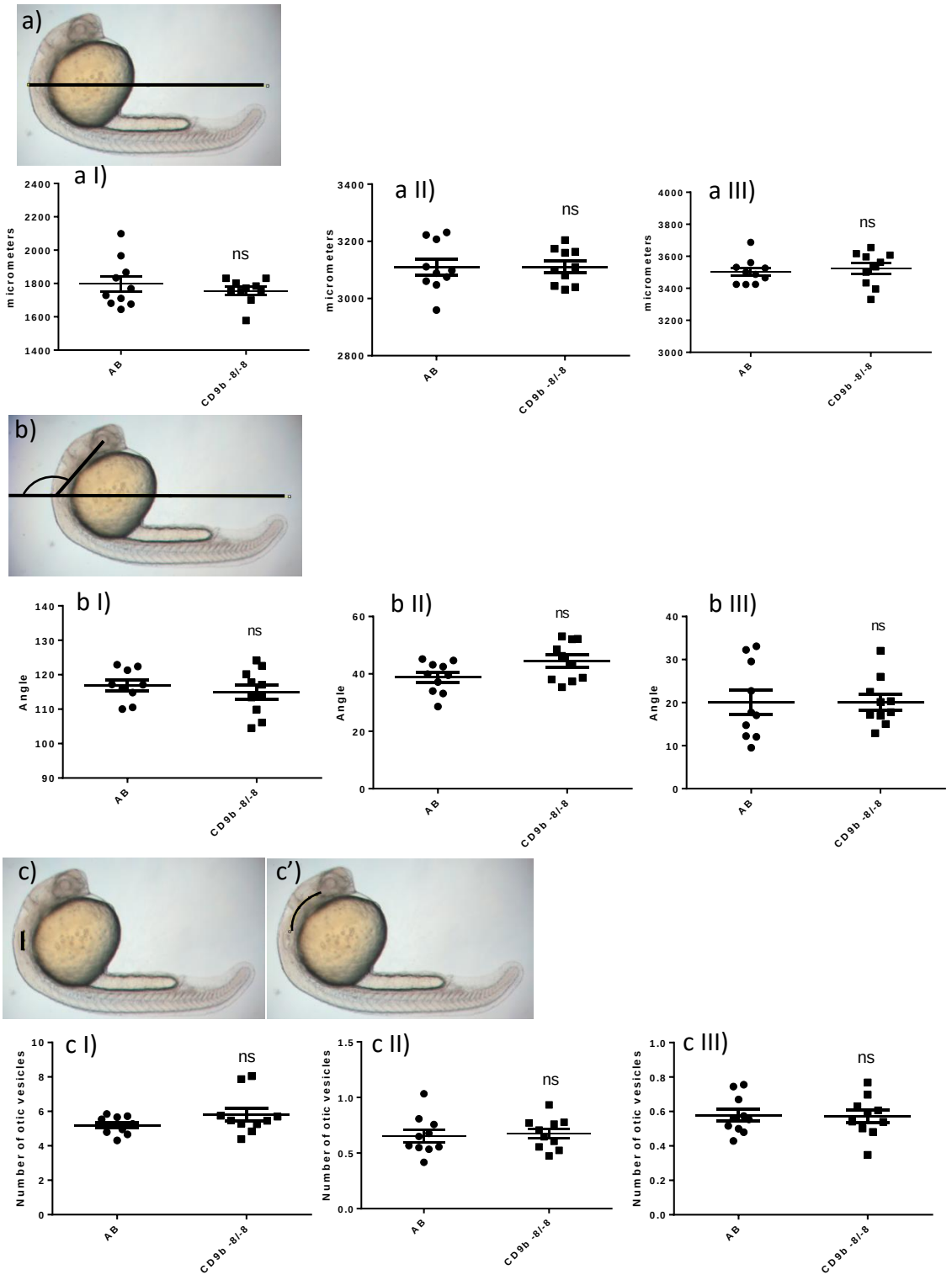

Figure 4.24 Developmental assays showed no significant difference in development between AB and CD9b -8/-8 embryos from AB and CD9b -8/-8 parents.

Embryo length (a), Head-Tail Angle (b) and Otic vesicle length (c) were measured at 24 (I), 48 (II)and 72 (III) hpf. All the assays had non-significant results. Otic vesicle length is defined as the number of otic vesicle that could fit in the distance between the eye and the ear. Unpaired T-test, significance calculated on $\log_{10}$ transformed data for c II. n= 10 per genotype. p=<0.05. Data from a single experiment.

The opposing phenotypes seen could be due to an overall developmental delay in the embryos from homozygous parents, which could then be masking any true lateral line phenotype. CD9b may be required during early development for efficient development and so the delay seen may not be specific to the lateral line. To determine whether this hypothesis was true, embryos from AB and CD9b -8/-8 adults were analysed using three different staging assays from Kimmel et al., 1995 at three different time points. No significant difference was found in any of the three assays: embryo length, head-tail angle or the otic-vesicle length at 24, 48 or 72hpf (Figure 4.24). This suggests that the delay phenotype seen in the lateral line is not due to general developmental delay and therefore may be specific to the lateral line.

Upon closer inspection of the pattern seen in Figure 4.22, it appears that there is a difference between the wildtype controls with the AB embryos showing higher results than WT siblings. To look into this, AB embryos from an AB in-cross and wildtype embryos from a CD9b +/-8 (female) x AB (male) cross were fixed at 36hpf and a *claudin b in situ* hybridisation carried out to assess the percentage of trunk length migrated by Prim I. No significant difference was seen in the percentage of trunk migrated or the number of neuromasts deposited by 36hpf between the two controls (Figure 4.25). This suggests that the difference seen in Figure 4.22 between the controls may be due to environmental differences between experiments or background genetic differences from using different tanks of ABs.

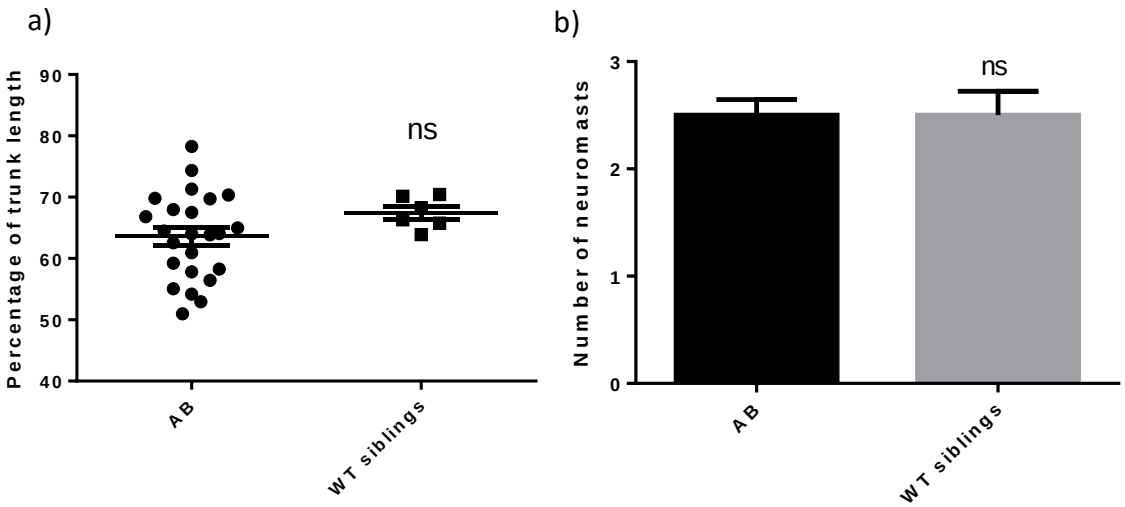

Figure 4.25 No difference in the percentage of trunk length migrated by Prim I (a) or in the number of neuromasts deposited (b) by 36hpf is seen between AB and WT siblings. n= minimum 6. Unpaired T test. p=<0.05. Data from a single experiment.

Whilst no hypothesis had been formed as to why embryos from heterozygous and homozygous parents would show opposite phenotypes, the phenotypes appeared to be significant and specific. The difference in position of Prim I and Prim II at 36 and 52hpf could either be due to a change in the onset of migration, a change in the speed of migration or a combination of the two. The speed of Prim I and Prim II migration was assessed using the claudinb:GFP line which had been crossed with CD9b -8/-8 adults to produce a line of double heterozygous fish (claudinb:GFP +/-, CD9b +/-). These fish were then crossed with CD9b -8/-8 fish and the claudinb:GFP+ embryos from the resulting offspring were selected. These embryos were then imaged at 26 and 31hpf for Prim I and 52 and 59hpf for Prim II. claudinb:GFP embryos were used as a control and the claudinb:GFP,cd9b-8/-8 embryos were identified after imaging by genotyping. As is evident from Figure 4.26 there was no difference in the speed of migration of Prim I or Prim II in the CD9b -8/-8 embryos. This could suggest that the onset of migration is affected but not the speed of migration.

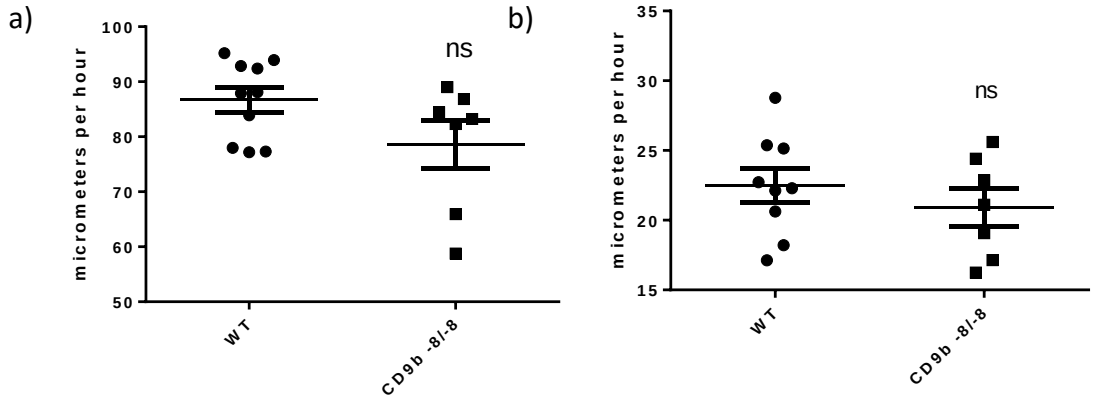

Figure 4.26 Migration speed of Prim I, or Prim II, is not affected in CD9b -8/-8 embryos. Speed of Prim I migration (a) and Prim II migration (b), between 26 - 31hpf and 52-59hpf respectively, was calculated for WT and CD9b -8/-8 embryos. No significant difference seen using an unpaired T test for either Prim I or Prim II migration speed. n= minimum 7, p=<0.05. Data from two experiments looking at either Prim I or Prim II.

A second CD9b knock out line was developed using F1s with the 46delA mutation, hereafter called CD9b -1, which causes a frameshift and an early stop codon (Figure 4.11). CD9b knockout was confirmed by *cd9b in situ* hybridisation (Figure 4.27). c*laudinb in situ* hybridisation experiments were carried out on 36 and 52hpf embryos to see if the migration phenotypes seen in CD9b-8/-8 embryos were replicated in a different CD9b mutant allele. Figure 4.28 shows there was no significant difference in the position of either Prim I or Prim II at 36 and 52hpf in the CD9b -1/-1 embryos which is surprising given the significance seen in Figure 4.22.

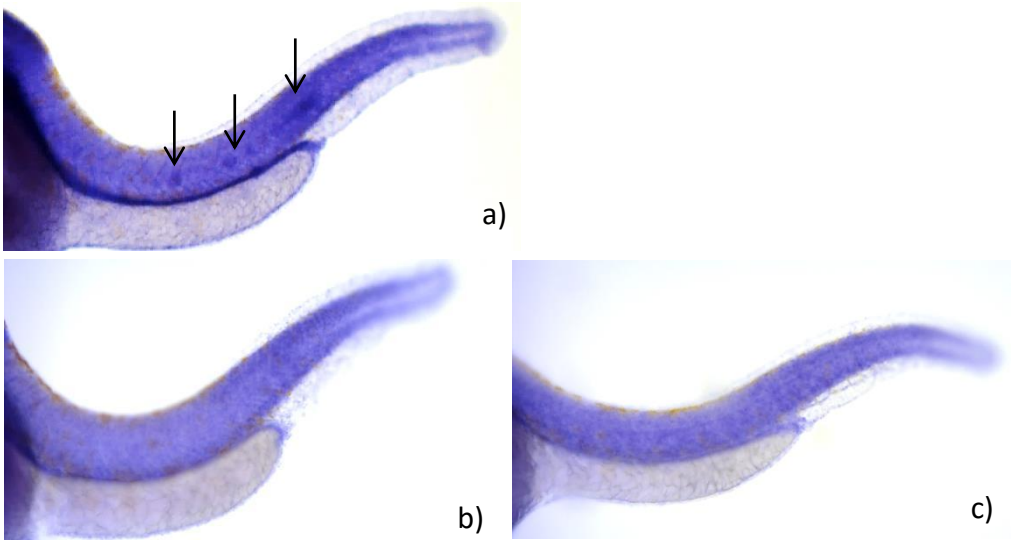

Figure 4.27 Expression of *cd9b* is reduced in 36hpfCD9b -8/-8 (b) and CD9b -1/-1 (c) homozygous mutants compared to AB embryos(a),. CD9b expression assessed using *in situ* hybridisation with a *cd9b* RNA probe. CD9b can be seen in the neuromasts and primordium of the posterior lateral line in WT embryos (black arrows, a), but is absent in CD9b mutants (b,c). n= minimum 3 imaged, 10 observed per genotype. Data from a single experiment.

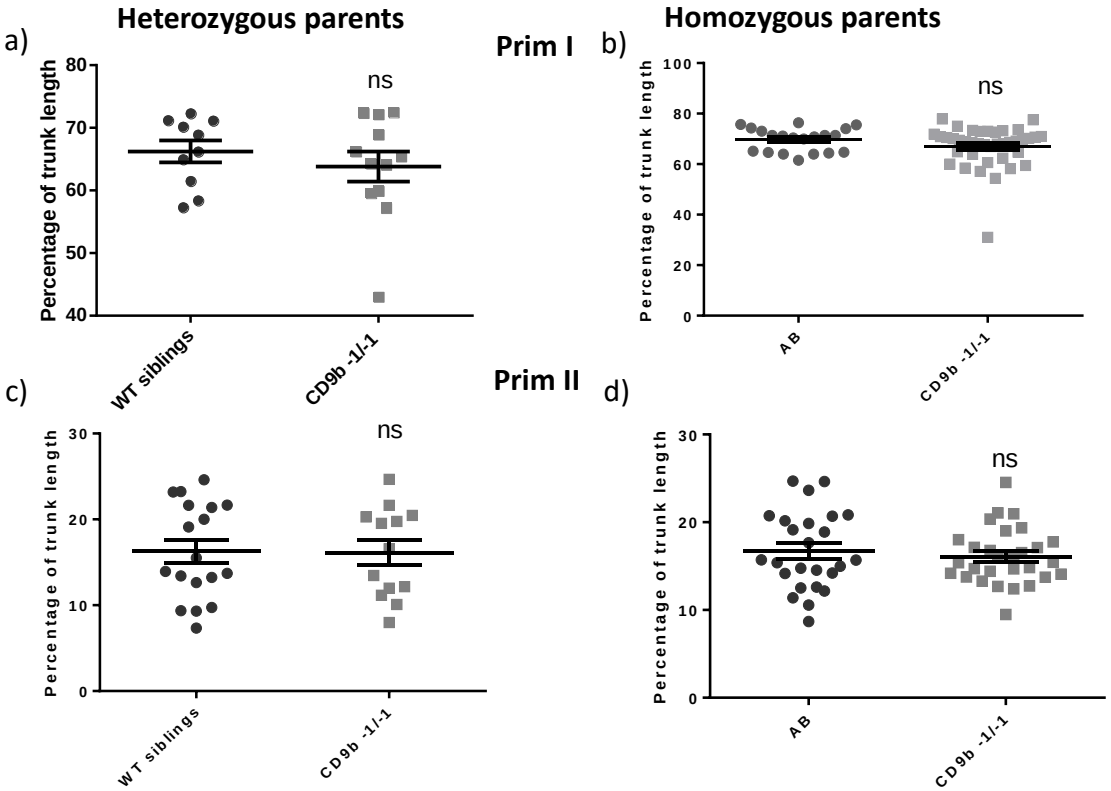

Figure 4.28 The migration phenotypes are not replicated in CD9b -1/-1 mutants. There is no significant difference in the percentage of trunk length migrated by 36hpf by Prim I in CD9b -1/-1 embryos from heterozygous (a) or homozygous (b) parents. There is also no difference in the percentage of trunk length migrated by Prim II by 52hpf in CD9b -1/-1 embryos from hetro- (c) or homo-zygous (d) parents. Unpaired T test on normal (d) or $\log_{10}$ transformed data (a-c). n= minimum 10 (a), 20 (b), 13 (c), 25 (d). p=<0.05. Data taken from four experiments.

Due to the lack of migration phenotype seen in CD9b -1/-1 embryos, I decided to repeat the *claudinb in situ* hybridisation experiments on 36 and 52hpf CD9b -8/-8 embryos from both heterozygous and homozygous parents. Each experiment was performed in triplicate but only the migration assay looking at Prim I migration in 36hpf embryos from heterozygous parents could be pooled and so the other conditions were analysed by looking for trends between the individual experiments (Figure 4.29). Representative graphs are shown for Figures 4.29b-d, for the experimental repeats see Figures 4.20, 4.21e and 4.30.

As shown in Figure 4.29e, the pattern starts to break down when the experimental repeats are taken into account. No significant difference was seen in the migration of Prim I in CD9b -8/-8 from heterozygous parents, both when looking at the pooled data and the individual experiments (Figure 4.29a,e). A significant decrease in Prim I migration at 36hpf was consistently seen in CD9b -8/-8 embryos from homozygous parents, suggesting that this phenotype may be specific and the developing embryos may need maternal CD9b for correct Prim I migration (Figure 4.29b,e). For Prim II migration, the data was much more varied (Figure 4.29e). In 52hpf CD9b -8/-8 embryos from heterozygous parents, each experiment gave a different result with significant increase, decrease and no significant difference seen (Figure 4.29e). Due to the opposing results, I concluded that the significant difference initially seen is most likely an artefact resulting from the variability of Prim II migration. I reached the same conclusion when looking at 52hpf CD9b -8/-8 embryos from homozygous parents as the significant decrease in migration was only observed in the initial experiment and not repeated (Figure 4.29e).

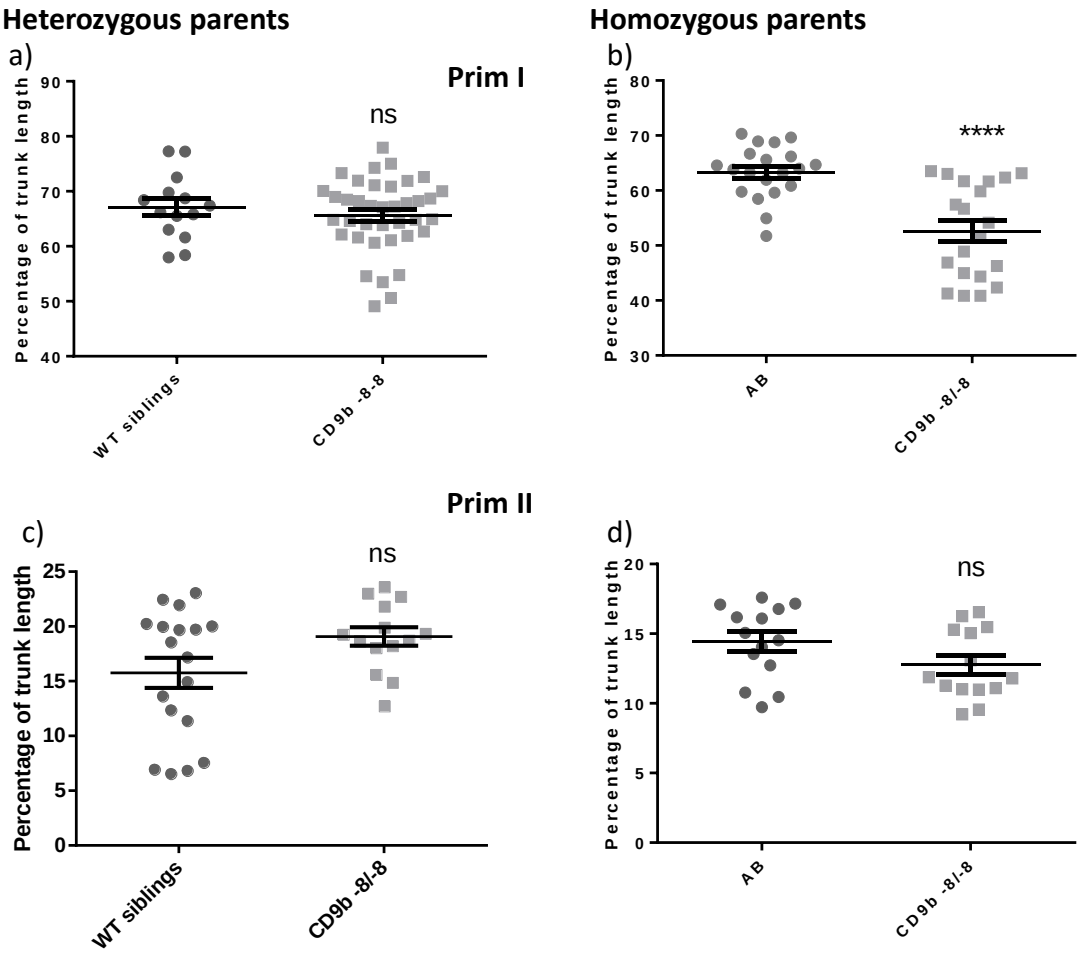

e)

	Heterozygous Parents			Homozygous parents		
Prim I	NS	NS	NS	↓	↓	↓
Prim II	↑	NS	↓	↓	NS	NS

Figure 4.29 The migration pattern is not replicated in further experiments.

The percentage of trunk migrated by Prim I by 36hpf only appears to be affected in embryos from homozygous parents (b) and not heterozygous parents (a). No significant difference is seen in the migration of Prim II by 52hpf in embryos from homozygous parents (d) and heterozygous parents (c). e) shows the outcome of each experimental repeat, with increase in migration in CD9b mutants displayed as a green arrow, a decrease as a red arrow and ns shows no significant difference.

Unpaired T test, n= minimum 14 (a,c,d), 20 (b). (a) shows pooled data of 3 experiments but the three repeats of b-d can't be pooled so a representative graph is shown, see Figures 4.20a,b, 4.21e and 4.30 for the experimental repeats of b-d. p=<0.05

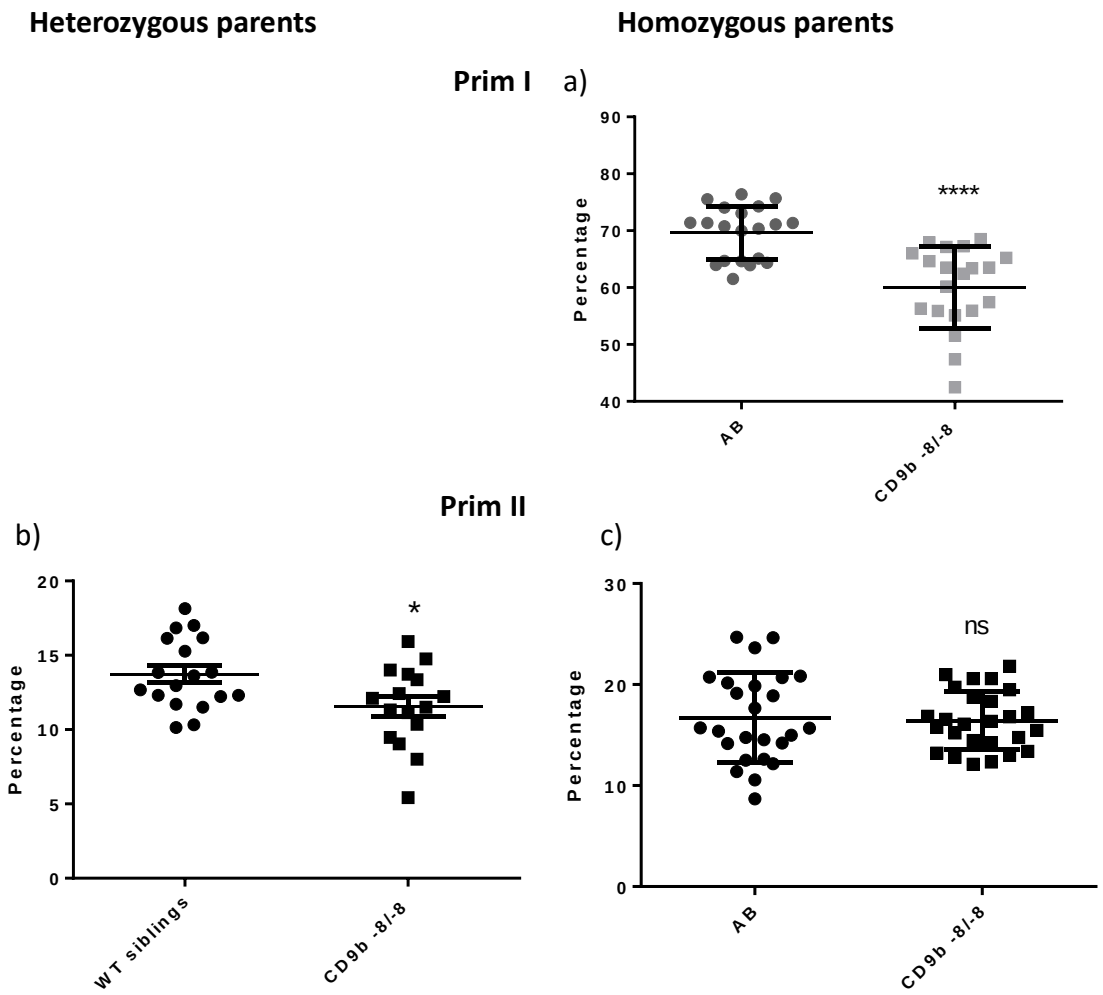

Figure 4.30 The migration pattern is not replicated in further experiments, experimental repeats of Figure 4.29.

The percentage of trunk migrated by Prim I by 36hpf appears to be consistently decreased in embryos from homozygous parents (a). No significant difference is seen in the migration of Prim II by 52hpf in embryos from homozygous parents (c) but a small decrease was seen in embryos from heterozygous parents (c) in this repeat. Unpaired T test, n= minimum 16 (b), 20 (a), 25 (c). p=<0.05

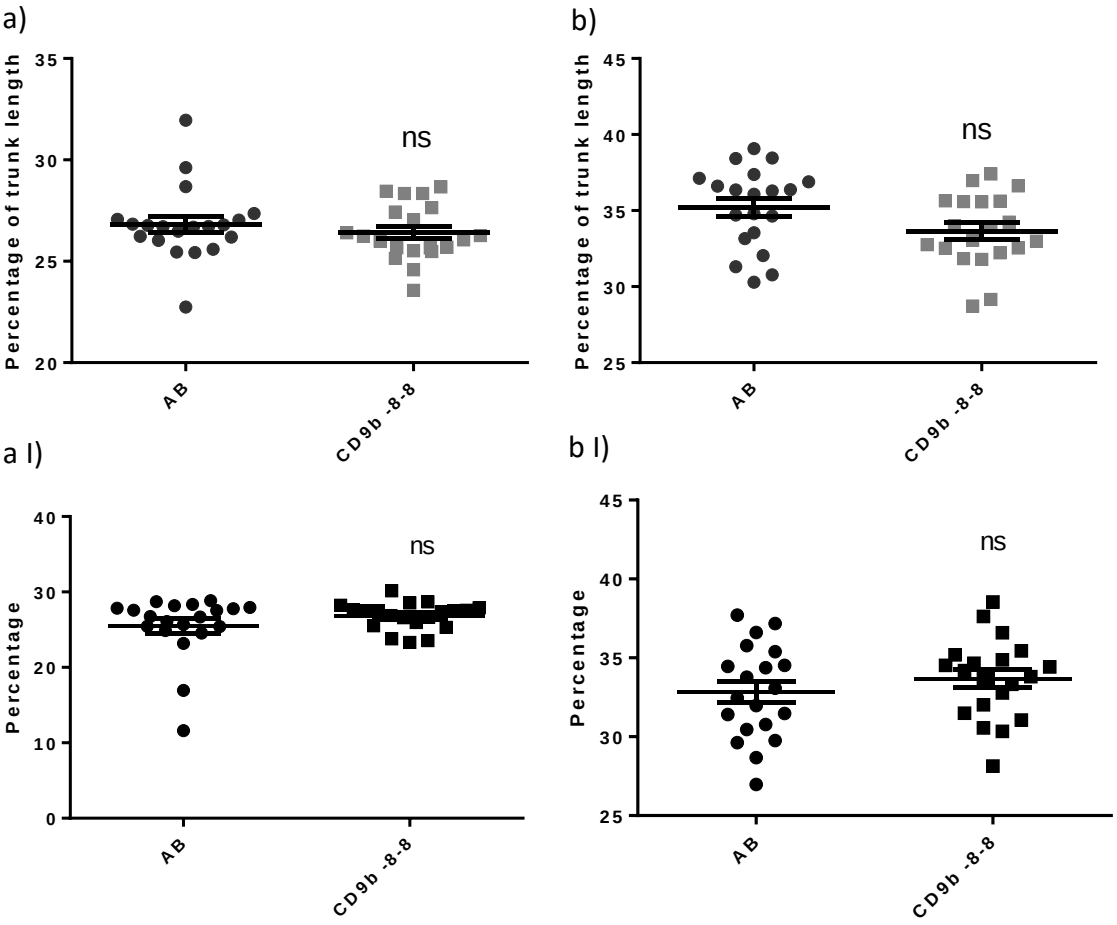

c)

hpf	Homozygous parents		
72	↓	NS	NS
96	↓	NS	NS

Figure 4.31 The delay in Prim II migration at 72 (a) and 96 (b) hpf in not observed in further experimental repeats.

Graphs of individual experiments showing the percentage trunk migrated by Prim II at 72 (a, a I) or 96 (b, b I) hpf. Unpaired T test on $\log_{10}$ transformed data (a, a I) and untransformed data (b, b I).n = 20. See Figure 4.23 for experimental repeats. c) shows the outcome of each experimental repeat, with increase in migration in CD9b mutants displayed as a green arrow, a decrease as a red arrow and ns shows no significant difference. p=<0.05

As well as the pattern seen in Figure 4.22 breaking down, the delay in Prim II migration seen at 72 and 96hpf previously also breaks down when the experiments are repeated. Only one of the three experiments showed a delay in Prim II migration, again suggesting that the initial delay seen is not a true CD9b deficiency phenotype (Figure 4.31).

The variability in percentage of trunk length migrated by Prim I and Prim II in both wildtype and mutant embryos suggests that any overall effect seen is not solely due to the CD9b mutation but could be due to a number of background environmental differences. One of these differences could be temperature fluctuations between experiments, which has been shown to affect penetrance in many other mutant lines (Johnson and Weston 1995, Dick et al. 2000, Poss et al. 2002, Parichy et al. 2003, Pei et al. 2007, Lin et al. 2013). Embryos are incubated at 28°C in a communal incubator, which is subject to temperature fluctuations depending on how often and for how long the incubator door is opened. The room temperature also changes throughout the year and so the extent to which the temperature changes will also depend on the room temperature during the experiment. To assess whether temperature fluctuations were affecting the migration of Prim I, AB and CD9b -8/-8 embryos were placed at 22°C for 72hpf, by which time they had developed to around stage Prim-25. Figures 4.32a and b show there is a decrease in the percentage of trunk migrated, however if this change is compared to the decrease seen in embryos from the same batch that were placed at 28°C until Prim-25, it is clear that the lower temperature is not exacerbating the delay (Figure 4.32). Whilst there appears to be no difference in the migration of Prim I in embryos incubated at 22°C compared to 28°C, there was a striking number of obvious abnormalities seen in the CD9b KO mutants kept at 22°C, which is explored later in Chapter 5 (Figure 4.32a).

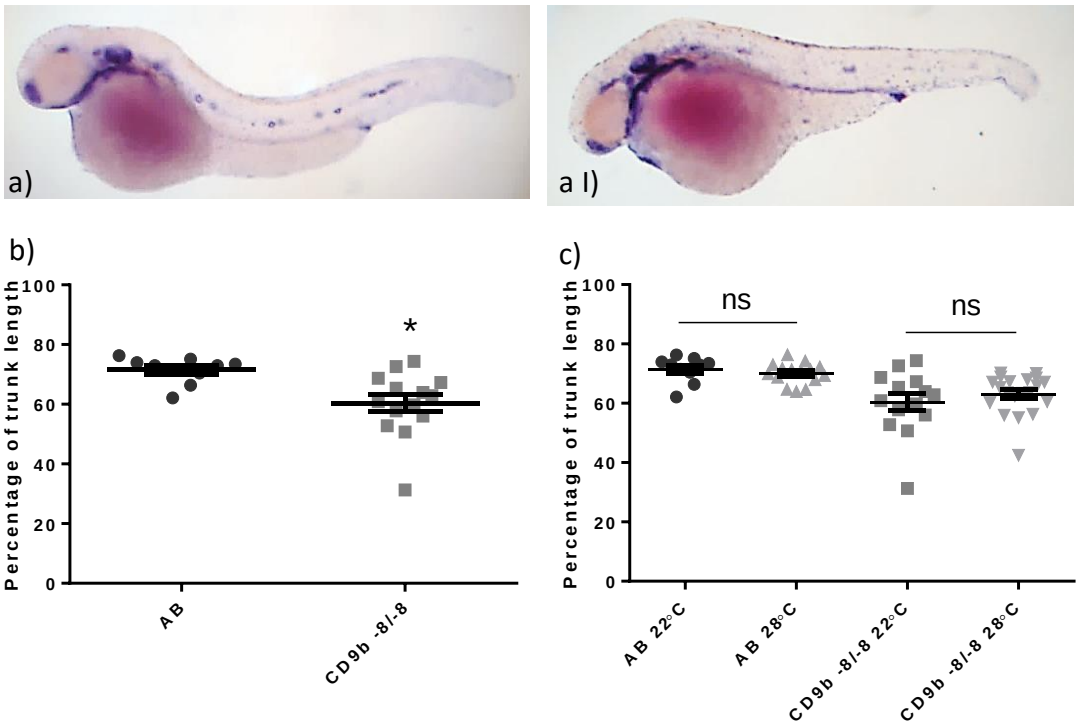

Figure 4.32 The variability in migration does not appear to be due to temperature sensitivity.

CD9b -8/-8 embryos (a I) raised at 22°C for 72hpf (to stage Prim-25) , stained for *claudin b,* show a decrease in the percentage trunk migrated by Prim I (b) compared to AB embryos (a). However, there is no difference in percentage trunk migrated by Prim I in stage matched embryos raised at 28°C (c) indicating the temperature is not causing or exacerbating the difference. Unpaired T test (b) and ANOVA with Sidak's multiple comparison test, which gave increased power (c), were both performed on $\log_{10}$ transformed data. n= minimum 10 p=<0.05. Data from a single experiment.

4.2.4.6 Is CXCR4b trafficking affected in CD9b homozygous mutants?

The original hypothesis of this project predicted that CD9b may play a role in regulating the signalling of CXCR4b. Leung et al. reported in 2011 that CD9 was up-regulated by CXCR4 and promoted CXCR4-mediated migration of HSCs. If CD9b played a similar role in the pLL, it would be expected that a pLL phenotype would have been observed in CD9b mutants. However, CXCR4 signalling has also been reported to be regulated by a tetraspanin through trafficking of CXCR4 (Yoshida et al. 2008). It has been suggested that we may not have expected to see a lateral line phenotype even if CD9b is regulating CXCR4b trafficking. Unpublished data looking at a mutant with a CXCR4b-internalisation defect showed no lateral line phenotype (personal communication, Dr. D. Gilmour, European Molecular Biology Laboratory Heidelburg). To investigate whether CD9b was required for CXCR4b internalisation, an internalisation assay was developed (Figure 4.33). CXCR4b-EGFP and CXCL12a-Venus constructs were provided by Prof. E.Raz, University of Münster (Minina et al. 2007), mRNA produced and injected individually into single blastocysts at the 8-cell stage in separate AB embryos (Figure 4.33a-b). Expression of both CXCR4b-EGFP and CXCL12a-venus were as expected, with CXCR4b expressed on the cell membrane and the ligand CXCL12a dispersing from CXCL12a-producing cells (Figure 4.33a-b) (Minina et al. 2007). The constructs were then injected into individual blastocysts in single 8-cell stage AB embryos, incubated for 3-4 hours and imaged, to see if the CXCR4b-EGFP and CXCL12a-Venus would co-localise and internalise, replicating endogenous CXCR4b and CXCL12a (Figure 4.33c) (Tarasova et al. 1998). As shown in Figure 4.33c, the CXCR4b-EGFP and CXCL12a-Venus can be seen co-localised in intracellular puncta, suggesting that the ligand bound the receptor, inducing internalisation and re-localisation for degradation.

The internalisation assay was then used on both AB and CD9b -8/-8 embryos to assess CXCR4b internalisation in CD9b deficient cells. Puncta were seen in both AB and CD9b -8/-8 embryos with CXCR4b-EGFP and CXCL12a-Venus co-localising inside the cells (Figure 4.34). This shows that CXCR4b is able to internalise in CD9b -8/-8 embryos, however, it does not rule out CD9b playing a role in CXCR4b internalisation in the lateral line. Tetraspanins are well known for their redundancy and a lack of phenotype could be explained by this (Hemler 2005, 2008, Hassuna et al. 2009). It may also be that CD9b only aids CXCR4b internalisation in certain tissues such as the lateral line,

which would not be seen at such an early embryonic stage. Whilst CD9b may aid CXCR4b internalisation in the lateral line, there is no positive data to support continuing this investigation.

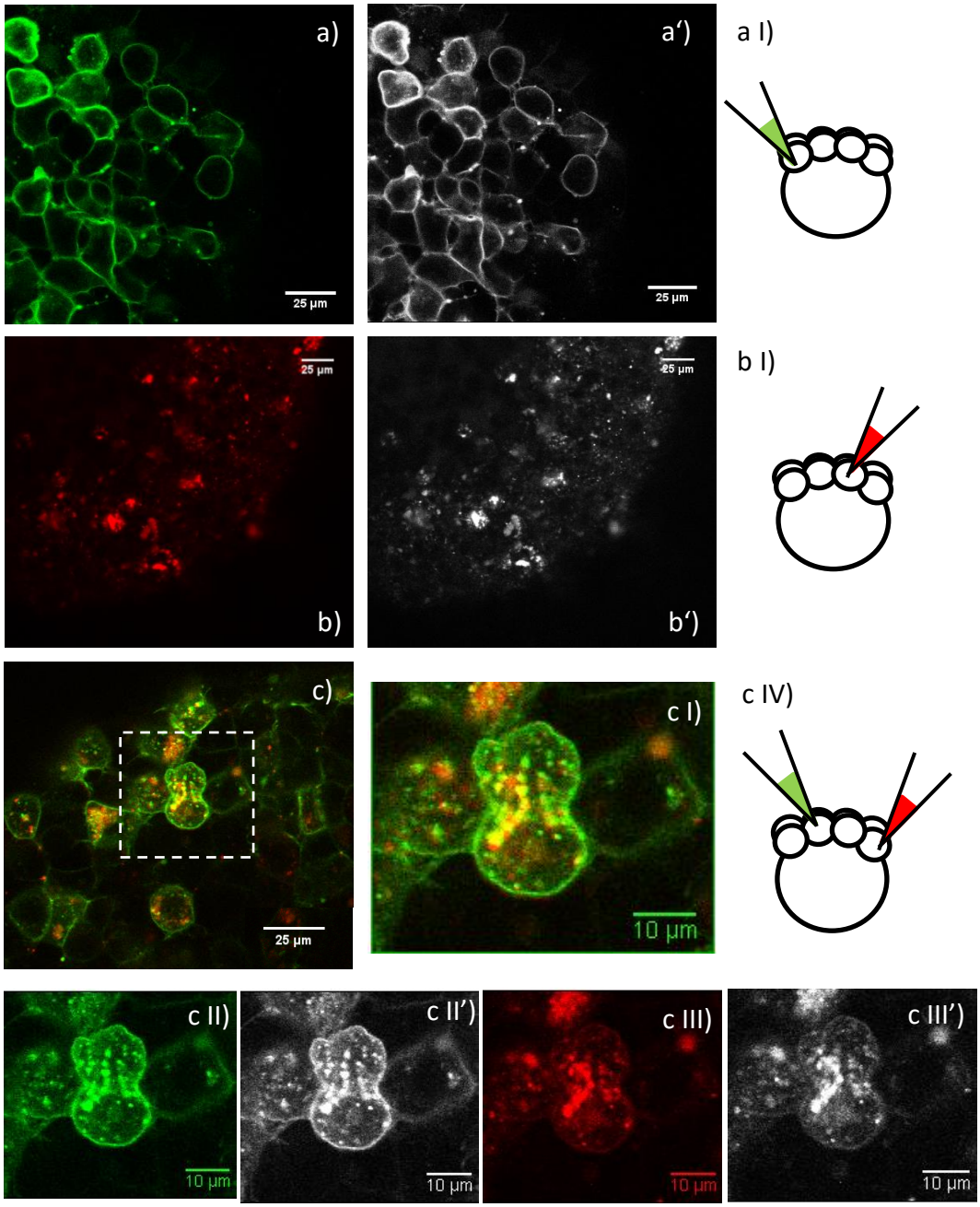

Figure 4.33 The CXCR4b-EGFP and CXCL12a-Venus co-localise and internalise like wildtype CXCR4b and CXCL12a.
Individual injections of CXCR4b-EGFP (a) and CXCL12a-Venus (b) into single blastocysts at the 8-cell stage (a I, b I) shows the membrane localisation of CXCR4b and the dispersion of CXCL12a. Co-injection of CXCR4b-EGFP and CXCL12a-Venus at 8-cell stage (c) displays co-localisation inside the cell. Magnification of the white box is shown in c I-III), with both channels shown in c I), CXCR4b only in c II) and CXCL12a only in c III). n= 3 (a), 2 (b), 5 (c) images, minimum 3 embryos observed per condition. Data from a single experiment.

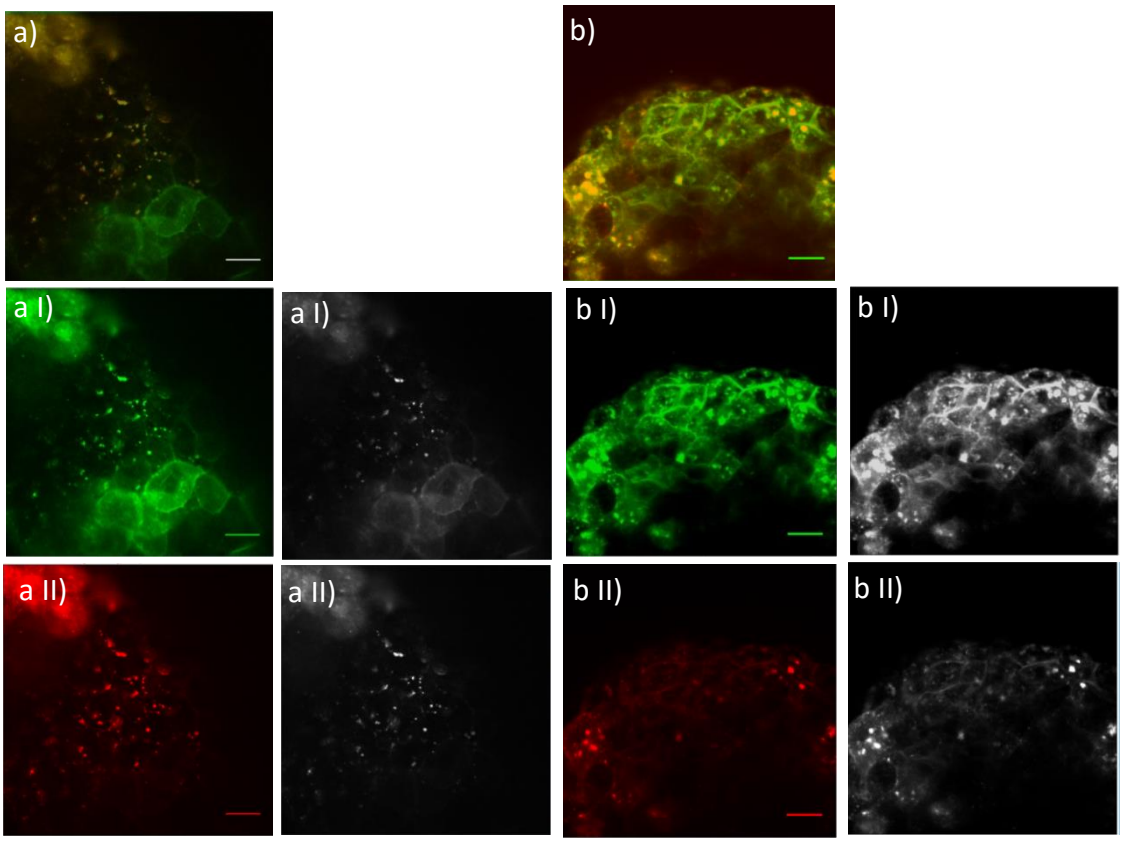

Figure 4.34 Co-localisation of CXCR4b and CXCL12a in intracellular puncta can be seen in both WT (a) and CD9b -8/-8 (b) embryos.
AB (a) and CD9b -8/-8 embryos (b) injected with CXCR4b-EGFP (a I, b I) and CXCL12a-Venus (a II, b II) in different blastocysts at the 8-cell stage and imaged 3-4 hours later. Scale bars 25µM. n= 2(a), 5(b) images, minimum 3 embryos observed. Data from a single experiment.

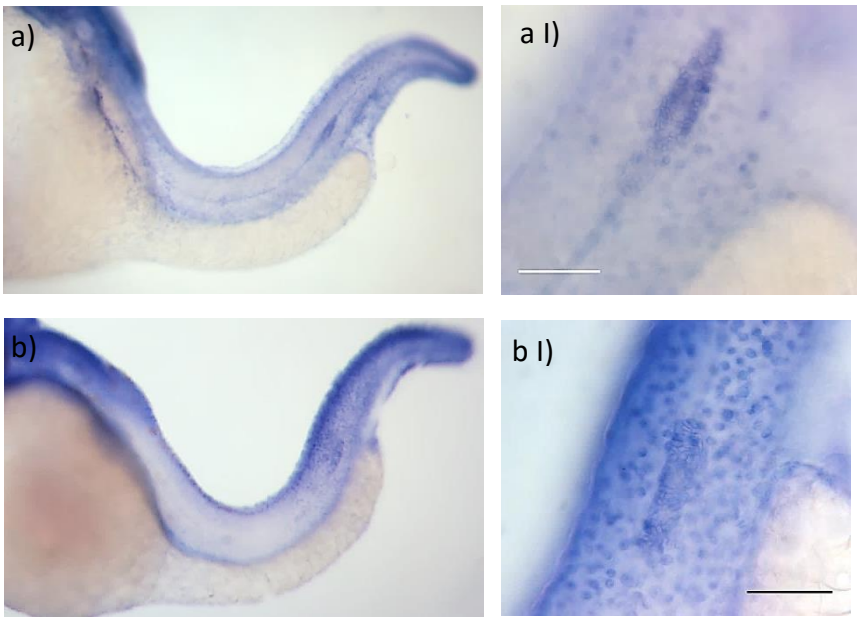

Figure 4.35 AB and CD9b -8/-8 embryos show no clear difference in *cd9a* RNA staining in the pLLP.
cd9a in situ hybridisation in 36hpf AB (a) and CD9b -8/-8 (b) embryos. a I) and b I) show the staining in the posterior lateral line primordium. Scale bars 50µM. n= 3(a), 4(b) images, minimum 10 embryos observed per genotype. Data from a single experiment.

4.2.4.7 Why do CD9b morphants and mutants display different pLL phenotypes?

At the beginning of this project the gold standard for reverse genetics was the creation of a mutant line. However, a recent paper by Rossi et al., 2015 showed that mutations in *egfl7*and *vegfaa* induced redundancy whereas knock-down technologies did not. In light of this, a *cd9a in situ* hybridisation was carried out on 36hpf AB and CD9b -8/-8 embryos to look for an upregulation of expression of the *cd9b* paralog, *cd9a,* in the lateral line primordium (Figure 4.35). *cd9a* was shown to be expressed in both AB and CD9b -8/-8 embryos with no obvious difference between the two, suggesting that *cd9a* expression is not noticeably upregulated (Figure 4.35). This was unexpected as *cd9a* has not previously been shown to be expressed in the lateral line in wildtype embryos, however, the expression was reproduced in multiple experiments.

Rossi et al.,2015 also demonstrated that injecting morpholinos into mutants, of the same target gene, can help to describe why phenotypes were seen with morphants but not mutants. Injecting CD9b MOs into CD9b mutants and seeing no phenotype would rule out the possibility that the CD9b MO phenotypes were caused by off-target effects, it would also show that the mutants are complete knock-outs and have no residual WT protein. AB, CD9b -8/-8 and CD9b -1/-1 embryos were left uninjected or injected with CD9b MO1, CD9b i2e3 or Mismatch MO at the 1-cell stage to give a final concentration of 0.1µM after which lateral line phenotypes were assessed by *claudin b in situ* hybridisation at 52hpf (Figure 4.36). AB embryos injected with CD9b MO1 or CD9b i2e3 replicated the phenotypes seen previously, showing decreased numbers of neuromasts deposited and irregular spacing between neuromasts, with CD9b MO1 causing a stronger phenotype. No difference in the percentage of trunk length migrated by Prim I or the percentage of trunk length between the 1st and last neuromasts was seen in AB embryos injected with CD9b i2e3, however, a significant decrease was seen in CD9b MO1 injected embryos (Figure 4.36). This suggests that Prim I may not have completed migration in the AB CD9b MO1 morphants, whereas it had in CD9b i2e3 morphants.

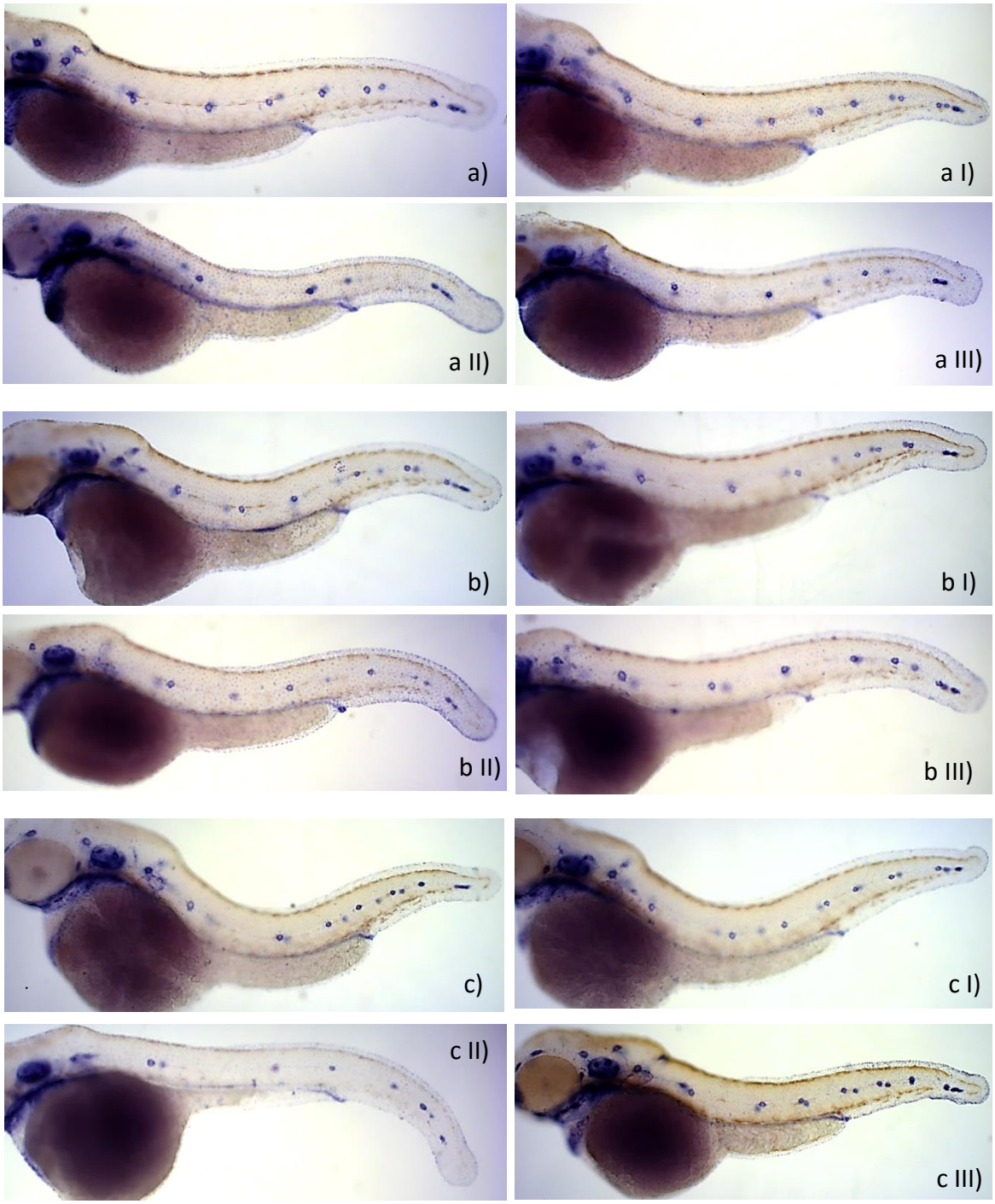

Figure 4.36 CD9b MO1 but not CD9b i2e3 causes abnormal pLL structure in CD9b mutant embryos.
Representative images of a *claudin b in situ* hybridisation on 52hpf AB (a), CD9b -8/-8 (b) and CD9b -1/-1 (c) embryos. Embryos were left uninjected (a,b,c) or injected with 0.1µM Mismatch MO (I), CD9b MO1 (II) or CD9b i2e3 (III).

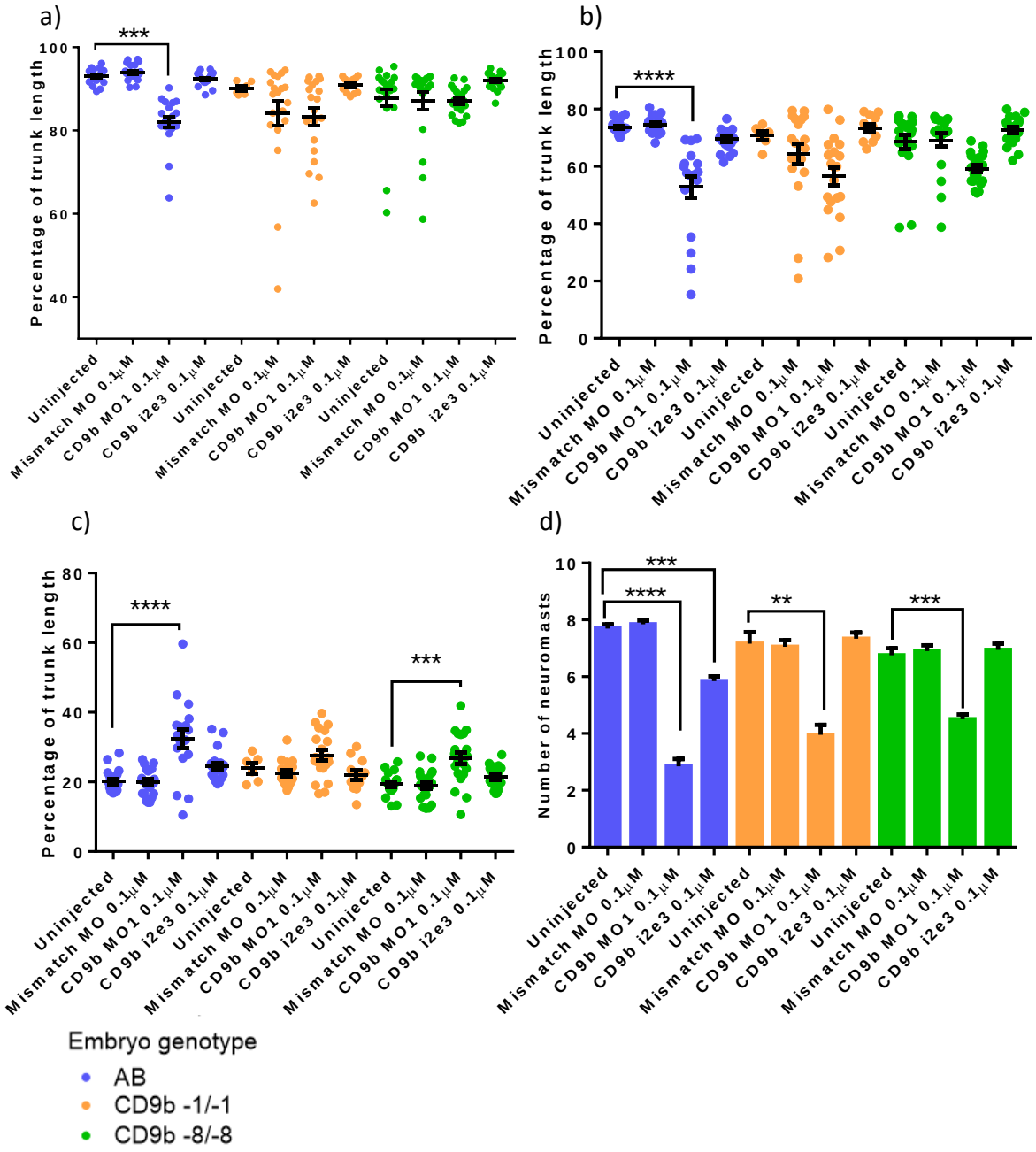

Figure 4.36 continued.CD9b MO1 but not CD9b i2e3 causes abnormal pLL structure in CD9b mutant embryos.

52hpf AB (blue), CD9b -8/-8 (orange) and CD9b -1/-1 (green) embryos were left uninjected or injected with 0.1μM Mismatch MO, CD9b MO1 or CD9b i2e3. Lateral line phenotypes were assessed using four assays: percentage of trunk length migrated by Prim I (a), percentage of trunk length between the 1st and last neuromast (b), percentage of trunk length between 1st and 2nd neuromasts (c) and the number of neuromasts deposited (d). Significance was analysed using an ANOVA with Sidak's multiple comparison test on $\log_{10}$ transformed data (a-c) or a Kruskal-Wallis test with Dunn's multiple comparisons test (d). n= 20 except for CD9b -1/-1 uninjected where n=6 and CD9b -1/-1 i2e3 where n=12. Many CD9b -1/-1 embryos died or were severely developmentally delayed and so were not analysed. Injected embryos were compared against the uninjected group of the same genotype. p=<0.05. Data from a single experiment.

CD9b -1/-1 and CD9b -8/-8 embryos injected with CD9b i2e3 showed no significant difference, compared to uninjected, in any of the assays indicating that no lateral line phenotypes were caused by this MO. CD9b MO1, however, did appear to cause a lateral line phenotype with less neuromasts deposited and varied spacing between the 1st and 2nd neuromasts. This induced phenotype in the CD9b mutants appears milder than the one seen in AB embryos injected with CD9b MO1 (Figure 4.36).

The lack of lateral line phenotypes in CD9b mutants injected with CD9b i2e3 suggests that the lateral line phenotypes seen in CD9b morphants are not due to general off-target effects or morpholino toxicity. If this were the case, it would be expected that both MOs would induce a phenotype in the CD9b mutants. The presence of lateral line phenotypes in CD9b MO1 injected CD9b mutants could suggest that CD9b MO1 is knocking down a secondary target, which could explain the more severe phenotypes seen with CD9b MO1. Alternatively it could suggest that there is residual functioning protein in the CD9b mutants.

BLAST (Basic local alignment search tool) was used to look for potential secondary targets of CD9b MO1 (Figure 4.37a). The only complete match was to *cd9b* as expected and all the potential secondary targets were predicted sequences, of which none were tetraspanins (Figure 4.37a). This suggests that CD9b MO1 is only binding *cd9b.*

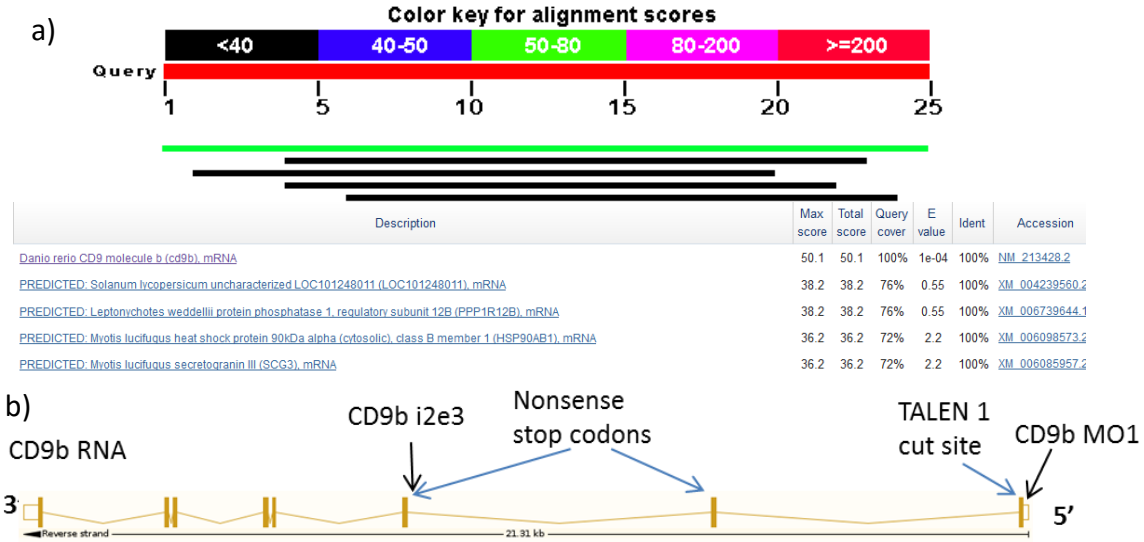

Description	Max score	Total score	Query cover	E value	Ident	Accession
Danio rerio CD9 molecule b (cd9b), mRNA	50.1	50.1	100%	1e-04	100%	NM_213428.2
PREDICTED: Solanum lycopersicum uncharacterized LOC101248011 (LOC101248011), mRNA	38.2	38.2	76%	0.55	100%	XM_004239560.2
PREDICTED: Leptonychotes weddellii protein phosphatase 1, regulatory subunit 12B (PPP1R12B), mRNA	38.2	38.2	76%	0.55	100%	XM_006739644.1
PREDICTED: Myotis lucifugus heat shock protein 90kDa alpha (cytosolic), class B member 1 (HSP90AB1), mRNA	36.2	36.2	72%	2.2	100%	XM_006098573.2
PREDICTED: Myotis lucifugus secretogranin III (SCG3), mRNA	36.2	36.2	72%	2.2	100%	XM_006085957.2

Figure 4.37 CD9b MO1 appears to only bind and affect *cd9b* (a) but CD9b i2e3 may not affect *cd9b* in the CD9b mutants.
CD9b MO1 appears to only bind *cd9b* (a), and not *cd9a*, according to BLAST. All other alignments with high query cover were just predicted sequences and no other tetraspanins were included in the list. It appears that only CD9b MO1, and not CD9b i2e3, may affect the two CD9b mutants as the mutations induce non-sense stop codons before the splice site affected by CD9b i2e3 (b).

Looking at the target sites for CD9b i2e3 and CD9b MO1 in *cd9b,* it became apparent that CD9b i2e3 binds after the nonsense stop codons induced in the CD9b mutants (Figure 4.37b). This could suggest that CD9b i2e3 may not have any additional effect on knocking down *cd9b*, whereas CD9b MO1 binds at the 5'UTR which would prevent translation of any mutant RNA not degraded by nonsense mediated decay (Figure 4.37b). The two mutants have cut sites in the first *cd9b* exon, which induced frameshifts; however the N-terminus and the beginning of the first transmembrane domain remain wildtype (Figure 4.1,4.11). It has been shown by multiple groups that the N- and C- termini of tetraspanins can play an important role in their function, for example the N-terminus of CD63 is required for its correct localisation and partner protein trafficking function (Yoshida et al. 2008). Taken together this could suggest that the N-terminal of CD9b is needed for CD9b to function correctly in the lateral line, with the CD9b N-terminus present in CD9b mutants but knocked down when using CD9b MO1.

To investigate whether the CD9b N-terminus RNA is present in CD9b mutants or degraded by nonsense mediated decay, qPCR was used to assess the levels of CD9b N- and C-terminals relativet to a reference gene, β-actin2 (Tang et al. 2007). Three primer pairs were designed to bind *cd9b*, with two targeting the 5'UTR and N-terminus and one targeting the 3'UTR and C-terminus. The primers for the control gene, β-actin2 were provided by Dr. P.Hua, University of Oxford. Primer pairs were initially tested on a cDNA mixture containing AB, CD9b -1/-1 and CD9b -8/-8 cDNA and dissociation curves studied to ensure that a single product was being produced by each primer pair, shown by the production of a single peak on the dissociation curve (Figure 4.38). I decided to use primers for β-actin2, CD9b C-terminus and CD9b N-terminus 1 but not CD9b N-terminus 2 as the primary N-terminus pair produced a cleaner dissociation peak.

These primers were then used for qPCR on cDNA from six single AB, CD9b -1/-1 or CD9b -8/-8 embryos. qPCR is highly sensitive to pipetting errors and so three technical repeats were conducted to highlight any abnormal results, which were later identified and removed blind before analysing the results. The results from CD9b C- or N-terminal primers were first normalised to β-actin2 expression results. The relative expression of CD9b N- and C- terminal RNA in CD9b mutants, compared to wildtype,

was then calculated. Figure 4.39a shows a significant decrease in the expression of CD9b C-terminal RNA in both CD9b mutants. The decrease is within the expected range for nonsense mediated decay (NMD), with 40-70% reductions due to NMD having been reported previously (Baker et al. 2006, Luan et al. 2015, Roman-Sanchez et al. 2015). Interestingly, CD9b N-terminus RNA does not show the same result. CD9b -1/-1 mutants appear to have no significant difference in the expression of CD9b N-terminal RNA, whereas CD9b -8/-8 mutants do show a significant decrease with approximately half the expression level compared to AB embryos (Figure 4.39b). Due to the differences in primer efficiencies, as shown by the standard curves in Figure 4.40, the CD9b C-terminal and CD9b N-terminal expression levels cannot be directly compared to each other. However, this qPCR has shown that CD9b N-terminal RNA is still present in CD9b mutants. If the N-terminus of CD9b does play a role in CD9b function in the lateral line, it would explain why a migration delay was seen in CD9b -8/-8 embryos from homozygous parents but not CD9b -1/-1 embryos and why CD9b MO1 causes an abnormal lateral line phenotype but CD9b i2e3 does not in CD9b mutants.

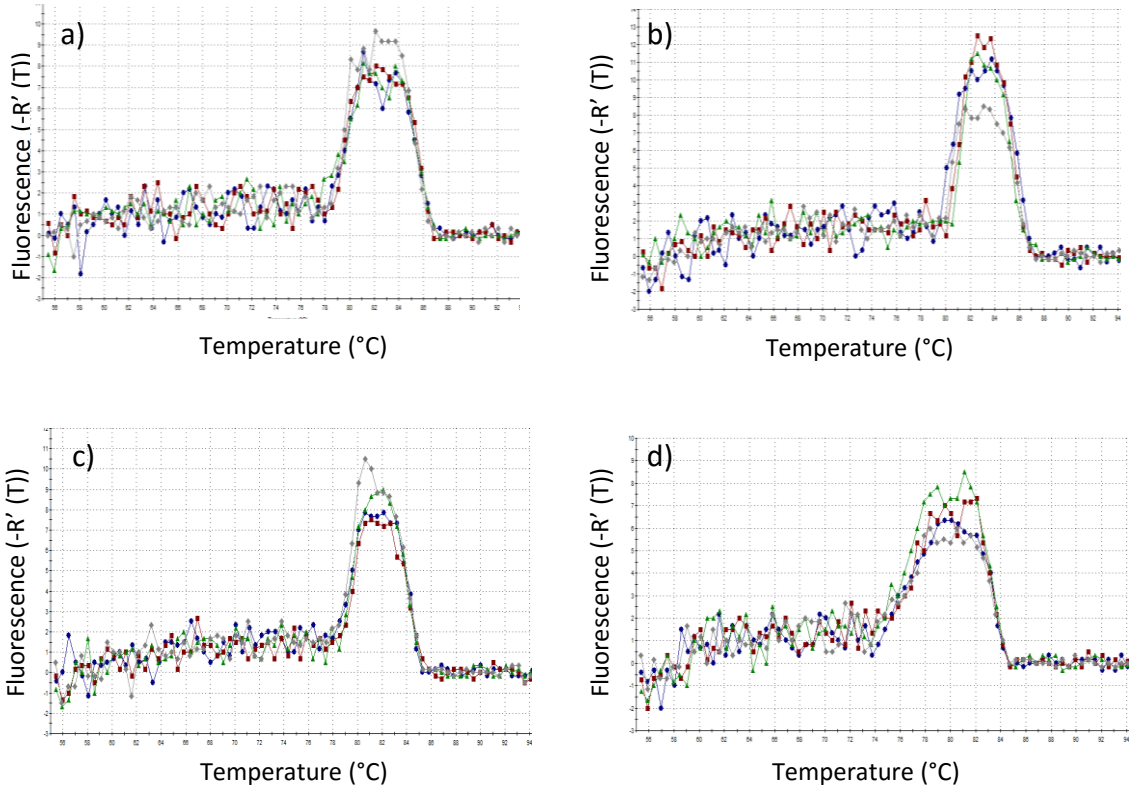

Figure 4.38 The qPCR primer pairs produce a single product.
Dissociation curves of β-actin 2 (a) and CD9b primer pairs: CD9b C-terminus (b), CD9b N-terminus 1 (c) and CD9b N-terminus 2 (d). n= 4 technical repeats

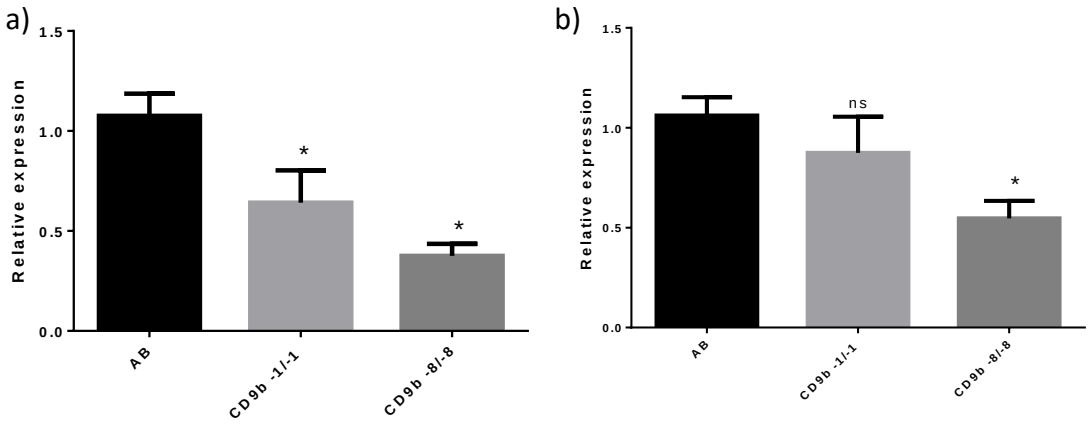

Figure 4.39 Expression of CD9b (a) C-Terminal but not (b) N-Terminal RNA is significantly reduced in both CD9b mutants compared to AB embryos.
qPCR on single 36hpf embryo cDNA using 6 biological samples and three technical repeats for each condition. Abnormal results, due to pipetting errors, were removed. Unpaired T-test with Holm-Sidak's multiple comparisons correction, p=<0.05. n= minimum 15 (a) and 11 (b) data points per genotype

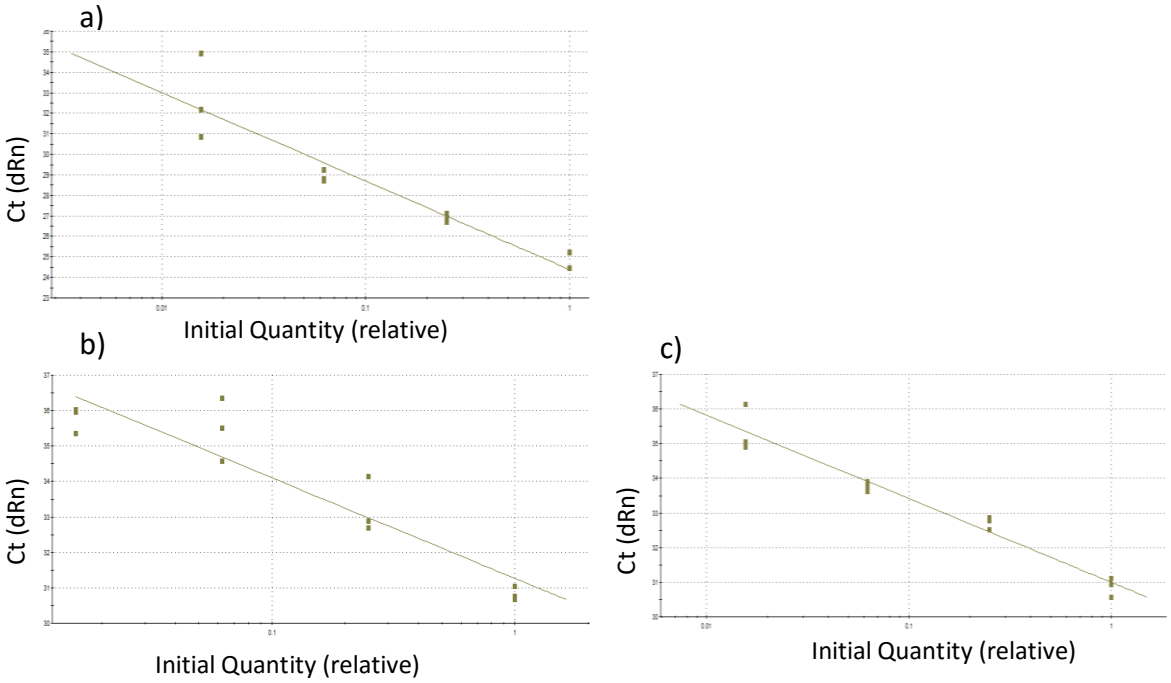

Figure 4.40 Primer pairs cannot be directly compared as primer efficiencies are not within 10-15% of each other.
Standard curves of β-actin 2 (a), CD9b C-terminal (b) and CD9b N-terminal (c). Primer efficiencies were 70.4 % (a), 125.0 % (b) and 159.67% (c) as calculated by MxPro. n=3 technical repeats

4.3 Discussion

Having created and studied two CD9b mutant lines for PGC and pLLP migratory defects, it has been shown that while the PGCs phenocopy the PGCs in CD9b morphants, the pLL does not. Homozygous CD9b mutants show no difference in the clustering of PGCs to wildtype controls, a phenotype which is seen in all of the CD9b morphants except embryos injected with the highest amounts of CD9b MO1(0.5-2.0µM) (Figure 4.16, Figure 3.6). These morphants also displayed increased morpholino toxicity, resulting in general morphological abnormalities (Figure 3.5). Interestingly this is mirrored by the CD9b mosaic embryos that were injected with either TALEN 1, which caused fewer morphological abnormalities, or TALEN 2, which caused greater amounts of morphological abnormalities (Figures 4.3-4.4). Only the TALEN 2 injected embryos showed a PGC phenotype, with increased distance between the most anterior and posterior PGC and increased numbers of ectopic PGCs (Figures 4.7-4.8). This supports the hypothesis that the significance seen in CD9b MO1 0.5-2.0µM morphants is due to general toxicity causing abnormal PGC migration and not a specific phenotype due to CD9b deficiency. The fact that TALEN 2 does not cut CD9b at the predicted site, unlike TALEN 1, may also suggest that any PGC phenotypes seen are due to general toxicity, however, the possibility of TALEN 2 causing DSBs elsewhere in *cd9b* or another gene cannot be ruled out.

While CD9b morphants did not show a consistent PGC phenotype, a consistent pLL phenotype was seen. CD9b morphants showed a decreased number of neuromasts deposited, irregular spacing between neuromasts and often a delay or stalling in primordium migration (Figures 3.10-3.12). Surprisingly, this phenotype is not recapitulated in CD9b homozygous mutants (Figure 4.19). This lack of phenotype could be due to a number of reasons. Firstly, the phenotype seen in CD9b morphants could be due to off target effects of the morpholinos and not due to CD9b knockdown. Secondly, the CD9b morphant phenotypes may be specific but tetraspanin redundancy could rescue the phenotype in CD9b mutants. Finally, the CD9b mutants could have some residual function.

It seems unlikely that the phenotypes seen in CD9b morphants are solely due to morpholino toxicity, as the same phenotype was seen with two independent morpholinos and at a range of concentrations. If the phenotypes were due to MO

toxicity, one would expect the lateral line phenotype to disappear with the general morphological defects seen in the embryos with higher concentrations of MO. This does not appear to be the case as the disrupted lateral line is present in embryos that do not show MO toxicity (Figures 3.11, 3.12). It would also be expected that injecting either of the CD9b MOs into CD9b mutants would cause lateral line phenotypes, if the cause was purely MO toxicity, however only CD9b MO1 and not CD9b i2e3 caused a phenotype (Figure 4.36).

Tetraspanins are well known for their redundancy within the tetraspanin family and mouse knockouts of single tetraspanins often appear healthy and viable with mild phenotypes, whereas double tetraspanin knockout mice often show increased numbers and severity of phenotypes (Knobeloch et al. 2000, Takeda et al. 2003, 2008, Wright et al. 2004, Hemler 2005, 2008, Hassuna et al. 2009, Gartlan et al. 2010). In zebrafish, this redundancy tendency may be amplified due to the occurrence of a fish-specific whole genome duplication in teleost fish. This means that many tetraspanins, for which there is one mammalian ortholog, have two paralogs in zebrafish (Meyer and Van de Peer 2005, Brunet et al. 2006, Garcia-España et al. 2008, Huang et al. 2010, Howe et al. 2013b). This is true for CD9, as mammals have a single CD9 whereas zebrafish have CD9a and CD9b. Initially it appeared that *cd9a* and *cd9b* were expressed in different tissues (Figure 1.7). However, this research has shown *cd9a* to also be expressed in the pLL. Whilst both *cd9a* and *cd9b* seem to be expressed in the pLL, CD9a does not appear to be upregulated in this organ in CD9b mutants (Figure 4.35). A CD9a mutant line has been developed using CRISPRs by another member of the lab, which is currently being studied for lateral line phenotypes. A double CD9a, CD9b mutant line is also in development using the CD9a CRISPR and my CD9b TALEN, which will be analysed for lateral line phenotypes in the future. However, the ISH data in Figure 3.35 suggests that redundancy is not the cause of the lack of phenotype seen in the CD9b mutants. If redundancy was rescuing the phenotype, no phenotype would be expected upon injection of CD9b MOs into CD9b mutants; however this was not the case (Figure 4.36).

CD9b *in situ* hybridisation experiments on CD9b -8/-8 and CD9b -1/-1 embryos showed no noticeable *cd9b* RNA and so it was expected that the mutant RNA was being degraded by nonsense mediated decay, resulting in a CD9b knockout (Figures

4.14,4.27). It was therefore unexpected to find that CD9b MO1 caused a lateral line phenotype in CD9b mutants. One hypothesis for this phenomenon was the presence of functioning CD9b protein in the CD9b mutants (Figure 4.36, 4.37). As CD9b -8/-8 and CD9b -1/-1 embryos have a frameshift causing mutation in Exon 1 of CD9b, only the N-terminus remains wildtype (Figure 4.11). It has been shown in a number of tetraspanins that the N- and C- termini are required for their correct function (Zhang et al. 2001, Stipp et al. 2003, Shoham et al. 2006, Wang et al. 2011a, Lapalombella et al. 2012). qPCR to investigate the relevant expression of the N- and C- termini of *cd9b* in CD9b mutants showed that while the C-terminal has decreased expression in both mutants, the N-terminal is only significantly decreased in CD9b -8/-8 but not CD9b -1/-1 (Figure 4.39). This fits with the observation that CD9b -8/-8 mutants from homozygous parents show a delayed Prim I migration but the equivalent CD9b -1/-1 embryos do not (Figures 4.28,4.29). This suggests that the N-terminal of maternal CD9b may be needed during early embryogenesis for correct migration of Prim I. It also supports the hypothesis that neuromast deposition may be influenced by the N-terminus of CD9b. While the relative expression of the *cd9b* N-terminal is significantly reduced in CD9b -8/-8 embryos, the levels are only 50% of wildtype which may be enough for normal function of the lateral line.

If, as hypothesised, the N-terminus is enough for and required for correct CD9b function in the lateral line and the CD9b morphant phenotypes are specific, the mechanism of CD9b function will need to be explored. One hypothesised mechanism was that CD9b could interact with and cycle CXCR4b; however, a CXCR4b internalisation mutant has since been shown to have no lateral line phenotype (personal communication, D. Gilmour, European Molecular Biology Laboratory Heidelburg). Recent papers have described an alternative mechanism in cell culture where CD9 is upregulated by CXCL12 signalling, which in turn causes the upregulation of RAC 1, polymerisation of actin and production of long actin protrusions which are used for CXCR4-mediated migration (Leung et al. 2011, Brzoska et al. 2015, Arnaud et al. 2015). However, this signalling pathway appears to be likely regulated by the C-terminus of CD9b (Arnaud et al. 2015).

A second model suggests that the N-terminus of CD9b may have signalling activity which could regulate the survival of lateral line cells. This model revolves around the

tyrosine residue in the N-terminus of CD9b. This tyrosine residue is part of the sequence IKYLLFI, which is similar to the sequence IKYFLFV in the N-terminus of human CD37 (Figure 4.41a). In CD37 this sequence is reported to be an immune tyrosine-based inhibitory motif (ITIM) -like domain. ITIM domains consist of a conserved sequence (S/I/V/LxYxxI/V/L, where x denotes any amino acid) within the cytoplasmic domains of many immune system inhibitory receptors. It was shown that although CD37 has an additional residue between the tyrosine and isoleucine /valine/leucine, the domain acts like other ITIM domains. The ITIM-like domain was tyrosine phosphorylated by Src-family kinases, which allowed association with and activation of a number of proteins including SHP1, LYN, SYK and PI3Kγ. The recruitment and activation of proteins such as SHP1 and LYN by the ITIM-like domain was shown to regulate apoptosis in B-cells (Lapalombella et al. 2012).

It appears that CD9 and Src-family kinases might regulate each other. As well as Src-family kinases phosphorylating ITIM domains, multiple Src-family kinases are regulated by CD9. Yamazaki et al. 2011 showed that expression of four members of the Src-family was regulated by the presence or absence of CD9 in human B-cells and that the Src protein was inactivated upon CD9 knockdown. This suggests there may be a feedback loop between CD9 and Src-family kinases, which may have implications for lateral line primordium migration and neuromast deposition.

It was recently shown that the Src-family kinase inhibitors Emodin, SU6656 and RBI caused delayed lateral line primordium migration in zebrafish embryos. A phenotype which was replicated with injection of CRISPRs targeting *src* or *tks5a*, a downstream target of src, indicating the involvement of the Src pathway in regulation of Prim I migration (Gallardo et al. 2015). It was also noted that embryos injected with *src* or *tks5a* CRISPRs showed a decreased primordium size, a phenotype which is reminiscent of decreased proliferation or increased apoptosis in the primordium.

Correct regulation of apoptosis and proliferation in Prim I is required for correct neuromast deposition with increase of the former and decrease of the latter resulting in decreased numbers of neuromasts deposited even though Prim I has reached the end of the tail (Aman et al. 2011, Valdivia et al. 2011). Cell survival in the primordium could be regulated by the ITIM-like domain in CD9b. In B-cells the protein SHP1 which

is activated by the ITIM-like domain in CD37 has been shown to downregulate Akt, and was suggested to downregulate MAPK, phosphorylation which then negatively regulates cell survival (Lapalombella et al. 2012). The Akt and MAPK pathways have also been shown to be regulated by CD9 in megakaryocytes (Desterke et al. 2015). In the same study, CD9 was shown to positively regulate CXCR4-mediated migration of megakaryocytes as well as CXCR4 and CXCL12 expression (Desterke et al. 2015).

It could be hypothesised that the IKYLLFIF sequence in the CD9b N-terminus is an ITIM-like domain, interacting with and regulating Src-family kinases, which in turn are activating CD9b to allow docking of proteins such as SHP1. This in turn could allow CD9b to regulate cell survival in the primordium by regulating Akt and MAPK signalling pathways (Figure 4.41b).

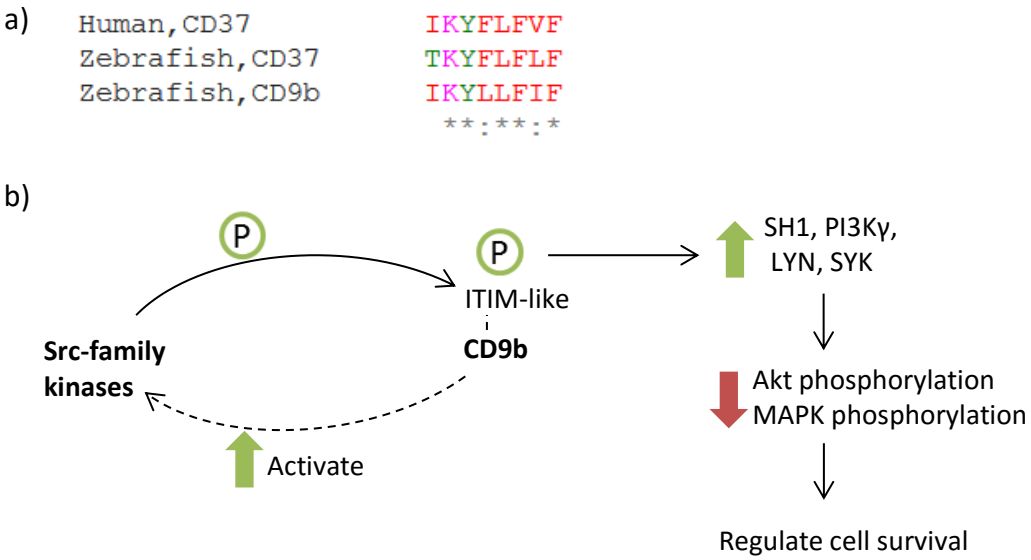

Figure 4.41 Model of the potential signalling properties of the CD9b N-terminus.Clustal multiple sequence alignment of Zebrafish CD9b with Human and Zebrafish CD37 using MUSCLE (Multiple Sequence Comparison by Log-Expectation) (a). Residue colour indicates residue physicochemical properties: red – small hydrophobic, magenta-basic, green- hydroxyl, sulfhydryl, amine or G, blue- acidic. Conserved residues are noted by *, strongly similar residues scoring >0.5 and weakly similar residues scoring <0.5 in the Gonnet PAM 250 matrix are noted by : and . respectively.
The proposed feedback loop between CD9b and Src-family kinases (b). This could regulate the activation of Src-family kinases as well as CD9b partner proteins such as SH1, LYN, PI3K and SYK (b). In turn this could help to regulate the migration and neuromast deposition of the lateral line by regulating primordium size through Akt and MAPK signalling. Dotted lines indicate hypothesised activities.

Chapter 5:
CD9b mutants raised at 22°C

5.1 Introduction

The tail phenotypes seen in CD9b -8/-8 embryos raised at 22°C were unexpected as CD9b is not specifically expressed in the tail during development (Figure 4.32, Table 1.4). Interestingly, a number of different chemical toxins are reported to induce a similar morphological phenotype, often including a shortened, kinked or curly tail with abnormal fin fold development (Samson and Shenker 2000, Saslowsky et al. 2010, Bakos et al. 2013, Yuan et al. 2014, Ahmad et al. 2015). Kinked and curly tails are also seen in a zebrafish hyperammonemia model (Feldman et al. 2014). As processing of toxins, including ammonia, is carried out by the kidneys this could suggest that CD9b may have a role in kidney function. In support of this, CD9b is strongly expressed in the pronephros during zebrafish development (Figures 4.14, 4.27, Table 1.4), and the mammalian homolog of CD9b, CD9, has been shown to be expressed in human, mouse, rat and canine kidney cells (Kaprielian et al. 1995, Sheikh-Hamad et al. 1996, 2000, Sincock et al. 1997, Yanez-Mo et al. 2001, Kuroda et al. 2001, Blumenthal et al. 2015). CD9 has been shown to play a role in the stress responses of kidney cells, where it is upregulated or increases survival when kidney cells are placed under osmotic, oxidative or mechanical stress (Sheikh-Hamad et al. 1996, 2000, Takemura et al. 1999, Blumenthal et al. 2015). Together this could suggest a hypothesis that CD9b in zebrafish is upregulated in the pronephros when under stress to allow the organ to function efficiently. Without this upregulation in the CD9b mutants the removal of bodily toxins, such as ammonia, could become impaired and lead to the tail phenotypes seen.

5.2 Results

Given that zebrafish are normally raised at 28°C, decreasing the incubator temperature to 22°C causes a temperature stress on the developing embryos. When raised at 22°C a large percentage of CD9b -8/-8 embryos showed dramatically shorter, kinked or curled tails, whereas their AB counterparts showed no abnormalities (Figure 5.1c). These phenotypes were observable by eye, as seen in Figure 5.1a-5.1b II, however some of the mutants looked normal overall. Embryos were categorised as having no obvious

phenotype or a mild, moderate or severe tail phenotype. Mild embryos were defined as having one trunk defect, moderate embryos showed two and severe showed the most extreme versions of these phenotypes. Although many CD9b mutants showed no obvious phenotype, upon measuring the trunk length of the embryos it became clear that the mutants had significantly shorter trunks than the ABs (Figure 5.1c-d). This decrease in trunk length at 22°C is only seen in CD9b -8/-8 embryos; AB embryos appear unaffected by the different raising temperatures (Figure 5.1e).

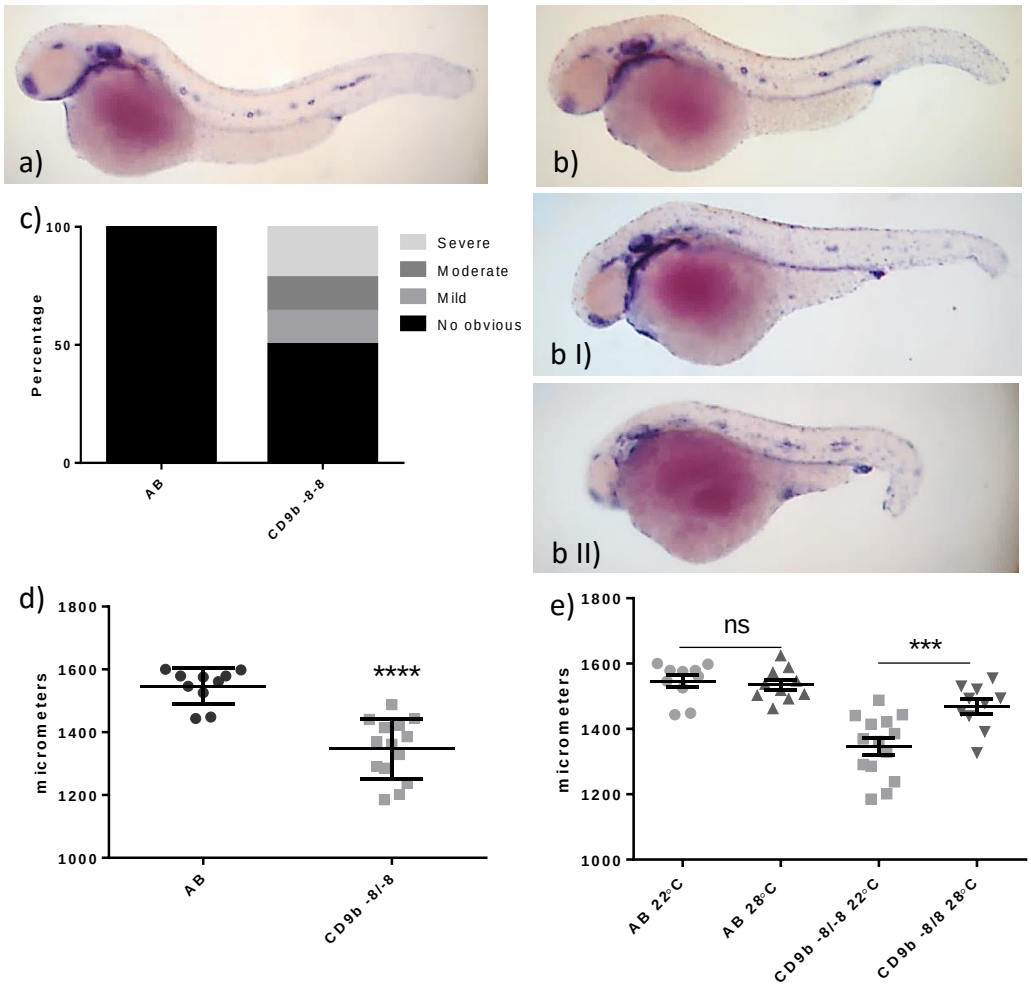

Figure 5.1 CD9b -8/-8 embryos (b), but not AB (a) embryos, show abnormal tail phenotypes when incubated at 22°C until reaching Prim-25 stage.

The embryos are stained for *claudin b* expression via *in situ* hybridisation. The wildtype AB embryos show a normal phenotype with no obvious defects (a). Some of the CD9b -8/-8 embryos also showed no obvious phenotype (b), although some showed shorter kinked or tightly curled tails (b I and b II). The percentage of embryos showing tail phenotypes is shown in (c). CD9b -8/-8 embryos show significantly shorter trunks when incubated at 22°C compared to AB embryos under the same conditions (d). This decrease in trunk length is only seen in CD9b -8/-8 embryos at 22°C whereas AB trunk lengths are the same at both 28°C and 22°C (e). All embryos were from the same AB or CD9b -8/-8 batch. An unpaired T test was used to analyse (d) and an ANOVA with Sidak's multiple comparisons test was used for (e). Sidak's test was used as it has increased power and corrects for multiple comparisons. n= minimum 10. p=<0.05. Data from a single experiment.

As many embryos died during development when raised at 22°, the experiment was repeated to assess whether the abnormal phenotypes seen were a result of selection bias through high embryo death in the previous batch. A larger number of AB and CD9b -8/-8 embryos were placed at 22°C for 72hpf then assessed by eye for obvious phenotypes, fixed and a randomly chosen subset imaged and measured (Figure 5.2). As seen in Figure 5.2a-5.2c, a range of tail phenotypes were observed again, including shorter, kinked or curled tails but also uneven or underdeveloped fin folds. Any fin fold phenotypes seen previously in Figure 5.1 would have been dismissed as potentially resulting from the use of proteinase K to digest the embryos during the *in situ* hybridisation. Whilst a large number of the CD9b -8/-8 embryos were labelled as no obvious phenotype, measurements showed that the tails were significantly shorter and the fin folds significantly smaller in the mutants (Figure 5.2d-5.2e).

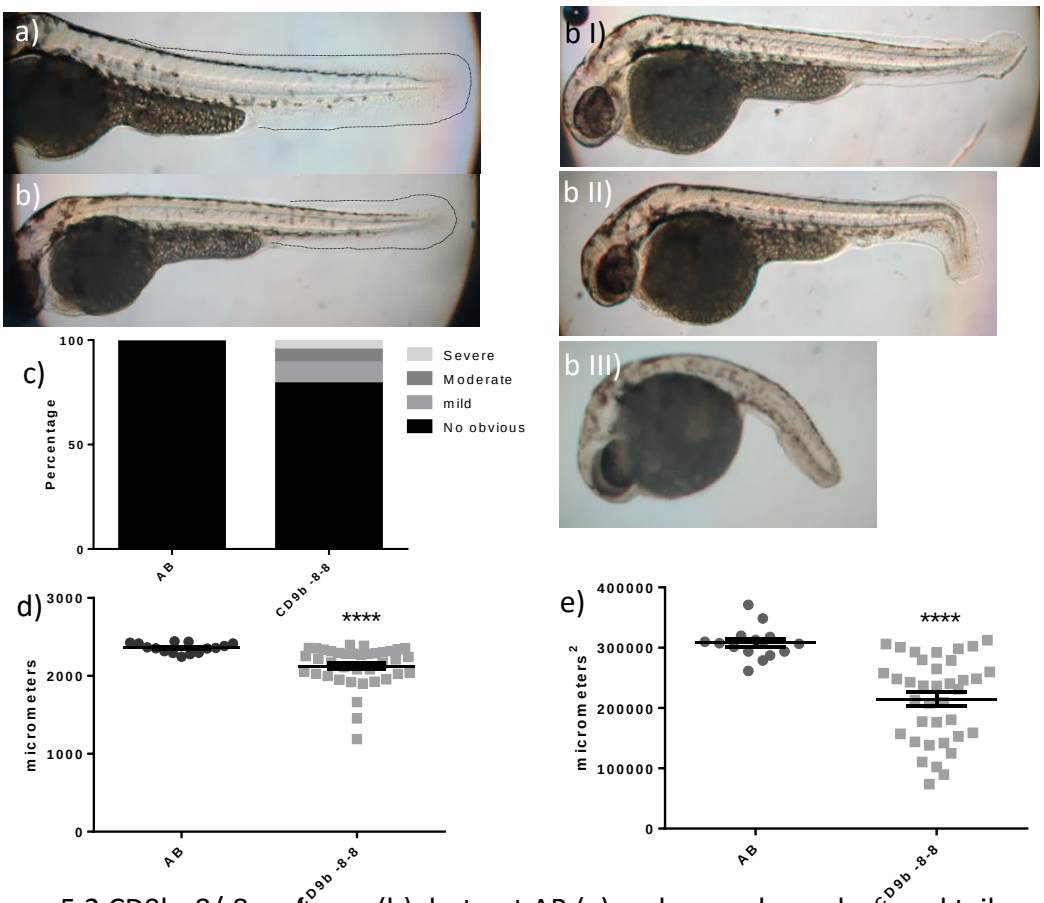

Figure 5.2 CD9b -8/-8 embryos (b), but not AB (a) embryos, show abnormal tail and finfold phenotypes when incubated at 22°C for 72hpf.

A range of phenotypes was seen in CD9b -8/-8 embryos from no obvious (b), mild (b I), moderate (b II) and severe (b III). Phenotypes were defined in the same way as Figure 5.1, except fin fold phenotypes were included in this repeat. A number of CD9b -8/-8 embryos show obvious trunk phenotypes (c), however the embryos that show no obvious phenotypes by eye have shorter trunks (d) and smaller fin fold areas (e). Fin folds outlined in a),b) in black. n= minimum 215 (c), 15(d,e). Mann-Whitney U test (d) and Unpaired T test (e). ****p<0.0001. Data from a single experiment.

To investigate whether the phenotypes also occurred in a different CD9b mutant allele, the experiment was repeated but CD9b -1/-1 embryos were also raised at 22°C for 72hpf. While a large percentage of CD9b -8/-8 and CD9b -1/-1 embryos did show tail phenotypes, surprisingly so did the AB embryos (Figure 5.3a). The significant difference seen previously in trunk length and fin fold area between AB and CD9b mutant embryos was not replicated (Figures 5.3b-5.3c). A final repeat confirmed that this loss of significance was not an isolated event (Figure 5.4).

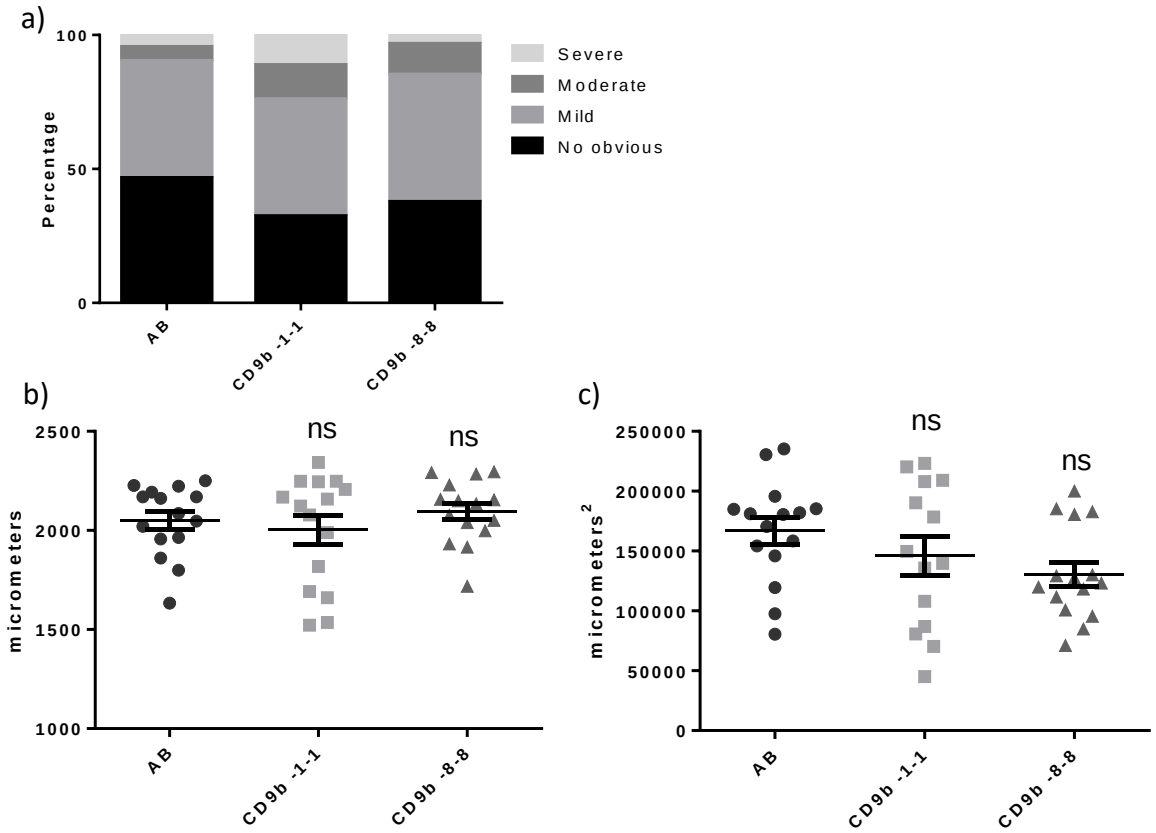

Figure 5.3 Further experimental repeats show AB embryos developing abnormal tail phenotypes as well as CD9b mutants when raised at 22°C.
The percentage of CD9b mutant embryos showing tail phenotypes is greatly increased in this repeat, however, many AB embryos also showed obvious tail phenotypes (a). n= minimum 60.
The change in AB tail phenotypes is also mirrored in the loss of significant difference in trunk length (b) and fin fold area (c). Significance was assessed using an ANOVA with Dunnett's multiple comparisons test. n= minimum 14. Data from a single experiment.

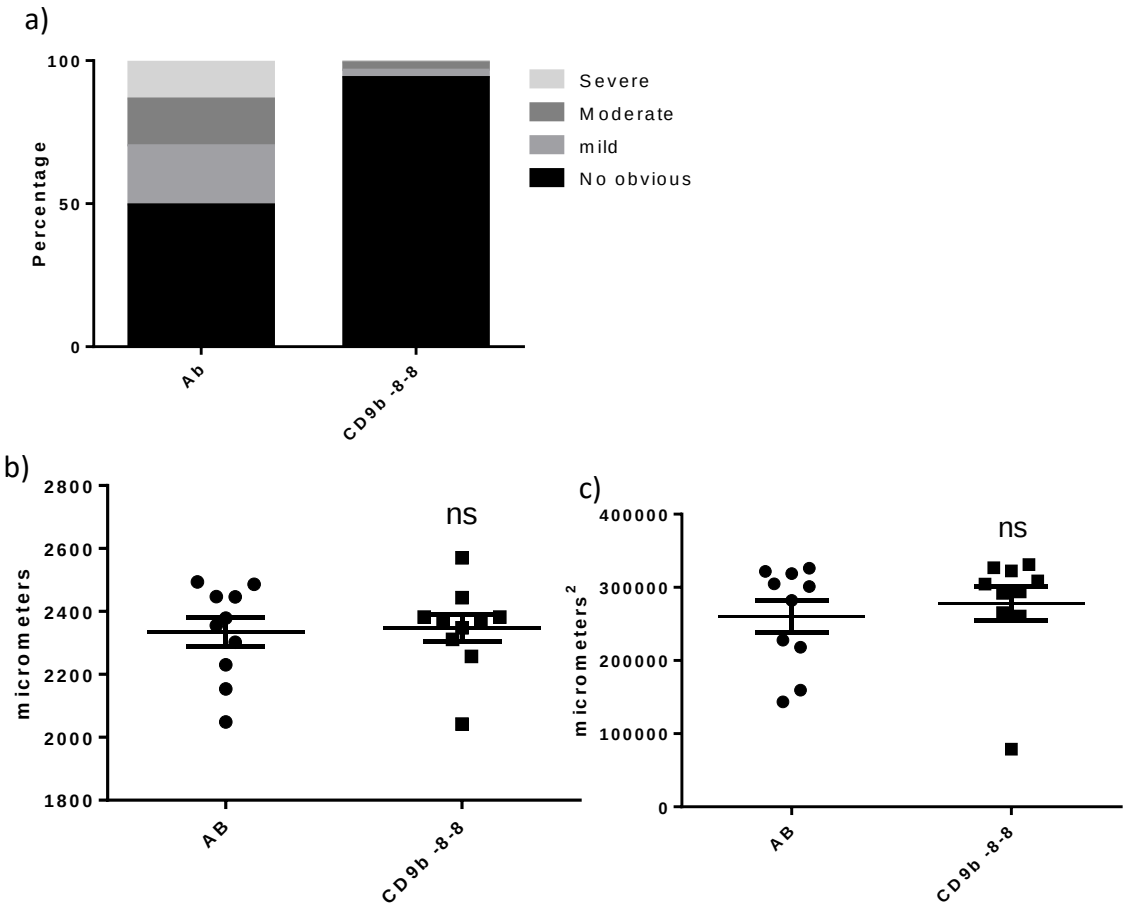

Figure 5.4. AB embryos develop abnormal tail phenotypes as well as CD9b mutants when raised at 22°C.
A large percentage of AB embryos display tail phenotypes, whereas less are seen in CD9b -8/-8 embryos, suggesting that the phenotypes seen are not due to CD9b deficiency (a). n= minimum 100
No significant difference is found in trunk length (b) and fin fold area (c). Significance was assessed using an unpaired T test (b) and a Mann-Whitney U test (c). n= minimum 10.

A large percentage of AB embryos showed tail phenotypes in two of four independent experiments. The data from these experiments cannot be pooled and so the means of individual experiments were compared for trunk length and fin fold area (Figure 5.5). The variation in experimental means suggest that the significance differences seen in Figures 5.1 and 5.2 were an artefact of the variable nature of embryo development at 22°C, and the lack of phenotypes shown by AB embryos occurred by chance.

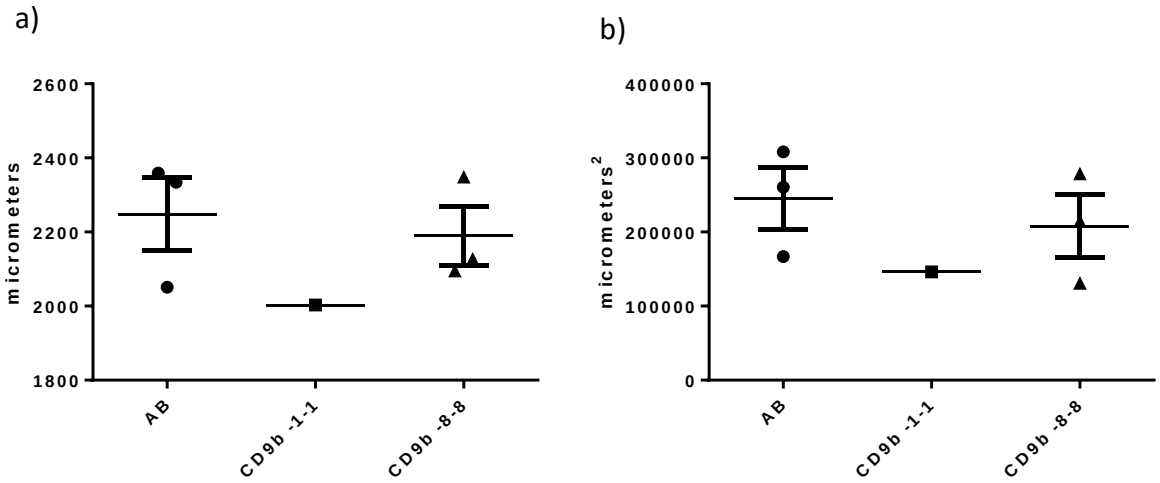

Figure 5.5 Large variation between the means of each experimental repeat suggests the initial significance difference in trunk length (a) and fin fold area (b) was an artefact. As the data cannot be pooled, the means from each experiment have been compared. A large variation can be seen between the experiments, suggesting that the significance initially seen was an artefact and not a true phenotype of CD9b deficiency. Mann-Whitney U tests between AB and CD9b -8/-8 embryos show no significant difference between the means. A Mann- Whitney U test was used as only one data point was reported for CD9b -1/-1 and ANOVAs need >1 data point per column. The lack of CD9b -1/-1 repeats is due to a lack of fertilised eggs being laid by CD9b -1/-1 adult pairs. n=minimum 1 experiment mean

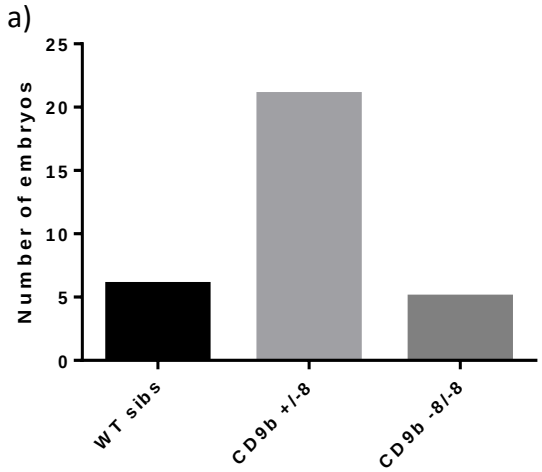

	WT sibs	CD9b +/-8	CD9b -8/-8
Observed	6	21	5
Expected	8	16	8

Figure 5.6 Tail phenotypes are found in embryos of all genotypes from CD9b +/-8 in-cross.

Embryos from CD9b +/-8 parents were raised at 22°C and embryos that developed tail phenotypes were genotyped (a). A chi-squared test showed the resulting number of embryos in each genotype did not differ significantly from Mendelian inheritance ratios (P=0.0832). The number of embryos observed by genotyping and expected by Mendelian inheritance is shown in (b). n= 32 embryos. Data from a single experiment.

Though AB embryos showed abnormal tail phenotypes in two of four repeats, CD9b mutant embryos showed abnormal phenotypes in all four. To determine whether CD9b deficiency was increasing the number of embryos with tail phenotypes, CD9b +/- 8 adults were paired and the resulting embryos collected the next day. The embryos were raised at 22°C for 72hpf before being assessed for tail phenotypes. Any embryos with abnormal tails or fin folds were then genotyped. If CD9b deficiency was increasing the occurrence of abnormal tail development, it would be expected that a large number of the embryos genotyped would be CD9b homozygous mutants and few would be wild type siblings. This appears not to be the case. An almost equal number of homozygous mutants and wildtype siblings were found in the genotyped embryos, with the number of embryos found in each genotype not significantly different to the number of embryos expected by Mendelian inheritance laws (Figure 5.6). This suggests any differences seen were not due to CD9b deficiency.

5.3 Discussion

While it is clear that CD9b deficiency in embryos raised at 22°C, instead of 28°C, does not promote abnormal tail development, it is still possible that CD9b could play a role in the zebrafish pronephros. CD9 has been shown to be expressed in kidney cells of a wide range of organisms and has been implicated in promoting survival during cellular stress by regulating signalling and augmenting both cell-cell and cell-matrix attachments through interactions with β_1-integrin and heparin-binding epidermal growth factor-like (HB-EGF) (Sheikh-Hamad et al. 1996, 2000, Takemura et al. 1999). Expression of CD9 in podocytes has also been shown to stimulate protrusion formation and increase migration speed during wound healing (Blumenthal et al. 2015). It would be interesting to see if any similar roles are found for CD9b in future research.

Chapter 6:
CD9b mutants and fertility

6.1 Introduction

In 1999, it was shown that CD9 is expressed on the cell membrane of murine oocytes and ovulated eggs. An anti-CD9 mAb, JF9, was shown to inhibit sperm- egg binding and fusion *in vitro* (Chen et al. 1999). A role for CD9 in fertilisation was confirmed with the generation of CD9 deficient mice (Kaji et al. 2000, Le Naour et al. 2000, Miyado et al. 2000). While CD9 deficient mice grew to adulthood with no obvious abnormalities, female CD9b -/- mice had severely reduced fertility with litter sizes <2% of wildtype (Miyado et al. 2000). It was observed that mating behaviour, number of oocytes ovulated, ovary morphology and sperm-egg binding were normal, however, the sperm and egg fusion was almost completely inhibited in CD9 -/- females (Kaji et al. 2000, Le Naour et al. 2000, Miyado et al. 2000).

CD9, as a member of the tetraspanin family, is well known for its ability to interact with other members of the tetraspanin family and multiple membrane surface proteins. In doing so, tetraspanins can act as 'molecular facilitators' for cellular processes (Rubinstein et al. 1996b, Maecker et al. 1997). It was therefore suggested that CD9 may organise partner proteins on the egg membrane to generate fusion competent sites (Zhu et al. 2002, Ziyyat et al. 2006, Jégou et al. 2011). Many potential CD9 partners, such as integrin-α6β1, have been shown to be non-essential for gamete fusion although recently the egg membrane protein Juno has been shown to be required for fertilisation (Miller 2000, He et al. 2003, Bianchi et al. 2014).

It was also proposed that CD9 could act as a direct receptor for a sperm membrane protein, as binding of the ligand PSG17 (pregnancy-specific-glycoprotein-17) to CD9 on the egg membrane can prevent sperm fusion. Although PSG17 is not a sperm protein, this suggests the binding site is needed for sperm-egg fusion (Ellerman et al. 2003). The sperm protein, Izumo, is required for gamete fusion but it's egg receptor is Juno not CD9 (Inoue et al. 2005, 2011, 2013, Satouh et al. 2012, Bianchi et al. 2014). It appears that CD9 may partner with Juno and regulate the binding of Izumo/Juno, after which Izumo dimerises and is passed to an alternative unknown egg receptor for tight

adhesion of the membranes (Chalbi et al. 2014, Inoue et al. 2015). Although CD9 is not required for Izumo/Juno binding, CD9 is required for correct formation and distribution of microvilli on the egg membrane (Kaji et al. 2000, Runge et al. 2007, Zyłkiewicz et al. 2010). Incorrect egg membrane structure in CD9 -/- eggs may account for the differences in Izumo/Juno binding kinetics (Runge et al. 2007, Chalbi et al. 2014).

While the majority of research on CD9 in fertility has focussed on female fertility, there is evidence suggesting that CD9 may play a role in male fertility also. CD9 has been shown to be expressed on spermatogonial stem cells and throughout the majority of spermatogenesis in mice (Kanatsu-Shinohara et al. 2004, Kierszenbaum et al. 2006, Ito et al. 2010).Like Izumo, CD9 is an inner acrosomal membrane associated protein in mature sperm and only becomes exposed after the acrosome reaction which occurs upon binding the zona pellucida (Ito et al. 2010, Inoue et al. 2011, Barraud-Lange et al. 2012). Whilst a role for CD9 in mature sperm has yet to be proposed, a role for CD9 in spermatogonial stem cells can be inferred from recent papers. Spermatogonial stem cells (SSCs) are located in specific niches in the testis that release the chemoattractant CXCL12, which is needed for both homing and maintenance of SSCs (Kanatsu-Shinohara et al. 2012, Yang et al. 2013, Westernströer et al. 2014). In order to access these niches, spermatogonial stem cells have to cross the blood-testes barrier. This transmigration requires the activation of Rac1 on the stem cells (Takashima et al. 2011). Recent publications have shown that CXCL12 upregulates CD9 and CD9 subsequently promotes Rac1 activation and actin polymerisation (Leung et al. 2011, Brzoska et al. 2015, Arnaud et al. 2015). It could be that a similar mechanism is present in spermatogonial stem cells.

To my knowledge there has been no research into a possible role for CD9a or CD9b in zebrafish sperm-egg fusion or spermatogenesis.

6.2 Results

In the CD9 knockout mouse, the main phenotype is a severe decrease in the number of pups born due to decreased sperm – egg fusion (Kaji et al., 2000; Le Naour et al., 2000; Miyado et al., 2000). We decided to check whether the total number of eggs laid per CD9b -8/-8 and CD9b -1/-1 pair, as well as the number of fertilised, dead and unfertilised eggs, was the same as those laid by their WT counterparts (Figure 6.1). AB, CD9b -1/-1 and CD9b -8/-8 in-cross pairs were set up in pair mating tanks and the total number of eggs laid per pair were collected and assessed the next morning (Figure 6.1a). Having only 5/6 pairs of CD9b -1/-1 and CD9b -8/-8 mutants, the experiment was repeated on multiple occasions to increase the reliability of the conclusions as laying behaviour varies largely between experiments. CD9b mutant pairs have a significantly decreased number of eggs per clutch, 31.36 ± 18.16 eggs and 38.97± 7.975 eggs compared to 170.3±18.16 (mean ± SEM) eggs from AB pairs. It is also apparent that CD9b mutant pairs often lay no eggs at all (Figure 6.1a).

The total clutch size assessed in Figure 6.1a included fertilised, dead and unfertilised eggs laid by each pair. The number of each egg type produced per pair that laid can be seen in Figures 6.1b-d. A significant decrease in the number of eggs fertilised per CD9b mutant pair (Figure 6.1b) mirrors the decrease seen in overall clutch size. This mirroring is not seen in the number of dead (Figure 6.1c) or unfertilised (Figure 6.1d) eggs. Due to significant differences between experimental repeats, the data for the number of dead eggs laid per pair cannot be pooled and so a representative experiment is shown in Figure 6.1c. An increase in the number of dead eggs laid by CD9b mutants can be seen in Figure 6.1c, however the number of pairs observed is low for CD9b -1/-1 as only pairs that laid any eggs were included. Whilst CD9b mutant pairs did not lay dead eggs in every experimental repeat (Figure 6.2), there was a trend of CD9b mutant pairs laying dead eggs with increased frequency, as shown in Figure 6.1c. The number of unfertilised eggs per CD9b mutant pair, in contrast to both fertilised and dead eggs, does not appear to change in comparison to AB pairs (Figure 6.1d).

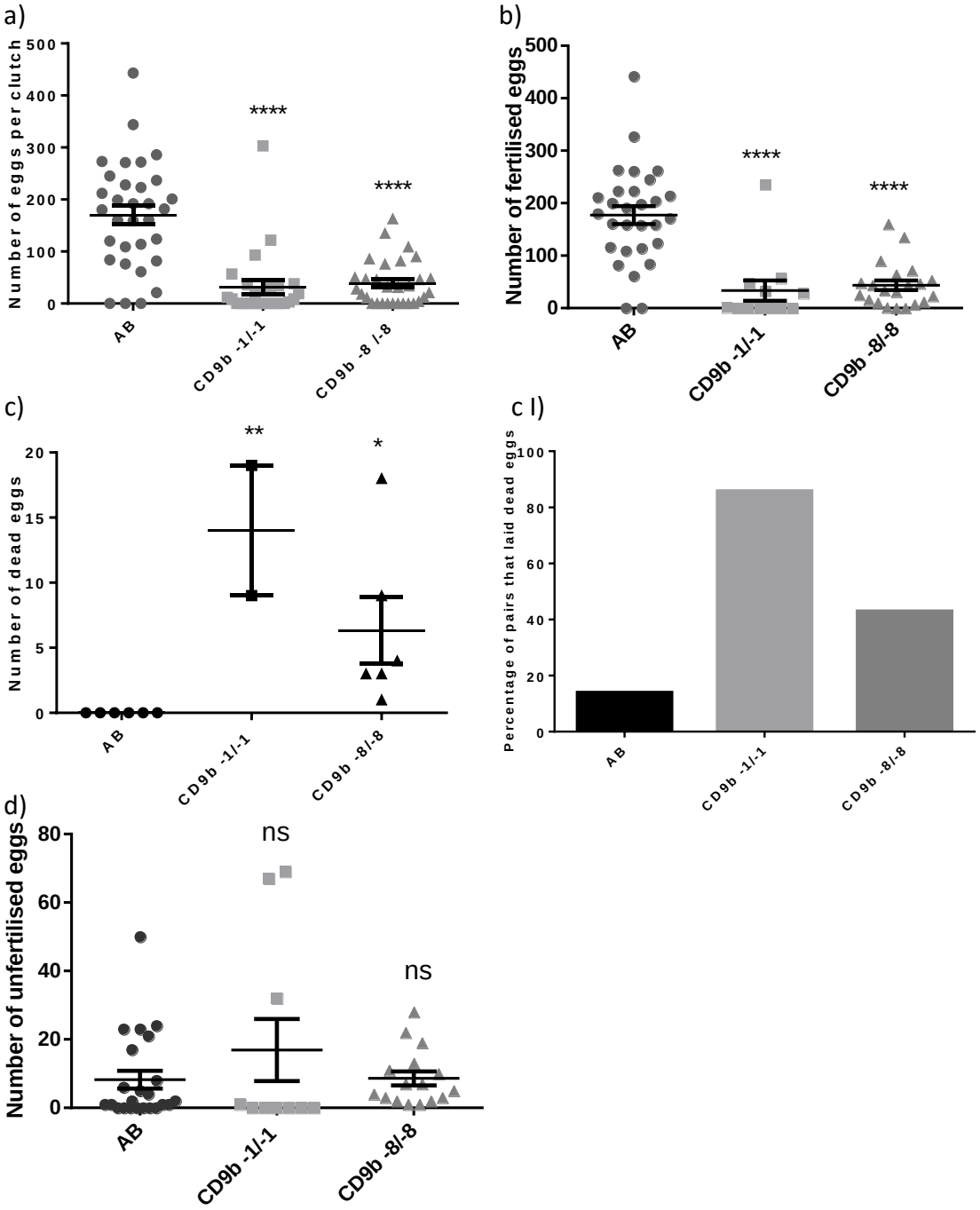

Figure 6.1 CD9b mutant pairs lay smaller clutches of eggs.
A significant decrease in the total number of eggs laid per pair, including fertilised, dead and unfertilised eggs, is seen with CD9b mutant pairs (a). The number of fertilised eggs laid per pair is also significantly decreased (b); however the numbers of dead (c) and unfertilised (d) eggs are increased or unchanged respectively. a),b) and d) represent pooled data from 4 -5 experimental repeats but c) is a representative experimental repeat as the data could not be pooled (for the repeats see Figure 6.2). Whilst the data for the number of dead eggs could not be pooled, the percentage of pairs that laid dead eggs was assessed to give an overview of the repeats (c I). Chi-squared analysis of (c I) shows a significant difference between the groups (p=<0.0001). All experiments, except (c I) were analysed using a Kruskal-Wallis test with Dunn's multiple comparisons test where p=<0.05. n=minimum 25 pairs (a), minimum 12 pairs (b), minimum 2 pairs (c) and minimum 10 pairs per genotype (c I) and (d). Only pairs that laid any eggs were included in b-d.

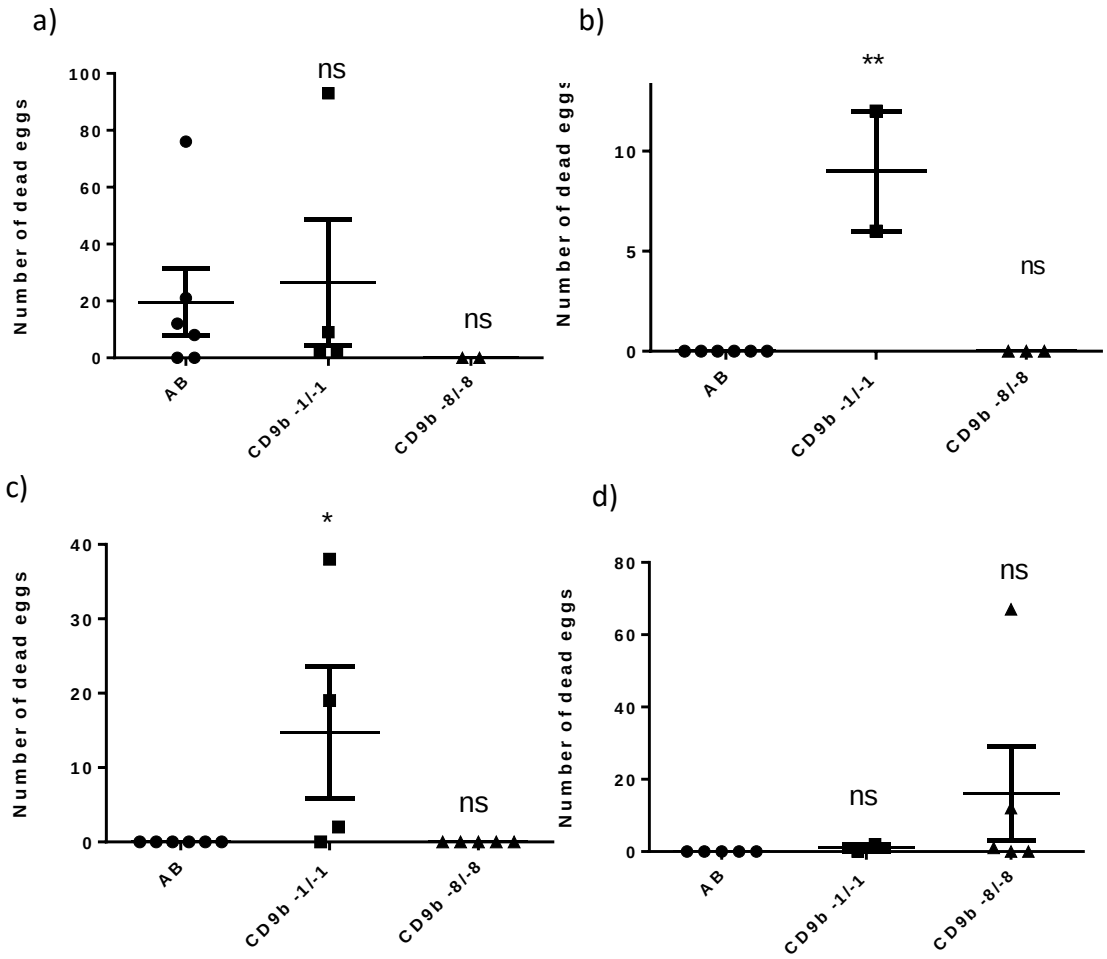

Figure 6.2 CD9b mutant pairs lay dead eggs more often than AB pairs. Experimental repeats (a-d) looking at the number of dead eggs laid per pair , all analysed using Kruskal-Wallis with Dunn's multiple comparisons test. Only pairs that laid were included in the data collection and CD9b mutant pairs often laid no eggs, leading to the low n numbers. n= minimum 2 pairs

If clutch size was the only laying phenotype seen from CD9b mutant pairs, it would be expected that the number of fertilised, dead and unfertilised eggs would also decrease. Figure 6.1 shows that while this is the case for the number of fertilised eggs, it is not true for the numbers of dead and unfertilised eggs. We therefore decided to look at the percentage of fertilised, dead and unfertilised eggs per clutch to see if the ratio of egg phenotypes within CD9b mutant clutches is affected (Figure 6.3).

CD9b mutant pairs have a significantly lower percentage of fertilised eggs per clutch 24.14 ±11.17 and 61.52±8.76 percent of eggs fertilised in comparison to AB clutches that have 96.54 ±0.89 percent of eggs fertilised (Figure 6.3a). It can therefore be inferred that CD9b mutants have a significant increase in the percentage of dead and unfertilised eggs per clutch. It can be seen in Figure 6.3b that both dead and unfertilised eggs appear to increase individually, with the percentage of dead eggs most dramatic with CD9b -1/-1 pairs.

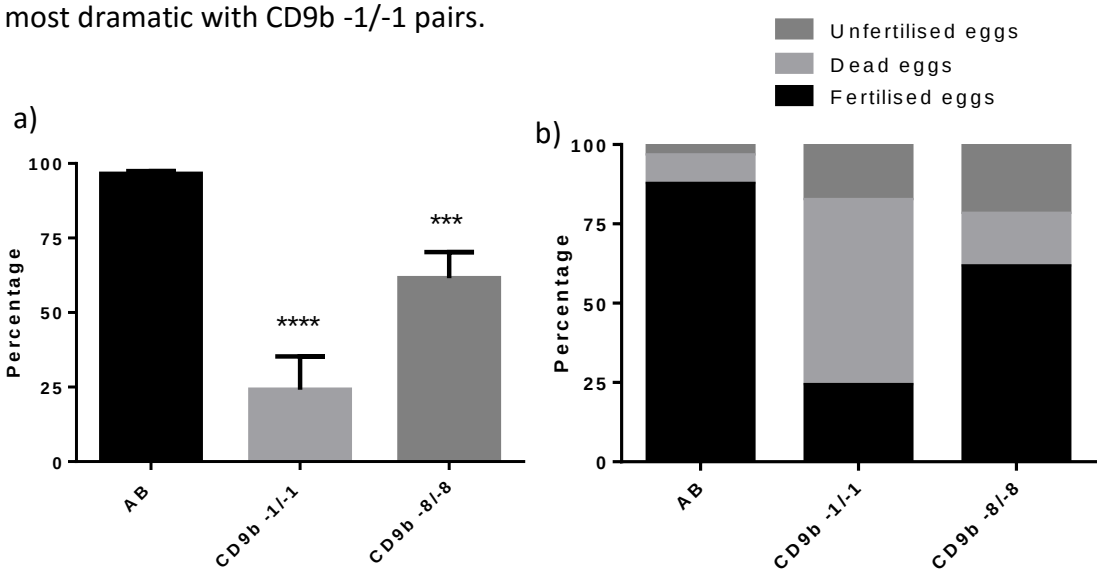

Figure 6.3 CD9b mutant pairs have a lower percentage of fertilised eggs per clutch. The percentage of fertilised eggs is significantly decreased in clutches from CD9b mutant pairs (a). n= minimum 10 pairs per genotype, with only pairs that laid counted, from four repeats. An ANOVA with Dunnett's multiple comparisons test was performed after removal of definitive outliers (3 outliers, ROUT, q=0.1) to give normally distributed data. p=<0.05
Given the significant decrease in fertilised eggs seen in (a), it can be inferred that there is a significant increase in the percentage of dead and unfertilised eggs per clutch from CD9b mutants. This increase is apparent in (b), where the average breakdown of clutches from wildtype and CD9b mutant pairs is shown.

While migration of PGCs to the embryonic gonadal ridge in CD9b mutants has been shown to be normal in a previous chapter, CD9b mutants may have fewer PGCs which could then result in a reduced clutch size. To investigate this, an ISH was carried out on 32hpf AB, CD9b -1/-1 and CD9b -8/-8 embryos using a *vasa* RNA ISH probe to stain the PGCs (Figure 6.4b-6.4b II). The number of PGCs per embryo was counted and no significant difference found between AB and CD9b mutant embryos (Figure 6.4a).

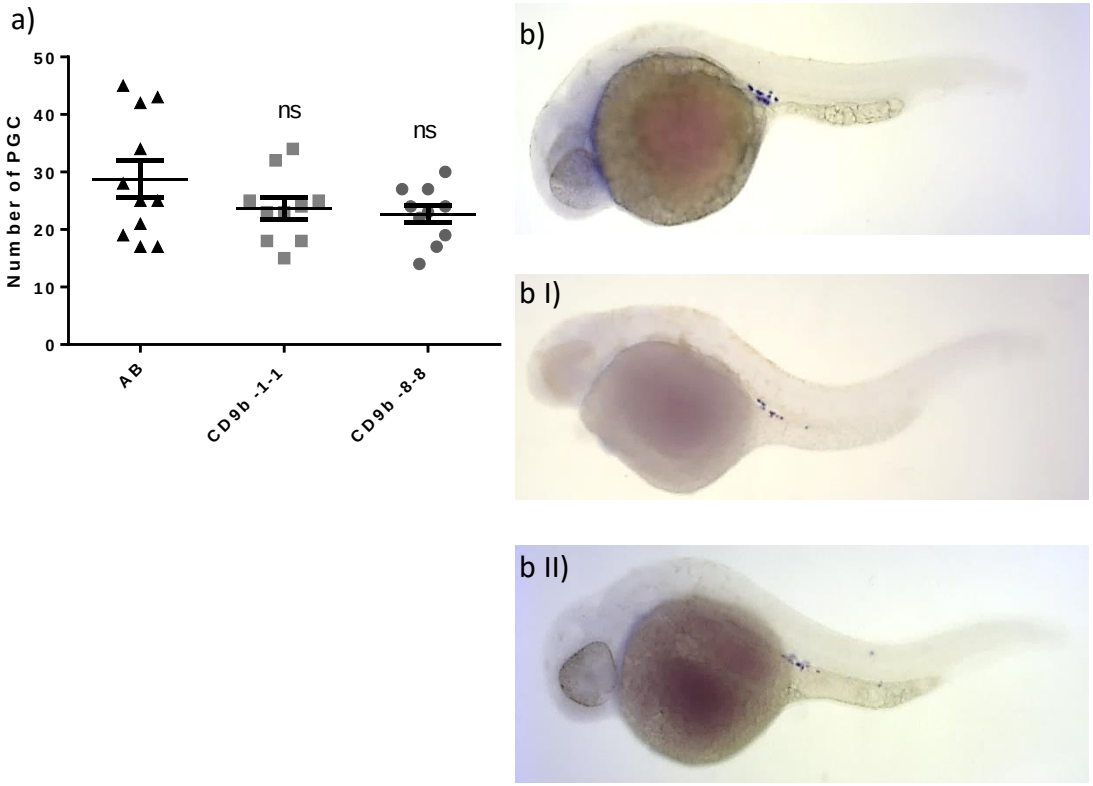

Figure 6.4 Number of PGCs per embryo at 32hpf is comparable between AB and CD9b mutant embryos.
There is no significant difference in the number of PGCs in AB and CD9b mutant embryos at 32hpf (a). This was shown using an ANOVA with Dunnett's multiple comparisons test on n= minimum 10 embryos per genotype. p=<0.05. Data from a single experiment.

The decrease in clutch size and decrease in percentage of eggs fertilised per clutch from CD9b mutant pairs are significant and interesting phenotypes, however, there are a number of factors that could be contributing to these results. Behavioural and physiological factors such as age, breeding interval and size can affect egg production (Eaton and Farley 1974, Niimi and LaHam 1974, Skinner and Watt 2007, Paull et al. 2008, Uusi-Heikkilä et al. 2010, Filby et al. 2010, Nasiadka and Clark 2012). Due to the use of communal AB stocks, the same tank of ABs was not used every time. This means there may be background genetic variations between the AB controls but all ABs used had been born in the same month and so negates any age effects. The CD9b mutants were born within two months of the ABs. The communal AB stocks may be less stressed than the mutants as they have an enforced breeding interval of two weeks between pairings, unlike the CD9b mutants which can be paired every week. This stress was controlled for by trying to limit CD9b mutant pairings to every two weeks and ensuring that the mutants, if paired in consecutive weeks, were then given two weeks rest before pairing again. Size differences were managed by pairing fish of similar sizes. Ideally, ABs and CD9b mutants would have been raised and bred under identical conditions to control for these variables, however, this was not viable at the time.

IVF was used to investigate whether the clutch size and fertilisation phenotypes were still significant after elimination of many of the behavioural and physiological factors in zebrafish spawning. AB, CD9b -1/-1 and CD9b -8/-8 in-cross pairs were set up in pair mating tanks overnight with eggs and sperm collected manually the next morning by gently squeezing anaesthetised fish. Eggs and sperm from the same genotype were then mixed and activated to induce fertilisation. Eggs were assessed for fertilisation two hours after the IVF procedure. This experiment focuses only on fertilised and unfertilised eggs as any dead eggs were immediately disposed of during the IVF. Of the females that laid suitable eggs, there is a significant decrease in the number of eggs per clutch from CD9b mutant females 37.33± 4.177 and 50.00±16.14 eggs on average compared to AB with 146.7±22.84 eggs (Figure 6.5a). Not only is the clutch size smaller from CD9b mutant pairs, but the percentage of eggs fertilised is also decreased (Figure 6.5b). The number of eggs fertilised and unfertilised per pair can be seen in Figure 6.5bI, with individual pairs aligned vertically.

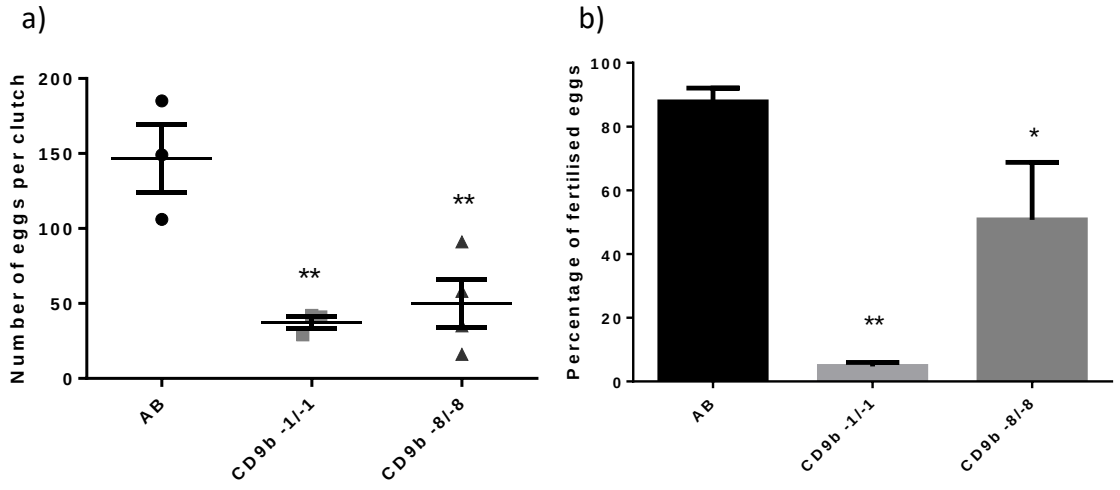

b I)

	AB			CD9b -1/-1			CD9b -8/-8			
Fertilised eggs	168	84	139	2	2	1	72	8	42	0
Unfertilised eggs	17	22	10	27	40	41	19	8	15	35

Figure 6.5 Clutches produced by IV,F from CD9b mutant pairs, have a decreased clutch size and lower percentage of eggs fertilised per clutch.
The number of eggs is significantly decreased in clutches from CD9b mutant pairs (a). Of the eggs laid, a significantly lower percentage were fertilised by CD9b mutant males (b). Dead eggs were immediately discarded during the IVF protocol and therefore (a) and (b) represent only fertilised and unfertilised eggs. The number of fertilised and unfertilised eggs is shown in b I), with individual pairs aligned vertically. n= minimum 3 pairs. ANOVA with Holm-Sidak multiple comparisons test was carried out on the original data from (a) and on arcsine transformed data in (b). The Holm-Sidak post-hoc test was chosen as it has more power than Dunnett's multiple comparisons test. p=<0.05. Data from a single experiment.

Due to the challenging nature of the IVF protocol, it was expected that not every fish would yield gametes for extraction; however, it appeared that sperm extraction was occurring less frequently from CD9b mutant males (Figure 6.6a and 6.6aI). Preliminary observations from the aquarium staff also suggests that the CD9b males also yielded a lower volume of sperm than AB males, although due to the time constraints on the IVF protocol, sperm volume could not be accurately measured.

Female CD9b mutants show no such difference in gamete extraction, with females from each genotype yielding eggs ~ 50% of the time (Figure 6.6b and 6.6bI). This may be a result of some of the AB fish laying prior to the IVF, whilst being held as a group in a large tank. This group laying is unusual and the males/females were separated as soon as the laying was observed. However, this could mean that some of the female ABs that did not yield eggs during the IVF could have already laid their ovulated eggs. The IVF experiments were repeated, however, due to high mortality rates of the procedure the experiment had to be terminated prematurely and the data could not be used.

a)

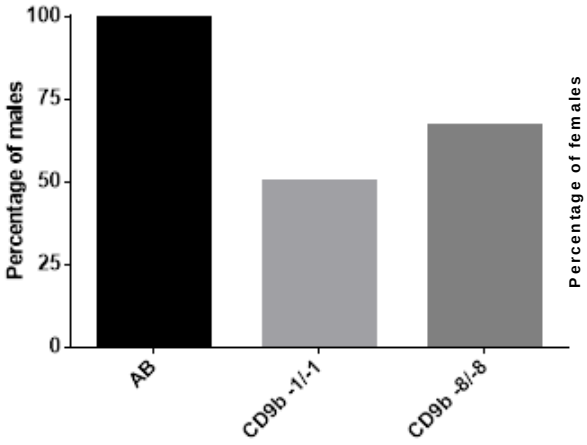

b)

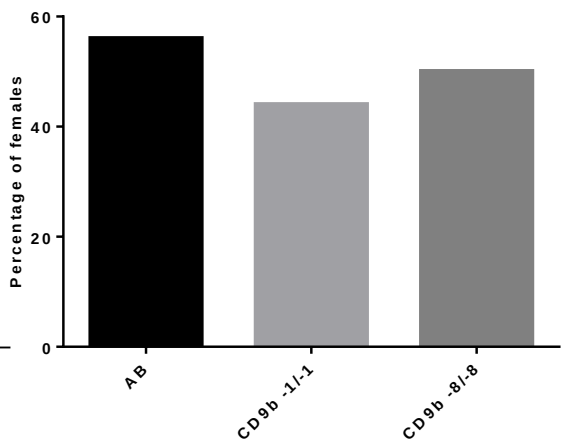

a I)

	Sperm extracted	No sperm extracted
AB	4	0
CD9b -1/-1	3	3
CD9b -8/-8	4	2

b I)

	Eggs extracted	No eggs extracted
AB	5	4
CD9b -1/-1	4	5
CD9b -8/-8	5	5

Figure 6.6 Sperm, but not oocytes, were extracted with a lower frequency from CD9b mutants. A decrease in the percentage of males from which sperm can be extracted is seen with CD9b mutant males (a, a I). This trend is not seen with female CD9b mutants; it appears that eggs can be extracted from female CD9b mutants as frequently as AB females (b, bI). n= minimum 4 males or 9 females per genotype. Data from a single experiment.

We decided to assess whether the phenotypes seen in CD9b mutant clutches were due to cumulative effects from both parents or due to a single gender as seen in the CD9b KO mice. Multiple pairs were set up including AB, CD9b -1/-1 and CD9b -8/-8 in-crosses as in previous experiments, as well as CD9b -1/-1 and CD9b -8/-8 out-crosses with AB for example CD9b -1/-1 female X AB male. The pairs were left in pair-mating tanks overnight and the eggs collected the following morning.

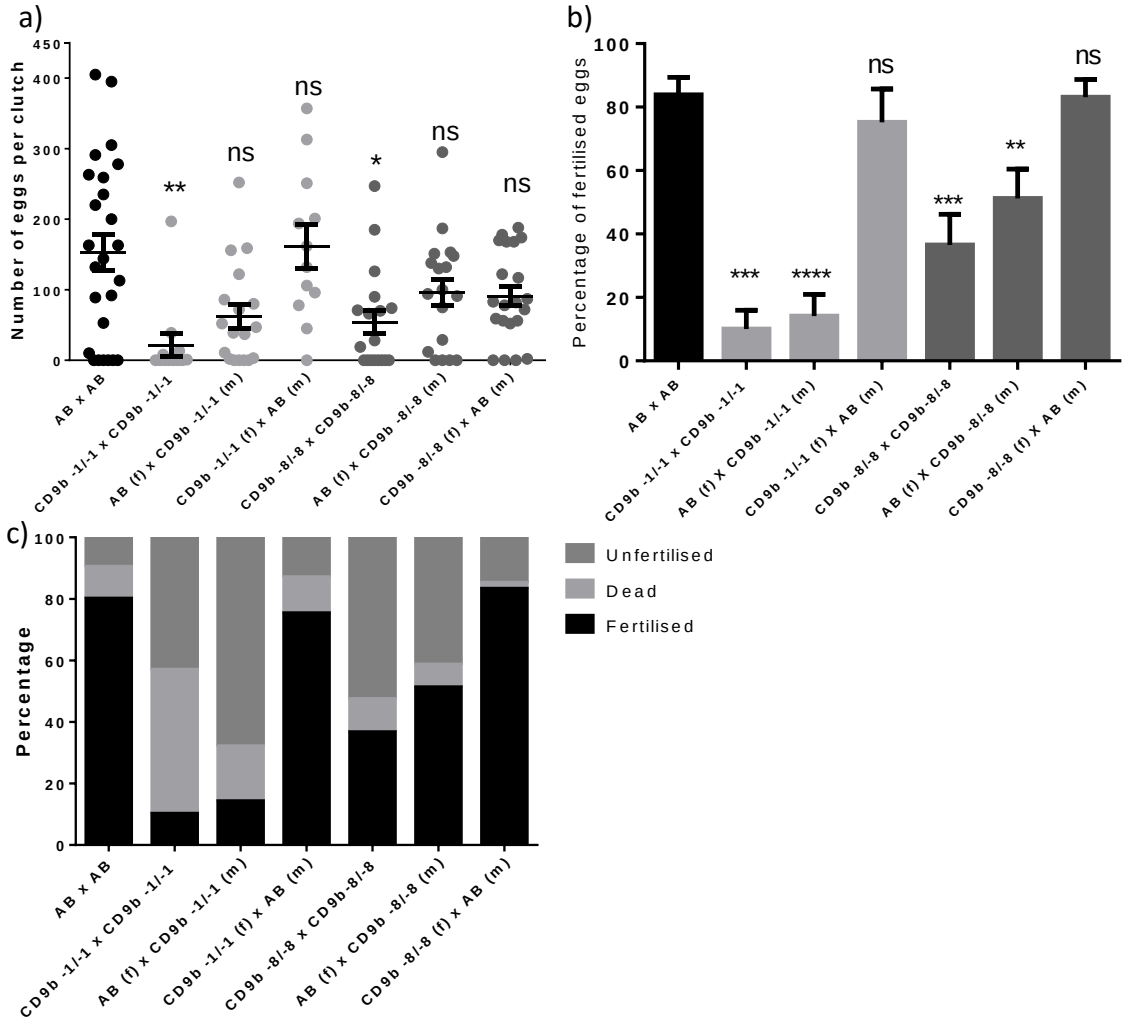

Figure 6.7 Clutch size can be rescued by substitution of either CD9b mutant partner but the decrease in the percentage of fertilised eggs can only be rescued by substitution of the CD9b mutant male for an AB male.
Clutch size can be rescued by substitution of a CD9b mutant partner, male (m) or female (f), with an AB (a). A Kruskal-Wallis test with Dunn's multiple comparisons test was carried out on the pooled data of three experimental repeats. n= minimum 12 pairs per cross. The percentage of fertilised eggs o only returns to wildtype levels upon substitution of a CD9b mutant male with an AB male (b). An ANOVA with Dunnett's multiple comparisons test was carried out on arcsine transformed data pooled from three experiments. The average percentage of fertilised, dead and unfertilised eggs per clutch is shown in (c). n= minimum 10 pairs per cross for (b) and (c), except CD9b -1/-1 x CD9b -1/-1 where only 4 of 12 pairs laid. p=<0.05

Clutch size can be partially or fully rescued by replacement of a CD9b mutant partner with an AB (Figure 6.7a). A significant decrease in clutch size, in comparison to AB clutches, is seen in clutches from CD9b -1/-1 and CD9b -8/-8 in-crosses; however this is not the case when an AB, either male or female, is paired with a CD9b mutant.

The percentage of eggs fertilised can also be rescued to wildtype levels, although only through substitution of a CD9b mutant male for an AB male (Figure 6.7b). This suggests that CD9b deficiency in females does not affect the ability of the eggs to be fertilised but CD9b deficiency in males dramatically reduces the males' ability to fertilise both wildtype and CD9b mutant eggs.

The mean percentage of fertilised, dead and unfertilised eggs can be seen in Figure 6.7c. It appears that a decrease in fertilised eggs comes with a dramatic increase in unfertilised eggs but the percentage of dead eggs does not vary hugely. This supports the hypothesis that CD9b mutant males cannot efficiently fertilise eggs, rather than the decrease in fertilised eggs being due to an increase in dead eggs (Figure 6.7c).

6.3 Discussion

In this chapter, it has been shown that CD9b -/- zebrafish pairs lay decreased clutch sizes and CD9b -/- males have severely reduced fertility. While the reduced number of fertilised eggs seen in Figure 6.1b is akin to the reduced fertility seen in CD9b -/- mice, the decreased clutch size is surprising as CD9b -/- mice show no ovulation defects (Le Naour et al. 2000, Miyado et al. 2000). Due to the previous investigation of PGCs in CD9b mutants, an immediate thought was to look for a decrease in the number of PGCs in CD9b mutants; however, it appears that both production and migration of PGCs is unchanged in CD9b mutants (Figure 6.4 and Figure 4.16). While this doesn't eliminate the possibility of impaired gametogenesis in later development, it does rule out a causative role for PGCs in both migration and numbers.

IVF was used to elucidate whether factors such as courting behaviour, adult size and mate choice were causing the decrease in clutch size. The reduction in clutch size seen in Figure 6.5a indicates that this is not the case. The protocol used for the IVF does not however eliminate any potential anatomical differences, between CD9b mutant females and AB females in their reproductive system, that could impede egg laying. This possible explanation for the decrease in clutch size seems unlikely though as CD9b mutant females paired with AB males in Figure 6.7 showed no significant difference in the number of eggs laid. This shows that the CD9b mutant females have the ability to ovulate and lay large numbers of eggs.

The decrease in clutch size seen from CD9b mutant pairs could be explained by the requirement of reproductive pheromones for successful zebrafish breeding (Van den Hurk and Lambert 1983, Lambert et al. 1986, van den Hurk et al. 1987). Zebrafish females only ovulate when in the presence of male zebrafish during the breeding process (Hisaoka and Firlit 1962, Eaton and Farley 1974, Lambert et al. 1986). Females are stimulated to ovulate overnight by steroid glucuronides, produced by the Leydig cells in the testis of male zebrafish, which are released into the water (Hisaoka and Firlit 1962, Eaton and Farley 1974, Lambert et al. 1986, van den Hurk et al. 1987, van den Hurk and Resink 1992, Gerlach 2006). During and after ovulation female zebrafish also produce steroid glucuronides, such as oestradiol-17β-glucuronide and testosterone-glucuronide, that are secreted from the ovaries to attract the males and

initiate courtship behaviour in the males which facilitates egg laying (Van den Hurk and Lambert 1983, Lambert et al. 1986, Kang et al. 2013) (Figure 6.8a).

During the IVF protocol, CD9b -1/-1, CD9b -8/-8 and AB in-cross pairs were left together overnight, therefore the females of each genotype were only exposed to pheromones from a male of the same genotype. The eggs were extracted manually the following morning. Using manual extraction removed any potential differences in courtship behaviour that could affect the number of eggs laid and the percentage of eggs fertilised. The reported decrease in clutch size after IVF suggests that ovulation is not being induced to the same extent in CD9b mutant females as in AB females. Decreased ovulation could be due to defective steroid glucuronide production by the males or recognition by the female CD9b mutants. If ovulation inducement was the sole cause of the decreased clutch size, then it would be expected that the phenotype would be rescued in Figure 6.7a with substitution of either the CD9b mutant male with an AB or the CD9b mutant female with an AB. Surprisingly the phenotype was rescued no matter which mutant partner was substituted with an AB (Figure 6.7a). Whilst it could be possible that both production of and response to male pheromones are defective, it would be expected that no rescue would be seen at all. However, it is more probable that the courtship inducing pheromones are also affected, either in the production of by the females or response to by the males. This would then explain why, although the CD9b mutant x AB pair clutch size is not significantly different to AB x AB pairs, the rescue of the phenotype appears partial and the numbers of eggs laid per pair are mostly lower than the AB x AB pairs (Figure 6.7a).

As well as a decreased clutch size, a decrease in the number and percentage of eggs fertilised was seen from CD9b mutant pairs (Figures 6.1 and 6.3). Although the impaired fertilisation is more aligned with the phenotype seen in CD9b -/- mice, it appears that the requirement for CD9b lies with male zebrafish, in contrast to CD9b-/- mice where CD9 is required for female fertility (Kaji et al. 2000, Le Naour et al. 2000, Miyado et al. 2000)(Figure 6.7b-c). The reduced fertilisation seen using IVF suggests that the defect seen in Figure 6.3 is not due to an absolute absence of sperm production, sperm release or sperm motility (Figure 6.5b). However, a reduced quantity or quality of sperm, due to a need for CD9b during spermatogenesis, could be causing the decreased male fertility seen. A decrease in the percentage of males from

which sperm could be extracted was shown in Figures 6.6a and 6.6aI and the mammalian homolog of CD9b, CD9, has been shown to be expressed throughout the majority of murine spermatogenesis (Kanatsu-Shinohara et al. 2004, Kierszenbaum et al. 2006, Ito et al. 2010) Interestingly, it appears that the steroid glucuronides that have been suggested to act as reproductive pheromones in zebrafish, such as oestradiol-17β-glucuronide and 17α,20β-dihydroxy-4-pregnen-3-one-glucuronide**,** can induce and regulate zebrafish spermatogenesis in their de-glucuronidated state (Van den Hurk and Lambert 1983, Lambert et al. 1986, van den Hurk et al. 1987, van den Hurk and Resink 1992, Miura and Miura 2003, Chen et al. 2010, 2013). A requirement of CD9b for efficient production of the steroids used as reproductive pheromones and spermatogenesis inducers would explain both the decreased clutch size and decreased percentage of eggs fertilized. This may also account for the results seen in Figure 6.7 where partial rescue of clutch size occurs by AB substitution of either partner but complete rescue of fertilization only occurs through substituting a mutant male for an AB male (Figure 6.8).

It could be that CD9b is needed for efficient recognition of these steroids, however, this is less likely as reproductive pheromones are detected in their glucuronidated state by olfaction whereas spermatogenesis occurs in the testis and requires de-glucuronidated steroids indicating that two different receptors are probably required (Van den Hurk and Lambert 1983, van den Hurk et al. 1987).

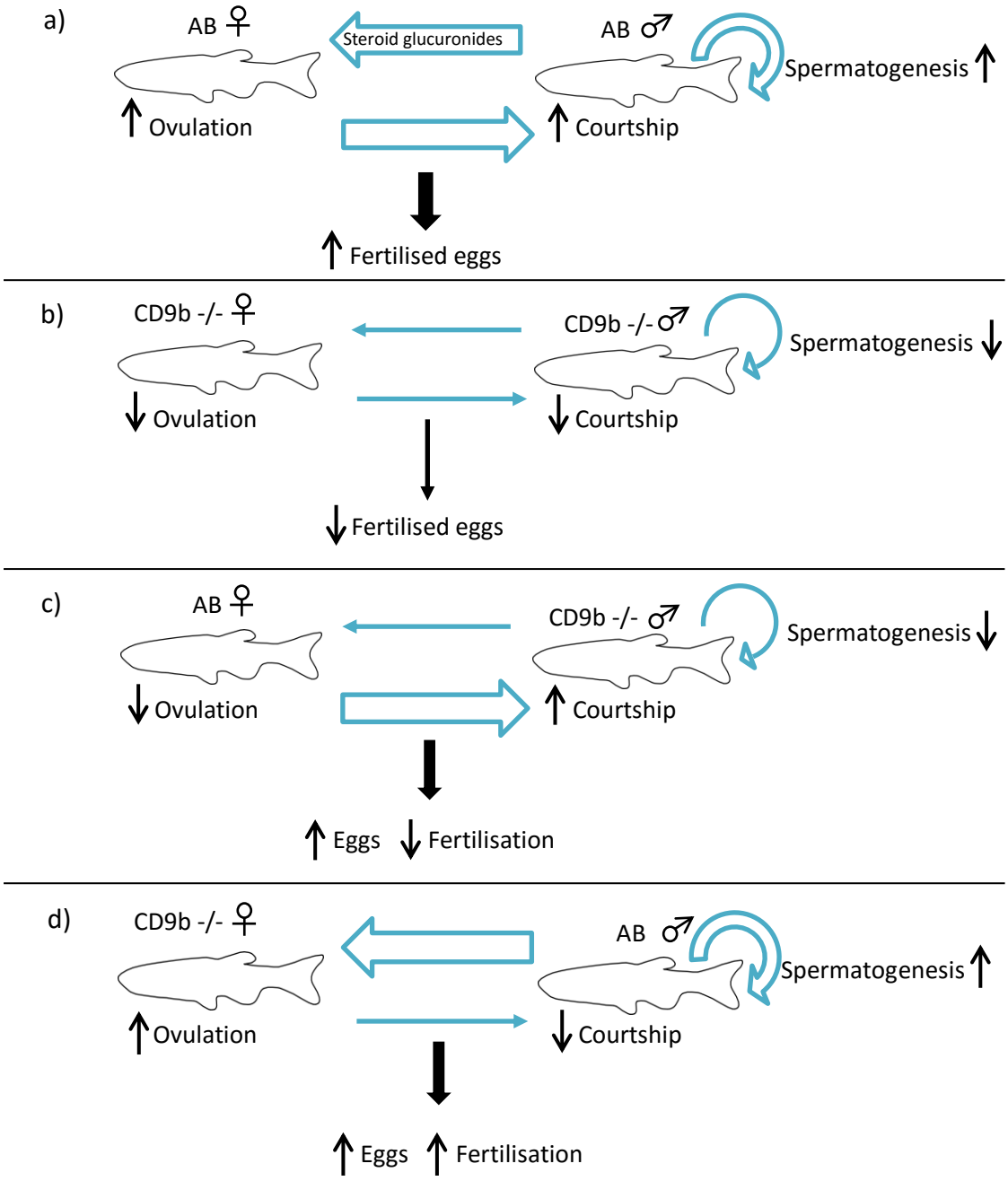

Figure 6.8 Model of potential outcomes from reduced production of reproductive steroids in CD9b mutants

Steroid glucuronides (blue arrows) are produced and released by both male and female zebrafish to induce ovulation and courtship respectively. This in turn leads to eggs being laid by the females and fertilised by the males. Fertilisation requires efficient spermatogenesis, which is under the control of the same steroids but de-glucuronidated (blue curly arrow), to produce mature sperm. In AB pairs this results in many fertilised eggs (a). In CD9b mutant pairs (b) it is hypothesised that less steroid glucuronides are produced leading to less ovulation and less courtship resulting in fewer eggs laid. Less sperm would also be predicted as fewer steroids would be produced to induce spermatogenesis, resulting in a lower percentage of eggs fertilised. The models for CD9b mutant x AB outcrosses are shown in (c) and (d).

Chapter 7: Discussion and future work

7.1 Summary of results

Treatment of embryos with CD9b MOs resulted in decreased neuromast deposition and irregular spacing between neuromasts in the embryonic posterior lateral line.

Homozygous CD9b mutants did not show the same phenotype, with the embryonic posterior lateral line appearing phenotypically normal. However, preliminary data suggested that this may be due to residual functionality of the remaining wild-type N-terminal portion of CD9b in homozygous mutants.

It appeared initially that CD9b homozygous mutants developed tail defects when raised at the lower temperature of 22°C, further experiments demonstrated that this is not the case and the observed defects were probably due to chance.

As with CD9-/- mice, CD9b homozygous mutant zebrafish showed fertility defects. CD9b mutant pairs laid fewer eggs and of the eggs laid, fewer were fertilised. The decrease in egg numbers can be rescued by exchanging either CD9b homozygous mutant partner, male or female, for a wildtype partner. However, the fertilisation defect was only rescued when the CD9b mutant male was exchanged for a wildtype male, suggesting the fertility defect is due to the male not the female partner.

7.2 Chapter 3: CD9b morphants

In this chapter, I characterised the effect of CD9b MO injection on two CXCR4b-mediated migratory processes: PGC and pLLP migration. Initially it seemed that the migration of PGCs was affect by CD9b knockdown. However this phenotype was not reproduced with a second CD9b morpholino and was only observed in embryos injected with the highest amounts of morpholino, many of which also appeared to be suffering from morpholino toxicity. Therefore I concluded that CD9b knockdown did not cause specific PGC migratory defects.

Unlike PGCs, the pLLP migration and neuromast deposition was consistently affected by CD9b morpholino injection. Fewer neuromasts were deposited in CD9b morphants and spacing between deposited neuromasts was irregular but often with an overall increase in the distance between. This work re-capitulated and then expanded on the results reported by Gallardo et al. 2010 in their brief proof-of-principle experiment. These authors reported a new method to assess tissue specific gene expression, during which they found high levels of *cd9b* mRNA in the lateral line primordium cells. To validate their method, they used a morpholino to knock-down *cd9b* and showed some images of *cd9b* morphants with a reduced number of neuromasts. By using two CD9b morpholinos, with different target sequences, at a range of concentrations and analysing the neuromast deposition phenotypes, this phenotype has been quantified, validated and characterised.

Due to the consistent observation of the neuromast deposition phenotype in this work, with multiple morpholino concentrations, two individual morpholinos, and the previous report by Gallardo et al., it appears likely that this phenotype is specific to *cd9b* knockdown.

The gold standard for confirming the specificity of the observed phenotype was, at the time, to determine if the phenotype is re-capitulated in deletion mutants. Unfortunately, the CD9b mutant lines I created did not replicate the phenotypes seen in CD9b morphants. This may be due to compensation by other genes. Rossi et al. 2015 recently reported that compensatory genes and proteins are upregulated in *egfl7* and *vegfaa* mutants but not in the corresponding morphants. This resulted in severe vasculature phenotypes in *egfl7* morphants but normal phenotypes in *egfl7* mutants.

Alternatively, it could suggest that CD9b retained some residual function in the CD9b mutant lines which is then lost upon CD9b MO1 injection.

In light of this, it would be better to confirm the specificity of the neuromast deposition phenotypes using mRNA rescue and so future work would include attempting to rescue the phenotypes using morpholino-resistant *cd9b* mRNA.

7.3 Chapter 4: CD9b mutants

Like CD9b morphants, CD9b deletion mutants showed no differences in PGC migration and so it was concluded that CD9b does not play a role in PGC migration.

CD9b homozygous mutants also showed no posterior lateral line defects. Only CD9b -8/-8 embryos from homozygous parents showed a consistent delay in Prim I migration, which was not replicated in CD9b -1/-1 embryos. This difference between CD9b mutant and morphant phenotypes was investigated by injecting CD9b morpholinos into homozygous mutants. If the morphant phenotype was due to an off-target effect, both morpholinos would produce neuromast phenotypes. If the mutant was rescued by redundancy then morpholino injection wouldn't produce any phenotype. However, only the start-site morpholino and not the splice-site morpholino produced the neuromast phenotype in CD9b mutant embryos. Knocking down translation of the mutant *cd9b* mRNA resulted in the abnormal neuromast phenotype seen in CD9b morphants. This suggested that the mutant CD9b protein in CD9b -1/-1 and CD9b -8/-8 embryos had a residual function which may be rescuing the mutants. As the mutation site is near the 5' of the gene, only the N-terminus of CD9b remains wildtype in CD9b -1/-1 and CD9b -8/-8 mutants. In the CD9b mutants, it would be expected that the mutation in *cd9b* would activate non-sense mediated decay, resulting in a knock-out of gene function. However, qPCR showed that the expression of 5' *cd9b* mRNA was not decreased in CD9b -1/-1 embryos and only 49% decreased in CD9b -8/-8 embryos. In contrast, both CD9b -1/-1 and CD9b -8/-8 embryos showed significant decreases in the expression of 3' *cd9b* mRNA. This preliminary data suggests that the N-terminus of *cd9b* is not cleared in CD9b mutants and has some residual function which is masking the phenotype seen in CD9b morphants. This function could occur through regulation of CXCR4b signalling.

Interaction and trafficking of CXCR4b by the tetraspanin CD63 has been shown to occur through the N-linked glycans of CD63 (Yoshida et al. 2008, 2009). In CD9 the only N-linked glycan is located in the EC1, after the mutation site, and therefore if CD9 played a role in CXCR4b internalisation it would be expected that trafficking differences would be observed in the CD9b mutants (Boucheix et al. 1991). However, internalisation of CXCR4b appears unaffected in the CD9b homozygous mutants.

Recent papers have described a mechanism where CXCL12-CXCR4 signalling up-regulates CD9 expression. CD9 in turn increases the ability of cells to migrate (Leung et al. 2011, Brzoska et al. 2015, Arnaud et al. 2015). In lymphoblastic leukemia, this occurs through CD9 enhancing RAC1 activation which promotes the formation of actin-rich lamellipodia for migration (Arnaud et al. 2015). However, this mechanism of CD9 promoting CXCR4-mediated migration has been reported to be facilitated through the C-terminus of CD9 and not the N-terminus (Arnaud et al. 2015). As the N-terminus is the only wildtype portion of CD9b remaining in the CD9b mutants, it appears unlikely that this mechanism is facilitating the residual function in CD9b mutants.

A recent report by Desterke et al. 2015 has shown that CD9 positively regulates CXCR4 and CXCL12 expression in megakaryocytes as well as CXCR4-mediated migration. It was also reported that CD9 regulated Akt and MAPK phosphorylation. These pathways have been reported to be regulated in a similar manner by an ITIM-like domain in CD37, which allows CD37 to regulate cell survival (Lapalombella et al. 2012). Interestingly, CD9b appears to also have an ITIM-like domain in its N-terminus. This suggests that the N-terminus of CD9b may still have signalling ability in the CD9b mutants.

To investigate whether CD9b in the CD9b mutants has retained some functionality, future work would include attempting to rescue CD9b morphants with morpholino-resistant mRNA which replicates the mRNA produced in CD9b mutants as well as investigating the possible ITIM-like domain in the N-terminus. To do this, the phosphorylation of the N-terminal tyrosine residue and association with proteins such as SHP1 would need to be analysed. Mutation of the tyrosine residue within the ITIM-like domain and assessment of Akt and MAPK phosphorylation would also help to confirm whether CD9b is regulating these pathways in a similar manner to CD37.

7.4 Chapter 5: CD9b mutants raised at 22°C

Initial experiments showed differences in tail development between wildtype and CD9b homozygous mutants raised at 22°C. Further experiments did not recapitulate this observed difference as wildtype embryos also had abnormal tail development and statistical tests showed no difference in tail length or fin fold area between CD9b mutant and wildtype embryos.

Whilst the initial observation and hypothesis for this chapter was proven invalid, it would still be interesting to investigate the function of CD9b in the developing pronephros. As shown in Figure 1.7 and Table 1.4, *cd9b* is highly expressed in the embryonic pronephros and in other models has been shown to be important in the stress response of kidney cells (Sheikh-Hamad et al. 1996, 2000, Takemura et al. 1999, Blumenthal et al. 2015). The CD9b mutants could be assessed for pronephros function, cell adhesion and cell survival under similar stress conditions.

7.5 Chapter 6: CD9b mutants and fertility

Fertility of CD9b -/- zebrafish was assessed for both the number of eggs laid and the percentage of eggs fertilised. It was found that CD9b -/- zebrafish pairs laid decreased numbers of eggs and CD9b -/- males had severely reduced fertility.

Fertility was assessed because CD9 -/- female mice have a severe fertility defect, where few pups were born due to defective sperm-egg fusion (Kaji et al. 2000, Le Naour et al. 2000, Miyado et al. 2000). CD9-/- mice appeared to produce normal numbers of eggs in contrast to CD9b-/- zebrafish which laid significantly fewer eggs than wildtype fish (Le Naour et al. 2000, Miyado et al. 2000). It was surprising that the fertilisation defect appears to reside in the CD9b -/- male partner not the female, unlike CD9-/- mice (Kaji et al. 2000, Le Naour et al. 2000, Miyado et al. 2000). However, CD9 has also been reported to be expressed in male mice throughout spermatogenesis and in mature sperm during fertilisation (Kanatsu-Shinohara et al. 2004, Ito et al. 2010).

In out-cross experiments, where one mutant partner was substituted for a wildtype partner, it was shown that substitution of either partner rescued the numbers of eggs laid but only the substitution of the male partner increased fertility. This apparent ability of both the male and female partner to affect the ovulation of the female might be explained by the mechanism of zebrafish breeding. Female zebrafish are induced to ovulate by steroid glucuronides produced by male zebrafish, which are released into the water. Courtship behaviour in males, to promote egg laying, is then induced by steroid glucuronides produced by the female (Eaton and Farley 1974, Van den Hurk and Lambert 1983, Lambert et al. 1986, van den Hurk et al. 1987, van den Hurk and Resink 1992). Interestingly, some of these steroids have also been reported to regulate spermatogenesis (Miura and Miura 2003, Chen et al. 2010, 2013). A role for CD9b in the production of these steroids would explain both of the fertility phenotypes seen in CD9b -/- pairs as well as the results of the out-cross experiments.

Steroid extraction from zebrafish holding water or rescue experiments using ovarian or testes homogenates from wildtype fish could be used to test whether CD9b -/- fish have deficient production, release or recognition of steroid glucuronides. To assess whether the fertility defect in male CD9b -/- fish is due to defective spermatogenesis, sperm count and quality could be assessed as well as conducting histological examinations of spermatogenesis in the testis.

7.6 Conclusions

- CD9b does not play a role in PGC migration.
- CD9b plays a role in neuromast deposition in the pLL and the 5’ of CD9b may be important for this function.
- CD9b deficiency does not result in abnormal tail development when embryos are raised at 22°C.
- CD9b functions in fertility, affecting both clutch size and egg fertilisation.

Bibliography

Ahmad, F., X. Liu, Y. Zhou, and H. Yao. 2015. An in vivo evaluation of acute toxicity of cobalt ferrite (CoFe2O4) nanoparticles in larval-embryo Zebrafish (Danio rerio). Aquatic toxicology (Amsterdam, Netherlands) 166:21–8.

Alsayed, Y., H. Ngo, J. Runnels, X. Leleu, U. K. Singha, C. M. Pitsillides, J. A. Spencer, T. Kimlinger, J. M. Ghobrial, X. Jia, G. Lu, M. Timm, A. Kumar, D. Côté, I. Veilleux, K. E. Hedin, G. D. Roodman, T. E. Witzig, A. L. Kung, T. Hideshima, K. C. Anderson, C. P. Lin, and I. M. Ghobrial. 2007. Mechanisms of regulation of CXCR4/SDF-1 (CXCL12)-dependent migration and homing in multiple myeloma. Blood 109:2708–17.

Aman, A., M. Nguyen, and T. Piotrowski. 2011. Wnt/β-catenin dependent cell proliferation underlies segmented lateral line morphogenesis. Developmental biology 349:470–82.

Aman, A., and T. Piotrowski. 2008. Wnt/beta-catenin and Fgf signaling control collective cell migration by restricting chemokine receptor expression. Developmental cell 15:749–61.

Aman, A., and T. Piotrowski. 2011. Cell-cell signaling interactions coordinate multiple cell behaviors that drive morphogenesis of the lateral line. Cell adhesion & migration 5:499–508.

Angers, A., and P. Drapeau. 2014. Itch is required for lateral line development in zebrafish. PloS one 9:e111799.

Araki, I., and M. Brand. 2001. Morpholino-induced knockdown of fgf8 efficiently phenocopies the acerebellar (ace) phenotype. Genesis (New York, N.Y. : 2000) 30:157–9.

Ariza-Cosano, A., A. Bensimon-Brito, J. L. Gómez-Skarmeta, and J. Bessa. 2015. sox21a directs lateral line patterning by modulating FGF signaling. Developmental neurobiology.

Arnaud, M.-P., A. Vallée, G. Robert, J. Bonneau, C. Leroy, N. Varin-Blank, A.-G. Rio, M.-B. Troadec, M.-D. Galibert, and V. Gandemer. 2015. CD9, a key actor in the dissemination of lymphoblastic leukemia, modulating CXCR4-mediated migration via RAC1 signaling. Blood 126:blood–2015–02–628560.

Artimo, P., M. Jonnalagedda, K. Arnold, D. Baratin, G. Csardi, E. de Castro, S. Duvaud, V. Flegel, A. Fortier, E. Gasteiger, A. Grosdidier, C. Hernandez, V. Ioannidis, D. Kuznetsov, R. Liechti, S. Moretti, K. Mostaguir, N. Redaschi, G. Rossier, I. Xenarios, and H. Stockinger. 2012. ExPASy: SIB bioinformatics resource portal. http://www.expasy.org/about.

Baker, M., I. R. Mackenzie, S. M. Pickering-Brown, J. Gass, R. Rademakers, C. Lindholm, J. Snowden, J. Adamson, A. D. Sadovnick, S. Rollinson, A. Cannon, E. Dwosh, D. Neary, S. Melquist, A. Richardson, D. Dickson, Z. Berger, J. Eriksen, T. Robinson, C. Zehr, C. A. Dickey, R. Crook, E. McGowan, D. Mann, B. Boeve, H. Feldman, and M. Hutton. 2006. Mutations in progranulin cause tau-negative frontotemporal dementia linked to chromosome 17. Nature 442:916–9.

Bakos, K., R. Kovács, Á. Staszny, D. K. Sipos, B. Urbányi, F. Müller, Z. Csenki, and B. Kovács. 2013. Developmental toxicity and estrogenic potency of zearalenone in zebrafish (Danio rerio). Aquatic toxicology (Amsterdam, Netherlands) 136-137:13–21.

Balabanian, K., B. Lagane, S. Infantino, K. Y. C. Chow, J. Harriague, B. Moepps, F. Arenzana-seisdedos, and M. Thelen. 2005a. The Chemokine SDF-1 / CXCL12 Binds to and Signals through the Orphan Receptor RDC1 in T Lymphocytes *. Journal of Biological Chemistry

280:35760–35766.

Balabanian, K., B. Lagane, J. L. Pablos, L. Laurent, T. Planchenault, O. Verola, C. Lebbe, D. Kerob, A. Dupuy, O. Hermine, J.-F. Nicolas, V. Latger-Cannard, D. Bensoussan, P. Bordigoni, F. Baleux, F. Le Deist, J.-L. Virelizier, F. Arenzana-Seisdedos, and F. Bachelerie. 2005b. WHIM syndromes with different genetic anomalies are accounted for by impaired CXCR4 desensitization to CXCL12. Blood 105:2449–57.

Balabanian, K., A. Levoye, L. Klemm, B. Lagane, O. Hermine, J. Harriague, F. Baleux, F. Arenzana-Seisdedos, and F. Bachelerie. 2008. Leukocyte analysis from WHIM syndrome patients reveals a pivotal role for GRK3 in CXCR4 signaling. The Journal of clinical investigation 118:1074–84.

Balkwill, F. 2004. Cancer and the chemokine network. Nature Reviews Cancer 4:540–550.

Barbolina, M. V, M. Kim, Y. Liu, J. Shepard, A. Belmadani, R. J. Miller, L. D. Shea, and M. S. Stack. 2010. Microenvironmental regulation of chemokine (C-X-C-motif) receptor 4 in ovarian carcinoma. Molecular cancer research : MCR 8:653–64.

Barraud-Lange, V., C. Chalas Boissonnas, C. Serres, J. Auer, A. Schmitt, B. Lefèvre, J.-P. Wolf, and A. Ziyyat. 2012. Membrane transfer from oocyte to sperm occurs in two CD9-independent ways that do not supply the fertilising ability of Cd9-deleted oocytes. Reproduction (Cambridge, England) 144:53–66.

Barreiro, O., M. Zamai, M. Yáñez-Mó, E. Tejera, P. López-Romero, P. N. Monk, E. Gratton, V. R. Caiolfa, and F. Sánchez-Madrid. 2008. Endothelial adhesion receptors are recruited to adherent leukocytes by inclusion in preformed tetraspanin nanoplatforms. The Journal of cell biology 183:527–42.

Bedell, V. M., S. E. Westcot, and S. C. Ekker. 2011. Lessons from morpholino-based screening in zebrafish. Briefings in functional genomics 10:181–8.

Beletkaia, E., S. F. Fenz, W. Pomp, B. E. Snaar-Jagalska, P. W. C. Hogendoorn, and T. Schmidt. 2016. CXCR4 signaling is controlled by immobilization at the plasma membrane. Biochimica et biophysica acta 1863:607–616.

Berditchevski, F., E. Gilbert, M. R. Griffiths, S. Fitter, L. Ashman, and S. J. Jenner. 2001. Analysis of the CD151-alpha3beta1 integrin and CD151-tetraspanin interactions by mutagenesis. The Journal of biological chemistry 276:41165–74.

Berditchevski, F., and E. Odintsova. 2007. Tetraspanins as regulators of protein trafficking. Traffic (Copenhagen, Denmark) 8:89–96.

Berditchevski, F., E. Odintsova, S. Sawada, and E. Gilbert. 2002. Expression of the palmitoylation-deficient CD151 weakens the association of alpha 3 beta 1 integrin with the tetraspanin-enriched microdomains and affects integrin-dependent signaling. The Journal of biological chemistry 277:36991–7000.

Bernhagen, J., R. Krohn, H. Lue, J. L. Gregory, A. Zernecke, R. R. Koenen, M. Dewor, I. Georgiev, A. Schober, L. Leng, T. Kooistra, G. Fingerle-Rowson, P. Ghezzi, R. Kleemann, S. R. McColl, R. Bucala, M. J. Hickey, and C. Weber. 2007. MIF is a noncognate ligand of CXC chemokine receptors in inflammatory and atherogenic cell recruitment. Nature medicine 13:587–96.

Berson, J. F., D. Long, B. J. Doranz, J. Rucker, F. R. Jirik, and R. W. Doms. 1996. A seven-transmembrane domain receptor involved in fusion and entry of T-cell-tropic human immunodeficiency virus type 1 strains. Journal of virology 70:6288–95.

Bianchi, E., B. Doe, D. Goulding, and G. J. Wright. 2014. Juno is the egg Izumo receptor and is essential for mammalian fertilization. Nature 508:483–7.

Blaser, H., S. Eisenbeiss, M. Neumann, M. Reichman-Fried, B. Thisse, C. Thisse, and E. Raz. 2005. Transition from non-motile behaviour to directed migration during early PGC development in zebrafish. Journal of cell science 118:4027–4038.

Blaser, H., M. Reichman-Fried, I. Castanon, K. Dumstrei, F. L. Marlow, K. Kawakami, L. Solnica-Krezel, C.-P. Heisenberg, and E. Raz. 2006. Migration of zebrafish primordial germ cells: a role for myosin contraction and cytoplasmic flow. Developmental cell 11:613–27.

Bleul, C. C., M. Farzan, H. Choe, C. Parolin, I. Clark-Lewis, J. Sodroski, and T. A. Springer. 1996a. The lymphocyte chemoattractant SDF-1 is a ligand for LESTR/fusin and blocks HIV-1 entry. Nature 382:829–33.

Bleul, C. C., R. C. Fuhlbrigge, J. M. Casasnovas, A. Aiuti, and T. A. Springer. 1996b. A highly efficacious lymphocyte chemoattractant, stromal cell-derived factor 1 (SDF-1). The Journal of experimental medicine 184:1101–9.

Blumenthal, A., J. Giebel, G. Warsow, L. Li, R. Ummanni, S. Schordan, E. Schordan, P. Klemm, N. Gretz, K. Endlich, and N. Endlich. 2015. Mechanical stress enhances CD9 expression in cultured podocytes. American journal of physiology. Renal physiology 308:F602–13.

Boch, J., H. Scholze, S. Schornack, A. Landgraf, S. Hahn, S. Kay, T. Lahaye, A. Nickstadt, and U. Bonas. 2009. Breaking the code of DNA binding specificity of TAL-type III effectors. Science (New York, N.Y.) 326:1509–12.

Boer, E. F., E. D. Howell, T. F. Schilling, C. A. Jette, and R. A. Stewart. 2015. Fascin1-dependent Filopodia are required for directional migration of a subset of neural crest cells. PLoS genetics 11:e1004946.

Boldajipour, B., M. Doitsidou, K. Tarbashevich, C. Laguri, S. R. Yu, J. Ries, K. Dumstrei, S. Thelen, J. Dörries, E.-M. Messerschmidt, M. Thelen, P. Schwille, M. Brand, H. Lortat-Jacob, and E. Raz. 2011. Cxcl12 evolution--subfunctionalization of a ligand through altered interaction with the chemokine receptor. Development (Cambridge, England) 138:2909–14.

Boldajipour, B., H. Mahabaleshwar, E. Kardash, M. Reichman-Fried, H. Blaser, S. Minina, D. Wilson, Q. Xu, and E. Raz. 2008. Control of Chemokine-Guided Cell Migration by Ligand Sequestration. Cell 132:463–473.

Boucheix, C., P. Benoit, P. Frachet, M. Billard, R. E. Worthington, J. Gagnon, and G. Uzan. 1991. Molecular cloning of the CD9 antigen. A new family of cell surface proteins. The Journal of biological chemistry 266:117–22.

Boucheix, C., and E. Rubinstein. 2001. Tetraspanins. Cell and molecular life science 58:1189–205.

Braat, A. K., T. Zandbergen, S. van de Water, H. J. Goos, and D. Zivkovic. 1999. Characterization of zebrafish primordial germ cells: morphology and early distribution of vasa RNA. Developmental dynamics : an official publication of the American Association of Anatomists 216:153–67.

Breau, M. A., D. G. Wilkinson, and Q. Xu. 2013. A Hox gene controls lateral line cell migration by regulating chemokine receptor expression downstream of Wnt signaling. Proceedings of the National Academy of Sciences of the United States of America 110:16892–7.

Brunet, F. G., H. Roest Crollius, M. Paris, J.-M. Aury, P. Gibert, O. Jaillon, V. Laudet, and M.

Robinson-Rechavi. 2006. Gene loss and evolutionary rates following whole-genome duplication in teleost fishes. Molecular biology and evolution 23:1808–16.

Brzoska, E., K. Kowalski, A. Markowska-Zagrajek, M. Kowalewska, R. Archacki, I. Plaskota, W. Stremińska, K. Jańczyk-Ilach, and M. A. Ciemerych. 2015. Sdf-1 (CXCL12) induces CD9 expression in stem cells engaged in muscle regeneration. Stem cell research & therapy 6:46.

Burger, M., A. Glodek, T. Hartmann, A. Schmitt-Gräff, L. E. Silberstein, N. Fujii, T. J. Kipps, and J. A. Burger. 2003. Functional expression of CXCR4 (CD184) on small-cell lung cancer cells mediates migration, integrin activation, and adhesion to stromal cells. Oncogene 22:8093–101.

Burns, J. M., B. C. Summers, Y. Wang, A. Melikian, R. Berahovich, Z. Miao, M. E. T. Penfold, M. J. Sunshine, D. R. Littman, C. J. Kuo, K. Wei, B. E. McMaster, K. Wright, M. C. Howard, and T. J. Schall. 2006. A novel chemokine receptor for SDF-1 and I-TAC involved in cell survival, cell adhesion, and tumor development. The Journal of experimental medicine 203:2201–13.

Busillo, J. M., and J. L. Benovic. 2007. Regulation of CXCR4 signaling. Biochimica et Biophysica Acta (BBA) - Biomembranes 1768:952–963.

Cabioglu, N., J. Summy, C. Miller, N. U. Parikh, A. A. Sahin, S. Tuzlali, K. Pumiglia, G. E. Gallick, and J. E. Price. 2005. CXCL-12/stromal cell-derived factor-1alpha transactivates HER2-neu in breast cancer cells by a novel pathway involving Src kinase activation. Cancer research 65:6493–7.

Cade, L., D. Reyon, W. Y. Hwang, S. Q. Tsai, S. Patel, C. Khayter, J. K. Joung, J. D. Sander, R. T. Peterson, and J.-R. J. Yeh. 2012. Highly efficient generation of heritable zebrafish gene mutations using homo- and heterodimeric TALENs. Nucleic acids research 40:8001–10.

Canals, M., D. J. Scholten, S. De Munnik, M. K. L. Han, M. J. Smit, and R. Leurs. 2012. Ubiquitination of CXCR7 Controls Receptor Trafficking. PloS one 7.

Cannon, K. S., and P. Cresswell. 2001. Quality control of transmembrane domain assembly in the tetraspanin CD82. The EMBO journal 20:2443–53.

Chalbi, M., V. Barraud-Lange, B. Ravaux, K. Howan, N. Rodriguez, P. Soule, A. Ndzoudi, C. Boucheix, E. Rubinstein, J. P. Wolf, A. Ziyyat, E. Perez, F. Pincet, and C. Gourier. 2014. Binding of sperm protein Izumo1 and its egg receptor Juno drives Cd9 accumulation in the intercellular contact area prior to fusion during mammalian fertilization. Development (Cambridge, England) 141:3732–9.

Charrin, S., S. Jouannet, C. Boucheix, and E. Rubinstein. 2014. Tetraspanins at a glance. Journal of cell science 127:3641–8.

Charrin, S., M. Latil, S. Soave, A. Polesskaya, F. Chrétien, C. Boucheix, and E. Rubinstein. 2013. Normal muscle regeneration requires tight control of muscle cell fusion by tetraspanins CD9 and CD81. Nature communications 4:1674.

Charrin, S., F. le Naour, O. Silvie, P.-E. Milhiet, C. Boucheix, and E. Rubinstein. 2009. Lateral organization of membrane proteins: tetraspanins spin their web. The Biochemical journal 420:133–54.

Chatterjee, S., B. Behnam Azad, and S. Nimmagadda. 2014. The intricate role of CXCR4 in cancer. Advances in cancer research 124:31–82.

Chen, M. S., K. S. Tung, S. A. Coonrod, Y. Takahashi, D. Bigler, A. Chang, Y. Yamashita, P. W. Kincade, J. C. Herr, and J. M. White. 1999. Role of the integrin-associated protein CD9 in binding between sperm ADAM 2 and the egg integrin alpha6beta1: implications for murine fertilization. Proceedings of the National Academy of Sciences of the United States of America 96:11830–5.

Chen, S. X., J. Bogerd, A. García-López, H. de Jonge, P. P. de Waal, W. S. Hong, and R. W. Schulz. 2010. Molecular cloning and functional characterization of a zebrafish nuclear progesterone receptor. Biology of reproduction 82:171–81.

Chen, S. X., J. Bogerd, N. E. Schoonen, J. Martijn, P. P. de Waal, and R. W. Schulz. 2013. A progestin (17α,20β-dihydroxy-4-pregnen-3-one) stimulates early stages of spermatogenesis in zebrafish. General and Comparative Endocrinology 185:1–9.

Chong, S., L. Nguyet, Y. Jiang, and V. Korzh. 2007. The chemokine Sdf-1 and its receptor Cxcr4 are required for formation of muscle in zebrafish. BMC developmental biology 14:1–14.

Chong, S. W., A. Emelyanov, Z. Gong, and V. Korzh. 2001. Expression pattern of two zebrafish genes , cxcr4a and cxcr4b. Mechanisms of Development 109:347–354.

Claas, C., C. S. Stipp, and M. E. Hemler. 2001. Evaluation of Prototype Transmembrane 4 Superfamily Protein Complexes and Their Relation to Lipid Rafts. Journal of Biological Chemistry 276:7974–7984.

Cook, G. A., C. M. Longhurst, S. Grgurevich, S. Cholera, J. T. Crossno, and L. K. Jennings. 2002. Identification of CD9 extracellular domains important in regulation of CHO cell adhesion to fibronectin and fibronectin pericellular matrix assembly. Blood 100:4502–11.

Copeland, B. T., M. J. Bowman, C. Boucheix, and L. K. Ashman. 2013. Knockout of the tetraspanin Cd9 in the TRAMP model of de novo prostate cancer increases spontaneous metastases in an organ-specific manner. International journal of cancer. Journal international du cancer 133:1803–12.

Corey, D. R., and J. M. Abrams. 2001. Morpholino antisense oligonucleotides: tools for investigating vertebrate development. Genome biology 2:REVIEWS1015.

Dahlem, T. J., K. Hoshijima, M. J. Jurynec, D. Gunther, C. G. Starker, A. S. Locke, A. M. Weis, D. F. Voytas, and D. J. Grunwald. 2012. Simple Methods for Generating and Detecting Locus-Specific Mutations Induced with TALENs in the Zebrafish Genome. PLoS Genetics 8.

Dambly-Chaudière, C., N. Cubedo, and A. Ghysen. 2007. Control of cell migration in the development of the posterior lateral line: antagonistic interactions between the chemokine receptors CXCR4 and CXCR7/RDC1. BMC developmental biology 7:23.

Dambly-Chaudière, C., D. Sapède, F. Soubiran, K. Decorde, N. Gompel, and A. Ghysen. 2003. The lateral line of zebrafish: a model system for the analysis of morphogenesis and neural development in vertebrates. Biology of the Cell 95:579–587.

David, N. B., D. Sapède, L. Saint-Etienne, C. Thisse, B. Thisse, C. Dambly-Chaudière, F. M. Rosa, and A. Ghysen. 2002. Molecular basis of cell migration in the fish lateral line: role of the chemokine receptor CXCR4 and of its ligand, SDF1. Proceedings of the National Academy of Sciences of the United States of America 99:16297–16302.

Décaillot, F. M., M. A. Kazmi, Y. Lin, S. Ray-Saha, T. P. Sakmar, and P. Sachdev. 2011. CXCR7/CXCR4 heterodimer constitutively recruits beta-arrestin to enhance cell migration. The Journal of biological chemistry 286:32188–97.

Deissler, H., E. Kuhn, G. E. Lang, and H. Deissler. 2007. Tetraspanin CD9 is involved in the migration of retinal microvascular endothelial cells 9:643–652.

Delandre, C., T. R. Penabaz, A. L. Passarelli, S. K. Chapes, and R. J. Clem. 2009. Mutation of juxtamembrane cysteines in the tetraspanin CD81 affects palmitoylation and alters interaction with other proteins at the cell surface. Experimental cell research 315:1953–63.

Desterke, C., C. Martinaud, B. Guerton, L. Pieri, C. Bogani, D. Clay, F. Torossian, J.-J. Lataillade, H. C. Hasselbach, H. Gisslinger, J.-L. Demory, B. Dupriez, C. Boucheix, E. Rubinstein, S. Amsellem, A. M. Vannucchi, and M.-C. Le Bousse-Kerdilès. 2015. Tetraspanin CD9 participates in dysmegakaryopoiesis and stromal interactions in primary myelofibrosis. Haematologica 100:757–67.

Detchokul, S., E. D. Williams, M. W. Parker, and A. G. Frauman. 2014. Tetraspanins as regulators of the tumour microenvironment: implications for metastasis and therapeutic strategies. British journal of pharmacology 171:5462–90.

Dick, A., M. Hild, H. Bauer, Y. Imai, H. Maifeld, A. Schier, W. Talbot, T. Bouwmeester, and M. Hammerschmidt. 2000. Essential role of Bmp7 (snailhouse) and its prodomain in dorsoventral patterning of the zebrafish embryo. Development 127:343–354.

Doitsidou, M., M. Reichman-Fried, J. Stebler, M. Köprunner, J. Dörries, D. Meyer, C. V. Esguerra, T. Leung, and E. Raz. 2002. Guidance of primordial germ cell migration by the chemokine SDF-1. Cell 111:647–659.

Donà, E., J. D. Barry, G. Valentin, C. Quirin, A. Khmelinskii, A. Kunze, S. Durdu, L. R. Newton, A. Fernandez-Minan, W. Huber, M. Knop, and D. Gilmour. 2013. Directional tissue migration through a self-generated chemokine gradient. Nature 503:285–9.

Draper, B. W., P. A. Morcos, and C. B. Kimmel. 2001. Inhibition of zebrafish fgf8 pre-mRNA splicing with morpholino oligos: a quantifiable method for gene knockdown. Genesis (New York, N.Y. : 2000) 30:154–6.

Dufourcq, P., and S. Vriz. 2006. The chemokine SDF-1 regulates blastema formation during zebrafish fin regeneration. Development genes and evolution 216:635–9.

Dumstrei, K., R. Mennecke, and E. Raz. 2004. Signaling pathways controlling primordial germ cell migration in zebrafish. Journal of cell science 117:4787–95.

Durdu, S., M. Iskar, C. Revenu, N. Schieber, A. Kunze, P. Bork, Y. Schwab, and D. Gilmour. 2014. Luminal signalling links cell communication to tissue architecture during organogenesis. Nature.

Eaton, R. C., and R. D. Farley. 1974. Spawning Cycle and Egg Production of Zebrafish, Brachydanio rerio, in the Laboratory. Copeia 1974:195–204.

Edgar, R. C. 2004. MUSCLE: multiple sequence alignment with high accuracy and high throughput. Nucleic acids research 32:1792–7.

Eisen, J. S., and J. C. Smith. 2008. Controlling morpholino experiments: don't stop making antisense. Development (Cambridge, England) 135:1735–43.

Ekker, S. C. 2000. Morphants: a new systematic vertebrate functional genomics approach. Yeast (Chichester, England) 17:302–306.

Ekker, S. C., and J. D. Larson. 2001. Morphant technology in model developmental systems.

Genesis (New York, N.Y. : 2000) 30:89–93.

Ellerman, D. A., C. Ha, P. Primakoff, D. G. Myles, and G. S. Dveksler. 2003. Direct binding of the ligand PSG17 to CD9 requires a CD9 site essential for sperm-egg fusion. Molecular biology of the cell 14:5098–103.

Encinas, P., M. A. Rodriguez-Milla, B. Novoa, A. Estepa, A. Figueras, and J. Coll. 2010. Zebrafish fin immune responses during high mortality infections with viral haemorrhagic septicemia rhabdovirus. A proteomic and transcriptomic approach. BMC genomics 11:518.

Feldman, B., M. Tuchman, and L. Caldovic. 2014. A zebrafish model of hyperammonemia. Molecular genetics and metabolism 113:142–7.

Filby, A. L., G. C. Paull, E. J. Bartlett, K. J. W. Van Look, and C. R. Tyler. 2010. Physiological and health consequences of social status in zebrafish (Danio rerio). Physiology & behavior 101:576–87.

Flannery, A. R., C. Czibener, and N. W. Andrews. 2010. Palmitoylation-dependent association with CD63 targets the Ca^{2+} sensor synaptotagmin VII to lysosomes. The Journal of Cell Biology 191:599–613.

Förster, R., E. Kremmer, A. Schubel, D. Breitfeld, A. Kleinschmidt, C. Nerl, G. Bernhardt, and M. Lipp. 1998. Intracellular and surface expression of the HIV-1 coreceptor CXCR4/fusin on various leukocyte subsets: rapid internalization and recycling upon activation. Journal of immunology (Baltimore, Md. : 1950) 160:1522–31.

Friedl, P., and D. Gilmour. 2009. Collective cell migration in morphogenesis, regeneration and cancer. Nature reviews. Molecular cell biology 10:445–457.

Gallardo, V. E., J. Liang, M. Behra, A. Elkahloun, E. J. Villablanca, V. Russo, M. L. Allende, and S. M. Burgess. 2010. Molecular dissection of the migrating posterior lateral line primordium during early development in zebrafish. BMC developmental biology 10:120.

Gallardo, V. E., G. K. Varshney, M. Lee, S. Bupp, L. Xu, P. Shinn, N. P. Crawford, J. Inglese, and S. M. Burgess. 2015. Phenotype-driven chemical screening in zebrafish for compounds that inhibit collective cell migration identifies multiple pathways potentially involved in metastatic invasion. Disease models & mechanisms 8:565–76.

Gamba, L., N. Cubedo, A. Ghysen, G. Lutfalla, and C. Dambly-Chaudière. 2010a. Estrogen receptor ESR1 controls cell migration by repressing chemokine receptor CXCR4 in the zebrafish posterior lateral line system. Proceedings of the National Academy of Sciences of the United States of America 107:6358–63.

Gamba, L., N. Cubedo, G. Lutfalla, A. Ghysen, and C. Dambly-Chaudiere. 2010b. Lef1 controls patterning and proliferation in the posterior lateral line system of zebrafish. Developmental dynamics : an official publication of the American Association of Anatomists 239:3163–71.

Ganju, R. K., S. A. Brubaker, J. Meyer, P. Dutt, Y. Yang, S. Qin, W. Newman, and J. E. Groopman. 1998. The -Chemokine, Stromal Cell-derived Factor-1 , Binds to the Transmembrane G-protein-coupled CXCR-4 Receptor and Activates Multiple Signal Transduction Pathways. Journal of Biological Chemistry 273:23169–23175.

Garcia-España, A., P.-J. Chung, I. N. Sarkar, E. Stiner, T.-T. Sun, and R. Desalle. 2008. Appearance of new tetraspanin genes during vertebrate evolution. Genomics 91:326–34.

Garner, J. M., M. J. Herr, K. B. Hodges, and L. K. Jennings. 2016. The utility of tetraspanin CD9 as a biomarker for metastatic clear cell renal cell carcinoma. Biochemical and biophysical research communications 471:21–5.

Gartlan, K. H., G. T. Belz, J. M. Tarrant, G. Minigo, M. Katsara, K.-C. Sheng, M. Sofi, A. B. van Spriel, V. Apostolopoulos, M. Plebanski, L. Robb, and M. D. Wright. 2010. A complementary role for the tetraspanins CD37 and Tssc6 in cellular immunity. Journal of immunology (Baltimore, Md. : 1950) 185:3158–66.

Gasteiger, E., C. Hoogland, A. Gattiker, S. Duvaud, M. R. Wilkins, R. D. Appel, and A. Bairoch. 2005. Protein Identification and Analysis Tools on the ExPASy Server (In) John M. Walker (ed): The Proteomics Protocols Handbook. Humana Press.

Gerlach, G. 2006. Pheromonal regulation of reproductive success in female zebrafish: female suppression and male enhancement. Animal Behaviour 72:1119–1124.

Ghysen, A., and C. Dambly-Chaudiere. 2004. Development of the zebrafish lateral line. Current Opinion in Neurobiology 14:67–73.

Gladson, C. L., and D. R. Welch. 2008. New insights into the role of CXCR4 in prostate cancer metastasis. Cancer biology & therapy 7:1849–51.

Gompel, N., N. Cubedo, C. Thisse, B. Thisse, C. Dambly-Chaudière, and A. Ghysen. 2001. Pattern formation in the lateral line of zebrafish. http://www.neurodvpmt.univ-montp2.fr/papers/pdf-MOD.pdf.

Gordón-Alonso, M., M. Yañez-Mó, O. Barreiro, S. Alvarez, M. A. Muñoz-Fernández, A. Valenzuela-Fernández, and F. Sánchez-Madrid. 2006. Tetraspanins CD9 and CD81 modulate HIV-1-induced membrane fusion. Journal of immunology (Baltimore, Md. : 1950) 177:5129–5137.

Goudarzi, M., T. U. Banisch, M. B. Mobin, N. Maghelli, K. Tarbashevich, I. Strate, J. van den Berg, H. Blaser, S. Bandemer, E. Paluch, J. Bakkers, I. M. Tolić-Nørrelykke, and E. Raz. 2012. Identification and regulation of a molecular module for bleb-based cell motility. Developmental cell 23:210–8.

Goudarzi, M., I. Strate, A. Paksa, A.-K. Lagendijk, J. Bakkers, and E. Raz. 2013. On the robustness of germ cell migration and microRNA-mediated regulation of chemokine signaling. Nature genetics 45:1264–5.

Grant, K. A., D. W. Raible, and T. Piotrowski. 2005. Regulation of latent sensory hair cell precursors by glia in the zebrafish lateral line. Neuron 45:69–80.

Haas, P., and D. Gilmour. 2006. Chemokine Signaling Mediates Self-Organizing Tissue Migration in the Zebrafish Lateral Line. Developmental Cell 10:673–680.

Harding, M. J., and A. V Nechiporuk. 2012. Fgfr-Ras-MAPK signaling is required for apical constriction via apical positioning of Rho-associated kinase during mechanosensory organ formation. Development (Cambridge, England) 139:3130–5.

Harrison, M. R. M., J. Bussmann, Y. Huang, L. Zhao, A. Osorio, C. G. Burns, C. E. Burns, H. M. Sucov, A. F. Siekmann, and C.-L. Lien. 2015. Chemokine-guided angiogenesis directs coronary vasculature formation in zebrafish. Developmental cell 33:442–54.

Hartwig, J., K. Tarbashevich, J. Seggewiß, M. Stehling, J. Bandemer, C. Grimaldi, A. Paksa, T. Groß-Thebing, D. Meyen, and E. Raz. 2014. Temporal control over the initiation of cell motility by a regulator of G-protein signaling. Proceedings of the National Academy of

Sciences of the United States of America 111:11389–94.

Hassuna, N., P. N. Monk, G. W. Moseley, and L. J. Partridge. 2009. Strategies for Targeting Tetraspanin Proteins Potential Therapeutic Applications in Microbial Infections. Biodrugs 23:1–19.

He, P., H. Kuhara, I. Tachibana, Y. Jin, Y. Takeda, S. Tetsumoto, T. Minami, S. Kohmo, H. Hirata, R. Takahashi, K. Inoue, I. Nagatomo, H. Kida, T. Kijima, T. Naka, E. Morii, I. Kawase, and A. Kumanogoh. 2013. Calretinin mediates apoptosis in small cell lung cancer cells expressing tetraspanin CD9. FEBS Open Bio 3:225–230.

He, Y., Z. Wang, S. Sun, D. Tang, W. Li, R. Chai, and H. Li. 2015. HDAC3 Is Required for Posterior Lateral Line Development in Zebrafish. Molecular neurobiology.

He, Z.-Y., C. Brakebusch, R. Fässler, J. A. Kreidberg, P. Primakoff, and D. G. Myles. 2003. None of the integrins known to be present on the mouse egg or to be ADAM receptors are essential for sperm–egg binding and fusion. Developmental Biology 254:226–237.

Heesen, M., M. A. Berman, J. D. Benson, C. Gerard, and M. E. Dorf. 1996. Cloning of the mouse fusin gene, homologue to a human HIV-1 co-factor. Journal of immunology (Baltimore, Md. : 1950) 157:5455–60.

Heesen, M., M. A. Berman, A. Charest, D. Housman, C. Gerard, M. E. Dorf, and C. Gerard. 1998. Cloning and chromosomal mapping of an orphan chemokine receptor : mouse RDC1. Immunogenetics:364–370.

Hemler, M. E. 2005. Tetraspanin functions and associated microdomains. Nature reviews. Molecular cell biology 6:801–11.

Hemler, M. E. 2008. Targeting of tetraspanin proteins--potential benefits and strategies. Nature reviews. Drug discovery 7:747–58.

Hernandez, P. A., R. J. Gorlin, J. N. Lukens, S. Taniuchi, J. Bohinjec, F. Francois, M. E. Klotman, and G. A. Diaz. 2003. Mutations in the chemokine receptor gene CXCR4 are associated with WHIM syndrome, a combined immunodeficiency disease. Nature genetics 34:70–4.

Herr, M. J., J. Kotha, N. Hagedorn, B. Smith, and L. K. Jennings. 2013. Tetraspanin CD9 promotes the invasive phenotype of human fibrosarcoma cells via upregulation of matrix metalloproteinase-9. PloS one 8:e67766.

Herrero, J., M. Muffato, K. Beal, S. Fitzgerald, L. Gordon, M. Pignatelli, A. J. Vilella, S. M. J. Searle, R. Amode, S. Brent, W. Spooner, E. Kulesha, A. Yates, and P. Flicek. 2016. Ensembl comparative genomics resources. Database : the journal of biological databases and curation 2016.

Higginbottom, A., E. R. Quinn, C. C. Kuo, M. Flint, L. H. Wilson, E. Bianchi, A. Nicosia, P. N. Monk, J. A. McKeating, and S. Levy. 2000. Identification of amino acid residues in CD81 critical for interaction with hepatitis C virus envelope glycoprotein E2. Journal of virology 74:3642–9.

Hisaoka, K. K., and C. F. Firlit. 1962. Ovarian Cycle and Egg Production in the Zebrafish, Brachydanio rerio Ovarian. Copeia 4:788–792.

Hoffmann, F., W. Müller, D. Schütz, M. E. Penfold, Y. H. Wong, S. Schulz, and R. Stumm. 2012. Rapid uptake and degradation of CXCL12 depend on CXCR7 carboxyl-terminal serine/threonine residues. The Journal of biological chemistry 287:28362–77.

Houle, C. D., X.-Y. Ding, J. F. Foley, C. A. Afshari, J. C. Barrett, and B. J. Davis. 2002. Loss of Expression and Altered Localization of KAI1 and CD9 Protein Are Associated with Epithelial Ovarian Cancer Progression. Gynecologic Oncology 86:69–78.

Howe, D. ., Y. Bradford, T. Conlin, A. . Eagle, D. Fashena, K. Frazer, J. Knight, P. Mani, R. Martin, S. Moxon, H. Paddock, C. Pich, S. Ramachandran, B. Ruef, L. Ruzicka, K. Schaper, X. Shao, A. Singer, B. Sprunger, C. . Van Slyke, M. Westerfield, B. Spunger, C. . Van Slyke, and M. Westerfield. 2013a. ZFIN, the Zebrafish Model Organism Database: increased support for mutants and transgenics.

Howe, K., M. D. Clark, C. F. Torroja, J. Torrance, C. Berthelot, M. Muffato, J. E. Collins, S. Humphray, K. McLaren, L. Matthews, S. McLaren, I. Sealy, M. Caccamo, C. Churcher, C. Scott, J. C. Barrett, R. Koch, G.-J. Rauch, S. White, W. Chow, B. Kilian, L. T. Quintais, J. A. Guerra-Assunção, Y. Zhou, Y. Gu, J. Yen, J.-H. Vogel, T. Eyre, S. Redmond, R. Banerjee, J. Chi, B. Fu, E. Langley, S. F. Maguire, G. K. Laird, D. Lloyd, E. Kenyon, S. Donaldson, H. Sehra, J. Almeida-King, J. Loveland, S. Trevanion, M. Jones, M. Quail, D. Willey, A. Hunt, J. Burton, S. Sims, K. McLay, B. Plumb, J. Davis, C. Clee, K. Oliver, R. Clark, C. Riddle, D. Elliot, D. Eliott, G. Threadgold, G. Harden, D. Ware, S. Begum, B. Mortimore, B. Mortimer, G. Kerry, P. Heath, B. Phillimore, A. Tracey, N. Corby, M. Dunn, C. Johnson, J. Wood, S. Clark, S. Pelan, G. Griffiths, M. Smith, R. Glithero, P. Howden, N. Barker, C. Lloyd, C. Stevens, J. Harley, K. Holt, G. Panagiotidis, J. Lovell, H. Beasley, C. Henderson, D. Gordon, K. Auger, D. Wright, J. Collins, C. Raisen, L. Dyer, K. Leung, L. Robertson, K. Ambridge, D. Leongamornlert, S. McGuire, R. Gilderthorp, C. Griffiths, D. Manthravadi, S. Nichol, G. Barker, S. Whitehead, M. Kay, J. Brown, C. Murnane, E. Gray, M. Humphries, N. Sycamore, D. Barker, D. Saunders, J. Wallis, A. Babbage, S. Hammond, M. Mashreghi-Mohammadi, L. Barr, S. Martin, P. Wray, A. Ellington, N. Matthews, M. Ellwood, R. Woodmansey, G. Clark, J. D. Cooper, J. Cooper, A. Tromans, D. Grafham, C. Skuce, R. Pandian, R. Andrews, E. Harrison, A. Kimberley, J. Garnett, N. Fosker, R. Hall, P. Garner, D. Kelly, C. Bird, S. Palmer, I. Gehring, A. Berger, C. M. Dooley, Z. Ersan-Ürün, C. Eser, H. Geiger, M. Geisler, L. Karotki, A. Kirn, J. Konantz, M. Konantz, M. Oberländer, S. Rudolph-Geiger, M. Teucke, C. Lanz, G. Raddatz, K. Osoegawa, B. Zhu, A. Rapp, S. Widaa, C. Langford, F. Yang, S. C. Schuster, N. P. Carter, J. Harrow, Z. Ning, J. Herrero, S. M. J. Searle, A. Enright, R. Geisler, R. H. A. Plasterk, C. Lee, M. Westerfield, P. J. de Jong, L. I. Zon, J. H. Postlethwait, C. Nüsslein-Volhard, T. J. P. Hubbard, H. Roest Crollius, J. Rogers, and D. L. Stemple. 2013b. The zebrafish reference genome sequence and its relationship to the human genome. Nature 496:498–503.

Huang, C., D. Liu, D. Masuya, K. Kameyama, T. Nakashima, H. Yokomise, M. Ueno, and M. Miyake. 2004. MRP-1/CD9 gene transduction downregulates Wnt signal pathways. Oncogene 23:7475–83.

Huang, P., A. Xiao, M. Zhou, Z. Zhu, S. Lin, and B. Zhang. 2011. Heritable gene targeting in zebrafish using customized TALENs. Nature Publishing Group 29:699–700.

Huang, S., H. Tian, Z. Chen, T. Yu, and A. Xu. 2010. The evolution of vertebrate tetraspanins : gene loss , retention , and massive positive selection after whole genome duplications:1–17.

Huang, S., S. Yuan, M. Dong, J. Su, C. Yu, Y. Shen, X. Xie, Y. Yu, X. Yu, S. Chen, S. Zhang, P. Pontarotti, and A. Xu. 2005. The phylogenetic analysis of tetraspanins projects the evolution of cell-cell interactions from unicellular to multicellular organisms. Genomics 86:674–84.

Huc-Brandt, S., N. Hieu, T. Imberdis, N. Cubedo, M. Silhol, P. L. A. Leighton, T. Domaschke, W. T. Allison, V. Perrier, and M. Rossel. 2014. Zebrafish prion protein PrP2 controls collective

migration process during lateral line sensory system development. PloS one 9:e113331.

Van den Hurk, R., and J. G. D. Lambert. 1983. Ovarian steroid glucuronides function as sex pheromones for male zebrafish Brachydanio rerio. Canadian journal of zoology 61:2381–2386.

van den Hurk, R., and J. W. Resink. 1992. Male reproductive system as sex pheromone producer in teleost fish. Journal of Experimental Zoology 261:204–213.

van den Hurk, R., W. G. E. J. Schoonen, G. A. van Zoelen, and J. G. D. Lambert. 1987. The biosynthesis of steroid glucuronides in the testis of the zebrafish, Brachydanio rerio, and their pheromonal function as ovulation inducers. General and Comparative Endocrinology 68:179–188.

Ikeyama, B. S., M. Koyama, M. Yamaoko, R. Sasada, T. C. Industries, and K. Hospital. 1993. Suppression of Cell Motility and Metastasis by Transfection with Human Motility-related Protein (MRP-1/CD9) DNA 177.

Inoue, N., Y. Hagihara, D. Wright, T. Suzuki, and I. Wada. 2015. Oocyte-triggered dimerization of sperm IZUMO1 promotes sperm-egg fusion in mice. Nature communications 6:8858.

Inoue, N., D. Hamada, H. Kamikubo, K. Hirata, M. Kataoka, M. Yamamoto, M. Ikawa, M. Okabe, and Y. Hagihara. 2013. Molecular dissection of IZUMO1, a sperm protein essential for sperm-egg fusion. Development (Cambridge, England) 140:3221–9.

Inoue, N., M. Ikawa, A. Isotani, and M. Okabe. 2005. The immunoglobulin superfamily protein Izumo is required for sperm to fuse with eggs. Nature 434:234–8.

Inoue, N., M. Ikawa, and M. Okabe. 2011. The mechanism of sperm-egg interaction and the involvement of IZUMO1 in fusion. Asian journal of andrology 13:81–7.

Inoue, S., S. Kondo, D. M. Parichy, and M. Watanabe. 2014. Tetraspanin 3c requirement for pigment cell interactions and boundary formation in zebrafish adult pigment stripes. Pigment cell & melanoma research 27:190–200.

Ito, C., K. Yamatoya, K. Yoshida, M. Maekawa, K. Miyado, and K. Toshimori. 2010. Tetraspanin family protein CD9 in the mouse sperm: unique localization, appearance, behavior and fate during fertilization. Cell and tissue research 340:583–94.

Itou, J., I. Oishi, H. Kawakami, T. J. Glass, J. Richter, A. Johnson, T. C. Lund, and Y. Kawakami. 2012. Migration of cardiomyocytes is essential for heart regeneration in zebrafish. Development (Cambridge, England) 139:4133–42.

Iwasaki, T., Y. Takeda, K. Maruyama, Y. Yokosaki, K. Tsujino, S. Tetsumoto, H. Kuhara, K. Nakanishi, Y. Otani, Y. Jin, S. Kohmo, H. Hirata, R. Takahashi, M. Suzuki, K. Inoue, I. Nagatomo, S. Goya, T. Kijima, T. Kumagai, I. Tachibana, I. Kawase, and A. Kumanogoh. 2012. Deletion of Tetraspanin CD9 Diminishes Lymphangiogenesis in Vivo and in Vitro. Journal of Biological Chemistry 288:2118–2131.

Janowski, M. 2009. Functional diversity of SDF-1 splicing variants. Cell adhesion & migration 3:243–9.

Jégou, A., A. Ziyyat, V. Barraud-Lange, E. Perez, J. P. Wolf, F. Pincet, and C. Gourier. 2011. CD9 tetraspanin generates fusion competent sites on the egg membrane for mammalian fertilization. Proceedings of the National Academy of Sciences of the United States of America 108:10946–51.

Jian, H., G. Yi, X. Jing, S. Wenjiong, Z. Wei, Z. Shuyu, C. Jianping, J. Jiang, Z. Liyuan, T. Ye, J. Huan, Y. Gao, J. Xu, W. Sheng, W. Zhu, S. Zhang, J. Cao, J. Ji, L. Zhang, and Y. Tian. 2015. Overexpression of CD9 correlates with tumor stage and lymph node metastasis in esophageal squamous cell carcinoma. International journal of clinical and experimental pathology 8:3054–61.

Jiang, W., P. Zhou, S. M. Kahn, N. Tomita, M. D. Johnson, and I. B. Weinstein. 1994. Molecular cloning of TPAR1, a gene whose expression is repressed by the tumor promoter 12-O-tetradecanoylphorbol 13-acetate (TPA). Experimental cell research 215:284–93.

Jiang, X., D. Zhang, M. Teng, Q. Zhang, J. Zhang, and Y. Huang. 2013. Downregulation of CD9 in keratinocyte contributes to cell migration via upregulation of matrix metalloproteinase-9. PloS one 8:e77806.

Jiang, X., J. Zhang, and Y. Huang. 2015. Tetraspanins in cell migration. Cell adhesion & migration 9:406–15.

Johnson, S. L., and J. A. Weston. 1995. Temperature-sensitive mutations that cause stage-specific defects in Zebrafish fin regeneration. Genetics 141:1583–95.

Johnston, I. a, H.-T. Lee, D. J. Macqueen, K. Paranthaman, C. Kawashima, A. Anwar, J. R. Kinghorn, and T. Dalmay. 2009. Embryonic temperature affects muscle fibre recruitment in adult zebrafish: genome-wide changes in gene and microRNA expression associated with the transition from hyperplastic to hypertrophic growth phenotypes. The Journal of experimental biology 212:1781–93.

Junge, H. J., S. Yang, J. B. Burton, K. Paes, X. Shu, D. M. French, M. Costa, D. S. Rice, and W. Ye. 2009. TSPAN12 regulates retinal vascular development by promoting Norrin- but not Wnt-induced FZD4/beta-catenin signaling. Cell 139:299–311.

Kaji, K., S. Oda, S. Miyazaki, and A. Kudo. 2002. Infertility of CD9-Deficient Mouse Eggs Is Reversed by Mouse CD9, Human CD9, or Mouse CD81; Polyadenylated mRNA Injection Developed for Molecular Analysis of Sperm–Egg Fusion. Developmental Biology 247:327–334.

Kaji, K., S. Oda, T. Shikano, T. Ohnuki, Y. Uematsu, J. Sakagami, N. Tada, S. Miyazaki, and a Kudo. 2000. The gamete fusion process is defective in eggs of Cd9-deficient mice. Nature genetics 24:279–282.

Kamisasanuki, T., S. Tokushige, H. Terasaki, N. C. Khai, Y. Wang, T. Sakamoto, and K. I. Kosai. 2011. Targeting CD9 produces stimulus-independent antiangiogenic effects predominantly in activated endothelial cells during angiogenesis: A novel antiangiogenic therapy. Biochemical and Biophysical Research Communications 413:128–135.

Kanatsu-Shinohara, M., K. Inoue, S. Takashima, M. Takehashi, N. Ogonuki, H. Morimoto, T. Nagasawa, A. Ogura, and T. Shinohara. 2012. Reconstitution of mouse spermatogonial stem cell niches in culture. Cell stem cell 11:567–78.

Kanatsu-Shinohara, M., S. Toyokuni, and T. Shinohara. 2004. CD9 is a surface marker on mouse and rat male germline stem cells. Biology of reproduction 70:70–5.

Kang, J., G. Nachtrab, and K. D. Poss. 2013. Local Dkk1 crosstalk from breeding ornaments impedes regeneration of injured male zebrafish fins. Developmental cell 27:19–31.

Kaprielian, Z., K. O. Cho, M. Hadjiargyrou, and P. H. Patterson. 1995. CD9, a major platelet cell surface glycoprotein, is a ROCA antigen and is expressed in the nervous system. The Journal of neuroscience : the official journal of the Society for Neuroscience 15:562–73.

Kardash, E., M. Reichman-Fried, J.-L. Maître, B. Boldajipour, E. Papusheva, E.-M. Messerschmidt, C.-P. Heisenberg, and E. Raz. 2010. A role for Rho GTPases and cell-cell adhesion in single-cell motility in vivo. Nature cell biology 12:47–53; sup pp 1–11.

Kersey, J. H., T. W. LeBien, C. S. Abramson, R. Newman, R. Sutherland, and M. Greaves. 1981. P-24: a human leukemia-associated and lymphohemopoietic progenitor cell surface structure identified with monoclonal antibody. The Journal of experimental medicine 153:726–31.

Kierszenbaum, A. L., C. Rosselot, E. Rivkin, and L. L. Tres. 2006. Role of integrins, tetraspanins, and ADAM proteins during the development of apoptotic bodies by spermatogenic cells. Molecular reproduction and development 73:906–17.

Kimmel, C. B., W. W. Ballard, S. R. Kimmel, B. Ullmann, and T. F. Schilling. 1995. Stages of embryonic development of the zebrafish. Developmental dynamics : an official publication of the American Association of Anatomists 203:253–310.

Kischel, P., A. Bellahcene, B. Deux, V. Lamour, R. Dobson, E. DE Pauw, P. Clezardin, and V. Castronovo. 2012. Overexpression of CD9 in human breast cancer cells promotes the development of bone metastases. Anticancer research 32:5211–20.

Kitadokoro, K., D. Bordo, G. Galli, R. Petracca, F. Falugi, S. Abrignani, G. Grandi, and M. Bolognesi. 2001. CD81 extracellular domain 3D structure: insight into the tetraspanin superfamily structural motifs. The EMBO journal 20:12–8.

Knaut, H., C. Werz, R. Geisler, and C. Nüsslein-Volhard. 2003. A zebrafish homologue of the chemokine receptor Cxcr4 is a germ-cell guidance receptor. Nature 421:279–282.

Knobeloch, K.-P., M. D. Wright, A. F. Ochsenbein, O. Liesenfeld, J. Lohler, R. M. Zinkernagel, I. Horak, and Z. Orinska. 2000. Targeted Inactivation of the Tetraspanin CD37 Impairs T-Cell-Dependent B-Cell Response under Suboptimal Costimulatory Conditions. Molecular and Cellular Biology 20:5363–5369.

Kovalenko, O. V, D. G. Metcalf, W. F. DeGrado, and M. E. Hemler. 2005. Structural organization and interactions of transmembrane domains in tetraspanin proteins. BMC structural biology 5:11.

Kovalenko, O. V, X. Yang, T. V Kolesnikova, and M. E. Hemler. 2004. Evidence for specific tetraspanin homodimers: inhibition of palmitoylation makes cysteine residues available for cross-linking. The Biochemical journal 377:407–17.

Kudoh, T., M. Tsang, N. . Hukriede, X. Chen, M. Dedekian, C. . Clarke, A. Kiang, S. Schultz, J. . Epstein, R. Toyama, and I. . Dawid. 2001. A gene expression screen in zebrafish embryogenesis.

Kumar, R., V. Tripathi, M. Ahmad, N. Nath, R. A. Mir, S. S. Chauhan, and K. Luthra. 2012. CXCR7 mediated Gi a independent activation of ERK and Akt promotes cell survival and chemotaxis in T cells. Cellular Immunology 272:230–241.

Kuroda, N., K. Inoue, L. Guo, E. Miyazaki, Y. Hayashi, K. Naruse, M. Toi, M. Hiroi, T. Shuin, and H. Enzan. 2001. Expression of CD9/motility-related protein 1 (MRP-1) in renal parenchymal neoplasms: consistent expression in papillary and chromophobe renal cell carcinomas. Human pathology 32:1071–7.

Lagane, B., K. Y. C. Chow, K. Balabanian, A. Levoye, J. Harriague, T. Planchenault, F. Baleux, N. Gunera-Saad, F. Arenzana-Seisdedos, and F. Bachelerie. 2008. CXCR4 dimerization and beta-arrestin-mediated signaling account for the enhanced chemotaxis to CXCL12 in

WHIM syndrome. Blood 112:34–44.

Lambert, J. G. D., R. van den Hurk, W. G. E. J. Schoonen, J. W. Resink, and P. G. W. J. van Oordt. 1986. Gonadal steroidogenesis and the possible role of steroid glucuronides as sex pheromones in two species of teleosts. Fish Physiology and Biochemistry 2:101 – 107.

Lapalombella, R., Y.-Y. Yeh, L. Wang, A. Ramanunni, S. Rafiq, S. Jha, J. Staubli, D. M. Lucas, R. Mani, S. E. M. Herman, A. J. Johnson, A. Lozanski, L. Andritsos, J. Jones, J. M. Flynn, B. Lannutti, P. Thompson, P. Algate, S. Stromatt, D. Jarjoura, X. Mo, D. Wang, C.-S. Chen, G. Lozanski, N. A. Heerema, S. Tridandapani, M. A. Freitas, N. Muthusamy, and J. C. Byrd. 2012. Tetraspanin CD37 directly mediates transduction of survival and apoptotic signals. Cancer cell 21:694–708.

Latysheva, N., G. Muratov, S. Rajesh, M. Padgett, N. A. Hotchin, M. Overduin, and F. Berditchevski. 2006. Syntenin-1 Is a New Component of Tetraspanin-Enriched Microdomains: Mechanisms and Consequences of the Interaction of Syntenin-1 with CD63. Molecular and Cellular Biology 26:7707–7718.

Ledent, V. 2002. Postembryonic development of the posterior lateral line in zebra sh. Development 604:597–604.

Legault, R. 1958. A technique for Controlling the Time of Daily Spawning and Collecting of Eggs of the Zebrafish. Copeia 1958:328–330.

Leung, K. T., K. Y. Y. Chan, P. C. Ng, T. K. Lau, W. M. Chiu, K. S. Tsang, C. K. Li, C. K. L. Kong, and K. Li. 2011. The tetraspanin CD9 regulates migration, adhesion, and homing of human cord blood CD34+ hematopoietic stem and progenitor cells. Blood 117:1840–50.

Levoye, A., K. Balabanian, F. Baleux, F. Bachelerie, and B. Lagane. 2009. CXCR7 heterodimerizes with CXCR4 and regulates CXCL12-mediated G protein signaling. Blood 113:6085–93.

Lewellis, S. W., D. Nagelberg, A. Subedi, A. Staton, M. Leblanc, and A. Giraldez. 2013. Precise SDF1-mediated cell guidance is achieved through ligand clearance and microRNA-mediated decay. Journal of Cell Biology 200:337–355.

Li, M.-Q., C.-L. Tang, M.-R. Du, D.-X. Fan, H.-B. Zhao, B. Xu, and D.-J. Li. 2011. CXCL12 controls over-invasion of trophoblasts via upregulating CD82 expression in DSCs at maternal-fetal interface of human early pregnancy in a paracrine manner. International journal of clinical and experimental pathology 4:276–286.

Li, Q., K. Shirabe, and J. Y. Kuwada. 2004. Chemokine signaling regulates sensory cell migration in zebrafish. Developmental Biology 269:123–136.

Li, Q., K. Shirabe, C. Thisse, B. Thisse, H. Okamoto, I. Masai, and J. Y. Kuwada. 2005. Chemokine signaling guides axons within the retina in zebrafish. The Journal of neuroscience : the official journal of the Society for Neuroscience 25:1711–7.

Li, X. 2011. Tetraspanin 18 regulates angiogenesis through VEGFR2 nd notch pathways. University of Southern California.

Libert, F., M. Parmentier, A. Lefort, C. Dinsart, J. Van Sande, C. Maenhaut, M. J. Simons, J. E. Dumont, and G. Vassart. 1989. Selective amplification and cloning of four new members of the G protein-coupled receptor family. Science (New York, N.Y.) 244:569–72.

Liedtke, D., I. Erhard, K. Abe, M. Furutani-Seiki, H. Kondoh, and M. Schartl. 2014. Xmrk-induced melanoma progression is affected by Sdf1 signals through Cxcr7. Pigment cell & melanoma research 27:221–33.

Lin, C.-Y., C.-C. Huang, W.-D. Wang, C.-D. Hsiao, C.-F. Cheng, Y.-T. Wu, Y.-F. Lu, and S.-P. L. Hwang. 2013. Low temperature mitigates cardia bifida in zebrafish embryos. PloS one 8:e69788.

Loetscher, M., T. Geiser, T. O'Reilly, R. Zwahlen, M. Baggiolini, and B. Moser. 1994. Cloning of a human seven-transmembrane domain receptor, LESTR, that is highly expressed in leukocytes. The Journal of biological chemistry 269:232–7.

López-Schier, H., and A. J. Hudspeth. 2005. Supernumerary neuromasts in the posterior lateral line of zebrafish lacking peripheral glia. Proceedings of the National Academy of Sciences of the United States of America 102:1496–501.

Lu, M., E. A. Grove, and R. J. Miller. 2002. Abnormal development of the hippocampal dentate gyrus in mice lacking the CXCR4 chemokine receptor. Proceedings of the National Academy of Sciences of the United States of America 99:7090–5.

Luan, C., W. Shen, Z. Yu, L. Chen, Y. Gu, L. Tang, Z. Wang, L. Dai, and M. Gu. 2015. Two nonsense mutations cause protein C deficiency by nonsense-mediated mRNA decay. Thrombosis research 135:733–8.

Ma, E. Y., and D. W. Raible. 2009. Signaling Pathways Regulating Zebrafish Lateral Line Development. Current Biology 19:R381–R386.

Ma, Q., D. Jones, P. R. Borghesani, R. A. Segal, T. Nagasawa, T. Kishimoto, R. T. Bronson, and T. A. Springer. 1998. Impaired B-lymphopoiesis, myelopoiesis, and derailed cerebellar neuron migration in CXCR4- and SDF-1-deficient mice. Proceedings of the National Academy of Sciences of the United States of America 95:9448–53.

Maecker, H. T., S. C. Todd, and S. Levy. 1997. The tetraspanin superfamily: molecular facilitators. The FASEB journal : official publication of the Federation of American Societies for Experimental Biology 11:428–442.

Mahabaleshwar, H., B. Boldajipour, and E. Raz. 2008. Killing the messenger. Cell adhesion & migration 2:69–70.

Mahabaleshwar, H., K. Tarbashevich, M. Nowak, M. Brand, and E. Raz. 2012. β-arrestin control of late endosomal sorting facilitates decoy receptor function and chemokine gradient formation. Development (Cambridge, England) 139:2897–902.

Marchese, A., and J. L. Benovic. 2001. Agonist-promoted ubiquitination of the G protein-coupled receptor CXCR4 mediates lysosomal sorting. The Journal of biological chemistry 276:45509–12.

Marchese, A., C. Raiborg, F. Santini, J. H. Keen, H. Stenmark, and J. L. Benovic. 2003. The E3 ubiquitin ligase AIP4 mediates ubiquitination and sorting of the G protein-coupled receptor CXCR4. Developmental cell 5:709–22.

Matsuda, M., and A. B. Chitnis. 2010. Atoh1a expression must be restricted by Notch signaling for effective morphogenesis of the posterior lateral line primordium in zebrafish. Development (Cambridge, England) 137:3477–87.

Matsuda, M., D. D. Nogare, K. Somers, K. Martin, C. Wang, and A. B. Chitnis. 2013. Lef1 regulates Dusp6 to influence neuromast formation and spacing in the zebrafish posterior lateral line primordium. Development (Cambridge, England) 140:2387–97.

Mazzinghi, B., E. Ronconi, E. Lazzeri, C. Sagrinati, L. Ballerini, M. L. Angelotti, E. Parente, R. Mancina, G. S. Netti, F. Becherucci, M. Gacci, M. Carini, L. Gesualdo, M. Rotondi, E.

Maggi, L. Lasagni, M. Serio, S. Romagnani, and P. Romagnani. 2008. Essential but diff erential role for CXCR4 and CXCR7 in the therapeutic homing of human renal progenitor cells. Journal of Experimental Medicine 205:479–490.

McGraw, H. F., M. D. Culbertson, and A. V Nechiporuk. 2014. Kremen1 restricts Dkk activity during posterior lateral line development in zebrafish. Development (Cambridge, England) 141:3212–21.

McGraw, H. F., C. M. Drerup, M. D. Culbertson, T. Linbo, D. W. Raible, and A. V Nechiporuk. 2011. Lef1 is required for progenitor cell identity in the zebrafish lateral line primordium. Development (Cambridge, England) 138:3921–3930.

Meeker, N. D., S. A. Hutchinson, L. Ho, and N. S. Trede. 2007. Method for isolation of PCR-ready genomic DNA from zebrafish tissues. BioTechniques 43:610, 612, 614.

Meng, Y., J. Shao, H. Li, Y. Hou, C. Tang, M. Du, and M. Li. 2012. CsA improves the trophoblasts invasiveness through strengthening the cross-talk of trophoblasts and de- cidual stromal cells mediated by CXCL12 and CD82 in early pregnancy 5:299–307.

Metcalfe, W. K. 1985. Sensory neuron growth cones comigrate with posterior lateral line primordial cells in zebrafish. The Journal of comparative neurology 238:218–24.

Metcalfe, W. K., C. B. Kimmel, and E. Schabtach. 1985. Anatomy of the posterior lateral line system in young larvae of the zebrafish. The Journal of comparative neurology 233:377–89.

Meyen, D., K. Tarbashevich, T. U. Banisch, C. Wittwer, M. Reichman-Fried, B. Maugis, C. Grimaldi, E.-M. Messerschmidt, and E. Raz. 2015. Dynamic filopodia are required for chemokine-dependent intracellular polarization during guided cell migration in vivo. eLife 4.

Meyer, A., and Y. Van de Peer. 2005. From 2R to 3R: evidence for a fish-specific genome duplication (FSGD). BioEssays : news and reviews in molecular, cellular and developmental biology 27:937–45.

Miao, Z., K. E. Luker, B. C. Summers, R. Berahovich, M. S. Bhojani, A. Rehemtulla, C. G. Kleer, J. J. Essner, A. Nasevicius, G. D. Luker, M. C. Howard, and T. J. Schall. 2007. CXCR7 (RDC1) promotes breast and lung tumor growth in vivo and is expressed on tumor-associated vasculature. Proceedings of the National Academy of Sciences of the United States of America 104:15735–15740.

Miller, B. J. 2000. Normal Fertilization Occurs with Eggs Lacking the Integrin alpha6beta1 and Is CD9-dependent. The Journal of Cell Biology 149:1289–1296.

Miller, J. C., S. Tan, G. Qiao, K. A. Barlow, J. Wang, D. F. Xia, X. Meng, D. E. Paschon, E. Leung, S. J. Hinkley, G. P. Dulay, K. L. Hua, I. Ankoudinova, G. J. Cost, F. D. Urnov, H. S. Zhang, M. C. Holmes, L. Zhang, P. D. Gregory, and E. J. Rebar. 2011. A TALE nuclease architecture for efficient genome editing. Nature biotechnology 29:143–8.

Minina, S., M. Reichman-fried, and E. Raz. 2007. Control of Receptor Internalization, Signaling Level, and Precise Arrival at the Target in Guided Cell Migration. Current Biology 17:1164–1172.

Mitra, S., S. Lukianov, W. G. Ruiz, C. Cianciolo Cosentino, S. Sanker, L. M. Traub, N. A. Hukriede, and G. Apodaca. 2012. Requirement for a uroplakin 3a-like protein in the development of zebrafish pronephric tubule epithelial cell function, morphogenesis, and polarity. PloS one 7:e41816.

Miura, T., and C. I. Miura. 2003. Molecular control mechanisms of fish spermatogenesis. Fish Physiology and Biochemistry 28:181–186.

Miyado, K., G. Yamada, S. Yamada, H. Hasuwa, Y. Nakamura, F. Ryu, K. Suzuki, K. Kosai, K. Inoue, a Ogura, M. Okabe, and E. Mekada. 2000. Requirement of CD9 on the egg plasma membrane for fertilization. Science (New York, N.Y.) 287:321–324.

Miyake, M., K. Nakano, Y. Ieki, M. Adachi, C. L. Huang, S. Itoi, T. Koh, and T. Taki. 1995. Motility related protein 1 (MRP-1/CD9) expression: inverse correlation with metastases in breast cancer. Cancer research 55:4127–4131.

Miyasaka, N., H. Knaut, and Y. Yoshihara. 2007. Cxcl12 / Cxcr4 chemokine signaling is required for placode assembly and sensory axon pathfinding in the zebrafish olfactory system. Development 2468:2459–2468.

Miyazaki, T., U. Müller, and K. S. Campbell. 1997. Normal development but differentially altered proliferative responses of lymphocytes in mice lacking CD81. The EMBO journal 16:4217–25.

Mizoguchi, T., H. Verkade, J. K. Heath, A. Kuroiwa, and Y. Kikuchi. 2008. Sdf1 / Cxcr4 signaling controls the dorsal migration of endodermal cells during zebrafish gastrulation. Development 2529:2521–2529.

Molyneaux, K. A., H. Zinszner, P. S. Kunwar, K. Schaible, J. Stebler, M. J. Sunshine, W. O'Brien, E. Raz, D. Littman, C. Wylie, and R. Lehmann. 2003. The chemokine SDF1/CXCL12 and its receptor CXCR4 regulate mouse germ cell migration and survival. Development (Cambridge, England) 130:4279–86.

Monk, P. N., and L. J. Partridge. 2012. Tetraspanins – Gateways for Infection. Infectious Disorders- Drug Targets.

Moore, F. E., D. Reyon, J. D. Sander, S. A. Martinez, J. S. Blackburn, C. Khayter, C. L. Ramirez, J. K. Joung, and D. M. Langenau. 2012. Improved somatic mutagenesis in zebrafish using transcription activator-like effector nucleases (TALENs). PloS one 7.

Morcos, P. A. 2007. Achieving targeted and quantifiable alteration of mRNA splicing with Morpholino oligos. Biochemical and Biophysical Research Communications 358:521–527.

Mori, M., K. Mimori, T. Shiraishi, M. Haraguchi, H. Ueo, G. F. Barnard, and T. Akiyoshi. 1998. Motility related protein 1 (MRP1/CD9) expression in colon cancer. Clinical cancer research : an official journal of the American Association for Cancer Research 4:1507–10.

Müller, A., B. Homey, H. Soto, N. Ge, D. Catron, M. E. Buchanan, T. McClanahan, E. Murphy, W. Yuan, S. N. Wagner, J. L. Barrera, A. Mohar, E. Verástegui, A. Zlotnik, A. Mu, A. Zlotnik, E. Murphy, W. Yuan, S. N. Wagner, J. Luis, A. Mohar, and E. Vera. 2001. Involvement of chemokine receptors in breast cancer metastasis. Nature 410:50–6.

Murakami, T., W. Maki, A. R. Cardones, H. Fang, A. Tun Kyi, F. O. Nestle, and S. T. Hwang. 2002. Expression of CXC Chemokine Receptor-4 Enhances the Pulmonary Metastatic Potential of Murine B16 Melanoma Cells. Cancer Res. 62:7328–7334.

Murayama, Y., J. Miyagawa, K. Oritani, H. Yoshida, K. Yamamoto, O. Kishida, T. Miyazaki, S. Tsutsui, T. Kiyohara, Y. Miyazaki, S. Higashiyama, Y. Matsuzawa, and Y. Shinomura. 2004. CD9-mediated activation of the p46 Shc isoform leads to apoptosis in cancer cells. Journal of cell science 117:3379–88.

Murayama, Y., Y. Shinomura, K. Oritani, J.-I. Miyagawa, H. Yoshida, M. Nishida, F. Katsube, M.

Shiraga, T. Miyazaki, T. Nakamoto, S. Tsutsui, S. Tamura, S. Higashiyama, I. Shimomura, and N. Hayashi. 2008. The tetraspanin CD9 modulates epidermal growth factor receptor signaling in cancer cells. Journal of cellular physiology 216:135–43.

Nagasawa, T., S. Hirota, K. Tachibana, N. Takakura, S. Nishikawa, Y. Kitamura, N. Yoshida, H. Kikutani, and T. Kishimoto. 1996a. Defects of B-cell lymphopoiesis and bone-marrow myelopoiesis in mice lacking the CXC chemokine PBSF/SDF-1. Nature 382:635–8.

Nagasawa, T., T. Nakajima, K. Tachibana, H. Iizasa, C. C. Bleul, O. Yoshie, K. Matsushima, N. Yoshida, T. A. Springer, and T. Kishimoto. 1996b. Molecular cloning and characterization of a murine pre-B-cell growth-stimulating factor/stromal cell-derived factor 1 receptor, a murine homolog of the human immunodeficiency virus 1 entry coreceptor fusin. Proceedings of the National Academy of Sciences of the United States of America 93:14726–9.

Le Naour, F., E. Rubinstein, C. Jasmin, M. Prenant, and C. Boucheix. 2000. Severely reduced female fertility in CD9-deficient mice. Science (New York, N.Y.) 287:319–321.

Nasevicius, A., and S. C. Ekker. 2000. Effective targeted gene “knockdown” in zebrafish. Nature genetics 26:216–20.

Nasiadka, A., and M. D. Clark. 2012. Zebrafish breeding in the laboratory environment. ILAR journal / National Research Council, Institute of Laboratory Animal Resources 53:161–8.

Naumann, U., E. Cameroni, M. Pruenster, H. Mahabaleshwar, E. Raz, A. Rot, and M. Thelen. 2010. CXCR7 Functions as a Scavenger for CXCL12 and CXCL11. PloS one 5.

Nechiporuk, A., and D. W. Raible. 2008. FGF-dependent mechanosensory organ patterning in zebrafish. Science (New York, N.Y.) 320:1774–7.

Niimi, A. J., and Q. N. LaHam. 1974. Influence of breeding time interval on egg number, mortality, and hatching of the zebra fish Brachydanio rerio. Canadian Journal of Zoology 52:515–517.

Nuñez, V. A., A. F. Sarrazin, N. Cubedo, M. L. Allende, C. Dambly-Chaudière, and A. Ghysen. 2009. Postembryonic development of the posterior lateral line in the zebrafish. Evolution & development 11:391–404.

Oberlin, E., A. Amara, F. Bachelerie, C. Bessia, J. L. Virelizier, F. Arenzana-Seisdedos, O. Schwartz, J. M. Heard, I. Clark-Lewis, D. F. Legler, M. Loetscher, M. Baggiolini, and B. Moser. 1996. The CXC chemokine SDF-1 is the ligand for LESTR/fusin and prevents infection by T-cell-line-adapted HIV-1. Nature 382:833–5.

Odemis, V., K. Boosmann, A. Heinen, P. Küry, and J. Engele. 2010. CXCR7 is an active component of SDF-1 signalling in astrocytes and Schwann cells. Journal of cell science 123:1081–8.

Odemis, V., J. Lipfert, R. Kraft, P. Hajek, G. Abraham, K. Hattermann, R. Mentlein, and J. Engele. 2012. The presumed atypical chemokine receptor CXCR7 signals through G(i/o) proteins in primary rodent astrocytes and human glioma cells. Glia 60:372–81.

Odintsova, E., T. Sugiura, F. Berditchevski, M. Nagira, T. Imai, I. Ishikawa, K.-I. Uwabe, O. Yoshie, J. T. Dong, P. W. Lamb, C. W. Rinker-Schaeffer, J. Vukanovic, T. Ichikawa, J. T. Isaacs, et al., M. Adachi, T. Taki, Y. Ieki, C. L. Huang, M. Higashiyama, M. Miyake, Y. Yu, J. L. Yang, B. Markovic, P. Jackson, G. Yardley, J. Barrett, et al., A. Takaoka, Y. Hinoda, S. Sato, F. Itoh, M. Adachi, M. Hareyama, et al., C. I. Huang, N. Kohno, E. Ogawa, M. Adachi, T. Taki, M. Miyake, M. E. Hemler, B. A. Mannion, F. Berditchevski, H. T. Maecker, S. C.

Todd, S. Levy, T. Sugiura, F. Berditchevski, N. Moghal, P. W. Sternberg, H. Waterman, I. Sabanai, B. Geiger, Y. Yarden, Y. Yarden, J. Schlessinger, T. Wada, X. Qian, M. I. Green, D. J. Riese, T. M. van Raaij, G. D. Plowman, G. C. Andrews, D. F. Stern, C. Mineo, G. L. James, E. J. Smart, R. G. W. Anderson, J. M. Couet, M. Sargiacomo, M. P. Lisanti, C. Mineo, G. N. Gill, R. G. W. Anderson, A. V. Vieira, C. Lamaze, S. L. Schmid, G. Levkowitz, H. Waterman, E. Zamir, Z. Kam, S. Oved, W. Y. Langdon, et al., P. P. Di Fiore, G. N. Gill, S. Levy, S. C. Todd, and H. T. Maecker. 2000. Attenuation of EGF receptor signaling by a metastasis suppressor, the tetraspanin CD82/KAI-1. Current biology : CB 10:1009–12.

Oren, R., S. Takahashi, C. Doss, R. Levy, and S. Levy. 1990. TAPA-1, the target of an antiproliferative antibody, defines a new family of transmembrane proteins. Molecular and cellular biology 10:4007–15.

Ovalle, S., M. D. Gutiérrez-López, N. Olmo, J. Turnay, M. A. Lizarbe, P. Majano, F. Molina-Jiménez, M. López-Cabrera, M. Yáñez-Mó, F. Sánchez-Madrid, and C. Cabañas. 2007. The tetraspanin CD9 inhibits the proliferation and tumorigenicity of human colon carcinoma cells. International Journal of Cancer 121:2140–2152.

Paksa, A., and E. Raz. 2015. Zebrafish germ cells: motility and guided migration. Current opinion in cell biology 36:80–5.

Palevitch, O., E. Abraham, N. Borodovsky, G. Levkowitz, Y. Zohar, and Y. Gothilf. 2010. Cxcl12a – Cxcr4b signaling is important for proper development of the forebrain GnRH system in zebrafish. General and Comparative Endocrinology 165:262–268.

Parichy, D. M., J. M. Turner, and N. B. Parker. 2003. Essential role for puma in development of postembryonic neural crest-derived cell lineages in zebrafish. Developmental Biology 256:221–241.

Paull, G. C., K. J. W. Van Look, E. M. Santos, A. L. Filby, D. M. Gray, J. P. Nash, and C. R. Tyler. 2008. Variability in measures of reproductive success in laboratory-kept colonies of zebrafish and implications for studies addressing population-level effects of environmental chemicals. Aquatic toxicology (Amsterdam, Netherlands) 87:115–26.

Pawig, L., C. Klasen, C. Weber, J. Bernhagen, and H. Noels. 2015. Diversity and Inter-Connections in the CXCR4 Chemokine Receptor/Ligand Family: Molecular Perspectives. Frontiers in immunology 6:429.

Pei, W., P. H. Williams, M. D. Clark, D. L. Stemple, and B. Feldman. 2007. Environmental and genetic modifiers of squint penetrance during zebrafish embryogenesis. Developmental biology 308:368–78.

Pols, M. S., and J. Klumperman. 2009. Trafficking and function of the tetraspanin CD63. Experimental Cell Research 315:1584–1592.

Poss, K. D., A. Nechiporuk, A. M. Hillam, S. L. Johnson, and M. T. Keating. 2002. Mps1 defines a proximal blastemal proliferative compartment essential for zebrafish fin regeneration. Development 129:5141–5149.

Powner, D., P. M. Kopp, S. J. Monkley, D. R. Critchley, and F. Berditchevski. 2011. Tetraspanin CD9 in cell migration. Biochemical Society transactions 39:563–7.

Pujic, Z., Y. Omori, M. Tsujikawa, B. Thisse, C. Thisse, and J. Malicki. 2006. Reverse genetic analysis of neurogenesis in the zebrafish retina. Developmental biology 293:330–47.

Rajagopal, S., J. Kim, S. Ahn, S. Craig, C. M. Lam, and N. P. Gerard. 2010. β -arrestin- but not G protein-mediated signaling by the " decoy " receptor CXCR7 107:628–632.

Rappa, G., T. M. Green, J. Karbanová, D. Corbeil, and A. Lorico. 2015. Tetraspanin CD9 determines invasiveness and tumorigenicity of human breast cancer cells. Oncotarget 6:7970–91.

Rauch, G.-J., D. . Lyons, I. Middendorf, B. Friedlander, N. Arana, T. Reyes, and W. . Talbot. 2003. Submission and curation of Gene expression data.

Raz, E., and M. Reichman-Fried. 2006. Attraction rules: germ cell migration in zebrafish. Current opinion in genetics & development 16:355–9.

Reichman-Fried, M., S. Minina, and E. Raz. 2004. Autonomous Modes of Behavior in Primordial Germ Cell Migration. Developmental Cell 6:589–596.

Rimland, J., W. Xin, P. Sweetnam, K. Saijoh, E. Nestler, and R. Duman. 1991. Sequence and expression of a neuropeptide Y receptor cDNA. Mol. Pharmacol. 40:869–875.

Robu, M. E., J. D. Larson, A. Nasevicius, S. Beiraghi, C. Brenner, S. A. Farber, and S. C. Ekker. 2007. p53 activation by knockdown technologies. PLoS genetics 3:e78.

Rocha-Perugini, V., F. Sánchez-Madrid, and G. Martínez Del Hoyo. 2015. Function and Dynamics of Tetraspanins during Antigen Recognition and Immunological Synapse Formation. Frontiers in immunology 6:653.

Roman-Sanchez, R., T. G. Wensel, and J. H. Wilson. 2015. Nonsense mutations in the rhodopsin gene that give rise to mild phenotypes trigger mRNA degradation in human cells by nonsense-mediated decay. Experimental eye research.

Rossi, A., Z. Kontarakis, C. Gerri, H. Nolte, S. Hölper, M. Krüger, and D. Y. R. Stainier. 2015. Genetic compensation induced by deleterious mutations but not gene knockdowns. Nature 524:230–233.

Rubinstein, E., F. Le Naour, C. Lagaudrière-Gesbert, M. Billard, H. Conjeaud, and C. Boucheix. 1996a. CD9, CD63, CD81, and CD82 are components of a surface tetraspan network connected to HLA-DR and VLA integrins. European Journal of Immunology 26:2657–2665.

Rubinstein, E., F. Le Naour, C. Lagaudrière-Gesbert, M. Billard, H. Conjeaud, and C. Boucheix. 1996b. CD9, CD63, CD81, and CD82 are components of a surface tetraspan network connected to HLA-DR and VLA integrins. European journal of immunology 26:2657–65.

Runge, K. E., J. E. Evans, Z.-Y. He, S. Gupta, K. L. McDonald, H. Stahlberg, P. Primakoff, and D. G. Myles. 2007. Oocyte CD9 is enriched on the microvillar membrane and required for normal microvillar shape and distribution. Developmental biology 304:317–25.

Saini, V., A. Marchese, and M. Majetschak. 2010. CXC chemokine receptor 4 is a cell surface receptor for extracellular ubiquitin. The Journal of biological chemistry 285:15566–76.

Sala-Valdes, M., Á. Ursa, S. Charrin, E. Rubinstein, M. E. Hemler, F. Sánchez-Madrid, and M. Yáñez-Mó. 2006. EWI-2 and EWI-F Link the Tetraspanin Web to the Actin Cytoskeleton through Their Direct Association with Ezrin-Radixin-Moesin Proteins. Journal of Biological Chemistry 281:19665–19675.

Samson, J. C., and J. Shenker. 2000. The teratogenic effects of methylmercury on early development of the zebrafish, Danio rerio. Aquatic Toxicology 48:343–354.

Sánchez-Alcañiz, J. A., S. Haege, W. Mueller, R. Pla, F. Mackay, S. Schulz, G. López-Bendito, R. Stumm, and O. Marín. 2011. Cxcr7 controls neuronal migration by regulating chemokine responsiveness. Neuron 69:77–90.

Sander, J. D., L. Cade, C. Khayter, D. Reyon, R. T. Peterson, J. K. Joung, and J. J. Yeh. 2011. Targeted gene disruption in somatic zebrafish cells using engineered TALENs. Nature Publishing Group 29:697–698.

Sapede, D., N. Gompel, C. Dambly-Chaudiere, and A. Ghysen. 2002. Cell migration in the postembryonic development of the fish lateral line. Development 129:605–615.

Sarrazin, A. F., V. A. Nunez, D. Sapede, V. Tassin, C. Dambly-Chaudiere, A. Ghysen, V. A. Nuñez, D. Sapède, V. Tassin, C. Dambly-Chaudière, and A. Ghysen. 2010. Origin and Early Development of the Posterior Lateral Line System of Zebrafish. The Journal of neuroscience : the official journal of the Society for Neuroscience 30:8234–44.

Saslowsky, D. E., J. A. Cho, H. Chinnapen, R. H. Massol, D. J.-F. Chinnapen, J. S. Wagner, H. E. De Luca, W. Kam, B. H. Paw, and W. I. Lencer. 2010. Intoxication of zebrafish and mammalian cells by cholera toxin depends on the flotillin/reggie proteins but not Derlin-1 or -2. The Journal of clinical investigation 120:4399–4409.

Satouh, Y., N. Inoue, M. Ikawa, and M. Okabe. 2012. Visualization of the moment of mouse sperm-egg fusion and dynamic localization of IZUMO1. Journal of cell science 125:4985–90.

Saur, D., B. Seidler, G. Schneider, H. Algül, R. Beck, R. Senekowitsch-Schmidtke, M. Schwaiger, and R. M. Schmid. 2005. CXCR4 expression increases liver and lung metastasis in a mouse model of pancreatic cancer. Gastroenterology 129:1237–1250.

Schindelin, J., I. Arganda-Carreras, E. Frise, V. Kaynig, M. Longair, T. Pietzsch, S. Preibisch, C. Rueden, S. Saalfeld, B. Schmid, J.-Y. Tinevez, D. J. White, V. Hartenstein, K. Eliceiri, P. Tomancak, and A. Cardona. 2012. Fiji: an open-source platform for biological-image analysis. Nature methods 9:676–82.

Schneider, C. A., W. S. Rasband, and K. W. Eliceiri. 2012. NIH Image to ImageJ: 25 years of image analysis. Nature methods 9:671–5.

Seigneuret, M., A. Delaguillaumie, C. Lagaudrière-Gesbert, and H. Conjeaud. 2001. Structure of the tetraspanin main extracellular domain. A partially conserved fold with a structurally variable domain insertion. The Journal of biological chemistry 276:40055–64.

Serru, V., F. Le Naour, M. Billard, D. Azorsa, F. Lanza, C. Boucheix, and E. Rubinstein. 1999. Selective tetraspan-integrin complexes (CD81/alpha4beta1, CD151/alpha3beta1, CD151/alpha6beta1) under conditions disrupting tetraspan interactions. The Biochemical journal 340:103–111.

Sethi, T., R. C. Rintoul, S. M. Moore, A. C. MacKinnon, D. Salter, C. Choo, E. R. Chilvers, I. Dransfield, S. C. Donnelly, R. Strieter, and C. Haslett. 1999. Extracellular matrix proteins protect small cell lung cancer cells againstapoptosis: A mechanism for small cell lung cancer growth and drug resistance in vivo. Nature Medicine 5:662–668.

Sheikh-Hamad, D., J. D. Ferraris, J. Dragolovich, H. G. Preuss, M. B. Burg, and A. Garcia-Perez. 1996. CD9 antigen mRNA is induced by hypertonicity in two renal epithelial cell lines. Am J Physiol Cell Physiol 270:C253–258.

Sheikh-Hamad, D., K. Youker, L. D. Truong, S. Nielsen, and M. L. Entman. 2000. Osmotically relevant membrane signaling complex: association between HB-EGF, beta 1-integrin, and CD9 in mTAL. Am J Physiol Cell Physiol 279:C136–146.

Shi, W., H. Fan, L. Shum, and R. Derynck. 2000. The Tetraspanin Cd9 Associates with Transmembrane TGF-α and Regulates TGF-α–Induced Egf Receptor Activation and Cell

Proliferation. The Journal of Cell Biology 148:591–602.

Shirozu, M., T. Nakano, J. Inazawa, K. Tashiro, H. Tada, T. Shinohara, and T. Honjo. 1995. Structure and chromosomal localization of the human stromal cell-derived factor 1 (SDF1) gene. Genomics 28:495–500.

Shoham, T., R. Rajapaksa, C.-C. Kuo, J. Haimovich, and S. Levy. 2006. Building of the tetraspanin web: distinct structural domains of CD81 function in different cellular compartments. Molecular and cellular biology 26:1373–85.

Si, Z., and P. Hersey. 1993. Expression of the neuroglandular antigen and analogues in melanoma. CD9 expression appears inversely related to metastatic potential of melanoma. International Journal of Cancer 54:37–43.

Siekmann, A. F., C. Standley, K. E. Fogarty, S. A. Wolfe, and N. D. Lawson. 2009. Chemokine signaling guides regional patterning of the first embryonic artery. Genes & development 23:2272–7.

Sierro, F., C. Biben, L. Martı, B. Woehl, H. Leung, J. Groom, M. Batten, R. P. Harvey, C. Martı, C. R. Mackay, F. Mackay, L. Martínez-Muñoz, M. Mellado, R. M. Ransohoff, M. Li, B. Woehl, H. Leung, J. Groom, M. Batten, R. P. Harvey, C. Martínez-A, C. R. Mackay, and F. Mackay. 2007. Disrupted cardiac development but normal hematopoiesis in mice deficient in the second CXCL12/SDF-1 receptor, CXCR7. Proceedings of the National Academy of Sciences of the United States of America 104:14759–64.

Sincock, P. M., G. Mayrhofer, and L. K. Ashman. 1997. Localization of the Transmembrane 4 Superfamily (TM4SF) Member PETA-3 (CD151) in Normal Human Tissues: Comparison with CD9, CD63, and 5 1 Integrin. Journal of Histochemistry & Cytochemistry 45:515–525.

Singh, S., U. P. Singh, W. E. Grizzle, and J. W. Lillard. 2004. CXCL12-CXCR4 interactions modulate prostate cancer cell migration, metalloproteinase expression and invasion. Laboratory investigation; a journal of technical methods and pathology 84:1666–76.

Skinner, A. M. J., and P. J. Watt. 2007. Strategic egg allocation in the zebra fish, Danio rerio. Behavioral Ecology 18:905–909.

Staton, A. A., H. Knaut, and A. J. Giraldez. 2011. miRNA regulation of Sdf1 chemokine signaling provides genetic robustness to germ cell migration. Nature Publishing Group 43:204–211.

Staton, A. A., H. Knaut, and A. J. Giraldez. 2013. Reply to: “On the robustness of germ cell migration and microRNA-mediated regulation of chemokine signaling.” Nature Publishing Group 45:1266–1267.

Steiner, A. B., T. Kim, V. Cabot, and A. J. Hudspeth. 2014. Dynamic gene expression by putative hair-cell progenitors during regeneration in the zebrafish lateral line. Proceedings of the National Academy of Sciences of the United States of America 111:E1393–401.

Stipp, C. S., T. V. Kolesnikova, and M. E. Hemler. 2003. Functional domains in tetraspanin proteins. Trends in Biochemical Sciences 28:106–112.

Stumm, R. K., C. Zhou, T. Ara, F. Lazarini, M. Dubois-Dalcq, T. Nagasawa, V. Höllt, and S. Schulz. 2003. CXCR4 regulates interneuron migration in the developing neocortex. The Journal of neuroscience : the official journal of the Society for Neuroscience 23:5123–30.

Suli, A., G. M. Watson, E. W. Rubel, and D. W. Raible. 2012. Rheotaxis in larval zebrafish is mediated by lateral line mechanosensory hair cells. PloS one 7:e29727.

Sumanas, S., and J. D. Larson. 2002. Morpholino phosphorodiamidate oligonucleotides in zebrafish: a recipe for functional genomics? Briefings in functional genomics & proteomics 1:239–56.

Summerton, J., and D. Weller. 1997. Morpholino Antisense Oligomers: Design, Preparation and Properties. Antisense & nucleic acid drug development 7:187–195.

Szala, S., Y. Kasai, Z. Steplewski, U. Rodeck, H. Koprowski, and A. J. Linnenbach. 1990, September 1. Molecular cloning of cDNA for the human tumor-associated antigen CO-029 and identification of related transmembrane antigens. National Academy of Sciences.

Tachibana, K., S. Hirota, H. Iizasa, H. Yoshida, K. Kawabata, Y. Kataoka, Y. Kitamura, K. Matsushima, N. Yoshida, S. Nishikawa, T. Kishimoto, and T. Nagasawa. 1998. The chemokine receptor CXCR4 is essential for vascularization of the gastrointestinal tract. Nature 393:591–4.

Takashima, S., M. Kanatsu-Shinohara, T. Tanaka, M. Takehashi, H. Morimoto, and T. Shinohara. 2011. Rac mediates mouse spermatogonial stem cell homing to germline niches by regulating transmigration through the blood-testis barrier. Cell stem cell 9:463–75.

Takeda, Y., P. He, I. Tachibana, B. Zhou, K. Miyado, H. Kaneko, M. Suzuki, S. Minami, T. Iwasaki, S. Goya, T. Kijima, T. Kumagai, M. Yoshida, T. Osaki, T. Komori, E. Mekada, and I. Kawase. 2008. Double deficiency of tetraspanins CD9 and CD81 alters cell motility and protease production of macrophages and causes chronic obstructive pulmonary disease-like phenotype in mice. The Journal of biological chemistry 283:26089–97.

Takeda, Y., A. R. Kazarov, C. E. Butterfield, B. D. Hopkins, L. E. Benjamin, A. Kaipainen, and M. E. Hemler. 2007. Deletion of tetraspanin Cd151 results in decreased pathologic angiogenesis in vivo and in vitro. Blood 109:1835–1842.

Takeda, Y., I. Tachibana, K. Miyado, M. Kobayashi, T. Miyazaki, T. Funakoshi, H. Kimura, H. Yamane, Y. Saito, H. Goto, T. Yoneda, M. Yoshida, T. Kumagai, T. Osaki, S. Hayashi, I. Kawase, and E. Mekada. 2003. Tetraspanins CD9 and CD81 function to prevent the fusion of mononuclear phagocytes. The Journal of cell biology 161:945–56.

Takemura, T., S. Hino, Y. Murata, H. Yanagida, M. Okada, K. Yoshioka, and R. C. Harris. 1999. Coexpression of CD9 augments the ability of membrane-bound heparin-binding epidermal growth factor-like growth factor (proHB-EGF) to preserve renal epithelial cell viability. Kidney international 55:71–81.

Tan, W., D. Martin, and J. S. Gutkind. 2006. The Galpha13-Rho signaling axis is required for SDF-1-induced migration through CXCR4. The Journal of biological chemistry 281:39542–9.

Tang, R., A. Dodd, D. Lai, W. C. Mcnabb, and D. R. Love. 2007. Validation of Zebrafish (Danio rerio) Reference Genes for Quantitative Real-time RT-PCR Normalization. Acta Biochimica et Biophysica Sinica 39:384–390.

Tarasova, N. I., R. H. Stauber, and C. J. Michejda. 1998. Spontaneous and Ligand-induced Trafficking of CXC-Chemokine:15883–15886.

Tarbashevich, K., M. Reichman-Fried, C. Grimaldi, and E. Raz. 2015. Chemokine-Dependent pH Elevation at the Cell Front Sustains Polarity in Directionally Migrating Zebrafish Germ Cells. Current biology : CB 25:1096–103.

Tashiro, K., H. Tada, R. Heilker, M. Shirozu, T. Nakano, and T. Honjo. 1993. Signal sequence trap: a cloning strategy for secreted proteins and type I membrane proteins. Science

(New York, N.Y.) 261:600–3.

Teicher, B. A., and S. P. Fricker. 2010. CXCL12 (SDF-1)/CXCR4 pathway in cancer. Clinical cancer research : an official journal of the American Association for Cancer Research 16:2927–31.

Tejera, E., V. Rocha-Perugini, S. Lopez-Martin, D. Perez-Hernandez, A. I. Bachir, A. R. Horwitz, J. Vazquez, F. Sanchez-Madrid, and M. Yanez-Mo. 2013. CD81 regulates cell migration through its association with Rac GTPase. Molecular Biology of the Cell 24:261–273.

Thisse, B., S. Pflumio, M. Furthauer, B. Loppin, V. Heyer, A. Degrave, R. Woehl, A. Lux, T. Steffan, X. Q. Charbonnier, and C. Thisse. 2001. Expression of the zebrafish genome during embryogenesis. http://zfin.org/cgi-bin/webdriver?MIval=aa-pubprintable.apg&OID=ZDB-PUB-010810-1&printable=yes.

Thisse, B., and C. Thisse. 2004. Fast release clones: A high throughput expression analysis. http://zfin.org/ZDB-PUB-040907-1.

Thisse, C., and B. Thisse. 2008. High-resolution in situ hybridization to whole-mount zebrafish embryos. Nature protocols 3:59–69.

Trikić, M. Z., P. Monk, H. Roehl, and L. J. Partridge. 2011. Regulation of zebrafish hatching by tetraspanin cd63. PLoS ONE 6.

Uusi-Heikkilä, S., C. Wolter, T. Meinelt, and R. Arlinghaus. 2010. Size-dependent reproductive success of wild zebrafish Danio rerio in the laboratory. Journal of fish biology 77:552–69.

Valdivia, L. E., R. M. Young, T. a Hawkins, H. L. Stickney, F. Cavodeassi, Q. Schwarz, L. M. Pullin, R. Villegas, E. Moro, F. Argenton, M. L. Allende, and S. W. Wilson. 2011. Lef1-dependent Wnt/{beta}-catenin signalling drives the proliferative engine that maintains tissue homeostasis during lateral line development. Development (Cambridge, England) 138:3931–3941.

Valentin, G., P. Haas, and D. Gilmour. 2007. The Chemokine SDF1a Coordinates Tissue Migration through the Spatially Restricted Activation of Cxcr7 and Cxcr4b. Current Biology 17:1026–1031.

Vasyutina, E., J. Stebler, B. Brand-saberi, S. Schulz, E. Raz, and C. Birchmeier. 2005. CXCR4 and Gab1 cooperate to control the development of migrating muscle progenitor cells. Genes & development:2187–2198.

Venkiteswaran, G., S. W. Lewellis, J. Wang, E. Reynolds, and C. Nicholson. 2013. Generation and Dynamics of an Endogenous , Self-Generated Signaling Gradient across a Migrating Tissue. Cell 155:674–687.

Vila-Coro, A. J., J. M. Rodríguez-Frade, A. Martín De Ana, M. C. Moreno-Ortíz, C. Martínez-A, and M. Mellado. 1999. The chemokine SDF-1alpha triggers CXCR4 receptor dimerization and activates the JAK/STAT pathway. FASEB journal : official publication of the Federation of American Societies for Experimental Biology 13:1699–710.

Walters, K. B., J. M. Green, J. C. Surfus, S. K. Yoo, and A. Huttenlocher. 2010. Live imaging of neutrophil motility in a zebrafish model of WHIM syndrome. Blood 116:2803–11.

Wang, H., N. Beaty, S. Chen, C. Qi, M. Masiuk, D. Shin, H. C. M. Iii, and W. Dc. 2012. The CXCR7 chemokine receptor promotes B-cell retention in the splenic marginal zone and serves as a sink for CXCL12 Brief report The CXCR7 chemokine receptor promotes B-cell retention in the splenic marginal zone and serves as a sink for CXCL12. Blood:465–468.

Wang, H.-X., T. V Kolesnikova, C. Denison, S. P. Gygi, and M. E. Hemler. 2011a. The C-terminal tail of tetraspanin protein CD9 contributes to its function and molecular organization. Journal of cell science 124:2702–10.

Wang, Y., G. Li, A. Stanco, J. E. Long, D. Crawford, G. B. Potter, S. J. Pleasure, T. Behrens, and J. L. R. Rubenstein. 2011b. CXCR4 and CXCR7 have distinct functions in regulating interneuron migration. Neuron 69:61–76.

Weidinger, G., J. Stebler, K. Slanchev, K. Dumstrei, C. Wise, R. Lovell-Badge, C. Thisse, B. Thisse, and E. Raz. 2003. dead end, a Novel Vertebrate Germ Plasm Component, Is Required for Zebrafish Primordial Germ Cell Migration and Survival. Current Biology 13:1429–1434.

Weidinger, G., U. Wolke, M. Köprunner, M. Klinger, and E. Raz. 1999. Identification of tissues and patterning events required for distinct steps in early migration of zebrafish primordial germ cells. Development (Cambridge, England) 126:5295–5307.

Weidinger, G., U. Wolke, M. Köprunner, C. Thisse, B. Thisse, E. Raz, M. Koprunner, C. Thisse, B. Thisse, and E. Raz. 2002. Regulation of zebrafish primordial germ cell migration by attraction towards an intermediate target. Development (Cambridge, England) 129:25–36.

Westernströer, B., N. Terwort, J. Ehmcke, J. Wistuba, S. Schlatt, and N. Neuhaus. 2014. Profiling of Cxcl12 receptors, Cxcr4 and Cxcr7 in murine testis development and a spermatogenic depletion model indicates a role for Cxcr7 in controlling Cxcl12 activity. PloS one 9:e112598.

Wetzler, M., M. Talpaz, E. S. Kleinerman, A. King, Y. O. Huh, J. U. Gutterman, and R. Kurzrock. 1990. A new familial immunodeficiency disorder characterized by severe neutropenia, a defective marrow release mechanism, and hypogammaglobulinemia. The American Journal of Medicine 89:663–672.

Wright, M. D., S. M. Geary, S. Fitter, G. W. Moseley, L.-M. Lau, K.-C. Sheng, V. Apostolopoulos, E. G. Stanley, D. E. Jackson, and L. K. Ashman. 2004. Characterization of mice lacking the tetraspanin superfamily member CD151. Molecular and cellular biology 24:5978–88.

Wright, M. D., and M. G. Tomlinson. 1994. The ins and outs of the transmembrane 4 superfamily. Immunology today 15:588–94.

Xing, C., B. Gong, Y. Xue, Y. Han, Y. Wang, A. Meng, and S. Jia. 2015. TGFβ1a regulates zebrafish posterior lateral line formation via Smad5 mediated pathway. Journal of molecular cell biology 7:48–61.

Xu, H., E. Kardash, S. Chen, E. Raz, and F. Lin. 2012. Gβγ signaling controls the polarization of zebrafish primordial germ cells by regulating Rac activity. Development (Cambridge, England) 139:57–62.

Xuan, H., X. Hu, and J. Huang. 2014. Role of motility-related protein-1 in promoting the development of several types of cancer (Review). Oncology letters 7:611–615.

Xue, B., W. Wu, K. Huang, T. Xie, X. Xu, H. Zhang, C. Qi, J. Ge, and Y. Yu. 2013. Stromal cell-derived factor-1 (SDF-1) enhances cells invasion by αvβ6 integrin-mediated signaling in ovarian cancer. Molecular and cellular biochemistry 380:177–84.

Yamada, M., Y. Sumida, A. Fujibayashi, K. Fukaguchi, N. Sanzen, R. Nishiuchi, and K. Sekiguchi. 2008. The tetraspanin CD151 regulates cell morphology and intracellular signaling on laminin-511. The FEBS journal 275:3335–51.

Yamazaki, H., C. W. Xu, M. Naito, H. Nishida, T. Okamoto, F. I. Ghani, S. Iwata, T. Inukai, K. Sugita, and C. Morimoto. 2011. Regulation of cancer stem cell properties by CD9 in human B-acute lymphoblastic leukemia. Biochemical and biophysical research communications 409:14–21.

Yáñez-Mó, M., O. Barreiro, M. Gordon-Alonso, M. Sala-Valdés, and F. Sánchez-Madrid. 2009. Tetraspanin-enriched microdomains: a functional unit in cell plasma membranes. Trends in cell biology 19:434–46.

Yanez-Mo, M., R. Tejedor, P. Rousselle, and F. Sanchez -Madrid. 2001. Tetraspanins in intercellular adhesion of polarized epithelial cells: spatial and functional relationship to integrins and cadherins. J. Cell Sci. 114:577–587.

Yang, D., Q. Liu, M. Yang, H. Wu, Q. Wang, J. Xiao, and Y. Zhang. 2012. RNA-seq liver transcriptome analysis reveals an activated MHC-I pathway and an inhibited MHC-II pathway at the early stage of vaccine immunization in zebrafish. BMC genomics 13:319.

Yang, Q.-E., D. Kim, A. Kaucher, M. J. Oatley, and J. M. Oatley. 2013. CXCL12-CXCR4 signaling is required for the maintenance of mouse spermatogonial stem cells. Journal of cell science 126:1009–20.

Yang, X., C. Claas, S.-K. Kraeft, L. B. Chen, Z. Wang, J. A. Kreidberg, and M. E. Hemler. 2002. Palmitoylation of tetraspanin proteins: modulation of CD151 lateral interactions, subcellular distribution, and integrin-dependent cell morphology. Molecular biology of the cell 13:767–81.

Yang, X. H., A. L. Richardson, M. I. Torres-Arzayus, P. Zhou, C. Sharma, A. R. Kazarov, M. M. Andzelm, J. L. Strominger, M. Brown, and M. E. Hemler. 2008. CD151 accelerates breast cancer by regulating alpha 6 integrin function, signaling, and molecular organization. Cancer research 68:3204–13.

Yang, Y.-G., I. N. Sari, M. F. Zia, S. R. Lee, S. J. Song, and H. Y. Kwon. 2016. Tetraspanins: Spanning from Solid Tumors to Hematologic Malignancies. Experimental hematology.

Yauch, R. L., F. Berditchevski, M. B. Harler, J. Reichner, and M. E. Hemler. 1998. Highly Stoichiometric, Stable, and Specific Association of Integrin alpha 3beta 1 with CD151 Provides a Major Link to Phosphatidylinositol 4-Kinase, and May Regulate Cell Migration. Molecular Biology of the Cell 9:2751–2765.

Yoon, C., K. Kawakami, and N. Hopkins. 1997. Zebrafish vasa homologue RNA is localized to the cleavage planes of 2- and 4-cell-stage embryos and is expressed in the primordial germ cells. Development (Cambridge, England) 124:3157–3165.

Yoshida, N., D. Kitayama, M. Arima, A. Sakamoto, A. Inamine, H. Watanabe-Takano, M. Hatano, T. Koike, and T. Tokuhisa. 2011. CXCR4 expression on activated B cells is downregulated by CD63 and IL-21. Journal of immunology (Baltimore, Md. : 1950) 186:2800–2808.

Yoshida, T., H. Ebina, and Y. Koyanagi. 2009. N-linked glycan-dependent interaction of CD63 with CXCR4 at the Golgi apparatus induces downregulation of CXCR4. Microbiology and immunology 53:629–635.

Yoshida, T., Y. Kawano, K. Sato, Y. Ando, J. Aoki, Y. Miura, J. Komano, Y. Tanaka, and Y. Koyanagi. 2008. A CD63 mutant inhibits T-cell tropic human immunodeficiency virus type 1 entry by disrupting CXCR4 trafficking to the plasma membrane. Traffic (Copenhagen, Denmark) 9:540–558.

Yu, F., C. C. Broder, P. E. Kennedy, and E. A. Berger. 1996. HIV-1 entry cofactor: Functional

cDNA clining of a seven-transmembrane, G protein-coupled receptor. Science (New York, N.Y.).

Yu, L., J. Cecil, S.-B. Peng, J. Schrementi, S. Kovacevic, D. Paul, E. W. Su, and J. Wang. 2006. Identification and expression of novel isoforms of human stromal cell-derived factor 1. Gene 374:174–9.

Yuan, G., Y. Wang, X. Yuan, T. Zhang, J. Zhao, L. Huang, and S. Peng. 2014. T-2 toxin induces developmental toxicity and apoptosis in zebrafish embryos. Journal of environmental sciences (China) 26:917–25.

Zabel, B. A., Y. Wang, S. Lewén, R. D. Berahovich, M. E. T. Penfold, P. Zhang, J. Powers, B. C. Summers, Z. Miao, B. Zhao, A. Jalili, A. Janowska-Wieczorek, J. C. Jaen, and T. J. Schall. 2009. Elucidation of CXCR7-mediated signaling events and inhibition of CXCR4-mediated tumor cell transendothelial migration by CXCR7 ligands. Journal of immunology (Baltimore, Md. : 1950) 183:3204–11.

Zeelenberg, I. S., L. Ruuls-Van Stalle, and E. Roos. 2001. Retention of CXCR4 in the endoplasmic reticulum blocks dissemination of a T cell hybridoma. The Journal of clinical investigation 108:269–77.

Zeelenberg, I. S., L. Ruuls-Van Stalle, and E. Roos. 2003. The Chemokine Receptor CXCR4 Is Required for Outgrowth of Colon Carcinoma Micrometastases. Cancer Res. 63:3833–3839.

Zhang, F., L. Cong, S. Lodato, S. Kosuri, G. M. Church, and P. Arlotta. 2011. Efficient construction of sequence-specific TAL effectors for modulating mammalian transcription. Nature biotechnology 29:149–53.

Zhang, F., J. Kotha, L. K. Jennings, and X. A. Zhang. 2009. Tetraspanins and vascular functions. Cardiovascular research 83:7–15.

Zhang, J., J. Dong, H. Gu, S. Yu, X. Zhang, Y. Gou, W. Xu, A. Burd, L. Huang, K. Miyado, Y. Huang, and H. C. Chan. 2012. CD9 is critical for cutaneous wound healing through JNK signaling. The Journal of investigative dermatology 132:226–36.

Zhang, X. A., A. L. Bontrager, and M. E. Hemler. 2001. Transmembrane-4 superfamily proteins associate with activated protein kinase C (PKC) and link PKC to specific beta(1) integrins. The Journal of biological chemistry 276:25005–13.

Zhu, G.-Z., B. J. Miller, C. Boucheix, E. Rubinstein, C. C. Liu, R. O. Hynes, D. G. Myles, and P. Primakoff. 2002. Residues SFQ (173-175) in the large extracellular loop of CD9 are required for gamete fusion. Development 129:1995–2002.

Ziyyat, A., E. Rubinstein, F. Monier-Gavelle, V. Barraud, O. Kulski, M. Prenant, C. Boucheix, M. Bomsel, and J.-P. Wolf. 2006. CD9 controls the formation of clusters that contain tetraspanins and the integrin alpha 6 beta 1, which are involved in human and mouse gamete fusion. Journal of cell science 119:416–24.

Zou, Y. R., A. H. Kottmann, M. Kuroda, I. Taniuchi, and D. R. Littman. 1998. Function of the chemokine receptor CXCR4 in haematopoiesis and in cerebellar development. Nature 393:595–9.

Zuidscherwoude, M., F. Göttfert, V. M. E. Dunlock, C. G. Figdor, G. van den Bogaart, and A. B. van Spriel. 2015. The tetraspanin web revisited by super-resolution microscopy. Scientific reports 5:12201.

Zyłkiewicz, E., J. Nowakowska, and M. Maleszewski. 2010. Decrease in CD9 content and reorganization of microvilli may contribute to the oolemma block to sperm penetration during fertilization of mouse oocyte. Zygote (Cambridge, England) 18:195–201.

Acknowledgments

Firstly, I would like to acknowledge and express my gratitude to the Department of Biomedical Science at the University of Sheffield for giving me the funding and opportunity to carry out this research.

For their continued support and advice I would like to thank my supervisors Dr. Peter Monk, Dr. Lynda Partridge and Dr. Henry Roehl.

Besides my supervisors, I thank my advisors Dr. Vincent Cunliffe and Dr. Andrew Peden for their encouragement and constructive comments on my work.

To my lab colleagues, both past and present, thank you for sharing your expertise with me and helping me develop into the researcher I am today. In particular, thank you to Kunal Chopra for your assistance in creating my CD9b mutant lines and to Katherine Marsay for your determined help with the extremely exasperating genotyping and PCR. I would also like to thank the staff at the Zebrafish Facility in the Bateson Centre at the University of Sheffield for their help with the genotyping of CD9b adult mutants and IVF experiments.

For kindly providing the CXCR4-EGFP and CXCL12a-Venus constructs used in the internalisation experiments, I thank Professor Erez Raz. I would also like to thank Dr. Stuart Casson and the members of his lab for all their advice, technical support and time in helping me set up my qPCR experiments.

For keeping me connected to the world outside of research and helping me laugh through the stressful times I thank my friends, in particular Laura and Emily.

Last but certainly not least, I thank my wonderful parents and my amazing fiancé. Without your love and support I am not sure that I would have completed this journey and research.